UNIVERSITY OF IOANNINA
SCHOOL OF SCIENCES
DEPARTMENT OF CHEMISTRY

"Design, synthesis and biological evaluation of bio-conjugates for selective drug delivery and tumour targeting"

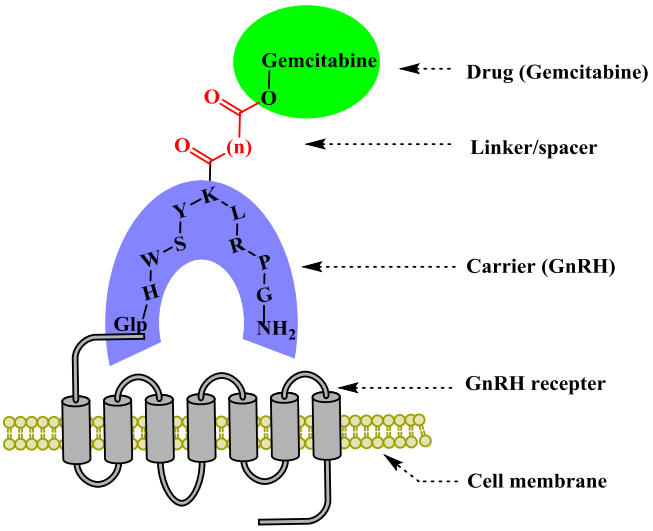

Mr. Sayyad Nisar Abdul
Chemist, Msc

PhD THESIS
Ioannina, 2015

UNIVERSITY OF IOANNINA
SCHOOL OF SCIENCES
DEPARTMENT OF CHEMISTRY

"Design, synthesis and biological evaluation of bio-conjugates for selective drug delivery and tumour targeting"

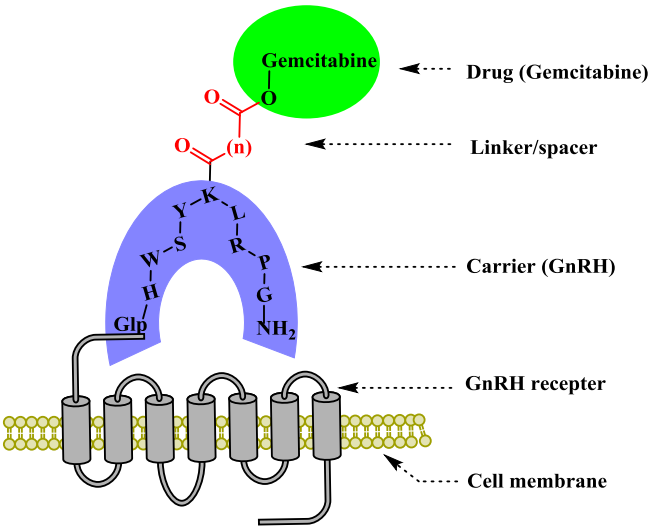

Mr. Sayyad Nisar Abdul
Chemist, Msc

PhD THESIS
Ioannina, 2015

«Η έγκριση της διδακτορικής διατριβής από το Τμήμα Χημείας της Σχολής Θετικών Επιστημών, του Πανεπιστημίου Ιωαννίνων δεν υποδηλώνει αποδοχή των γνωμών του συγγραφέα Ν. 5343/32, άρθρο 202, παράγραφος 2»

The financial support for this doctoral study was from Greek State Scholarships Foundation (I.K.Y.) for the period 2011-2015.

Ορισμός Τριμελούς Συμβουλευτικής Επιτροπής/Appointment of Three member committee από τη Γ.Σ.Ε.Σ.: 802^{A}/ 03-11-2010

Μέλη Τριμελούς Συμβουλευτικής Επιτροπής/Three member committee:

Επιβλέπων/Supervisor:

Assistant professor Tzakos Andreas

Μέλη/Members:

Professor Gerothanasis Ioannis
Professor Theodorou Vasiliki

Ημερομηνία ορισμού θέματος/Date appointed topic: 03-11-2010

Θέμα/Thesis: «**Design, synthesis and biological evaluation of bio-conjugates for selective drug delivery and tumour targeting**»

ΟΡΙΣΜΟΣ ΕΠΤΑ ΜΕΛΟΥΣ ΕΞΕΤΑΣΤΙΚΗΣ ΕΠΙΤΡΟΠΗΣ/ Apoitment of Seven member committee από τη Γ.Σ.Ε.Σ.: 899^{A}/10-12-2014

1. Assistant professor Tzakos Andreas
2. Professor Gerothanasis Ioannis
3. Professor Theodorou Vasiliki
4. Professor Varvounis George
5. Associate professor Skobridis Konstantinos
6. Associate professor Zarkadis Antonios
7. Associate professor Siskos Michail

Έγκριση Διδακτορικής Διατριβής μεβαθμό Αριστα στις 27-01-2015/Approval of PhD thesis «Excellent» at 27-01-2015

Η Πρόεδρος του Τμήματος Χημείας/	Η Γραμματές του Τμήματος Χημείας/
The Chairman of the Department of Chemistry	The Secretary of the Department of Chemistry
Lekka Maria-Eleni, Professor	Eleni Adamadiou

Acknowledgements

I wish to express my deep sense of gratitude to my research guide Dr. A.Tzakos for his valuable guidance, stimulating discussions and personal help during my PhD research. I would like to thank Prof. Gerothanassis Ioannis and Prof. Vassiliki Theodorou for their valuable supervision during my research work. Dr. A. Tzakos is highly creative and talented scientist, I have been inspired to watch his involvement with students. I thank him for allowing me to work independently on my projects. He also provided the opportunity to attend several conferences including EUROMAR 2013 in Crete, Greece. I learned how to convey scientific ideas clearly from him. I thank him for maintaining a group of intelligent and hard-working students who make the lab a wonderful and stimulating place to work.

I am also thankful to my dissertation committee members: 1) Prof. George Varvounis, 2) Asso. Prof. Konstantinos Skobridis, 3) Asso. Prof. Antonios Zarkadis and 4) Asso. Prof. Michael Siskos.

I wish to acknowledge, financial support from "The Greek State Scholarship Foundation" (IKY).

I also thank Dr. Makis Papas and Dr. Vassiliki Kontogianni for their help with mass spectrometric analysis experiments; and Dr. Kostas Tsiafoulis for helping me in NMR experiments.

I am very thankful to my colleagues who helped me during my good and bad times. Eleni Kyriakou, Alexandra Primikiri, Haralabos Papas, Alexandra Hatzikwnstantinou (Alex), Marianna Sakka, Maria Chatziathanasiadou and Christina now all of them are my best friends.

Finally, I would like to thank my family members. I owe everything I am today to my mom, Mrs. Hajarabee Abdul and my Dad Mr. Abdul Sayyad. I thank to my brother Altaf, sister Reshma and my wife Asma for supporting and encouraging me, they have taught me to be optimistic in any circumstances. They went through a lot of difficult situations but always allowed me to stick to my research work.

. **- Nisar Sayyad.**

List of Abbreviations

KOH = Potassium hydroxide
NaOH = Sodium hydroxide
ACN = Acetonitrile
amu = atomic mass unit
B(*i*-OPr)$_3$ = triisopropoxy borate
BNPC = Bis(4-nitrophenyl)carbonate
Boc = *tert*-Butoxycarbonyl
CuI = Copper Iodide, copper (I) iodide or cuprous iodide
DBDC = Boc_2O = di-*tert*-butyl dicarbonate
DCC = 1,3-Dicyclohexylcarbodiimide
DCM = CH_2Cl_2 = Dichloromethane
DIC = Diisopropylcarbodiimide
DIPEA = $NiPr_2Et$ = Diisopropylethylamine
DMAP = 4-Dimethylaminopyridine = 4-*N*,*N*-Dimethylaminopyridine
DMB = Dimethoxy benzene
DMF = *N*,*N*-Dimethylformamide
DMSO = Dimethylsulphoxide
DNA = deoxyribonucleic acid
EDC = EDCI = 1-Ethyl-3-(3-dimethylaminopropyl)carbodiimide
ESI = Electrospray ionization
EtOAc = Ethyl acetate
EtOH = Ethanol
GnRH = Gonadotropin-releasing hormone
GnRH-R = Gonadotropin-releasing hormone receptor
H_2O = Water
HATU = 1-[Bis(dimethylamino)methylene]-1H-1,2,3-triazolo[4,5-b]pyridinium 3-oxid hexafluorophosphate
HBTU = O-Benzotriazole-*N,N,N',N'*-tetramethyluronium-hexafluoro-phosphate.
HCl = Hydrocloride
$HClO_4$ = perchloric acid
HMBC = Heteronuclear Multiple Quantum Correlation
HOAt = 7-Aza-1-hydroxybenzotriazole
HOBt = 1-Hydroxybenzotriazole
HPLC = High-Performance Liquid Chromatography
HSQC = Heteronuclear Single Quantum Correlation,
MeOH = Methanol
MW = Mol.wt. = molecular weight
Na_2CO_3 = Sodium carbonate

$NaIO_4$ = Sodium periodate
n-BuLi = *n*- butyl lithium
NHS = *N*-Hydroxysuccinimide
NMR = Nuclear Magnetic Resonance
NOESY = Nuclear Overhauser Effect Spectroscopy
$Pd(PPh_3)_4$ = Tetrakis(triphenylphosphine)palladium(0)
PyBOP = benzotriazol-1-yl-oxy-tris-pyrrolidino-phosphonium hexafluorophosphate
RNA = ribonucleic acid
rt = room temperature
$SOCl_2$ = Thionyl chloride
*t*Bu = *tert*-Butyl
TEA = Triethylamine
TFA = Trifluoroacetic acid
THF = Tetrahydrofurane
THPTA = Tris(3-hydroxypropyltriazolylmethyl)amine :
TIS = Triisopropylsilane
TLC = Thin-Layer Chromatography
TOCSY = Total Correlation Spectroscopy
Trt = Trityl, triphenylmethyl
UV = Ultraviolet

Table of Contents

Chapter 3: Quercetin

Chapter 4: GnRH-Sunitinib conjugates

Chapter 5: Side projects I worked in the frame of PhD thesis

Chapter 1: Introduction

1.1 Targeted drug delivery:

Despite the progress in techniques for cancer prevention, detection and treatment, as well as for increasing the public awareness in recent years, this disease is projected to become the leading cause of death worldwide. Advancements in omics, analytical procedures and high throughput screening in the last five years have led to the realization that human diseases and especially cancer is more complex than was originally conceived. Cancer is not a static entity that can be easily monitored and manipulated. It is characterized by a dynamic and time dependent network of constantly altered molecular and cellular interactions between players in different pathways. This network is not invariable and rigid, but is constantly reshaped and altered conforming to the pliable signaling processes/responses implicated. Its complexity is apparent by the fact that the disease state is not a disruption of a single node or specific nodes in the network-organism, but is organism-patient dependent, thus, requiring personalized perspective approaches.

Numerous challenges hamper effective cancer treatment and development of effective drugs such as ineffective therapeutic drug concentration reaching the tumour site; life-threatening side-effects caused by nonspecific tissue distribution of anticancer agents; acquired resistance of the cancer cell upon chemotherapy that triggers cross-resistance to a wide range of different drugs.

Such multifactorial states require the development of very delicate approaches in the course of the drug discovery pipeline. The scientific roots of the drug development philosophy should be shifted from the traditional concept of the “magic bullet” drug (that is scalped for a single drug target) to the formulation of a navigated vehicle which could spatio-temporally deliver the drug in the correct location and the appropriate time. Thus, the term *targeted drug delivery* should give its place to *navigated drug delivery* since it is not only the cytotoxic drug that targets a specific cellular location but rather a vehicle that navigates the course of the loaded drug to the appropriate site of action. Such drug loaded and navigated vehicles in order to enhance the selective uptake of the cytotoxic agent by the tumour cells, and spare the normal cells, should consist of a multidimensional

architecture (*Figure 1 & 2*). The major components of these vehicles are: the transporting vehicle (i.e. lipid), the cytotoxic agent that is loaded, the "programmable" navigating/targeting agent (i.e. receptor specific ligand) that enables the appropriate delivery routes to avoid toxicity on healthy proliferating cells as also ineffective concentration of the cytotoxic agent to the tumour site (*Figure 2*) and the "stealth" nano-carriers (biocompatibility polymers, i.e. PEG) that extents the short plasma half-life of the drug-loaded transporting vehicle.

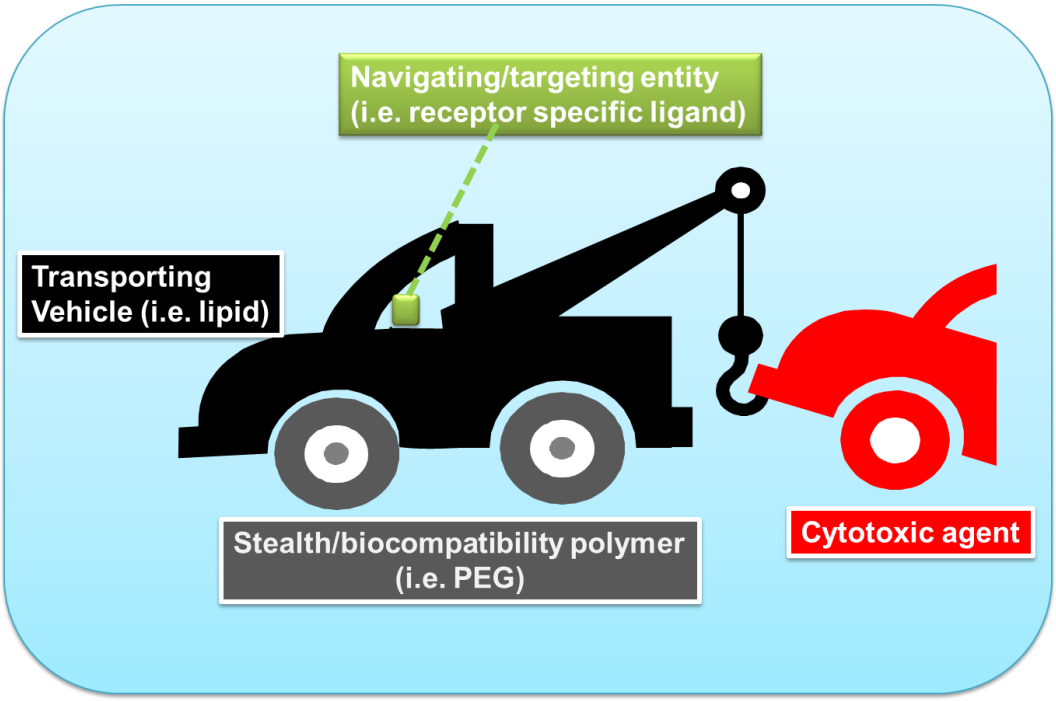

Figure 1: *Structural architecture and mechanical analogue of a navigated drug delivery nanoparticle.*

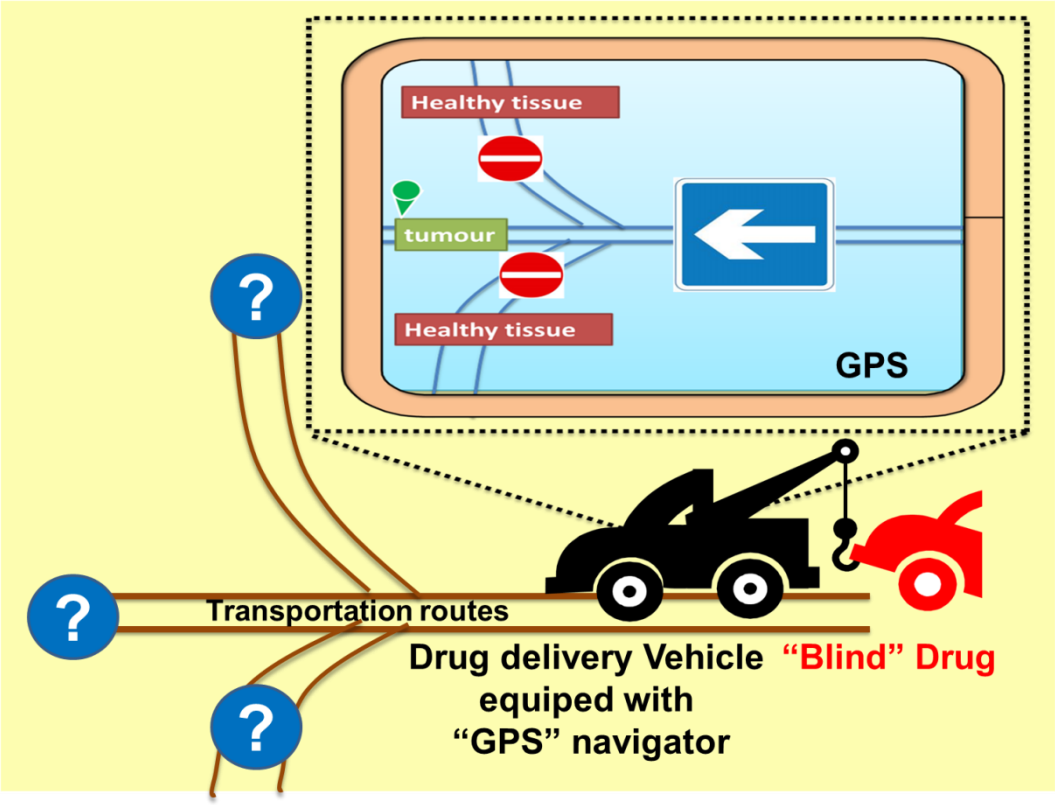

Figure 2: *Navigated drug delivery: The drug delivery vehicle is equipped with a "programmable navigation system" that allows the transportation of the "blind" cytotoxic agent in the correct cellular location. In the absence of the drug delivery vehicle that is tagged with navigating delivery routes, toxicity is triggered on healthy proliferating cells against the anticancer agent and ineffective therapeutic drug concentration reaches the tumour site.*

In line with the challenges raised by the complexity of cancer, the aim of the present thesis is to provide novel methods that could shed the basis for innovative molecularly targeted cancer therapies and entrepreneurial methods of drug delivery in cancer (*Table 1*).

Due to the complexity of the disease, efficient cancer therapy can emerge only upon inter-science collaboration. Current knowledge on molecularly targeted cancer therapies and innovative methods of drug delivery in cancer has to be rationally orchestrated. We believe that this accumulative knowledge will assist to accelerate progress developing more precise navigated drug delivery in cancer based on innovative tools.

Table 1: *Some of the delivery systems appeared in the literature.*

Vehicle	**Vehicle Description**	**Navigation device**	**Target Location**	**cancer type**
Bionanocapsules	A bio-nanocapsule (BNC) is a hollow nanoparticle consisting of an approximately 100-nm-diameter liposome with about 110 molecules of hepatitis B virus (HBV) surface antigen L protein embedded as a transmembrane protein.	chlorotoxin	MMP-2 protein	Brain tumour
enzyme-based cancer imaging agents	dual aromatase-steroid sulfatase inhibitor (DASSI) radiotracers	^{11}C-labelled inhibitors of steroid sulfatase (sulfamate derivatives)	enzymes of the "sulfatase pathway", particularly steroid sulfatase	breast, endometrial, ovarian, and colorectal cancer
Cytotoxic drugs coupled to OATP-substrates or OATP-directed antibodies	Substrates of membrane-located OATP isoforms, selctively expressed in cancer cells, e.gmicrocystins as substrates for OATP1B3	Selective ligands for OATP e.g. microcystins or OATP-directed antibodies in cancer cells	organic anion transporting polypeptides (OATPs)	gastrointestinal tract, breast, prostate, lung, brain, bladder, kidney, liver, testis.
lipid-based nanoparticles	Genuine particles (approx 100 nm in dimension) assembled from varieties of lipid and other chemical components that act collectively to overcome biological barriers (biobarriers).	*bona fide* biological receptor specific ligands		
PEGylated Span 80 vesicles PEGylated Span 80 vesicles with immobilized ESA	Span 80 is a heterogeneous mixture of sorbitan mono-, di- tri-, and tetra- esters	Lectin-sugar binding protein (Eucheumaserra agglutinin)	sugar chains on the tumour cell-surface	Osteosarcoma
Doxorubicin (DOX)-loaded liposomes	liposomes composed of DSPG, DSPC, cholesterol, and DSPE-PEG-2000	a triple-helical sequence derived from type IV collagen	CD44/chondroitin sulfate proteoglycan	CD44-overexpressing tumour cells
Mannan	Oxidized or reduced mannan, a poly-mannose, conjugated to cancer antigen	mannan	Mannose receptor	Adenocarcinoma
GnRH	It is 10 residue peptide	It act as a navigating device as its own.	GnRH-R	Prostate, breast, bladder etc.

1.2 Drug-Peptide Conjugates:

1.2.1 The Peptide-Carrier:

Chemotherapy is still one of the primary modalities for the treatment of cancer. However, the application of free anticancer drugs has several drawbacks. Frequently applied high doses are required for the efficacy because of the fast elimination of the drugs from the circulation. Furthermore, the lack of selectivity generally results in toxic side effects. Also, the acquired or intrinsic multidrug resistance (MDR) of cancer cells may restrict the use of chemotherapy. Targeted chemotherapy has been developed to overcome these disadvantages and it has been suggested as an alternative for differentiating healthy and cancer cells.

Tumour targeting is usually achieved by conjugation of the chemotherapeutic agent to a targeting moiety consisting of sugars, lectins, receptor ligands, or antibodies, which is specifically directed to certain types of binding sites on cancer cells. One of the various targeted chemotherapeutic approaches is based on the finding that receptors of several peptide hormones (e.g. gonadotropin-releasing hormone (GnRH), bombesin, and somatostatin) are over-expressed on cancer cells compared to normal cells and organs. GnRH receptor (GnRHR) expression was identified on different tumours (breast, ovarian, endometrial, prostate, renal, brain, pancreatic, melanomas, and non-Hodgkins lymphomas) with high percentages in specimens.

A modern approach to improve conventional chemotherapy is by direct targeting of chemotherapeutic agents to cancer cells in order to enhance the tumouricidal effect and reduce peripheral toxicity of a specific drug. Linking chemotherapeutic agents to peptide ligands or antibodies directed towards cell surface proteins/receptors, expressed or over-expressed uniquely in cancer cells.

Even though peptides have advantages as carriers with respect to proteins, there are some essential requirements for a peptide to become a convenient carrier. For instance, the peptide should have binding affinity and selectivity for the receptor which is present or over-expressed on targeted cells surface. To achieve the required drug efficacy (effective concentration) at the targeted cells the carrier peptide should have sufficient stability in the

studied system. The most important part is that, after conjugation the peptide must not alter the microenvironments required for its binding with the targeted receptor.

The gonadotropin-releasing hormone (GnRH) as a drug-carrier: The GnRH-R is a member of the G-protein-coupled receptor family with the characteristic seven trans-membrane domains.[1, 2] It is normally present in the pituitary gland but upregulation of its expression has been reported in prostate, breast and other cancers[1, 3] often linked to a poor prognosis[4]. The main ligand for this receptor is the decapeptide hormone GnRH which upon binding transmits signals from the GnRH-R to the nucleus through activation of protein kinase C, regulating reproduction.[5] GnRH is a deca aminoacids peptide (pGlu-His-Trp-Ser-Tyr-Gly-Leu-Arg-Pro-Gly-NH_2) and substitution of the 6^{th} aminoacid glycine with D-Lys stabilizes the folded conformation and increases the peptides binding affinity as also reduces the metabolic clearance of the peptide.

GnRH-R has provided valuable paradigms for targeted drug delivery.[6–9] One representative example of a cytotoxic analogue targeting the GnRH-R is AN-152, a conjugate molecule of a peptide analogue of GnRH, ([D-Lys^6]-GnRH), linked to doxorubicin.[10] Other examples of molecules linked to GnRH for targeted delivery include daunorubicin,[11] curcumin[12] and docetaxel.[13] Importantly, AN-152 has been evaluated in Phase I and Phase II clinical studies in GnRH-R positive cancer patients demonstrating anticancer activity with only moderate side effects.[14]

1.2.2 The Cytotoxic Drug:

Cytotoxic drugs such as gemcitabine, doxorubicin, methotrexate (MTX), campethecin (CPT) and sunitinib etc. in most of the cases are not able to exploit their full therapeutic efficacy because they lack selectivity for cancer over normal cells. Such molecules enter the cell by different mechanisms (i.e. gemcitabine enter cells by nucleoside transporters) and trigger their cytotoxic effects. What is important to note is that due to low bioavailability or low efficacy patients need to take high doses of drugs and this overdose may induce drug resistance.

Thus, conjugation of these drugs to carriers that could direct them to the specific population of cancer cells could lead to lesser side effect (since lower doses will be required) as also to enhanced pharmacokinetics and tuned therapeutic action. What is important in such conjugates is the very careful design of linkers that will connect the drug

to the targeting vehicle (peptide carrier). This conjugation has to be done in such a way that the carrier's ability to bind to the specific bio-receptor should not be perturbed. In addition, special care has to be taken on the type of linkage between the carrier (peptide) and drug since the drug has to be released when it will reach the target site/cell so as to exert its cytotoxic activity.

1.3 The Chemistry of Drug-peptide Conjugation:

There is currently available a large pool of bioactive compounds and approved drugs that evolved after effortless and numerous medicinal chemistry projects in pharma industry and in academy. What is to note, in the drug discovery process, there is a large number of these compounds that due to late stage identification of toxicity, side effect identification or lack of targeting make their development halted. There are also numerous examples of approved drugs that their associated developmental cost was enormous but after their launch had to be withdrawn due to side effects identification. Since for all these compounds there was large investment and careful shape of their bioactivity, a very challenging issue will be carefully exploit ways on how to put back on track these compounds and surmount all these associated drawbacks. Peptides as drugs carriers, cell penetrating agents and cellular targeting vehicles have seen an enormous application recently. A very challenging issue though is the development of appropriate chemical entities that will function as the conjugation chain between the drug and the peptide. There are numerous characteristics and careful design should be met for this linking to permit the drug-peptide conjugation to fulfill the desired properties. Herein, we will present the array of biolinkers used in drug peptide conjugation, we will describe the mechanism of their function and present recent advances in the field as also we will provide basic guides on to select the appropriate linker dependent on the functional groups that the drug is decorated.

Different approaches are available for the conjugation of peptide carriers with cytotoxic drugs. The conjugation can be achieved by using specific linkers-spacers or in some cases through utilization of traceless linkers. The linkers are used to avoid the development of potent steric hindrance among the peptide and the drug as also to sustain the microenvironment required for receptor binding. The type of chemical bond used for the bioconjugation is directly affecting the stability of bio-conjugates and consequently affects

the spatiotemporal delivery of the drug. The chemical bonds that are used to form the conjugates could be either of a single type (i.e. esters) or in combination (i.e. ester bonds and oxime bonds).

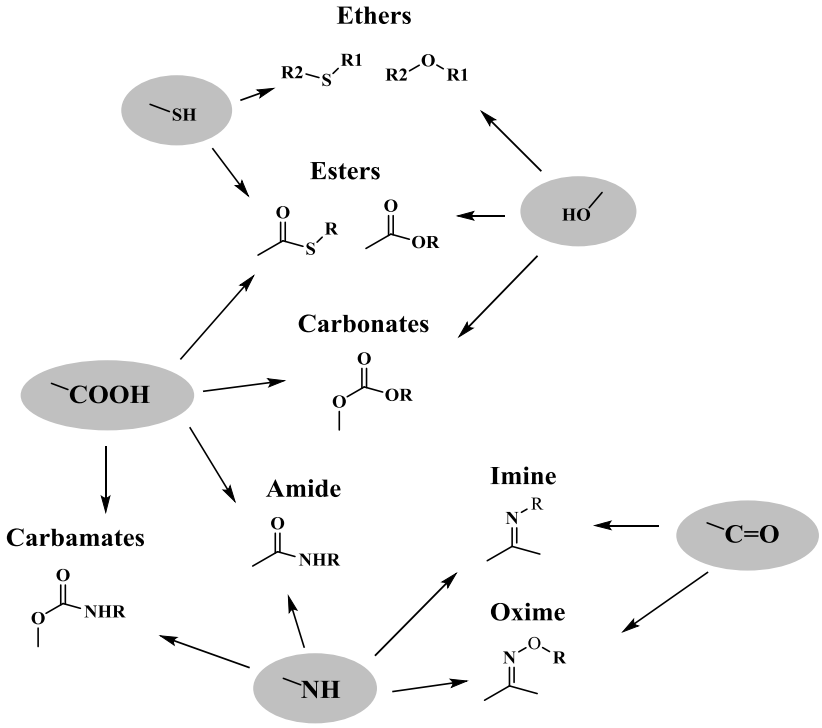

Figure 3: *Example of Drug – peptide linkers used in medicinal chemistry*

On the frame of this thesis we explored different types of chemical bonds as also spacers of various lengths and exploited their effect such as cytotoxicity, binding affinity to targeted receptor, pharmacokinetics, and in vivo studies to understand the selectivity, stability and efficacy of cytotoxic drugs. We have conducted different **GnRH-Gemcitabine conjugates.** The designing of these conjugates was based on improving the therapeutic potential of gemcitabine through: a) Reduction of gemcitabine's metabolic inactivation, b) surmount developed resistance related to the loss of gemcitabine transporters; c) Targeted delivery in cancer cells. In addition, we studied **GnRH-Sunitinib conjugates.** Specifically, we investigated whether targeting of GnRH-R expressing cancer cells in parallel with tumour angiogenesis could lead to enhanced tumour growth inhibition by conjugating [D-Lys^6]-GnRH to novel antiangiogenic analogues of sunitinib (SANs).

1.3.1 Amide Bonds in Chemical Linkers

The amide bond conjugation is carried out by the reaction between a carboxylic acid of one constituent and the amine from other. This is a simple reaction and the amide bond has immense chemical/enzymatic stability with respect to other bonds. The enzymatic cleavage of this conjugation may be slow but it has very high possibility to reach the cell target leading in the same time to high drug efficacy. Another benefit that this reduced bond susceptibility could offer is that for some drugs could slow down the rate of their metabolic inactivation.

The synthesis of amide bioconjugation can be achieved by activation of carboxylic acids (it may be from the carrier, the drug or the spacer) using coupling reagents such as HBTU, HATU, EDCI-HOBt, PyBOP etc. and then addition of the complementary amine (from drug, peptide or spacer) in the presence of a base (DIPEA) and solvent DMF or DMSO.

1.3.2 Oxime Bonds in Chemical Linkers:

The Oxime bond is also conisdered as a stable bond (more stable than the carboxylic ester) for bioconjugation. The oxime bond formation is of importance in bio conjugation chemistry due to its chemoselectivity, stability and compatibility with other groups. The reaction of a ketone or an aldehyde with aminoxy or hydrazide form the imine called oxime and hydrazone, respectively. Even though the oxime formation is more sluggish than the hydrazone, its hydrolytic stability makes the oxime bond more preferable than the hydrazone[15]. The alfa nucleophile of the aminoxy is stronger nucleophile than amines, and its low basicity allows the formation of more stable imines (oxime).[16]

The enhanced chemoselectivity of the oxime bond formation provides great opportunities in orthogonal coupling in bioconjugation. The basic characteristics of the oxime bond are: 1) Its ease of synthesis due to high chemoselectivity, therefore laborious protection/deprotection steps are avoided,[17] 2) High chemical stability in the pH range 3-8.

1.3.3 Carboxylic Acid Ester Bonds in Chemical Linkers:

The carboxylic ester formation is the condensation reaction between carboxylic acid and hydroxyl group. The carboxylic acid ester is the commonly used bond in the bioconjugation[18,19] because it can be hydrolyzed chemically or enzymatically (e.g.

esterase) to release the drug. However its sensitivity for hydrolysis may release the drug before the reaching target cell/tissue. The stability of the ester bond may be improved by the length of the linker between the carrier peptide and the cytotoxic drug or by selection of hydroxyl group (primary vs. secondary) for carboxylic ester formation.[18] A series of gemcitabine conjugates with [D-Lys^6]-GnRH, an agonistic peptide with enhanced receptor binding activity,[20] were synthesized on the frame of the current thesis for selective drug targeting to cancer cells over-express GnRH-Rs.

1.3.4 Carbamate Bond in Chemical Linkers:

Carbamate is a chemical moiety where carbonyl group holds two nucleophiles together: an amine and an alcohol. This carbonyl may come from phosgene; 1, 1'-Carbonyldiimidazole (CDI); Bis(4-nitrophenyl)carbonate (BNPC); isocynates; or chloroformates. This bond can be characterized as the shortest traceless linker in Bioconjugation. Its higher stability in plasma than the carboxylic ester gives higher possibility of reaching drugs to the target.[21]

1.4 The Molecular hybridism concept:

Molecular hybridization is a new concept in drug design and developement based on the combination of pharmacophoric moieties of different bioactive substances to produce a new hybrid compound with improved affinity and efficacy, when compared to the parent drugs. New innovative hybrid compounds have appeared in the literature presenting analgesic, anti-inflammatory, platelet anti-aggregating, anti-infectious, anticancer, cardio and neuro properties. Additionally, this strategy can result in compounds presenting modified selectivity profile, different and/ or dual models of action and reduced undesired side effects.

Herein, we have prepared an array of different hybrids using different strategies for drug design, discovery and pharmacomodulation focused on new innovative hybrid compounds.

1.4.1 Gemcitabine 4N-acyl derivatives:

Gemcitabine is an anticancer agent that acts against a wide range of solid tumours such as pancreatic, non small lung, breast, and ovarian cancers. It is transported across the plasma

membrane by sodium-dependent (concentrative nucleoside transporter hCNTs) and by sodium independent (equilibrative nucleoside transporter hENTs) mechanisms. However, many cancers develop resistance against this drug, such as loss of transporters and kinases responsible for the first phosphorylation step. Furthermore, gemcitabine, is known to be rapidly deaminated in blood to the inactive metabolite 2′,2′-difluorodeoxyuridine and to be rapidly excreted by the urine. To increase its therapeutic levels, gemcitabine is administered at high doses (1000 mg/m2) causing side effects (neutropenia, nausea, and so forth). To improve its metabolic stability and cytotoxic activity and to limit the phenomena of resistance strategies that provide both enhanced transport and high metabolic bioevasion by chemical modification could potentially lead to new therapeutic strategies. To overcome these drawbacks, we have established a novel methodology for regioselective N-acylation of gemcitabine with chloroformates bearing different functionality that are suitable to result to an array of different molecular hybrids.

1.4.2 Quercetin-aminoacids:

Quercetin is one of the prominent antioxidant consumed daily but suffers from its low solubility and bioavailability.[22] On the frame of this thesis in order to surmount these issues we have synthesized different Quercetine-aminoacids analogues.

1.4.3 Quercetin-Captopril/Losartan:

Diseases such as cancer and hypertension are interlinked to oxidative stress. Thus construction of hybrids equipped with compounds that carry multifunctional activities (antioxidant, anti-hypertensive and anticancer) is of immense importance in therapy.

Herein, we designed and synthesized Losartan-quercetin and Captopril-quercetin hybrids that carry in a single core an anticancer/antihypertensive functional group (losartan/captopril) and an antioxidant functional group (quercetin).

Chapter 2: Gemcitabine

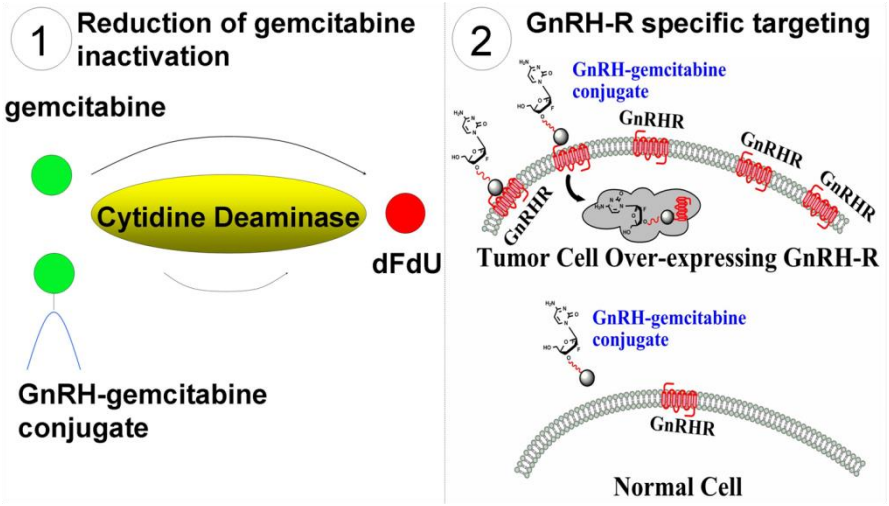

2.1 Introduction:

2.1.1 Biological background of gemcitabine:

Cell is the building block of life; it consists of protoplasm enclosed within the membrane which contains numerous biomolecules such as proteins and nucleic acids. Nucleic acids which include the deoxyribonucleic acids (DNA) and ribonucleic acids (RNA), the DNA and RNA, respectively, are made from monomeric nucleotides. The sequence of nucleotides in DNA and RNA are responsible for encoding, transmitting and expressing the genetic information of an organism. Each nucleotide is consisted of three components, 1) a 5-carbon sugar, 2) phosphate group and 3) the nitrogenous base.

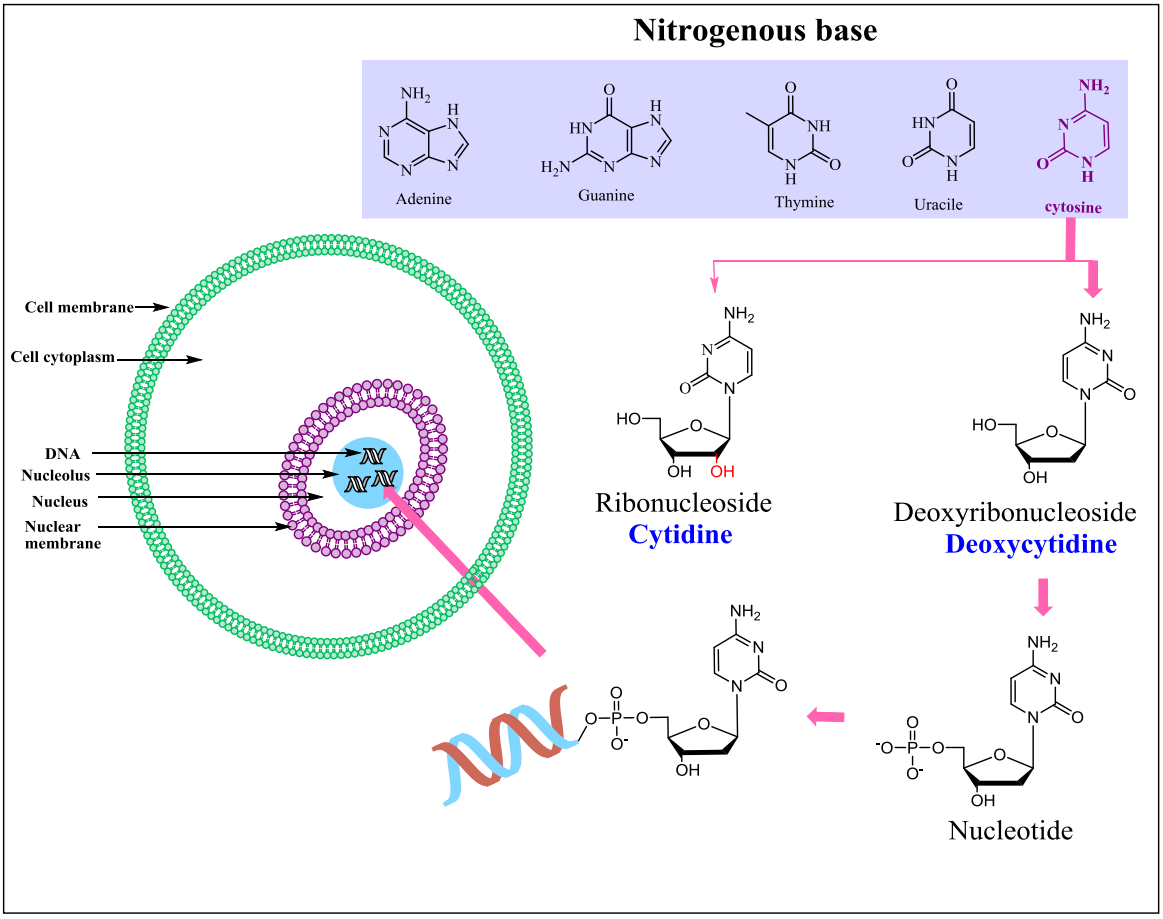

Figure 1: *Schematic path of nitrogenous bases in cell growth (DNA synthesis).*

Gemcitabine is a nucleoside analogue of deoxycytidine where two hydrogen atoms from the 2' position are replaced by fluorine. Incorporation of the fluorine atom enhances the physico-chemical and biological properties of gemcitabine and doesn't alter the shape

and size of this molecule significantly despite the fact that the C-F bond is stronger than the C-H bond, these feature enhance the physico-chemical and biological properties of gemcitabine.

Nucleosides and their analogues are an important class of anticancer and antiviral agents. Gemcitabine is one of the Deoxycytidine nucleoside analogues, being used as chemotherpetic agents alone or in combination and presents anticancer activity against a wide spectrum of solid tumour such as non-small cell lung cancer, pancriatic cancer, bladder cancer, breast cancer, prostate cancer, ovarian cancer.[23] However, gemcitabine lacks an effective therapeutic window to be used as an efficient anticancer drug since:

1) It presents high and non-selective toxicity to normal cells.

2) It is inactivated, through deamination, to its inactive metabolite 2', 2'-difluorodeoxyuridine (dFdU).

3) Its high hydrophilicity causes hydrolytic degradation[24] consequently reduces the effective concentration of gemcitabine.

Cellular uptake of gemcitabine:

Gemcitabine cross the cell plasma membrane through the nucleoside transpoters (NTs). Human NTs are the concentrative (hCNTs) and equlibrative (hENTs) types, both of them are responsible for gemcitabine transport in cells.[25]

Mechanism of gemcitabine's action:

Gemcitabine (dFdC) is taken up by cells via the nucleoside transporters. Intracellular phosphorylation of gemcitabine into its active metabolites by nucleoside (deoxycytidine) kinases at its hydroxyl groups gives sequentially mono (dFdCMP), di (dFdCDP) and triphosphates (dFdCTP). Among these dFdCDP and dFdCTP are the most important metabolites responsible for gemcitabine's cytotxicity[26]. In addition, dFdCDP inhibits the enzyme ribonucleotide reductase, which is responsible for the synthesis of deoxycytidine triphosphate (dCTP) required for DNA synthesis. In this way, dFdCDP reduces the intracellular concentration of dCTP, and due to a concentration gradient dFdCTP competes with dCTP and is implemented into DNA. After the implementation of dFdCTP in the DNA sequence one additional nucleotide is added and then termination of DNA synthesis takes place, so-called "Mask termination" and subsequently follows apoptosis.

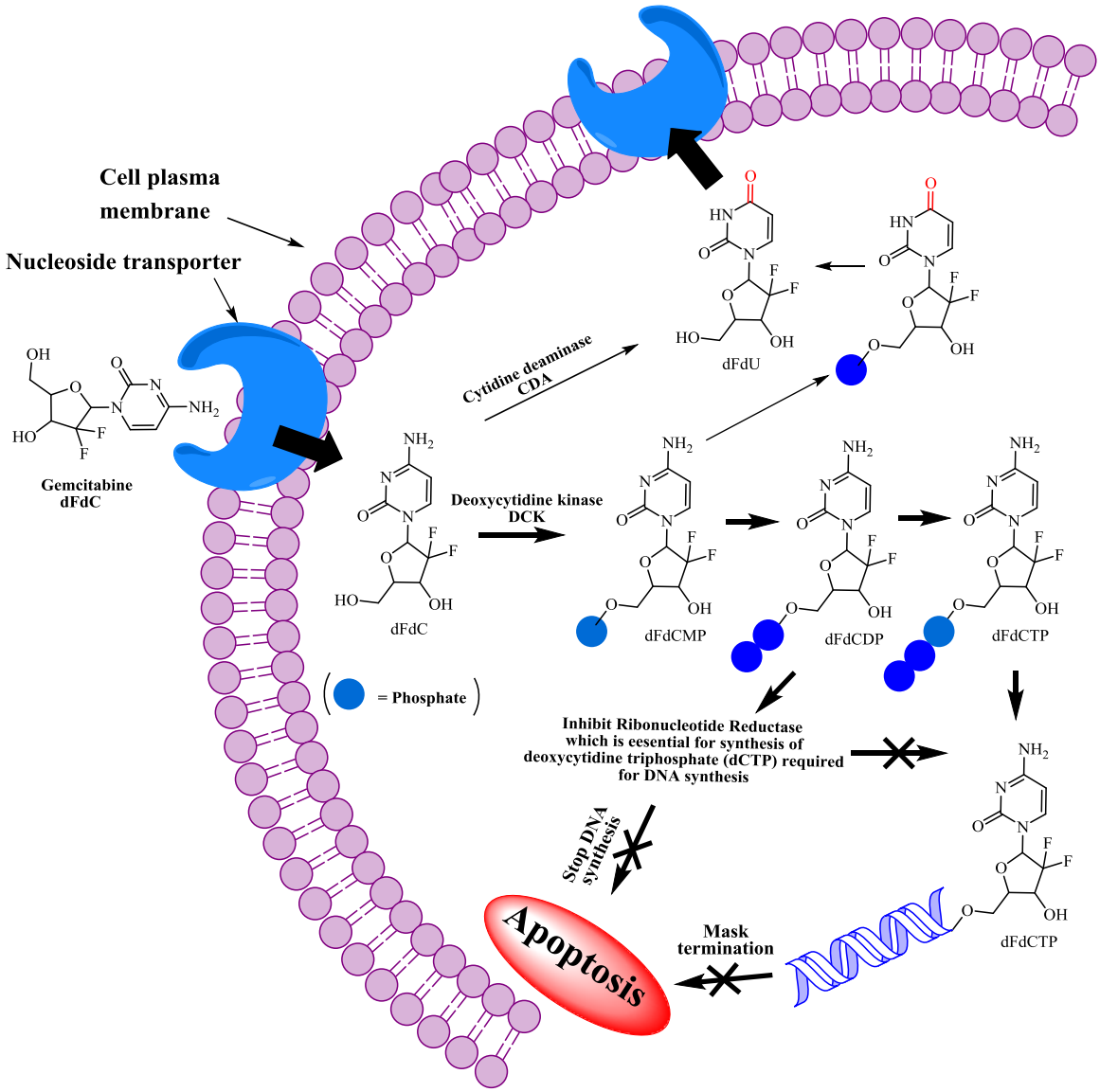

Figure 2: *Intracellular Gemcitabine metabolism.*

Deamination of gemcitabine:

Gemcitabine lacks optimal pharmacokinetics since it has reduced stability in plasma[26] and in liver[27], due to its rapid conversion to its inactive metabolite 2',2'-deoxydifluorouridine (dFdU) via hydrolytic deamination in its 4-amine by the enzyme cytidine deaminase.

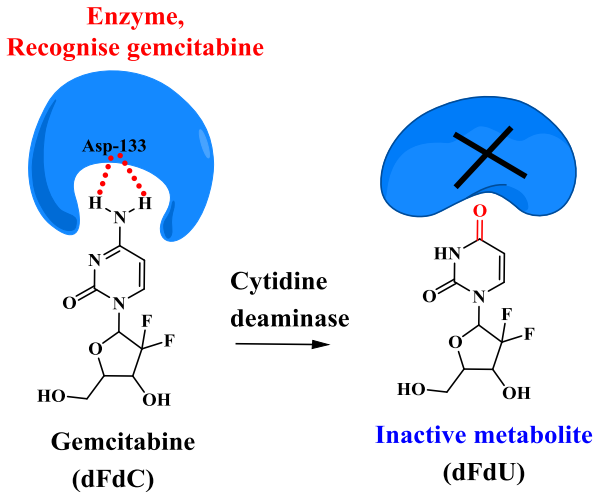

Figure 3: *Enzymatic recognition of Gemcitabine by* cytidine *deaminase and its deamination to the inactive metabolite.*

This deamination results an obstacle in enzyme-substrate recognition, since there is no hydrogen bonding between amino acid (Asp. 133) of the enzyme and the group 4-O of dFdU[28] (*Figure 3*). This is the main reason for the low bioavailability and gastrointestinal toxicity of gemcitabine. To overcome plasma instability (half life 1.5 h)[28] gemcitabine is being injected intravenously instead of oral administration.[29]

2.1.2 Gemcitabine's Chemistry:

The above mentioned limitations of gemcitabine can be surmounted by synthesis of prodrugs or through conjugation with carrier or navigating molecules (e.g. peptides) targeting receptors that are over-expressed in cancer cells.

Herein, we aimed a targeted drug (gemcitabine) delivery utilizing as a navigation vehicle the GnRH (Gonadotropin Releasing Hormone) peptide (carrier) which is recognized by the GnRH receptor that is over-expressed in cancer cells. The conjugation of gemcitabine to the GnRH peptide was achieved with various linkers (spacer) consisted of different chemical functionalities. Gemcitabine has three functional groups (reactive sites) where we can have possible chances for conjugation of Gemcitabine and GnRH with variable linkers via different bonds (functional groups). These reactive sites are the primary hydroxyl group (5'-OH), the secondary hydroxyl (3'-OH) and the amine (4-NH_2) group. Thus, conjugation possibilities are the formation of amide, carbamate or imine at

the 4-amine position and carbonate, carbamate or ether at the 5' and the 3' hydroxyl position (*Figure 4*).

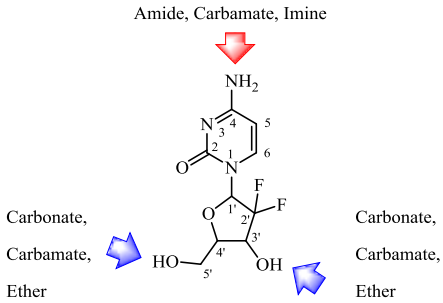

Figure 4: *Gemcitabine, possible sites for conjugation.*

Following the principle of targeted drug delivery, gemcitabine should be enzymatically or chemically[30] released (hydrolyzed into the parent drug) in the tumour cells and should carry its native activity (antitumour). So, the linker/spacer should be designed in such a way that the linker should be labile at the acidic pH (4.8) of the tumour cell organelles (especially endosome and lysosomes[31, 32, 30]) and get hydrolyzed. The order of hydrolysable bonds (functional groups) is as follows:

Carbonate > Carbamate > Hydrazone or Oxime > Amide

To achieve a regioselective coupling at one site (5'-OH, 3'-OH or 4-NH_2) we need to go through a protection/deprotection scheme.

Table 1*: The possible ways of protecting alcohol and amine.*

1) Benzoate (Bz)[33, 34, 35]	6) Triisopropylsilyl ether (TIPS)
2) Benzyl ether (Bn)	7) Acetate (Ac)
3) tert-Butyldimethylsilylether (TBDMS)[33, 34, 35]	8)Trt-Butyldiphenylsilyl ether (TBDPS)[12, 17]
4) Trimethylsilyl ether (TMS)[4, 14–16]	9) tert-Butoxy carbonyl (Boc)[33, 26, 40, 37, 18, 41]
5) triethyl sisyl ether (TES)	

According to the reported procedure[41] we have synthesised different "Boc" protected derivatives of gemcitabine (i.e. Gem 1, Gem 2 and Gem 3 , see *Figure 5*) leaving the primary hydroxy, secondary hydroxy and amine groups, respectively free for the conjugation reactions.

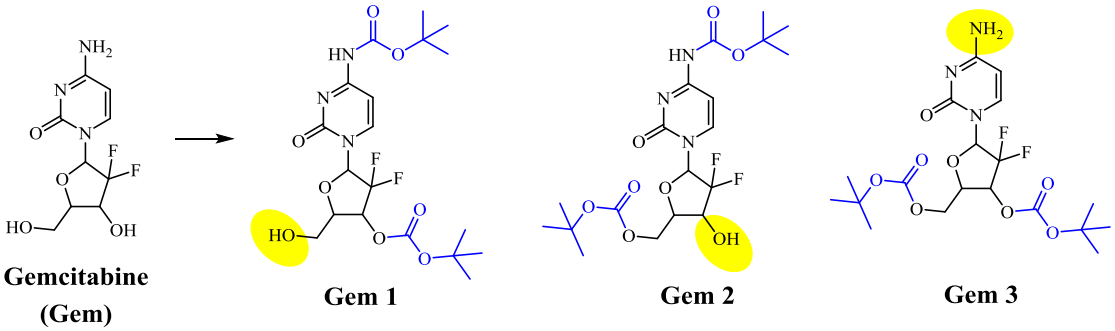

Figure 5: *Synthesis of different Gemcitabine-boc derivatives.*

2.2 Conjugation of Gemcitabine via Carbonate linkers

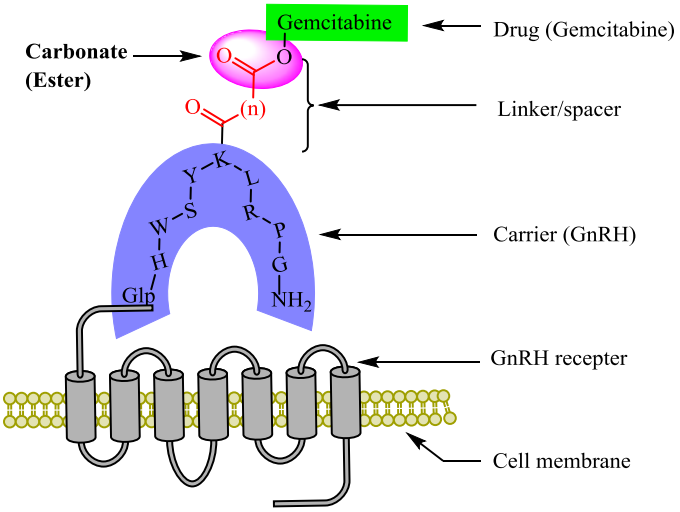

General concept of medium linkers ($3G_1$, $3G_2$, GSG_1, GSG_2) via carbonate.

Published:

Theodoros Karampelas[1], Nisar Sayyad et. al. **GnRH-Gemcitabine Conjugates for the Treatment of Androgen-Independent Prostate Cancer: Pharmacokinetic Enhancements Combined with Targeted Drug Delivery**. *Bioconjugate Chemistry, 2014, (4), 25, 813-823.*

2.2.1 Introduction:

Despite advancements in methods for early cancer detection and improved insights into the molecular mechanisms and treatment options, advanced prostate cancer (CaP) remains a major health problem for the aging man.[21, 22] Hormonal therapy is usually the first line of defense for CaP treatment by using drugs that lead to chemical castration, suppression of testosterone and dihydrotestosterone (DHT) biosynthesis.[23, 24] The hormonal ablation approach has been achieved successfully using agonist (through desensitization) or antagonist analogue drugs, of the native Gonadotropin Releasing Hormone (GnRH). These drugs exert their effects primarily on the pituitary gland through the GnRH-R by lowering gonadotropins and downstream gonadal sex steroids. Nevertheless, in many cases after treatment, following initial tumour regression, CaP progresses to an androgen-independent state with poor prognosis, which presents a major challenge for the physician and the patient.[23, 25–30] Research on the GnRH-R has shown that its expression is not confined solely to the pituitary but that is also present in several other tissues such as prostate, breast[52–54] and the GnRH-R level of expression along with cell context is critical for cell responses to either agonist or antagonist drugs of the receptor.[3] It is also well established that GnRH-R gene expression is upregulated in patients with androgen-independent CaP, making the GnRH-R an attractive target for the design of novel and specific therapeutics.[55]

A modern approach to improve conventional chemotherapy is by direct targeting of chemotherapeutic agents to cancer cells in order to enhance the tumouricidal effect and reduce peripheral toxicity of a specific drug. Linking chemotherapeutic agents to peptide ligands or antibodies directed towards cell surface proteins/receptors, expressed or over-expressed uniquely in cancer cells (such as the GnRH-R), provides valuable paradigms for this approach.[6–9] One representative example of a cytotoxic analogue targeting the GnRH-R is AN-152, a conjugate molecule of a peptide analogue of GnRH, ([D-Lys^6]-GnRH), linked to doxorubicin.[10] Other examples of molecules linked to GnRH for targeted delivery include daunorubicin[11], curcumin[12] and docetaxel[13]. Importantly, AN-152 has been evaluated in Phase I and Phase II clinical studies in GnRH-R positive cancer patients demonstrating anticancer activity with only moderate side effects.[14]

Gemcitabine(2', 2'- difluorodeoxycytidine, dFdC), is an established and highly potent cytotoxic drug with a broad spectrum of cancer targets including colon, lung,

pancreatic, breast, bladder and ovarian cancer.[56] Upon administration, gemcitabine is transported into cells by nucleoside transporters.[57] Gemcitabine is then phosphorylated by cytidine kinase to gemcitabine monophosphate (dFdCMP) which is subsequently phosphorylated to gemcitabine diphosphate (dFdCDP) and gemcitabine triphosphate (dFdCTP). Gemcitabine exerts its cytotoxic action mainly through the incorporation of dFdCTP into the DNA strand leading to inhibition of DNA synthesis and subsequent cell apoptosis. dFdCDP also has an indirect cytotoxic effect by inhibiting ribonucleotide reductase. A major impediment related to gemcitabine efficacy is its rapid inactivation, since upon administration more than 90% of gemcitabine is converted to its inactive metabolite, 2, 2'- difluorodeoxyuridine(dFdU) and its monophosphate derivative (dFdUMP);[47, 48] another important drawback regarding gemcitabine therapy is that after initial tumour regression, tumours develop different forms of drug resistance. The most common form of gemcitabine induced resistance is the one related to nucleoside transporter deficiency.[48, 49] Previous *in vitro* studies demonstrated that gemcitabine has exceptional antiproliferative effects in androgen-independent CaP cell lines[61] but modest clinical benefit when tested as monotherapy or combination therapy, mainly due to its severe peripheral side effects.[62–64]

Many efforts aiming to enhance the therapeutic status of gemcitabine by chemical modifications have been reported.[60] These modifications have been focused on either improving gemcitabine's pharmacokinetics or reducing resistance induction. In this study, the design of GnRH-gemcitabine conjugates was based on improving the therapeutic potential of gemcitabine as follows:

1) Reduction of gemcitabine's metabolic inactivation. It has been shown that gemcitabine prodrugs can be designed specifically to affect its interaction with cytidine deaminase, the enzyme responsible for gemcitabine's poor pharmacokinetic properties.

2) Targeted delivery. Such a strategy would be advantageous since an effective drug (gemcitabine) would be delivered to the tumour site through conjugation to a peptide with a strong affinity for a cell surface receptor over-expressed in the tumour cell.

3) Reduction of induced resistance. The suggested conjugation potentially offers gemcitabine an alternative entrance route (GnRH-R) to the cell, possibly a crucial advantage for treating tumours that develop nucleoside transporter deficiency.

Herein, we achieved the synthesis of different Gemcitabine-GnRH conjugates via carbonate (ester) linkage. Carbonate functional group is widely used in the bio-conjugation

of drug-peptides both for targeted drug delivery as also for imaging purposes due to its susceptibility for chemical and enzymatic hydrolysis[30]. The carbonate bond can be synthesised from the reaction of the hydroxyl group of Gemcitabine (5'-OH and 3'-OH) with linker consisted of 1) Acid anhydride, 2) Acyl chloride and 3) Carboxylic acid. We have selected the carbonate formation at Gemcitabine hydroxyl with acid anhydrides with variable length of linkers. This study has been divided in two parts based on the length of linker (medium and long linkers)

2.2.2 $3G_1$, $3G_2$, GSG_1 and GSG_2 bearing medium linkers.

2.2.3 GSHG conjugate bearing a long linker.

Final bio-conjugates have been assigned according to the following criteria: the position and the type of linkers e.g. **GSG_1** stands for **G**emcitabine-**S**uccinic acid-**G**nRH (**1**: for primary hydroxyl and **2** for secondary hydroxyl).

2.2.2 $3G_1$, $3G_2$, GSG_1 and GSG_2 bearing medium linkers.

2.2.2.1 Design and synthesis of $3G_1$, $3G_2$, GSG_1 and GSG_2:

In our current research we are going to describe the chemical synthesis and biological evaluation of different analogues of Gemcitabine-GnRH conjugates. These conjugate analogues vary according to the site of carbonate (primary vs. secondary hydroxyl) and length of linker (four vs. five carbon atoms).

As shown in *Figure 6*, for the synthesis of Gemcitabine-GnRH conjugates we went through the following three steps:

a. Protection/deprotection of alcohol and amine
b. hemisuccinate or hemiglutarate coupling
c. Amide coupling with [D-Lys^6]-GnRH

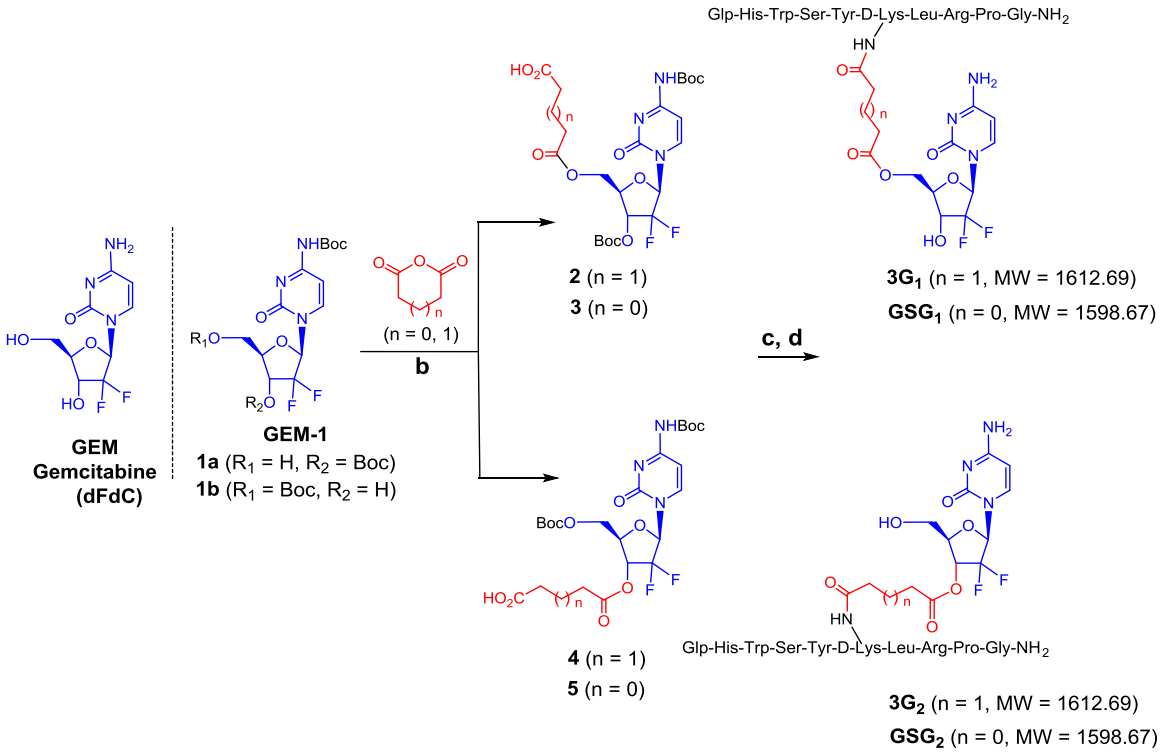

Figure 6: *Chemical synthesis of Gemcitabine-GnRH conjugates: Reagents and conditions: b) $NiPr_2Et$, ACN, rt; c) [D-Lys^6]-GnRH, DMF, HATU, $NiPr_2Et$, rt; d) TFA-H_2O-TIS (95:2.5:2.5), rt.*

a/d. Protection/deprotection of alcohol and amine: Selective Boc-protection of alcohols and amine (**1a** and **1b)** were done as same as reported by Zhi-wei Guo et.al.[41] Boc-deprotection was performed under one cleavage step using Trifluoroacetic acid (TFA): Triisopropylsilane (TIS): Water (H_2O) (95:2.5:2.5, v/v) for 4 h at room temperature. TIS is used as a cation scavenger (tert.butyl cation formed after deprotection must not interfere with the active sites (e.g. serine, tyrosine tryptophan side chain) present in the GnRH peptide.

b. Hemisuccinate or hemiglutarate coupling to gemcitabine: The optimal reaction conditions we found for the coupling of hemisuccinate or hemiglutrate to the 5'-OH group of gemcitabine were: GEM-1 (1 equiv.) and Succinic anhydride (2 equiv.) or Glutaric anhydride (8 equiv.), were dissolved in anhydrous acetonitrile under inert atmosphere, diisopropyl ethyl amine (DIPEA) (40 equiv.) was added and the reaction progress was monitored with TLC. After 4-12 h TLC shows almost consumption of GEM-

1, addition of water for the protonation and then purification was perform with HPLC to remove additional equivalents of glutaric or succinic acid.

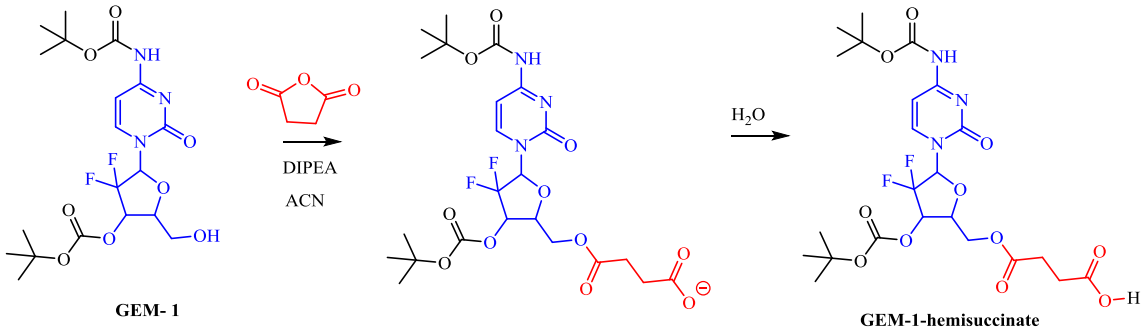

Figure 7: *Acylation of Gemcitabine with hemisuccinate or hemiglutarate.*

Type and molar ratio of the anhydrides: Interesting thing to note was for the completion of one mol of GEM-1 it was requested 2 moles of succinic anhydride and 8 moles of glutamic anhydride. This mapped differentiation is due to the different strain and stability of the five and six member ring of the different unhydrides. Since, the five memberring of succinic anhydride has a higher strain; it becomes unstable/ reactive and assists the reaction. Therefore, less succinic anhydride was required with respect to the glutaric anhydride. The purity of succinic and glutaric anhydride was confirmed with ^{1}H NMR. The methyle protons present different chemical shift in diacids (open ring) than in anhydrides.

Type and molar ratio of the base: There are many possible organic or inorganic bases which we could use for this reaction e.g. Diisopropyl ethyl amine (DIPEA / *NiPr₂Et*), Triethyl amine (TEA), Pyridine, Potassium carbonate (K_2CO_3), Sodium carbonate (Na_2CO_3) etc., Out of these DIPEA (40 equiv.) illustrated the best performance for this reaction.

Reaction solvents: Tetrahydrofuran (THF), dichloromethane (DCM) and 1,4-Dioxane, acetonitrile (ACN) and N, N-Dimethylformamide (DMF) etc. are the solvents generally being used for this reaction, but because of the insolubility of anhydride in other solvents we had two choices i.e. in ACN or DMF. Acetonitrile

was the best option due to its low boiling point and its miscibility in water allowing protonation at the end of the reaction by addition of water.

c. Amide coupling with [D-Lys^6]-GnRH: The coupling of GEM-1-hemisuccinate and the primary amine from the side chain of D-Lys amino acids (6th amino acid) from GnRH peptide was performed using 1-[Bis(dimethylamino)methylene]-1H-1,2,3-triazolo[4,5-b]pyridinium 3-oxid hexafluorophosphate (HATU) in the presence of organic base (DIPEA) in Dimethylformamide (DMF) as solvent. The reaction progress was monitored with TLC; For TLC, solvent system (mobile phase) used was the mixture of n-Butanol-water-Acetic acid (3:1:1, v/v). This is very convenient TLC mobile phase for most peptides. The [D-Lys^6]-GnRH peptide is UV light visible because of aromatic aminoacids (e.g. Tyrosine, Histidine, Tryptophan etc.) and the primary amine of D-Lys, is helpful to monitor the reaction with TLC after staining with Ninhydrine solution. On TLC [D-Lys^6]-GnRH shows a purple colour in ninhydrine.

To optimize this reaction, we have tried variable molar ratio of HATU with respect to the acid (Gem-1 hemisuccinate). Initially we used 1equiv. HATU, but in TLC we detected unreacted [D-Lys^6]-GnRH. To consume all [D-Lys^6]-GnRH and consequently to improve reaction yield, it was necessary to increase the HATU upto 1.5 equiv. and we obtained a ~30% yield after HPLC purification. Interestingly, we detected in the MS spectrum the expected mass and an additional product which illustrated a higher than the expected mass (M) by 99 amu (M + 99 m/z). This observation triggered us to explore this side product and this is presented in the chapter entitled ***"2.2.4 Guanidino side product in HATU/HBTUmediated liquid phase amide coupling reaction".***

Similarly, we have synthesized different analogues of Gemcitabine-GnRH conjugates; such as, GSG_1, GSG_2, $3G_1$, $3G_2$.

The details on the synthesis of different compounds are given below.

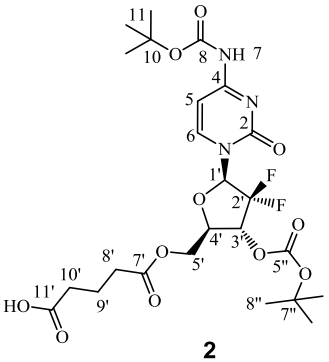

2

5′-*O*-Gemcitabine hemiglutarate 2: To a solution of protected gemcitabine **1a** (200 mg, 0.43 mmol) and glutaric anhydride (394 mg, 3.45 mmol) in 20 mL of ACN was added DIPEA (0.75 mL, 4.30 mmol). The reaction mixture was stirred at room temperature overnight and then treated with 10 mL of water. The resulting mixture was concentrated under reduced pressure to give the crude product which was purified by HPLC to give hemiglutarate **2** (170 mg, 68%) as a white solid.

^{1}H-NMR (500 MHz, DMSO-d_6, 25^{o}C): δ = 12.05 (s, 1 H), 10.62 (s, 1 H, 7-NH), 8.01 (d, J = 7.6 Hz, 1 H, 6-H), 7.14 (d, J = 7.6 Hz, 1 H, 5-H), 6.33 (t, J = 8.7 Hz, 1 H, 1'-H), 5.33 (m, 1 H, 3'-H), 4.49 (m, 1 H, 5'a-H), 4.48 (m, 1 H, 4'-H), 4.41 (m, 1 H, 5'b-H), 2.43 (t, J = 7.4 Hz, 2 H, 8'-H), 2.30 (t, J = 7.3 Hz, 2 H, 10'-H), 1.78 (m, 2 H, 9'-H), 1.50 (s, 9 H), 1.49 (s, 9 H) ppm. Mass: MS (ESI$^-$) *m/z* for $C_{24}H_{32}F_2N_3O_{11}$: calcd, 576.5; found, 576.1 [M-H].

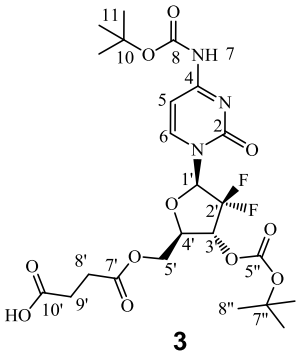

3

5′-*O*-Gemcitabine hemisuccinate 3: It was prepared from protected gemcitabine **1a** and succinic anhydride in a similar .way as compound **2**. It was isolated after HPLC purification as a white solid (190 mg, 78%).

^{1}H-NMR (500 MHz, DMSO-d_6, 25^{o}C): δ = 12.30 (s, 1 H), 10.60 (s, 1 H, 7-NH), 8.01 (d, J = 7.6 Hz, 1 H, 6-H), 7.15 (d, J = 7.6 Hz, 1 H, 5-H), 6.33 (t, J = 8.7 Hz, 1 H, 1'-H), 5.32 (m, 1 H, 3'-H), 4.51 (m, 1 H, 5'a-H), 4.48 (m, 1 H, 4'-H), 4.41 (m, 1 H, 5'b-H), 2.60 (t, 2 H, C8'-H), 2.54 (t, 2 H, C9'-H), 1.50 (s, 9 H), 1.49 (s, 9 H) ppm. Mass: MS (ESI$^-$) *m/z* for $C_{23}H_{30}F_2N_3O_{11}$: calcd, 562.5; found, 562.1 [M-H].

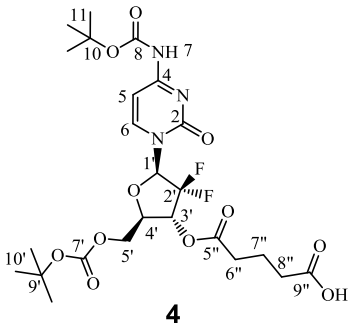

4

3′-*O*-Gemcitabine hemiglutarate 4: It was prepared from protected gemcitabine **1b** and glutaric anhydride in a similar .way as compound **2**. It was isolated after HPLC purification as a white solid (30 mg, 80%).

^{1}H-NMR (500 MHz, DMSO-d_6, 25^{o}C): δ = 12.0 (s, 1 H), 10.59 (s, 1 H, 7-NH), 8.04 (d, J = 7.7 Hz, 1 H, 6-H), 7.12 (d, J = 7.7 Hz, 1 H, 5-H), 6.33 (t, J = 8.4 Hz, 1 H, 1'-H), 5.44 (m, 1 H, 3'-H), 4.47 (m, 1 H, 4'-H), 4.45 (m, 1 H, 5'a-H), 4.39 (m, 1 H, 5'b-H), 2.54 (t, J = 7.4 Hz, 2 H, 6"-H), 2.32 (t, J = 7.3 Hz, 2 H, 8"-H), 1.81 (m, 2 H, 7"-H), 1.49 (s, 9 H), 1.45 (s, 9 H) ppm. Mass: MS (ESI$^-$) *m/z* for $C_{24}H_{32}F_2N_3O_{11}$: calcd, 576.5; found, 576.1 [M-H].

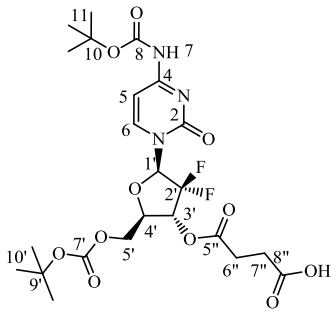

5

3′-*O*-Gemcitabine hemisuccinate 5: It was prepared from protected gemcitabine **1b** and succinic anhydride in a similar way as compound **2**. It was isolated after HPLC purification as a white solid (16 mg, 44%).

^{1}H-NMR (500 MHz, DMSO-d_6, 25ºC): δ = 12.29 (s, 1 H), 10.60 (s, 1 H, 7-NH), 8.05 (d, J = 7.6 Hz, 1 H, 6-H), 7.12 (d, J = 7.6 Hz, 1 H, 5-H), 6.34 (t, J = 8.5 Hz, 1 H, 1'-H), 5.46 (m, 1 H, 3'-H), 4.46 (m, 1 H, 4'-H), 4.42 (m, 1 H, 5'a-H), 4.37 (m, 1 H, 5'b-H), 2.70 (t, J = 6.3 Hz, 2 H, C6"-H), 2.57 (t, J = 6.4 Hz, C7"-H), 1.49 (s, 9 H), 1.46 (s, 9 H) ppm. Mass: MS (ESI$^-$) *m/z* for $C_{23}H_{30}F_2N_3O_{11}$: calcd, 562.5; found, 562.1 [M-H].

Conjugate 3G$_1$: To a solution of acid **2** (60 mg, 0.104 mmol), HATU (59.3 mg, 0.156 mmol) and DIPEA (90 μL, 0.52 mmol) in 15 mL of DMF, a solution of D-Lys^6-GnRH (130 mg, 0.104 mmol) in 5 mL of DMF was added drop wise. The reaction mixture was stirred at room temperature for 12 h and the solvent was removed under reduced pressure to give the crude Boc-protected conjugate which was then treated with 5 mL of a solution of TFA-H_2O-TIS (95:2.5:2.5). The resulting solution was stirred at room temperature for 30 min and then concentrated under reduced pressure to give the crude product which was purified by HPLC to give conjugate **3G$_1$** as a white solid (25 mg, 15%).

Mass: MS (ESI$^+$) *m/z* for $C_{73}H_{100}F_2N_{21}O_{19}$: calcd, 1613.7; found, 1613.5 [M+1], 807.6 [M+2]/2, 538.6 [M+3]/3.

Conjugate GSG$_1$: It was prepared in a similar way from acid **3** and was isolated after HPLC purification as a white solid (27 mg, 19%). Mass: MS (ESI$^+$) *m/z* for $C_{72}H_{98}F_2N_{21}O_{19}$: calcd, 1599.7; found, 1599.3 [M+1], 800.7 [M+2]/2, 534.1 [M+3]/3.

Conjugate 3G$_2$: It was prepared in a similar way from acid **4** and was isolated after HPLC purification as a white solid (31 mg, 16%). Mass: MS (ESI$^+$) *m/z* for $C_{73}H_{100}F_2N_{21}O_{19}$: calcd, 1613.7; found, 1613.4 [M+H], 807.5 [M+2]/2, 538.6 [M+3]/3.

Conjugate GSG$_2$: It was prepared in a similar way from acid **5** and was isolated after HPLC purificationas a white solid (4.5 mg, 13%). Mass: MS (ESI$^+$) *m/z* for $C_{72}H_{98}F_2N_{21}O_{19}$: calcd, 1599.7; found, 1599.4 [M+H], 800.2 [M+2]/2, 534.2 [M+3]/3.

2.2.2.2 Characterization of the GnRH-Gemcitbine conjugates by 2D NMR (TOCSY):

Nuclear Magnetic Resonance (NMR) based mapping of possible changes induced in the environment of [D-Lys^6]-GnRH upon gemcitabine conjugations. To assess the chemical perturbation induced in the environment of [D-Lys^6]-GnRH upon conjugation of the gemcitabine variants, NMR spectroscopy was used. All the NMR spectra were recorded on a Bruker AV-500 spectrometer (Bruker Corporation, Billerica, MA, USA) equipped with a cryoprobe. The NMR samples were prepared by dissolving the solid material in H_2O/D_2O (90:10) at a concentration of 5 mM. 2D ^{1}H-^{1}H TOCSY (Total Correlation Spectroscopy) l and 2D ^{1}H-^{1}H NOESY (Nuclear Overhauser Effect Spectroscopy) experiments were performed for [D-Lys^6]-GnRH, 3G$_1$ and GSG$_1$, at 298 K using standard Bruker pulse sequences. For water suppression excitation, sculpting with gradients was used. The mixing time for TOCSY spectra was 80 ms. Mixing time. for NOESY experiments were set to 100, 200, 350 and 400 ms to determine NOE build-up rates. A mixing time of 350 ms provided sufficient cross-peak intensity without introducing spin-diffusion effects in the 2D – NOESY

Conjugation of gemcitabine to [D-Lys^6]-GnRH does not alter drastically the conjugate's GnRH-R binding domains. GnRH-gemcitabine conjugates were evaluated by NMR. The described study allowed the assessment of potential conservation of microenvironments responsible for binding to the GnRH-R (*Figure 8B*). NMR studies

using 2D NMR TOCSY experimentation indicate that conjugation of gemcitabine to the bioactive peptide does not perturb the chemical environment known to be important for receptor binding. The part of the **GnRH** peptide which is important for the receptor binding is aminoacids 1-3 and 8-10. The conjugation of the drug (gemcitabine) on the backbone of lysine 6 perturbed only the chemical environment (chemical shift) of the neighboring aminoacids Leu-7 and Tyr-5 (*Figure 8A*), however the structure (N-terminus or C-terminus) of the peptide sequence which is functionally important for receptor binding[5, 27, 28] was not affected.

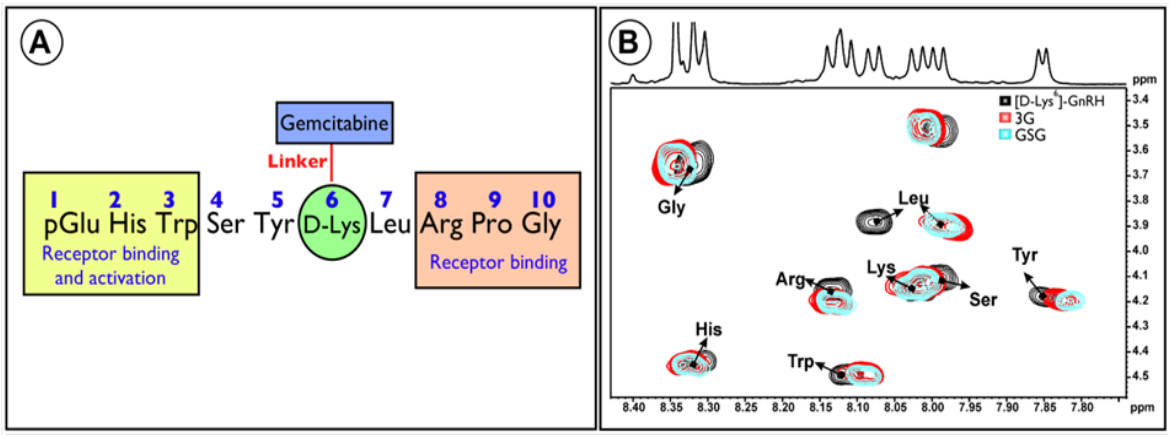

Figure 8: *Evaluation of the binding potential of representative GnRH-gemcitabine conjugates against the GnRH-R using 2D NMR.* ***A)*** *Schematic representation of a GnRH-gemcitabine conjugate indicating the residues that are responsible for binding to the GnRH-R.* ***B)*** *Superimposition of the selected region NH- of 2D NMR TOCSY spectrum of [D-Lys^6]-GnRH (black) with 3G$_1$ (red) and GSG$_1$ (blue). The conjugated molecules, GSG$_1$ and 3G$_1$ do not perturb the structure of the [D-Lys^6]-GnRH region that is important for binding to the GnRH-R.*

2.2.2.3 Biological evaluation of the GnRH-gemcitbine conjugates:

The biological evaluation of the synthesized GnRH-Gemcitbine conjugateswas conducted in collaboration with the groups of Dr. Constantin Tamvakopoulos (Bioacademy of Athens) and Prof. George Liapakis (Department of Pharmacology, University of Crete).

Binding affinity (IC$_{50}$) of GnRH-gemcitabine conjugates:

The binding affinity (IC_{50}) of GnRH-gemcitabine conjugates ($3G_1$, GSG_1, $3G_2$, GSG_2) on the GnRH-R was evaluated in comparison to the binding affinity of the known GnRH-R superagonist leuprolide as well as the binding affinity of ([D-Lys^6]-GnRH). Competition binding isotherms of GnRH analogues to human GnRH – I receptor are also shown. Competition of [^{125}I-D-Tyr^6, His^5] GnRH specific binding by increasing concentrations of the analogues was performed on membranes from HEK 293 cells stably expressing the human GnRH – I receptor. The mean values and S.E. are shown from 3 – 4 different experiments. The data were fit to a one – site competition model by nonlinear regression and the IC_{50} values were determined as described.

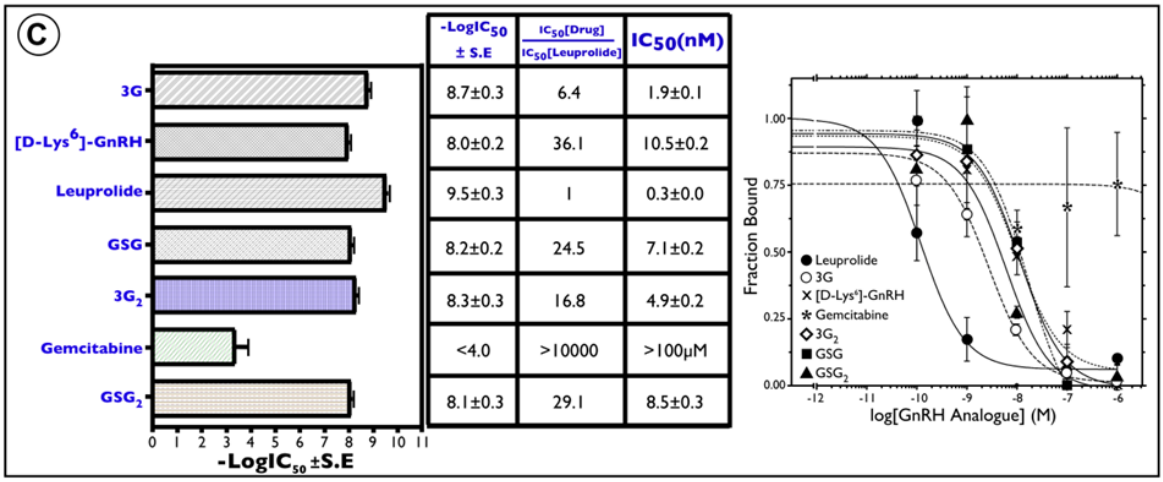

Figure 9: *Evaluation of the binding potential of representative GnRH-gemcitabine conjugates against the GnRH-R using radioligand binding assays.*

GnRH-gemcitabine conjugates exhibit antiproliferative potential in vitro:

The antiproliferative effect of the GnRH-gemcitabine conjugates was evaluated in two androgen-independent CaP cell lines (DU145 and PC3) with gemcitabine and [D-Lys^6]-GnRH as points of reference (results shown in *Table 2*). GSG_1 and GSG_2 had the highest potencies which were comparable with that of gemcitabine in the examined cell lines (Average IC_{50} values for GSG_1 and GSG_2 of 308 and 439 nM respectively versus 231 nM for gemcitabine). $3G_2$ was also potent with an average IC_{50} value of 663 nM. Following stability studies in cell culture medium, GSG_1 and $3G_2$ were selected for further evaluation in pharmacokinetic experiments based on the criteria of: i) sufficient stability in cell culture medium (approximately 40% of drug conjugate remaining intact following 8 h incubation) and ii) *in vitro* antiproliferative effects.

Table 2: *Antiproliferative effect of GnRH-gemcitabine conjugates in androgen-independent cell lines (PC3, DU145).*

IC_{50} (nM)	**Gemcitabine**	**$3G_1$**	**$3G_2$**	**GSG_1**	**GSG_2**
DU145	231 ± 34	1171 ± 83	663 ± 273	308 ± 170	439 ± 217
PC3	585 ± 68	1161 ± 130	729 ± 193	670 ± 352	786 ± 125

Cells were plated in 96-well plates (5,000 cells/well) and incubated for 72 h with either GnRH-gemcitabine conjugates or gemcitabine at selected concentrations. IC_{50} values shown represent means of three experiments performed in triplicates ± SD. [D -Lys^6]-GnRH treatment had no effect in the selected concentrations.

Pharmacokinetics:

GSG_1 provides enhanced systemic exposure of gemcitabine following administration in mice. Administration of GSG_1 in mice led to blood gemcitabine concentrations averaging 500 ng/mL (1.7 μM) at 1 h following dosing. Importantly, levels of gemcitabine were sustainable for at least 2 h after dosing of GSG_1 (average concentration: 85 ng/mL or 0.3 μM). In comparison, following equimolar dosing of gemcitabine in mice, gemcitabine was rapidly absorbed reaching highest blood concentrations averaging 685 ng/mL (2.3 μM) at 0.5 h following dosing. Levels of gemcitabine dropped significantly 2 h after dosing (average concentration: 15 ng/mL or 0.05 μM). In *Figure 10A*, comparative curves of gemcitabine levels are depicted, following dosing in mice of GSG_1, $3G_2$ or gemcitabine. Administration of GSG_1 also resulted in significantly lower levels of dFdU in blood (*Figure 10B*) in comparison to gemcitabine treatment in which rapid conversion to dFdU was observed. The findings from the pharmacokinetic experiments suggest that administration of GSG_1 can lead to appreciable gemcitabine formation and blood exposure ($AUC_{15\text{-}480min}$: 4.3 x 10^4 min x ng/mL for GSG_1 versus $AUC_{15\text{-}480min}$: 2.9 x 10^4 min x ng/mL for gemcitabine) and a lower rate of formation of the inactive metabolite dFdU ($AUC_{15\text{-}480min}$: 1.8 x 10^6 min x area for GSG_1 versus $AUC_{15\text{-}480min}$: 4.5 x 10^6 min x area for gemcitabine). Based on the described pharmacokinetic advantages, GSG_1 was selected as the lead candidate compound among the GnRH-gemcitabine conjugates for efficacy studies in mice.

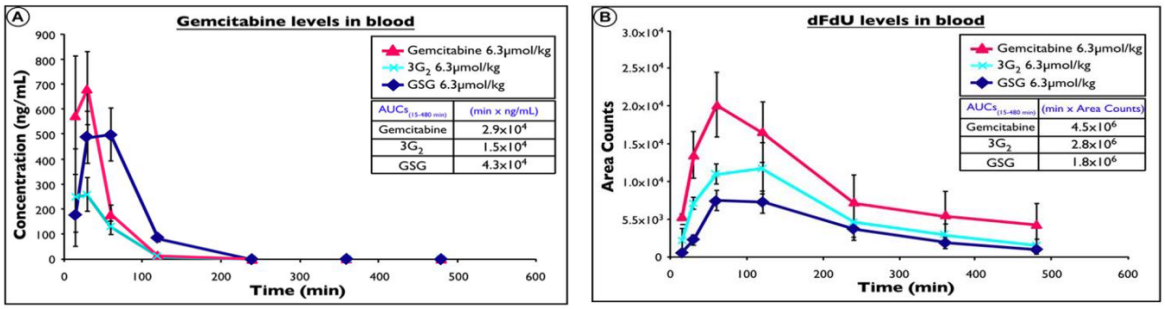

Figure 10: *Pharmacokinetic evaluation of GnRH-gemcitabine conjugates versus gemcitabine.*

Male C57BL/6N mice (n = 5) were dosed (IP) with either gemcitabine, GSG_1, or $3G_2$ at a dose of 6.3 µmol/kg and blood samples were collected at selected time points. Gemcitabine and dFdU were monitored by LC-MS/MS. The areas under the curve (AUCs) for each treatment were calculated as a measure of gemcitabine or dFdU exposure over time.

Efficacy studies in mice:

GSG_1 **biodistribution in xenografted mice:** Administration of GSG_1 in tumour bearing NOD-SCID mice led to the following important findings: GSG_1 has tumour bioavailability as it can be delivered at the tumour site at appreciable levels (average GSG_1 concentration of 184 ng/g or 115 nM at 1 h) even at a lower dose (6.3 µmol/kg) in comparison to the efficacious dose (18.8 µmol/kg, see efficacy section). Blood level measurements of gemcitabine and dFdU indicated that the inactivation of gemcitabine (formation of dFdU) after GSG_1 administration was less extensive when compared to gemcitabine administration (*Table 3*) a finding that was consistent with pharmacokinetic experiments in naïve mice. Although this significant pharmacokinetic advantage was not as pronounced at the tumour site, a slight increase of the $AUC_{(0\text{-}24\ h)}$ Gemcitabine:dFdU ratio was observed with GSG_1 dosing in comparison to gemcitabine (0.016 vs. 0.013).

Table 3: *Bioavailability of gemcitabine, dFdU in blood and tumours*

Gemcitabine:dFdU $AUC_{(0\text{-}24\ h)}$	Gemcitabine Administration	GSG_1 Administration
Blood	0.023	0.202
Tumour	0.013	0.016

Cell uptake:

GSG_1 enters the cell and affords sustained gemcitabine levels. The expression of GnRH-R levels was confirmed in the tested CaP cell lines by Western Blot analysis (*Figure 11A*). The cell uptake of GSG_1 in DU145 cells and the intracellular release of gemcitabine were evaluated in comparison to gemcitabine. Following incubation of cells with gemcitabine, was rapidly inactivated forming dFdU. Incubation of GSG_1 with cells led to a relatively slow formation of gemcitabine and what appeared to be sustained levels of gemcitabine over time (up to 8 h). In contrast, incubation of gemcitabine with cells, led to higher dFdU levels in comparison to dFdU formed upon incubation of GSG_1, further supporting our hypothesis that GSG_1's efficacy could be partially based on a mechanism of action associated with a "slow down" of gemcitabine's inactivation. The ratio of the intracellular levels of gemcitabine over dFdU as a function of time is depicted in *Figure 11B*. Moreover, pre-incubation of DU145 cells for 1 h with 1 μM [D-Lys^6]-GnRH affected the kinetics of GSG_1 (10 μM) uptake. An approximate 40% reduction in intra-cellular concentrations of GSG_1 was measured in the pre-treated cells (data not shown), an observation that supports the hypothesis of selective GSG_1 entrance to the cell through the GnRH-R.

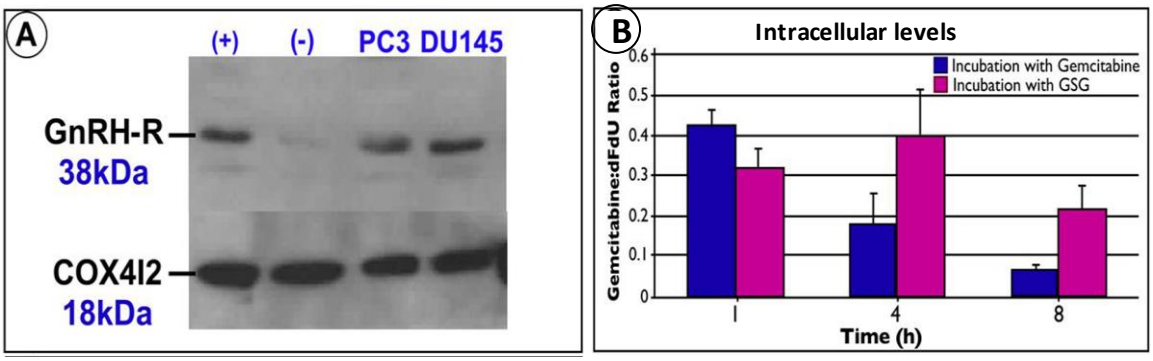

Figure 11: *Cell culture GnRH-R expression and cell uptake of a GnRH-gemcitabine conjugate*

A) *GnRH-R expression in the two androgen-independent cell lines used (DU145, PC3) for the evaluation of the antiproliferative effects of the GnRH-gemcitabine conjugates. MCF-7 and RAW264.7 cells were used as positive (+) and negative (-) controls respectively. Expression of the GnRH-R in androgen-independent cell lines was confirmed by Western blot analysis as a band at 38 kDa.* ***B)*** *GSG_1 vs. gemcitabine cell uptake in DU145 cells. Cells were incubated with 10 μM GSG_1 or gemcitabine for selected time points (1 h, 4 h,*

and 8 h) and were then lysed in order to determine intracellular levels of gemcitabine and its inactive metabolite (dFdU) by LC-MS/MS. Experiments were performed in triplicates.

GSG_1 inhibits tumour growth:

The efficacy of GSG_1 was tested on a GnRH-R positive prostate cancer animal model using the DU145 CaP cell line. Efficacy was compared to equimolar dose of gemcitabine or the peptide used for targeting the GnRH-R ([D-Lys^6]-GnRH). Pharmacokinetic studies of GSG_1 at 6.3 μmol/kg, demonstrated that average circulating levels of gemcitabine could reach 85 ng/mL (or 323 nM) at 2 h post-dose (see *Figure 10*). Evaluation on antiproliferative *in vitro* effects of gemcitabine in cell lines indicated that the IC_{50} of gemcitabine was approximately 230 nM (see *Table 2*). Based on the above observations, in order to ensure an efficacious dose, the dose chosen for efficacy studies of GSG_1 was 18.8 μmol/kg. A clear inhibitory effect of GSG_1 on tumour growth was observed when compared to the control group (vehicle) or equimolar doses of gemcitabine or [D-Lys^6]-GnRH. Average tumour volume of GSG_1 treated group at day 18 was 506 $mm^3 \pm 152$, significantly lower ($P<0.001$) when compared to vehicle (1266 $mm^3 \pm 421$), low dose gemcitabine (1110 $mm^3 \pm 270$) or [D-Lys^6]-GnRH (1030 $mm^3 \pm 290$) treatments (*Figure 12A*). Efficacy was achieved also with a high dose of gemcitabine of 454.5 μmol/kg or 120 mg/kg (tumour volume at day 18 of 482 $mm^3 \pm 198$). Mice treated with GSG_1 or high dose gemcitabine showed significant ($P<0.001$) tumour inhibition when compared to vehicle, low dose gemcitabine or [D-Lys^6]-GnRH treatments, measured as area under the tumour volume – time curve (AUC) until day 18 (*Figure 12B*). No morbidity or significant changes in body weight were observed in the animals during the course of the experiment, suggesting that all the treatments were well tolerated.

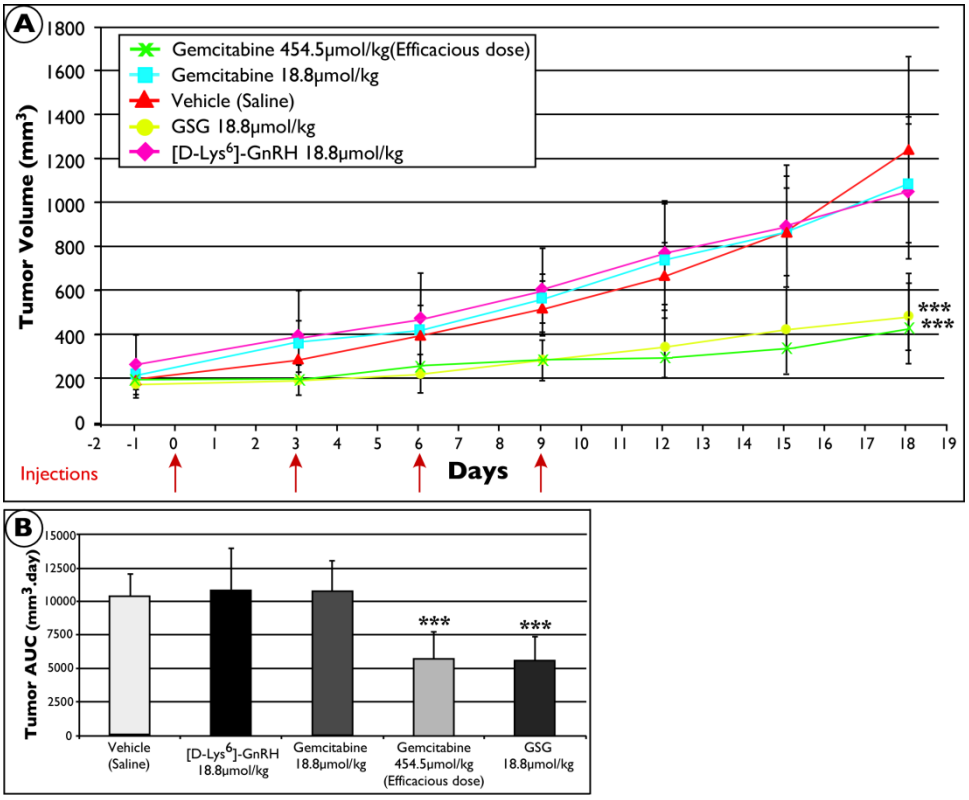

Figure 12: *Therapeutic efficacy of GSG in NOD/SCID mice xenografted with DU145 cells*

A) *Tumour growth inhibition. Mice were dosed (IP) with GSG, [D-Lys^6]-GnRH, gemcitabine (low and high dose) or vehicle (saline). Red arrows indicate the day of dosing. Each point represents mean of at least 8 tumour volumes resulting from at least 5 mice ± SD. ***, P<0.001 vs. controls.*

B) *AUC (mm$^{3.}$ day) calculated for each treatment group from the tumour volumes of mice.*

2.2.3 GSHG conjugate bearing a long linker

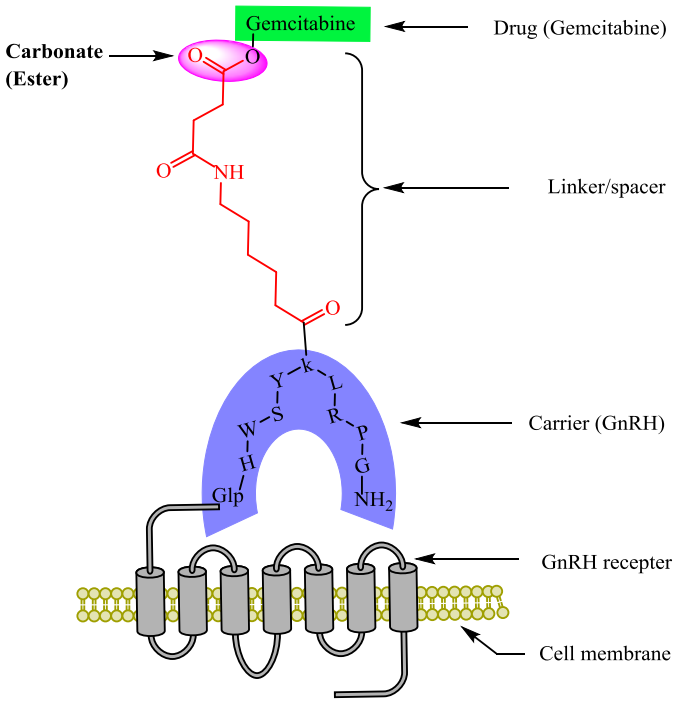

General concept of long linker (GSHG) conjugate via carbonate.

2.2.3.1 Introduction:

In our former studies we have reported the conjugation of Gemcitabine and peptide GnRH via hemiglutarate and hemisuccinate linkers. These studies highlighted the dominant role that the linker adopted towards the compounds bioactivity profile. On these lines and aiming to enhance the therapeutic potency of these compounds we further exploited new GnRH-Gemcitabine conjugates either bearing a long linker connecting the two parent compounds or very short traceless cleavable carbamate linkers (see section *"2.4.2 Carbamate bond formation at Gemcitabine's hydroxyl (3'-OH or 5'-OH) groups using Bis(4-nitrophenyl)carbonate (BNPC)).* The relevant biocompounds were explored on their cytotoxicity in different cancer cell lines equipped with the GnRH-R, metabolic stability, as also the formation of inactive metabolite of gemcitabine (dFdU).

2.2.3.2 Design, synthesis and characterization:

Gemcitabine was coupled to the GnRH peptide via a long linker to result to the GSHG conjugate. Amine of ε-amino caproic acid was Boc-protected [65] and the free carboxylic acid was coupled with the ε-amino group of the Lys^6 of the [D-Lys^6]-GnRH by 1-[Bis(dimethylamino)methylene]-1H-1,2,3-triazolo[4,5-b]pyridinium 3-oxid hexafluorophosphate (HATU). In a subsequent step Boc protection was removed and the resulted free amine ε-amino caproic acid linker was coupled with the carboxylic acid of the hemiglutarate conjugate with gemcitabine (compound **4**, which was synthesized according to previously reported synthetic scheme[66]) using HATU to result to GSHG.

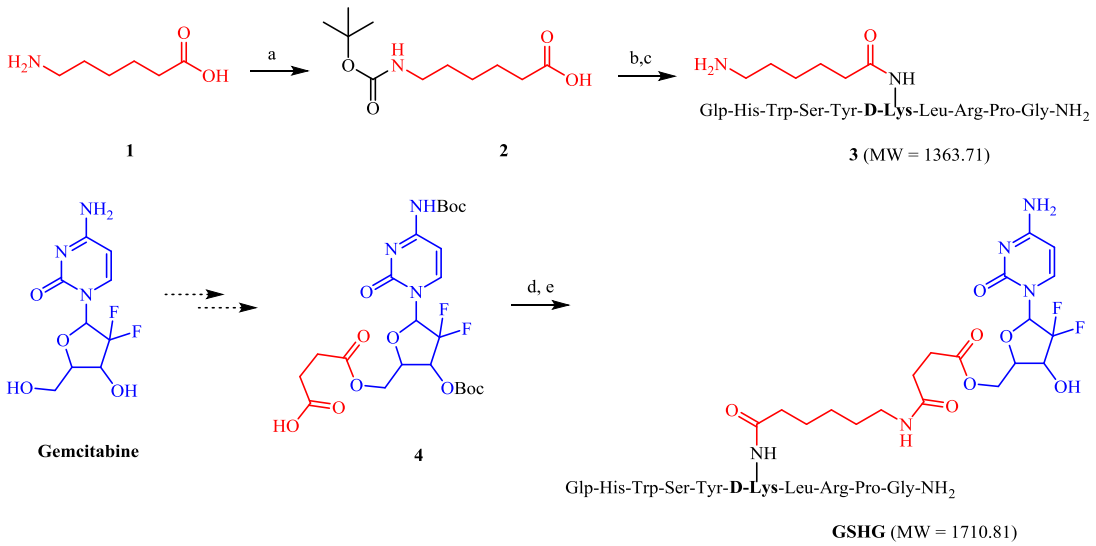

Figure 13: *Synthesis of the long linker ester based GnRH-Gemcitabine conjugate. a) Boc-protection: Boc_2O, NaOH, Dioxane: water, rt; b) [D-Lys^6]-GnRH, HATU, N,N´-Diisopropylethylamine (DIPEA), DMF, rt; c) TFA/H_2O/TIS (9.5/0.25/0.25, v/v), rt; d) 3, HATU, DIPEA, DMF, rt; e) TFA/ H_2O/ TIS (9.5/0.25/0.25, v/v), rt.*

Synthetic part:

Synthesis of 6-N-(tert-Butyloxycarbonyl)aminocaproic Acid 2: To the solution of **1** (100 mg, 131.17 mmol) in 10 mL Dioxane/H_2O (2/1, v/v), 1M aq. NaOH (0.762 mL, 131.17 mmol) was added drop wise, at ice cooling (0^0C). After 5 min Boc_2O was added and the reaction was continued 0^0C-rt for 3 h. Reaction progress was monitored with TLC (5% methanol in CH_2Cl_2). Solvent was evaporated with rotary evaporator; the aqueous reaction mixture was extracted with ethyl acetate (5 mL X 2). The aqueous phase was acidified (pH ~ 1) with 1M aq. HCl and extracted with ethyl acetate (10 mL X 3). The combined organic phases was washed with brine, dried over sodium sulfate, the solvent was concentrated and dried well to give compound **2** (170 mg, 96.47%) as a colourless liquid.

^{1}H-NMR (400 MHz, DMSO-d_6, 25^{o}C): δ = 12.01 (bs, 1 H), 6.78 (t, J = 5.06 Hz, 1 H), 2.91 (q, J = 6.66, 6.26 Hz, 2 H), 2.21 (t, J = 7.33 Hz, 2 H), 1.54 - 1.47 (m, 2 H), 1.43 - 1.35 (m, 2 H), 1.40 (s, 9 H), 1.30 - 1.22 (m, 2 H) ppm; ^{13}C-NMR (400 MHz, DMSO-d_6, 25^{o}C): δ = 175.39 (C), 156.53 (C), 78.26 (C), 40.65 (CH_2), 34.57 (CH_2), 30.15 (CH_2), 29.21 (CH_3),

26.78 (CH_2), 25.15 (CH_2) ppm; Mass:ESI-MS (*m/z)* for $C_{11}H_{21}NO_4$: calcd, 231.15; found, 254.55 $[M+Na]^+$.

Synthesis of 3: To the solution of **2** (2.58 mg, 0.011 mmol) and HATU (6.37 mg, 0.016 mmol) in 3 mL of DMF, DIPEA (9.7 µL, 0.055 mmol) was added drop wise under inert atmosphere. After 5 min, a solution of [D-Lys^6]-GnRH (14 mg, 0.011 mmol) in 2 mL DMF was added drop wise in the reaction and the reaction was continued for 12 h at rt. TLC in n-butanol/ Acetic acid/ water (6/2/2, v/v) illustrated complete consumption of both **2** and [D-Lys^6]-GnRH and formation of a new spot. DMF was removed under reduced pressure and the residue was washed with acetonitrile (1 mL X 3) to give 16 mg white solid compound. The crude compound was used for the next Boc-deprotection reaction without further purification.

Boc-deprotection was perform with 2 mL mixture of TFA/TIS/ H_2O (9.5/0.25/0.25, v/v) at 0^0C to rt for 1 h. Solvent was removed under reduced pressure and the residue was washed with cold diethyl ether (2 mL X 3) to result to a solid compound which was dried under high vacuum to give compound **3** (14 mg, 91.92%) as a white solid.
Mass: ESI-MS (*m/z*): $[M+H]^+$ for $C_{65}H_{95}N_{19}O_{14}$: calcd, 1365.73; found 1368.22, $[M+2H]^{2+}$ calcd, 683.86; found, 684.71.

5′-*O*-Gemcitabine hemisuccinate 4: To a solution of Boc-4NH-boc-3'-O-Gemcitabine (200 mg, 0.43 mmol) and succinic anhydride (108 mg, 1.08 mmol) in 20 mL of ACN was added DIPEA (0.75 mL, 4.30 mmol) drop wise. The reaction mixture was stirred at rt for 12 h and then treated with 10 mL of water. The resulting mixture was then concentrated under reduced pressure to give the crude product which was purified by HPLC (60/40% H_2O.TFA/ACN.TFA to 100% ACN.TFA for 30 min, at λ= 254 nm wavelength.) to give **4** (190 mg, 78%) as a white solid.

^{1}H-NMR (400 MHz, DMSO-d_6, 25^{o}C): δ = 12.31 (s, 1 H), 10.61 (s, 1 H), 8.01 (d, J = 7.6 Hz, 1 H), 7.15 (d, J = 7.6 Hz, 1 H), 6.33 (t, J = 8.7 Hz, 1 H), 5.33 (m, 1 H), 4.51 (m, 1 H), 4.48 (m, 1 H), 4.41 (m, 1 H), 2.6 (t, 2 H), 2.54 (t, 2 H), 1.50 (s, 9 H), 1.49 (s, 9 H) ppm. ^{13}C-NMR (400 MHz, DMSO-d_6, 25^{o}C): δ = 174.27 (C), 172.84 (C), 164.67 (C), 154.72

(C), 152.84 (C), 152.02 (C), 146.18 (C), 122.13 (CF_2), 96.32 (CH), 85.60 (CH), 84.81 (C), 82.32 (C), 76.91 (CH), 73.88 (CH), 63.24 (CH_2), 29.51 (CH_2), 28.66 (CH_3), 28.05 (CH_3) ppm. Mass: ESI-MS (*m/z)* for $C_{23}H_{30}F_2N_3O_{11}$: calcd, 562.2; found, 562.1 $[M\text{-}H^+]^-$.

Synthesis of GSHG: To the solution of **4** (6.6 mg, 0.011 mmol) and HATU (6.7 mg, 0.017 mmol) in 3 mL of DMF, DIPEA (10.2 μL, 0.058 mmol) was added drop wise under inert atmosphere. After 5 min a solution of **3** (16 mg, 0.011 mmol) in 2 mL DMF was added drop wise and the reaction was continued for 12 h at rt. TLC in n-butanol/ Acetic acid/ water (6/2/2, v/v) presented complete consumption of both **3** and **4** and formation of a new spot. DMF was removed under reduced pressure; the residue was washed with acetonitrile (1 mL X 3) to give 11 mg of white solid compound. The crude compound was used for the next Boc-deprotection reaction without further purification.

Boc-deprotection was performed with 2 mL mixture of TFA/TIS/ H_2O (9.5/0.25/0.25, v/v) at 0^0C to rt for 1 h. Solvent was removed under reduced pressure and the residue was washed with cold diethyl ether (2 mL X 3) to obtained white solid compound. After HPLC (90/10% H_2O.TFA/ACN.TFA to 70% H_2O.TFA for 30 min, at 254λ wavelength) purification **GSHG** (5 mg, 24.91%) was obtained as a white solid compound.
Mass: ESI-MS (*m/z*): $[M+2H]^{2+}$ for $C_{78}H_{108}F_2N_{22}O_{20}$: calcd, 856.4; found 856.3, $[M+3H]^{3+}$ calcd, 571.0; found, 571.3.

2.2.3.3 Biological evaluation:

Note: *Biological evaluation of GSHG was explained (In section "2.4.2 Carbamate bond formation at Gemcitabine's hydroxyl (3'-OH or 5'-OH) groups using Bis(4-nitrophenyl)carbonate (BNPC)) with $2G_1$ and $2G_2$ short and traceless linkers, for better understanding and comparitive study of Short and Long linkers in biconjugation.*

2.2.4 Guanidino side product in HATU/HBTU mediated liquid phase amide coupling reaction.

To be submitted:

Paper: Nisar Sayyad et. al. Challenging the Selectivity of Guanidinium Peptide Coupling Reagents: Orthogonal Coupling Problems and Solutions, Amino acids.

Among many coupling reagents for peptide synthesis in solid and solution phase, the guanidinium salts HXTU are the most usually utilized: the N-[(dimethylamino)-1H-1,2,3-triazo[4,5-b]pyridin-1-ylmethylene]-N-methylmethanaminium hexafluorophosphate N-oxide, HATU (**1**)**,** and the N-[(1H-benzotriazol-1-yl)(dimethylamino)methylene]-N-methylmethanaminium hexafluorophosphateN-oxide, HBTU (**2**)[67]**.**

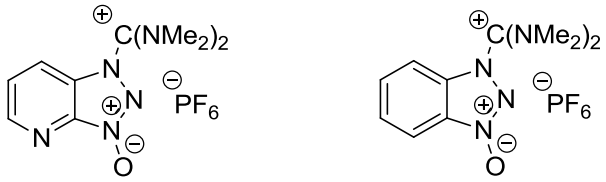

Figure 14: *Guanidinium salts of HATU and HBTU coupling reagents*

Since its innovation,[68] HATU has been established as a very famous coupling reagent since it does not result in formation of side products. However, it has been reported[69] that during the peptide coupling reaction by the use of uronium coupling reagents, formation of a guanidine side product on the N-terminus amine group could be observed.

During the liquid phase synthesis of the GnRH-gemcitabine conjugate presented in ***Chapter 1.2.1*** through the coupling of the Boc-protected Gemcitabine hemiglutarate (**3**) and the ε-amino group of Lys derived from the [D-Lys]^6-GnRH (**4**), using HATU as the

coupling reagent, we recorded in the ESI-MS spectra, in addition to the desired compound, the formation of a side product. This side product presented an increased mass by +99 m/z with respect to the mass of the desired compound.

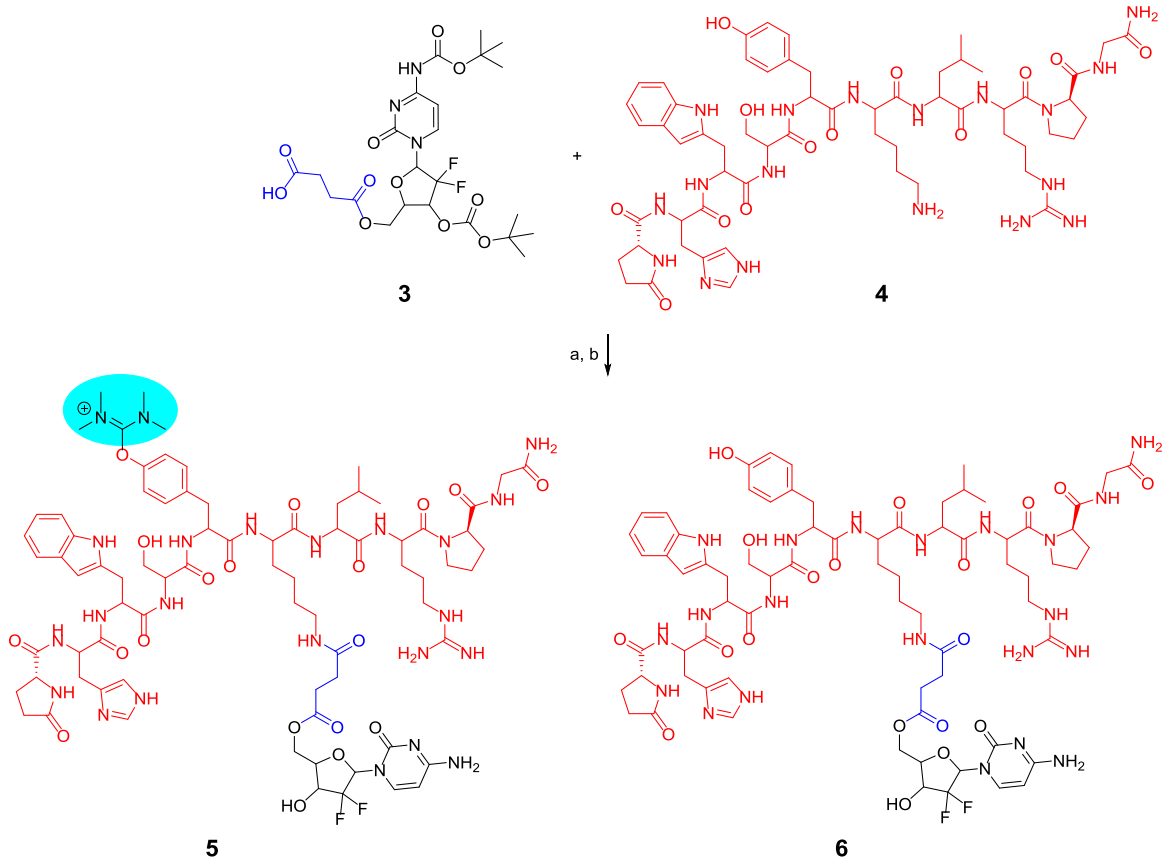

Figure 15: *Synthesis of Gemcitabine-GnRH conjugate: (a) HATU (1.5 equiv.), DIPEA, DMF (b) TFA/TIS/H2O (95/2.5/2.5%).*

After challenging different hypotheses we suggested that the side product could be a guanidine side product since it corresponded to the mass of the relevant group and could originate from the used coupling reagent HATU. Indeed, it had been reported that the amine group of the *N*-terminal amino acid, during solid phase peptide synthesis, could form a guanidino derivative by the use of HATU that could interrupt the peptide bond formation.[70] In our case, since we lacked an N-terminal amine and since we got the expected coupled product plus the mass of the guanidine group, it was suggested that the guanidino formation occurred at a different site to the relevant one that was reported in the literature since the peptide bond formation was not interrupted.

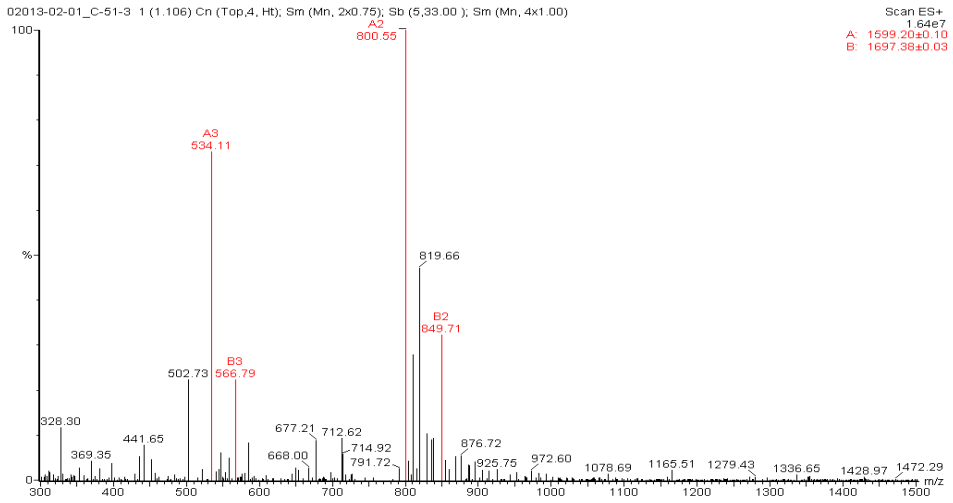

Figure 16: *ESI-MS spectra of compound **5** and **6**. The molecular ions of compound **5** [M + 2H]$^{2+}$ = 849.71 and [M + 3H]$^{3+}$ = 566.79. The molecular ions of compound **6**[M + 2H]$^{2+}$ = 800.55 and [M + 3H]$^{3+}$ = 534.11.*

In order to confirm the potential of a HATU mediated orthogonal coupling of the guanidino group to the side chain of any amino acid present in the sequence of the GnRH peptide, we designed a template reaction (*Figure 17)* between different amino acid methyl esters carrying unprotected side-chains (**8**), where both the N-terminus amine and side chain reactive groups are present (mimic the GnRH peptide) and Fmoc-Ser(*t*Bu)-OH (**7**), that has a free carboxylic acid for peptide bond formation, using the same reaction conditions, as in *Figure 15*.

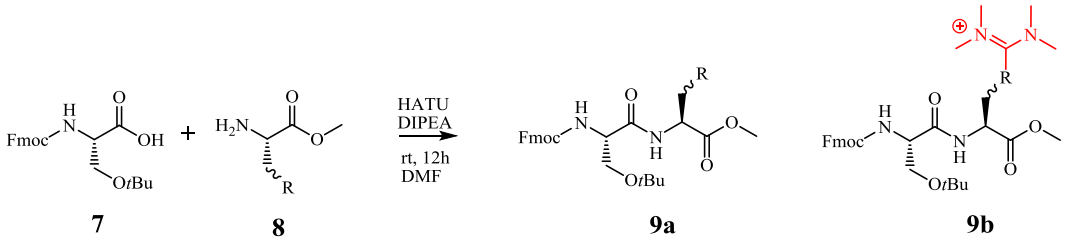

Figure 17: *General amide coupling of **7** and **8** with HATU (1.5 equiv.), DIPEA (5 equiv.), DMF.*

The reaction was performed according to the classical method of peptide bond formation; i.e. activation of acid (**7)** with HATU and DIPEA for 5 min [71] prior to the addition of nucleophile (**8)**. Interestingly, we observed that when Fmoc-Ser(*t*Bu)-OH (**7**) was treated with 1.5 equivalent of HATU, DIPEA (5 equiv) and Tyr/Lys in DMF, the formation of

guanidino side product was detected by mass spectroscopy, where as with the other amino acids this side product was not observed (*Table 4*).

Table 4: *Coupling of* Fmoc-Ser(*t*Bu)-OH *with different amino acids using HATU.*

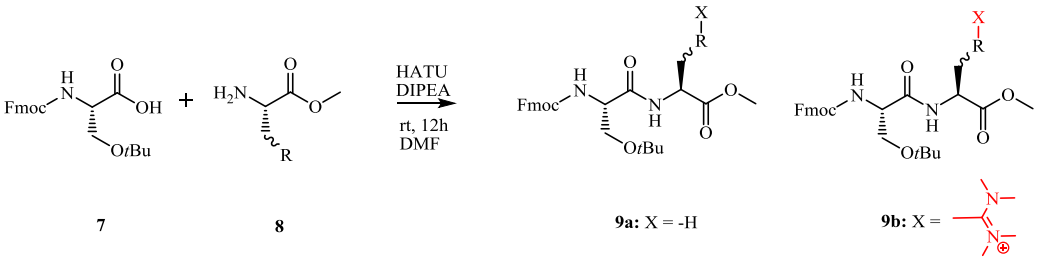

Sr.no.	R	HATU (equivalents)	X (monitored with mass)	
			a	**b**
i	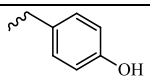 **10**	1.5	✓	✓
		1.0	✓	×
ii	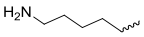 **11**	1.5	×	✓
		1.0	✓	✓
iii	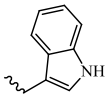 **12**	1.5	✓	×
		1.0	✓	×
iv	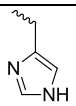 **13**	1.5	✓	×
		1.0	✓	×
v	 **14**	1.5	✓	×
		1.0	✓	×
vi	 **15**	1.5	✓	×
		1.0	✓	×
vii	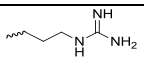 **16**	1.5	✓	×
		1.0	✓	×

The possibility of having the HATU mediated activated ester of Fmoc-Ser(*t*Bu)-OH to react with the hydroxyl group of Tyr (to obtain an ester linkage) is ruled out by the recorded MS spectra of the resulted products. As it is shown in *Figure 18*, compound **19** that bears an ester linkage between Fmoc-Ser(*t*Bu)-OH and Tyr has a mass of 658.78 but we recorded a 660.14 m/z which refers to compound **18**. This concludes that the guanidine side product formation occurs without interrupting peptide bond formation and takes place in the side chain of Tyrosine.

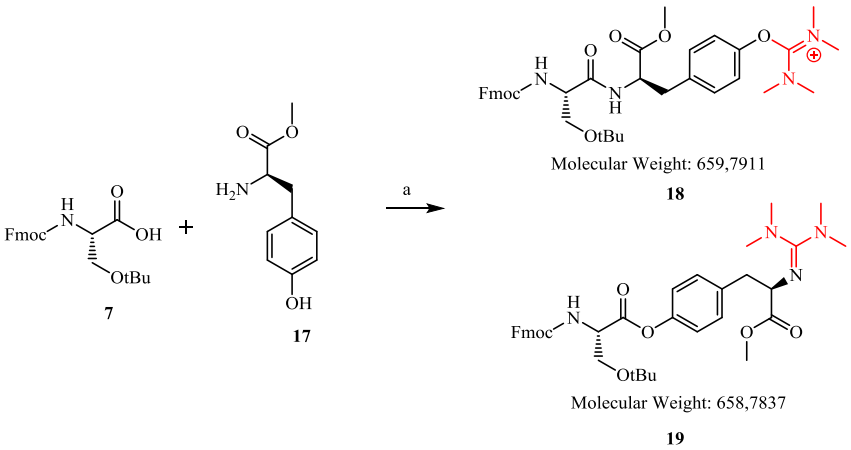

Figure 18: .*Coupling of* Fmoc-Ser(*t*Bu)-OH *with Tyr methyl ester: (a) HATU (1.5 equiv.), DIPEA, DMF.*

Interestingly, the side product formation was not observed by utilizing 1.0 instead of 1.5 equiv of HATU in the coupling reaction. These results clearly indicate that special care should be taken when coupling reagents are used with unprotected peptides for orthogonal reactions. In the case of HATU the conditions that the specific side-reaction happens as also the conditions to avoid the formation of the side product were monitored and presented.

A possible mechanism for the formation of the guanidine side product on the amino acid side chain is shown in *Figure 19*. In the first step the deprotonated acidic carboxylic group of the Fmoc-Ser(*t*Bu)-OH attacks the electrophilic carbon of HATU. Then, the resulting anion HATU-N-oxide reacts with the initially formed activated ester of Fmoc-Ser(*t*Bu)-OH (I) to another activated ester (II), which is coupled with the primary amino group of the amino acids to the desired product (III). The excess of HATU in the reaction mixture

seems to react further with the unprotected side chain to the undesirable product, bearing the guanidine group (IV).

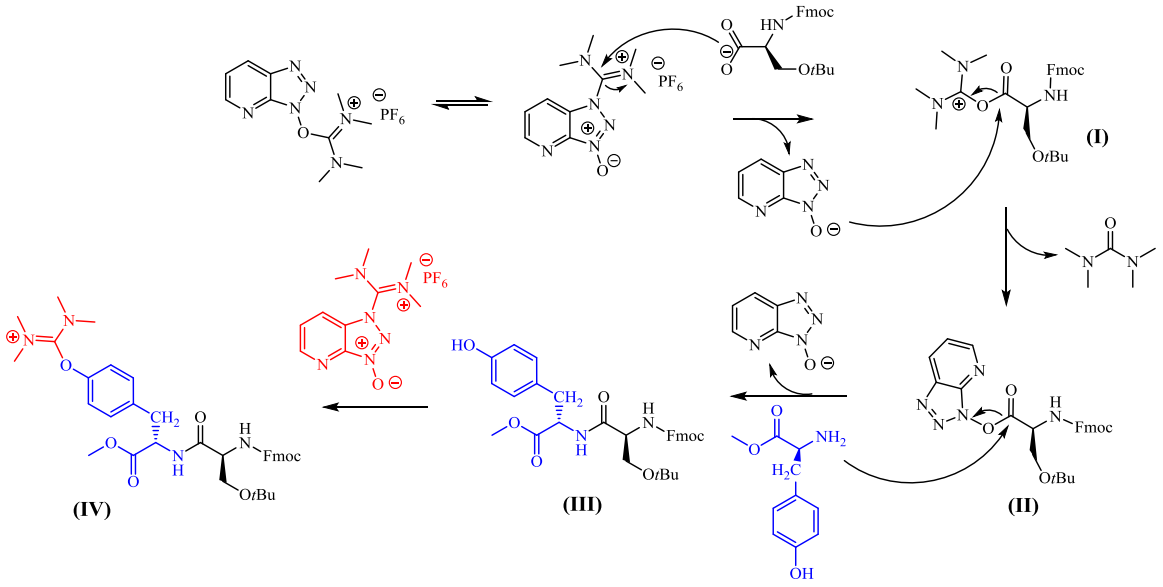

Figure 19: *Plausible reaction mechanism for guanidine side product formation.*

2.3 Gemcitabine – GnRH conjugates bearing in the conjugate linker oxime and carbonate bond

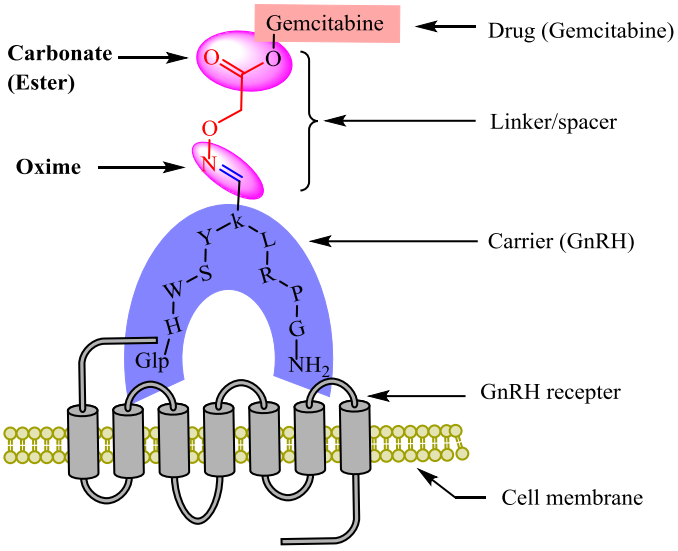

General concept of Carbonate and Oxime linker.

In preparation:

Title: Nisar Sayyad et. al., Gemcitabine-GnRH derivative bio-conjugates with different oxime bond linkages: synthesis, in vitro drug release and cytostatic effect.

2.3.1 Introduction:

Oxime Bond in Bioconjugation: The reaction of a ketone or an aldehyde with aminoxy or hydrazide form the imine called oxime and hydrazone, respectively. Even though the oxime formation is more sluggish than the hydrazone, its hydrolytic stability makes the oxime bond more preferable than the hydrazone.[15] The alfa nucleophile of the aminoxy is stronger nucleophile than amines, and its low basicity allows the formation of more stable imines (oxime).[16]

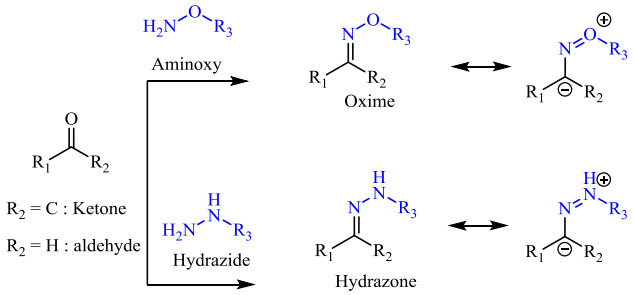

Figure 20: *Oxime and hydrazone formation.*

Chemoselectivity of oxime bond formation provides an orthogonal approach for coupling macro molecules (proteins and peptides) in bioconjugation. Oxime bond has the following characteristics: 1) Easy synthesis due to high chemo selectivity, therefore there is no requirements of protection/deprotection schemes;[17] 2) high chemical stability in the pH range 3-8; 3) Even though oxime formation is faster in acidic pH (4-5), oxime can be formed at neutral pH.[17] These properties of oxime bond-linked bio-conjugates make them appealing to be explored in targeted drug delivery.

Role of catalyst in oxime formation*:* Oxime formation reaction is favorable in acidic condition (pH 4-5), but the reaction rate is reduced at neutral pH. This reaction request: 1) acidic conditions (pH 4-5), 2) high concentration (mM) of reagents and 3) high temperature. Unfortunately, since biomolecules are naturally present at neutral pH, it is difficult to obtain oxime bond ligation in biomolecules. Thus catalyst is used in most of the cases; for example aniline[15] is being used as a nucleophilic catalyst. Aniline gives good results at neutral pH (7), but p-methoxyaniline is a better option for acidic pH (4.5). Aniline is a nucleophilic catalyst which forms a Schiff base intermediate with the aldehyde

or ketone, after protonation (that's why fast in acidic and quit slow in neutral) intermediate undergoes transimination with aminoxy to get oxime.[15] Recent research resulted in different catalysts such as anthranilic acid derivatives;[15] 4-aminophenylalanine;[72] 3,5-diaminobezoic acid;[72] m- phenylenediamine;[15] p- phenylenediamine[15] etc. to enhance the reaction rate at wide range of reaction pH and low concentration of regents.

Oxime vs. Carbonate: The carbonate bond is susceptible for chemical or enzymatic hydrolysis, and the degradation of carboxylic ester based bio-conjugates is fast with a half-life of about 2 h in human serum and 20 min in mouse serum (In mouse serum there is high content of caboxylesterases).[30] Among the GnRH-gemcitabine conjugates we synthesized linked via carbonate bond, GSG_1 was the most stable and showed almost complete hydrolysis in 2 h.[18] This chemical or enzymatic susceptibility of carbonate bond raises the issue of stability/degradation of such bio-conjugates. On the contrary oxime bond stability is higher; therefore oxime/hydrazone bonds may provide a better alternative to the carbonate bonds in bio-conjugates.

Demand of bifunctional bio-conjugates: In literature the drug-peptide conjugates are linked via single functional groups like carbonate,[18] oxime,[73, 74] carbamate[22] etc.. Although the fact that the oxime bond is more stable than the carbonate bond at neutral pH[30] could be beneficial in bioconjugation to avoid ectopic release of the cytotoxic drug, this stability may create obstacles in the release of the drug upon delivery in the tumour cells. Since the utilization of bifunctional linkers (loaded with combination of different functional groups-bonds, i.e. oxime and thioether used in doxorubicine and cell penetrating peptide conjugation[75]) has not been explored in detail in the literature we went on to exploit and design linkers bearing hybrid functionality: (carbonate and oxime bonds. Such linkers could potentially improve the cytotoxicity, stability, degradation and pharmacokinetics profile of gemcitabine as compared to bio-conjugation with only one hydrolysable functional group.

2.3.2 Design, synthesis and characterization:

The usefulness of Boc-aminoxy acetic acid as an oxime linkage is very convenient since the terminal carboxylic acid is useful to perform reactions with any amine (e.g. ε-amine of lysine residue from peptide), or any alcohol of drug like Gemcitabine. The

aminoxy group, after boc-deprotection is then able to provide reaction with any ketones or aldehydes.

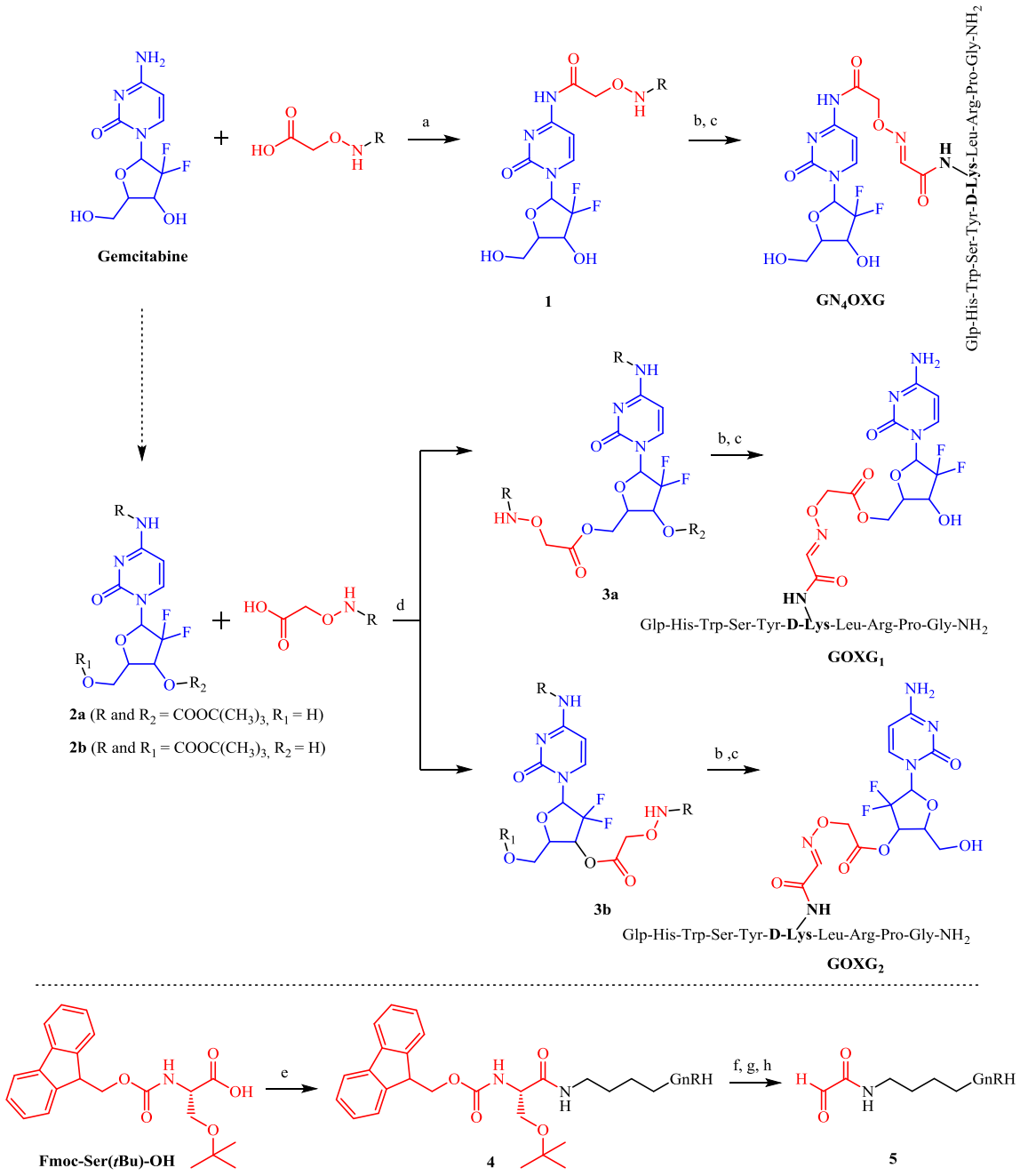

Figure 21: Synthetic scheme of GNRH-Gemcitabine Conjugate via oxime and carbonate linker: *a) DCC, NHS, Pyridine/DMF; b) DCM: TFA 95:5, 3 h, rt; c)* ***5****, ACN: H_2O, 5:1, 24 h; d) PyBOP, HOBt, DMAP, DIPEA, DCM; e) [D-Lys^6]- GnRH, PyBOP, HOBt, DIPEA, DMF; f) 20% pyridine in DMF, rt, 10 min; g) TFA/TIS/H_2O (95/2.5/ 2.5, v/v); h) $NaIO_4$, imidazole, H_2O, rt, 5 min. ([**D-Lys^6]-GnRH:** Glp-His-Trp-Ser-Tyr-D-Lys-Leu-Arg-Pro-Gly-NH_2).*

The Boc-aminoxy acetic acid was covalently coupled, using N,N'-dicyclohexylcarbodiimide (DCC) and N-Hydroxysiccinimide (NHS)[38] (*Figure 21*), with the gemcitabine to obtained compound **1** (amide); and using PyBOP, HOBt, DMAP and DIPEA with gemcitabine analogues which had selective Boc-potection at 5'-OH/4-NH_2 (**2b**) and 3'-OH/4-NH_2 (**2a**)[18, 41] to gives **3b** and **3a** (carbonate), respectively. After TFA treatment the aminoxy group (resulted compound is very hygroscopic, and should be maintained under inert atmosphere) is available to react with aldehyde group of compound **5.** The compound **5** resulted after orthogonal coupling and subsequent oxidation of a serine at the ε-amino group of [D-Lys^6]-GnRH. Specifically, amide coupling of Fmoc-Ser(*t*Bu)-OH and ε-amino group of [D-Lys^6]-GnRH with PyBOP, HOBt and DIPEA as base. After Fmoc removal (20% piperidine in DMF) and *tert*-Butyl deprotection (TFA/TIS/H_2O, 95/2.5/2.5, v/v) in liquid phase gave NH_2-Ser-[D-Lys^6]-GnRH (**4b**). Compound **4b** was purified with HPLC. Selective oxidaion of **4b** at the terminal serine in the presence of $NaIO_4$ and imidazole[74] gave HCO-CO-[D-Lys^6]-GnRH (**5**). Nonacylated N-terminal serine and threonine residue of peptide and proteins can be oxidised into aldehyde by periodate[76, 77], (*Figure 22)* that formed aldehyde can be modified by various hydrazine, hydroxyl amine, amines and aminoxy derivatives.

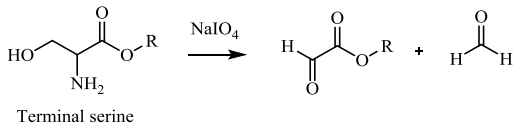

Figure 22: *Sodiumperiodate oxidation of an N-terminal serine residue to aldehyde with release of formaldehyde.*

Precautions to be taken while handling the aminoxy group: The aminoxy group formed after Boc-deprotection is very reactive with electrophiles (such as ketones and aldehydes) and especially with the acetone from the glass tubes that was not properly dried. In the onset of our studies we had not dried well on high vacuum our compounds (**1, 3a, 3b**), after column purification in DCM/Acetone, and traces of acetone were enough to react with aminoxy to form side product, characterized (*see experimental part*). To avoid side product formation a better option is to perform the Boc-deprotection of the aminoxy group and oxime bond formation insitu[78] and in one pot.

As we mentioned above oxime bond formation in bio-conjugates normally requests a catalyst,[58, 61] acidic particular pH,[75, 74] excess use of one reagents, temperature[17, 78] etc. but still the reaction requests days to be completed as is reported in the literature. We discovered a simple and rapid method of oxime bond formation in bio-conjugates that does not require buffers, excess molar ratio of reagents, catalyst and it can be performed at room temperature within few hours. We used the solvent mixture ACN/H_2O (5/1, v/v), for the first time to form oxime bonds in bio-conjugates leading to quantitative formation of the desired product and the resulting product is pure without the need for further purification.[79]

Synthesis of the bio-conjugates:

Selective Boc-protection of alcohols and amine (**2a** and **2b)** were done as same as reported by Zhi-wei Guo et.al.[41]

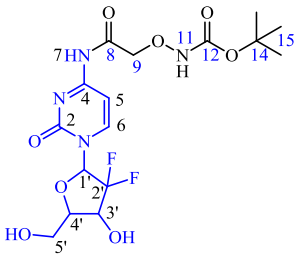

1

Synthesis of 1: The solution of Boc-aminooxy acetic acid (30 mg, 0.1570 mmol), DCC (32.39 mg, 0.157 mmol) and NHS (18.06 mg, 0.157 mmol, in 8 mL DMF/pyridine (1:1, v/v) stirred at rt, under nitrogen atmosphere. After 4 h a solution of Gemcitabine (123.9 mg, 0.471 mmol) in 4 mL pyridine was added drop wise and the reaction was continued for 24 h. Solvent was evaporated on high vacuum, the residue was purified with column chromatography in DCM/methanol. Expected pure spot collected at 6% methanol in DCM, the solvent was evaporated on rotary evaporator and dried to gives **1** (30 mg, 43.81%) as a white solid.

^{1}H-NMR (500 MHz, DMSO-d_6, 25^{o}C): δ = 10.89 (s, 1 H, 7-NH), 10.33 (s, 1 H, 11-NH), 8.32 (d, J = 7.5 Hz, 1 H, 6-H), 7.26 (d, J = 7.5 Hz, 1 H, 5-H), 6.36 (d, J = 6.6 Hz, 1 H, 3'-OH), 6.21 (t, J = 7.4 Hz, 1 H, 1'-H), 5.34 (t, J = 5.5 Hz, 1 H, 5'-OH), 4.49 (s, 2 H, 9-H), 4.26- 4.18 (m, 1 H, 3'-H), 3.95- 3.92 (m, 1 H, 4'-H), 3.86- 3.82 (m, 1 H, 5'a-H), 3.71- 3.67

(m, 1 H, 5'b-H), 1.44 (s, 9 H, 15-H) ppm. ^{13}C-NMR (500 MHz, DMSO-d_6, 25^{o}C): δ = 170.51 (C8), 163.20 (C4), 154.92 (C2), 145.90(C6), 123.80 (C2'), 96.64 (C5), 84.85 (C1') 81.74 (C4'), 81.19 (C14), 75.39 (C9), 69.07 (C3´), 59.45 (C5'), 28.73 (C15) ppm. Mass: MS (ESI$^+$) *m/z*: $[M-H]^+$ for $C_{16}H_{22}F_2N_4O_8$:calcd, 436.14; found, 435.13.

Synthesis of 3a/3b: To a solution of **2a/2b** (50 mg, 0.107 mmol)**,** Boc-aminooxy acetic acid (30.9 mg, 0.161 mmol), PyBOP (112.30 mg, 0.215 mmol), HOBt (29.1 mg, 0.215 mmol) and DMAP (19.7 mg, 0.161 mmol) in 10 mL anhydrous DCM, DIPEA (75.2 µL, 0.431 mmol) was added under nitrogen atmosphere; the reaction was continued for 12 h at rt. TLC (DCM/acetone, 10/1, v/v) indicated almost complete consumption of **2a** and formation of new non polar spot. The solvent was evaporated from reaction mixture and the crude compound was purified with column chromatography. The pure compound was collected at 10% acetone in DCM, the solvent was evaporated and the compound was dried well on high vacuum, to give **3a** (90 mg, 72.8%) as a white solid.

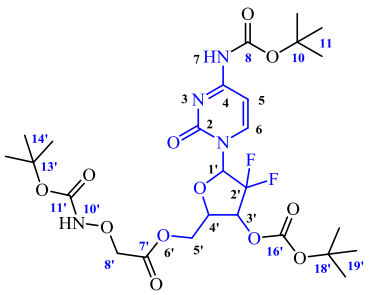

3a

^{1}H-NMR (500 MHz, DMSO-d_6, 25^{o}C): δ = 10.61 (s, 1 H, 7-NH), 10.25 (s, 1 H, 10'-NH), 8.02 (d, J = 7.7 Hz, 1 H, 6-H), 7.15 (d, J = 7.7 Hz, 1 H, 5-H), 6.33 (t, J = 8.4 Hz, 1 H, 1'-H), 5.37 (m, 1 H, 3'-H), 4.57 (dd, J = 11.7 Hz, 2 Hz, 1 H, 5a'-H), 4.52 (m, 1 H, 4'-H) , 4.49 (dd, J = 11.6 Hz, 6.3 Hz, 1 H, 5'b-H), 1.49 (s, 18 H, 11-H and 19'), 1.43 (s, 9 H, 14'-H) ppm; ^{13}C-NMR 500 MHz, DMSO-d_6, 25^{o}C: δ = 169.27 (C7'), 164.65 (C4), 157.25 (C11'), 154.65 (C2), 146.05 (C6), 96.13 (C5), 85.42 (C1') 84.85 (C10), 82.28 (C18'), 81.05 (C13´), 76.63 (C4´), 73.43 (C3'), 72.69 (C8'), 63.24 (C5'), 28.59 (C14'), 28.11 C11 and C19') ppm. Mass: MS (ESI$^+$) *m/z*: $[M+H]^+$ for $C_{26}H_{38}F_2N_4O_{12}$:calcd, 636.25; found, 637.25.

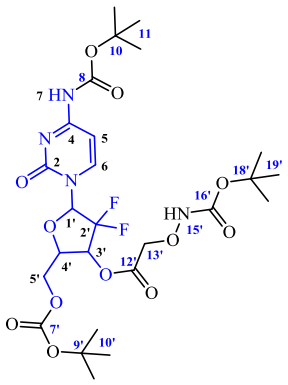

3b

^{1}H-NMR (500 MHz, DMSO-d$_6$, 25^{o}C): δ = 10.63 (s, 1 H, 7-NH), 10.33 (s, 1 H, 15'-NH), 8.06 (d, J = 7.7 Hz, 1 H, 6-H), 7.13 (d, J = 7.7 Hz, 1 H, 5-H), 6.36 (t, J = 8.3 Hz, 1 H, 1'-H), 5.52 (m, 1 H, 3'-H), 4.56 (dd, J = 21.1 Hz, 16.4 Hz, 2 H, 13'-H), 4.55- 4.51 (m, 1 H, 4'-H) , 4.48 (dd, J = 12.0 Hz, 2.5 Hz, 1 H, 5'a-H), 4.41 (dd, J = 12 Hz, 7 Hz, 1 H, 5'b-H), 1.50 (s, 9 H, 19'-H), 1.46 (s, 9 H, 10'-H), 1.44 (s, 9 H, 11-H) ppm; ^{13}C-NMR (500 MHz, DMSO-d$_6$, 25^{o}C): δ = 168.62 (C12'), 164.81 (C4), 157.43 (C16'), 154.69 (C2), 153.36 (C7'), 146.4 (C6), 96.03 (C5), 85.78 (C1') 83.16 (C9'), 82.42 (C18'), 81.23 (C10), 76.59 (C4′), 72.57 (C13'), 71.58 (C3'), 65.93 (C5'), 28.71 (C11), 28.51 (C19') ppm. Mass: MS (ESI^{+}) *m/z*: [M+H]$^{+}$ for $C_{26}H_{38}F_2N_4O_{12}$:calcd, 636.25; found, 637.25.

Fmoc-Ser(*t*Bu)-[D-Lys^{6}]-GnRH 4: To a solution of Fmoc-Ser(*t*Bu)-OH (6.1 mg, 0.015 mmol)**,** PyBOP (12.42 mg, 0.023 mmol) and HOBt (3.23 g, 0.023 mmol) in DMF (3 mL), DIPEA (13.9 ul, 0.079 mmol) was added under nitrogen atmosphere. After 5 min [D-Lys^{6}]- GnRH (19.94 mg, 0.015 mmol) in DMF (2 mL) added drop wise, and the reaction was continued for 12 h at rt. TLC (n-butanol/H_2O/AcOH, 6/2/2, v/v) indicatedthe consumption of the starting material and formation of new spot. Solvent was evaporated under high vacuum, the residue was washed with acetonitrile (1 mL X 2) to give compound **4** (20 mg, 81.59%) as a white solid.

Mass: MS (ESI^{+}) *m/z* for $C_{81}H_{107}N_{19}O_{17}$: calcd, 1617.81; found, 1619.77 [M+H]$^{+}$, 810.78 [M+2H]$^{2+}$.

NH_2-Ser(*t*Bu)-[D-Lys^6]-GnRH 4a: Compound **4** (15 mg) was dissolved in 2 mL 20% piperidine in DMF (at ice cooling) and stirred till rt for 10 min. Solvent was removed under high vacuum and the residue was washed with acetonitrile (0.5 mL X 2) to give **4a** (12 mg, 92.73%) as a white solid. TLC (n-butanol/ H_2O/AcOH, 6/2/2, v/v) indicated the formation of new spot that was ninhydrine active.

Mass: MS (ESI^+) *m/z* for $C_{66}H_{97}N_{19}O_{15}$: calcd, 1395.74; found, 1398.19 $[M+H]^+$, 699.62 $[M+2H]^{2+}$, 466.68 $[M+3H]^{3+}$

Ser-[D-Lys^6]-GnRH 4b: The solution of **4a** (12 mg) was stirred in 2 mL of TFA/TIS/H_2O (95/2.5/2.5, v/v) for 4 h at rt. The solvent was evaporated on rotary evaporator, the residue was washed with acetonitrile (0.5 mL X 2) and the crude compound was purified with semi preparative HPLC (85/15 to 55/45% of H_2O.TFA/ ACN.TFA, flow rate 5 mL/min for 30 min at 214 nm); The purified fraction was lyophilized to give **4b** (10 mg, 86.80%) as a white solid.

Mass: MS (ESI^+) *m/z* for $C_{62}H_{89}N_{19}O_{15}$: calcd, 1339.68; found, 1342.07 $[M+H]^+$, 671.48 $[M+2H]^{2+}$, 447.88 $[M+3H]^{3+}$

HCO-CO-[D-Lys^6]-GnRH 5: To the solution of **4b** (10 mg, 7.464 μmol) in 0.5 mL H_2O, imidazole (2.54 mg, 0.037 mmol) and sodium periodate (1.91 mg, 8.957 μmol) was added simultaneously; the resulting mixture was stirred on rt for 5 min. The reaction was quenched with ethylene glycol (4.16 μL, 0.074 mmol). TLC (n-butanol/ H_2O/AcOH, 6/2/2, v/v) indicated the consumption of **4b** and formation of a new non polar spot, that was ninhydrine active. The crude compound was purified with semi preparative HPLC (85/15 to 50/50% of H_2O.TFA/ ACN.TFA, flow rate 5 mL/min for 30 min, at 214 nm); the pure fraction was lyophilized to give **5** (6 mg, 61.47%) as a white solid.

Mass: MS (ESI^+) *m/z* for $C_{61}H_{84}N_{18}O_{15}$: calcd, 1308.64; found, 1310.91 $[M+H]^+$, 656.07 $[M+2H]^{2+}$, Monohydrated: MS (ESI^+) *m/z* for $C_{61}H_{84}N_{18}O_{15}.H_2O$: calcd, 1326.64; found, 1328.96 $[M+H]^+$, 665.06 $[M+2H]^{2+}$, Dihydrated: MS (ESI^+) *m/z* for $C_{61}H_{84}N_{18}O_{15}.2H_2O$:calcd, 1344.64; found, 1348.74 $[M+H]^+$

GOXG$_1$, GOXG$_2$ and GN$_4$OXG: Compound **3a/3b/1** (7.331 μmol) was dissolved in 1 mL DCM/TFA (95/5%), in ice, the resulting mixture was left for 3 h at rt. The solvent was evaporated and the residue was dissolved in 20 mL ACN/H_2O (5/1, v/v).Compound **5** (9.6 mg, 7.331 μmol) was added the reaction was continued at rt for 24 h. The reaction was lyophilized to give **GOXG$_1$**, **GOXG$_2$** and **GN$_4$OXG** (11.8 mg, 98.9%) as a white solid compound.

GOXG$_1$: Mass: ESI-MS (*m/z*): $[M+H]^+$ calcd. for $C_{72}H_{96}F_2N_{22}O_{20}$, 1626.71; found 1629.59, $[M+2H]^{2+}$ calcd. 814.35; found 815.15, $[M+3H]^{3+}$ calcd. 543.23; found 543.81.

GOXG$_2$: Mass: ESI-MS (*m/z*): $[M+H]^+$calcd. for $C_{72}H_{96}F_2N_{22}O_{20}$, 1626.71; found 1629.84, $[M+2H]^{2+}$ calcd. 814.35; found 815.15, $[M+3H]^{3+}$ calcd. 543.23; found 543.81.

GN$_4$OXG: Mass: ESI-MS (*m/z*): $[M+H]^+$calcd. for $C_{72}H_{96}F_2N_{22}O_{20}$, 1626.71; found 1630.02, $[M+2H]^{2+}$ calcd. 814.35; found 815.28.

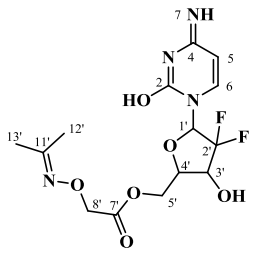

^{1}H-NMR (500 MHz, DMSO-d$_6$, 25^{o}C): δ = 8.9 (s, 1 H, 2-OH), 8.34 (s, 1 H, 7-NH), 7.76 (d, J = 7.7 Hz, 1 H, 6-H), 6.56 (bs, 1 H, 3'-OH), 6.21 (t, J = 8.2 Hz, 1 H, 1'-H), 6.06 (d, J = 7.7 Hz, 1 H, 5-H), 4.67 (s, 2 H, 8'-H), 4.51 (dd, J = 6.3 Hz, 2 Hz, 1 H, 5a'-H) , 4.40 (dd, J = 6.3 Hz, 5.6 Hz, 1 H, 5'b-H), 4.25 (m, 1 H, 3'-H), 4.12 (m, 1 H, 4'-H), 3.20 (s, 2 H), 1.87 (s, 3 H, 13'-H), 1.82 (s, 3 H, 12'-H) ppm; ^{13}C-NMR (500 MHz, DMSO-d$_6$, 25^{o}C): δ = 170.53 (C7'), 162.58 (C4), 157.13 (C11'), 150.82 (C2), 123.40 (C2'), 95.59 (C5), 84.51 (C1'), 78.31 (C4'), 70.21 (C3'), 70.03 (C8′), 62.84 (C5′), 43.28 (C6), 21.98 (C13'), 16.38 (C12') ppm. Mass: MS (ESI$^+$) *m/z*: $[M-H]^+$ for $C_{14}H_{18}F_2N_4O_6$: calcd, 376.12; found, 375.11.

2.3.3 Biological evaluation:

1) In vitro cytotoxicity

2) Stability in cell culture medium

3) In vitro stability in human plasma

4) Pharmacokinetics (In progress)

1) In vitro cytotoxicity of $GOXG_1$, $GOXG_2$ and GN_4OXG:

Cells (DU145, PC3) were plated at a density of 5 x 10^3 cells per well on 96-well plates. After 24 h incubation (37ºC, 5% CO_2), the cell medium was removed, and compounds were added at selected concentrations (10-20,000 nM for $GOXG_1$, $GOXG_2$), followed by incubation for 72 h. The medium was then removed and the MTT solution (0.3 mg/mL in PBS) was added to cells for 3 h, after which the MTT solution was removed and the formazan crystals were dissolved in 100 µL DMSO. The optical density was measured at 570 nm and a reference wavelength of 690 nm using an absorbance micro plate reader. The 50% cytostatic concentration (IC_{50}) was calculated based on a four-parameter logistic equation using Sigma Plot 12 software. Each point was the result of three experiments performed in triplicate. Results are summarized in the table below:

***Table 5**: IC_{50} for $GOXG_1$, $GOXG_2$ and GN_4OXG in DU145 and PC3 cells.*

IC_{50} (nM)	**$GOXG_1$**	**$GOXG_2$**	**GN_4OXG**
DU145	613 ± 62 (n=6)	494 ± 93 (n=6)	580 ± 47 (n=6)
PC3	754 ± 142 (n=6)	675 ± 82 (n=6)	833 ± 27 (n=6)

2) In vitro stability of GSG_1, $GOXG_1$, $GOXG_2$ and GN_4OXG in cell culture:

Cells (DU145) were plated at a density of 2 x 10^5 cells on 25 cm^2 flasks. After 24 h incubation (37ºC, 5% CO_2), cell medium (RPMI, 10%FBS, 1%P/S) was removed and was refreshed with medium containing 1µM of either gemcitabine, GSG_1, $GOXG_1$, $GOXG_2$,

and GN_4OXG. Samples (triplicates of 20 µL) were collected at selected time points (t = 0, 0.5, 1, 2, 4, 8, 24 h) and were stored at -80°C after mixing with 180 µL of initial mobile phase (90% H_20, 10%ACN, 2 mM ammonium acetate, 0.1% formic acid). The degradation of the tested molecules and the formation of gemcitabine from the conjugates over time are presented below.

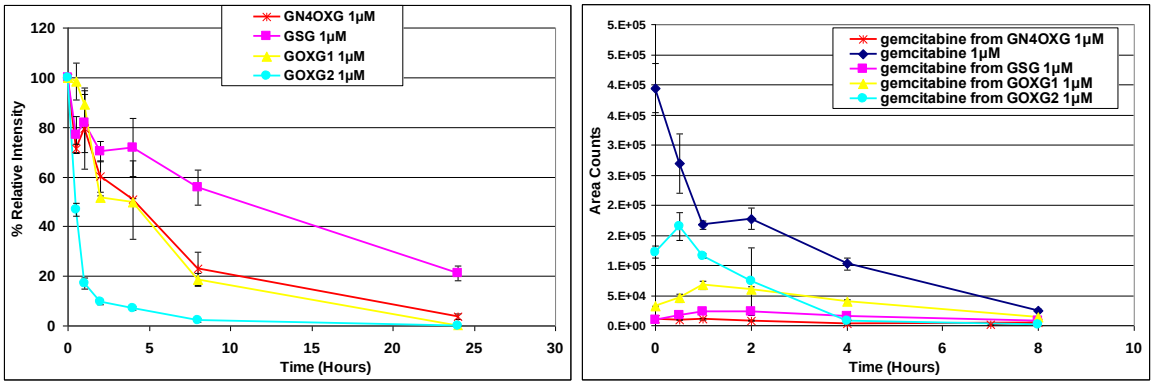

Figure 23: *In vitro stability of GSG_1, $GOXG_1$, $GOXG_2$, GN_4OXG, in cell culture and degradation. (**Note**: GSG = GSG_1)*

Note: *In forthcoming bilogical evaluation of oxime conjugates, we have included GSG_1 as a reference for comparitive study of oxime-carbonate and carbonate bond. Because in our previous work*[18] *GSG_1 showed the best result (on the basis of cytotoxicity, stability, pharmacokinetics and cell uptake) than others analogues.*

3) In vitro stability of $GOXG_1$, $GOXG_2$, GN_4OXG, GSG_1 in human plasma:

1µg/mLof $GOXG_1$, $GOXG_2$, GN_4OXG or GSG_1 were incubated with human plasma in a shaking water bath at 37°C. Samples (triplicates of 50 µL) were collected at selected time points (t = 0, 0.08, 0.5, 1, 4 h) were stored at -80°C after mixing with 150 µL acetonitrile. Samples were then extracted using protein precipitation. The degradation of the tested molecules is presented below.

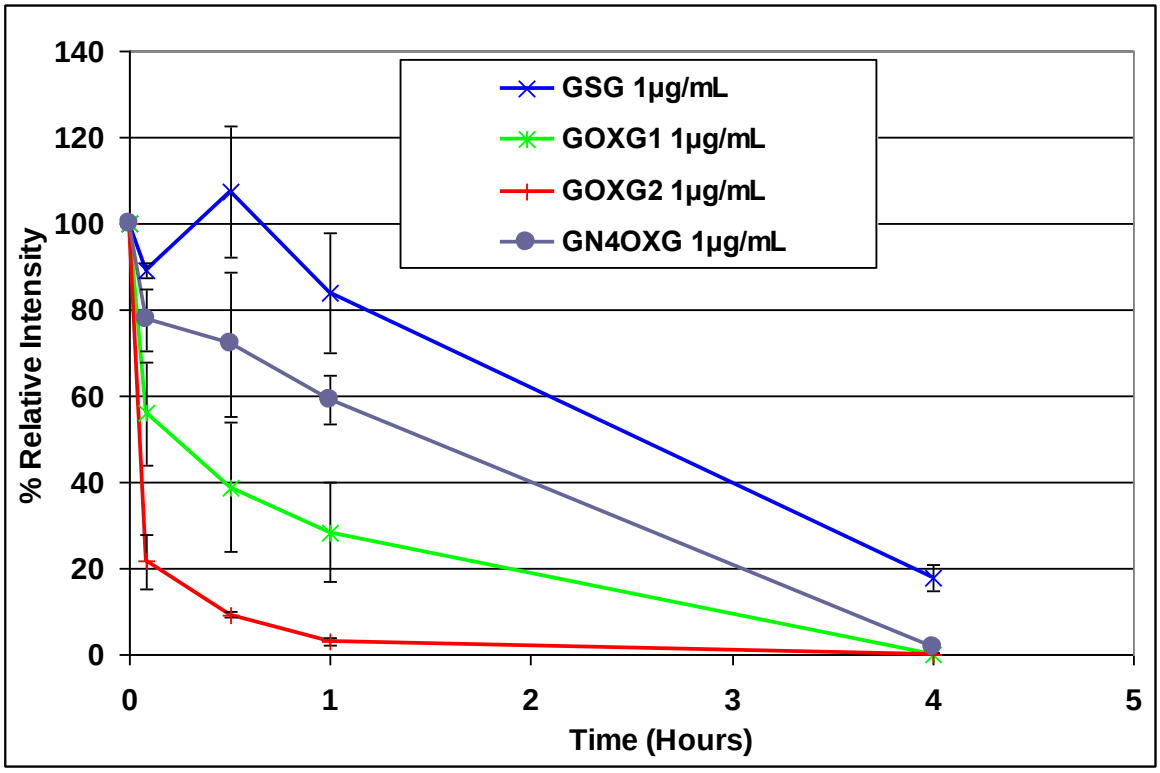

Figure 24: *In vitro stability of $GOXG_1$, $GOXG_2$, GN_4OXG and GSG_1 in human plasma. (Note: GSG = GSG_1)*

2.4 Gemcitabine – GnRH conjugates bearing in the conjugate linker carbamate (urethane) bond: a traceless linker

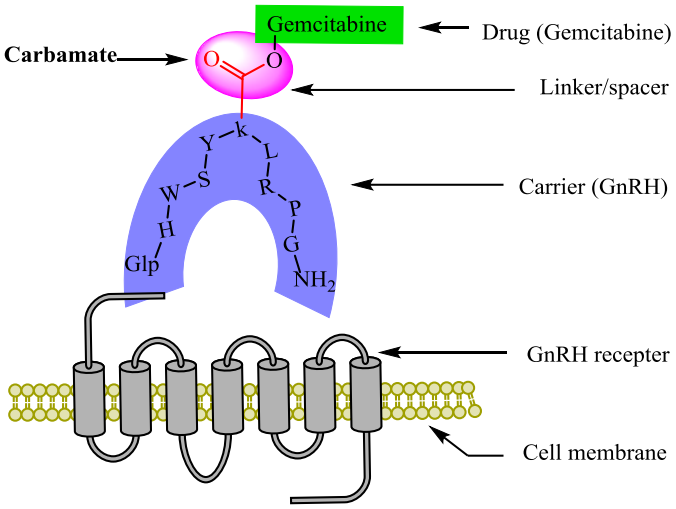

General concept of traceless linker ($2G_1$, $2G_2$) conjugates via carbamate bond.

In preparation:

Nisar Sayyad et al., GnRH-*gemcitabine* bio-conjugates with traceless cleavable linkers,

2.4.1 Introduction

In our former studies we have reported the conjugation of gemcitabine and peptide GnRH via hemiglutarate and hemisuccinate linkers. These studies highlighted the dominant role that the linker adopted towards the compound bioactivity profile. On these lines and aiming to enhance the therapeutic potency of these compounds we further exploited new GnRH-gemcitabine conjugates bearing very short traceless cleavable carbamate linkers connecting the two parent compounds as shown in *Figure 25*.

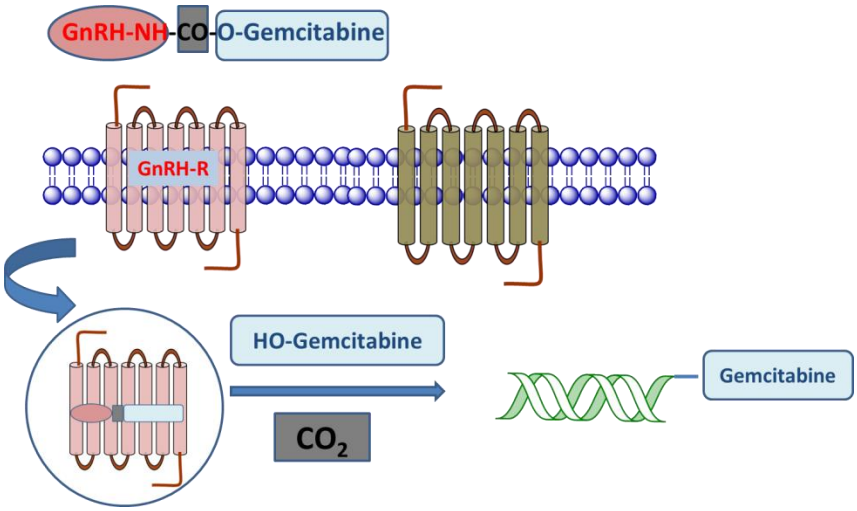

***Figure 25**: GnRH-gemcitabine bio-conjugates with traceless cleavable linkers.*

The relevant biocompounds were explored on their cytotoxicity in different cancer cell lines equipped with the GnRH-R, metabolic stability, as also the formation of inactive metabolite of gemcitabine (dFdU).

Carbamate is a chemical moiety where carbonyl group links a nucleophile amine and an alcohol together. This carbonyl could originate from phosgene; 1,1'-Carbonyldiimidazole (CDI); Bis(4-nitrophenyl)carbonate (BNPC); isocynates; or chloroformates as shown in *Figure 26*. Among these phosgene is of limited usage due to its gaseous phase and enhanced toxicity. CDI and BNPC are the two most convenient

reagents, though we prefer BNPC since its nitro at para position makes it a more active electrophile than CDI.

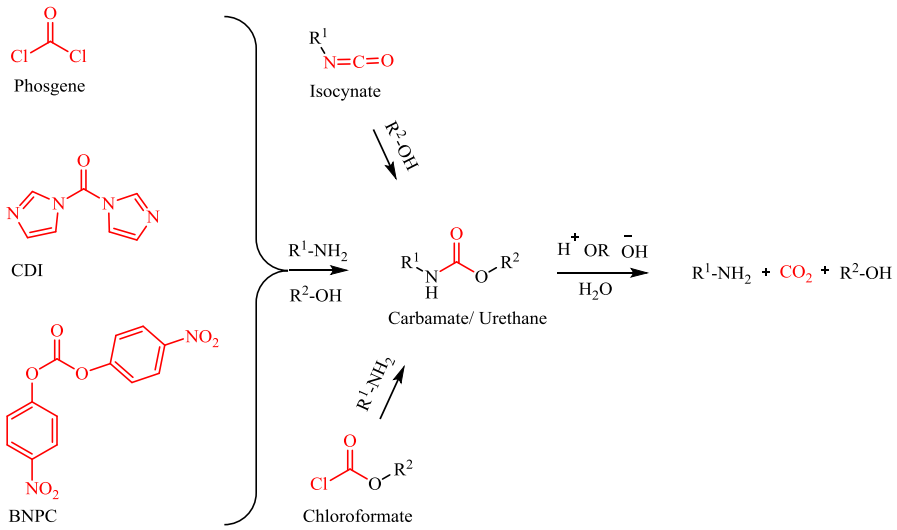

Figure 26: *Reagents used for formation of carbamate bonds and degradation (hydrolysis) products of carbamates.*

According to the principles of targeted drug delivery, bio-conjugates should be susceptible for chemical or enzymatic hydrolysis. Indeed, carbamate is also labile in aqueous acidic or basic conditionsand upon its hydrolysis it releases carbon dioxide as gas (traceless linker) and the parent compounds (*Figure 26*).

Gemcitabine has two hydroxyl and one amine groups that are available for carbamate bond formation with the ε-amine group of [D-Lys]^6-GnRH. On the basis of these different nucleophiles, we divided this work in two parts:

2.4.2 Carbamate bond formation at Gemcitabine's hydroxyl (3'-OH or 5'-OH) groups using Bis(4-nitrophenyl)carbonate (BNPC).

2.4.3 Carbamate bond formation at Gemcitabine's amine (4-NH_2) group using Chloroformates.

2.4.2 Carbamate bond formation at Gemcitabine's hydroxyl (3'-OH or 5'-OH) groups using Bis(4-nitrophenyl)carbonate (BNPC).

2.4.2.1 Design, synthesis and characterization:

The Bio-conjugation of GnRH-gemcitabine via traceless linker carbamate was achieved by the reaction of nucleophile 5'-OH primary or 3'-OH secondary alcohol of gemcitabine and the ε-amine of Lys[6] of [D-Lys]^6-GnRH. Gemcitabine was initially regioselectively Boc-protected at the amine and the one alcohol to give **1a** and **1b**[41, 18], which have the 5'-OH primary and 3'-OH secondary alcohol, respectively free for the subsequent acylation with BNPC. Application of BNPC to **1a** and **1b** gave the intermediate **2a** and **2b**, respectively. These were then reacted with the *ε*-amino group of [D-Lys^6]-GnRH in the presence of DIPEA, to give the bio-conjugates **2G$_1$** and **2G$_2$** (after Boc-deprotection with TFA/ TIS/ H_2O, 9.5/0.25/0.25, v/v), respectively where Gemcitabine and GnRH are linked via carbamate bond.

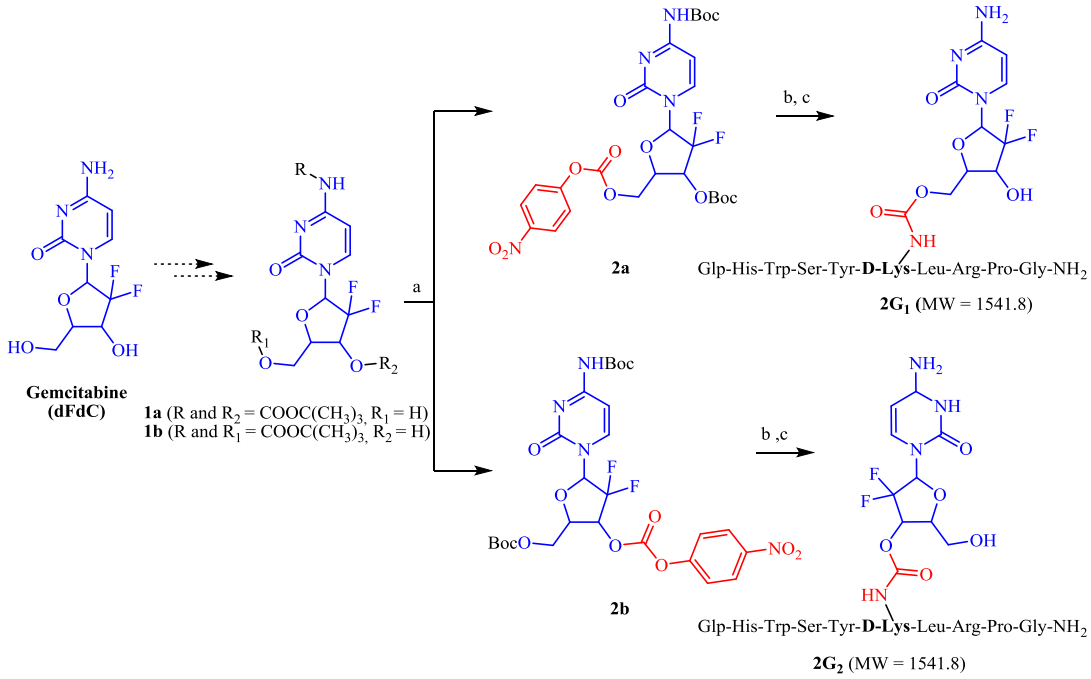

Figure 27: *Synthesis of GnRH-gemcitabine conjugates linked via carbamate bond. Reagents and conditions: a) Bis(4-nitrophenyl)carbonate, N,N´-Diisopropylethylamine (DIPEA), acetonitrile, rt; b) [D-Lys^6]-GnRH, DIPEA, DMF, rt; c) TFA/ H_2O/ TIS (9.5/0.25/0.25, v/v), rt.*

We followed the published protocols for carbamate bond formation where it was indicated that the intermediate required almost 12 h[22] and then the addition of the next nucleophile was done *insitu* without further purification of the intermediate.[28] According to this published protocols we faced the following problems: a) The reaction was going reverse after 4 h. i.e. the intermediate was hydrolyzed back to Gemcitabine and b) We recorded cyclisation of GnRH (Intramolecular carbamate formation) even after a 1:1 molar ration of Gemcitabine, BNPC and GnRH. (*Figure 28*).

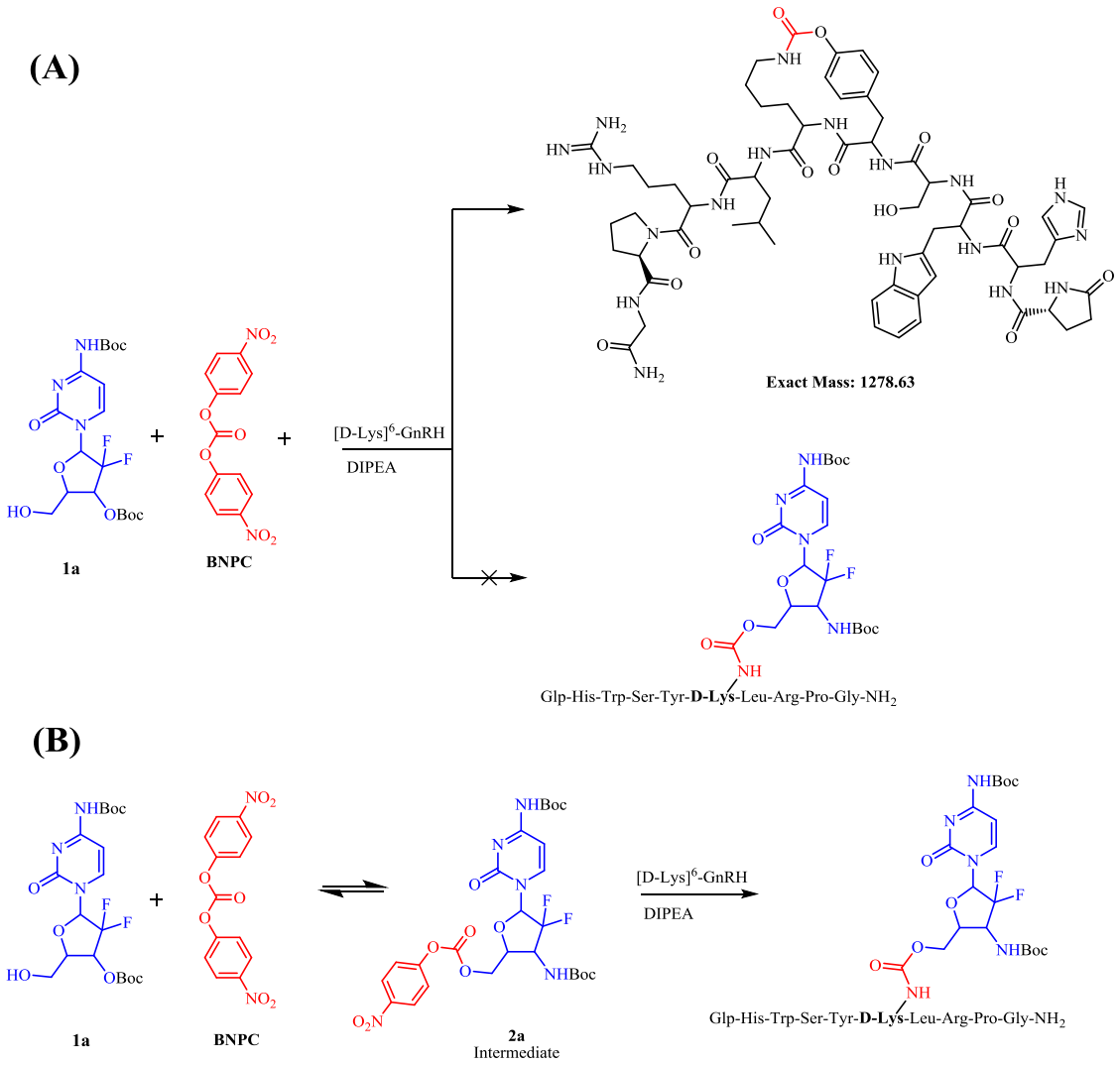

Figure 28: *(A) Literature synthetic protocol for Carbamate bond formation had not resulted in the desired product. (B) The protocol we followed resulted in the desired product formation.*

To avoid the hydrolysis of the intermediate, it was necessary to stop reaction after 4 h and addition of more equivalents of BNPC (8 equiv.) and DIPEA (40 equiv.) to shift equilibrium to the right and minimize the hydrolysis of the product.

GnRH has many nucleophile (amine and alcohol) unprotected which .can undergo intramolecular coupling via carbamate bond (*Figure 28-A and Figure 28-B*). We hypothesized that the detected intramolecular cyclization in GnRH would have happened between tyrosine and lysine, due to the high pKa of tyrosine hydroxyl (10.07) and ε-amine of lysine (10.53). To surmount this problem we isolated the resulted intermediate performed the reaction in a step wise manner. Purification of the intermediate and removal of the extra equivalents of BNPC was performed with column chromatography. The most crucial step was to isolate intermediate as they were very active electrophile (ester), depending upon nucleophile (hydroxyl or amine group) when come in contact will give cabonate or carbamate stable product. Characterisation of **2a** and **2b** was performed with NMR and mass spectrometry. While preparing the sample for mass in methanol (0.1% formic acid in methanol), methanol can act as a nucleophile and replace nitro phenol group (transesterification) from **2a** and **2b**. Mass spectrum (*Figure 29-A*) clearly shows that molecular ion peak in spectrum (ESI-MS (*m/z)* Calcd. for $C_{21}H_{29}F_2N_3O_{10}$: 521.18, found: 522.79 $[M+H]^+$).

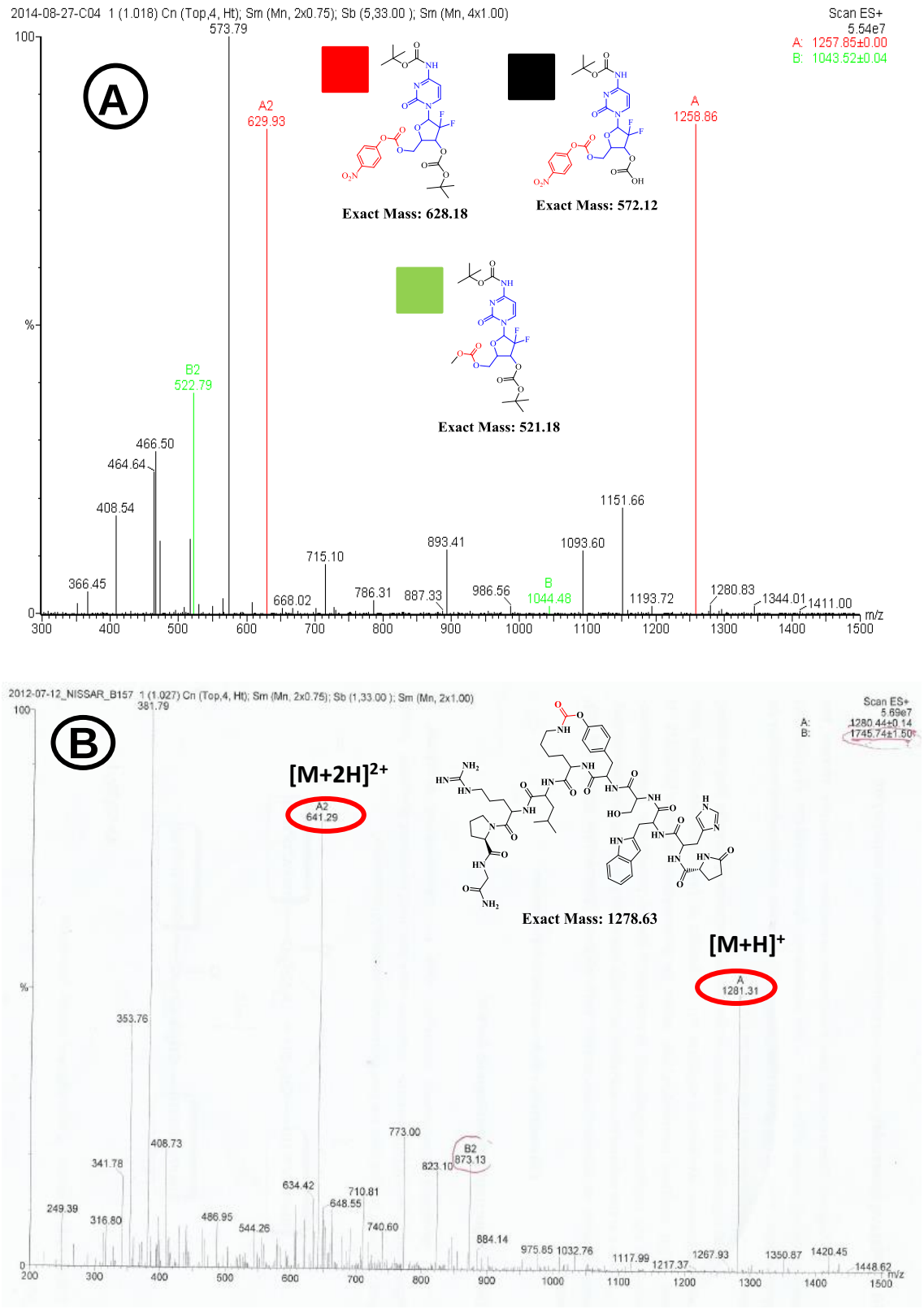

Figure 29: *Mass spectrum of A) Gemcitabine-BNPC intermediate and B) Cyclized GnRH peptide by carbamate bond.*

Synthesis part:

Synthesis of 2a/2b: DIPEA (752.4 µL, 4.319 mmol) was added to the solution of **1a/1b** (50 mg, 0.107 mmol) in anhydrous acetonitrile (10 mL), under inert atmosphere, at -10^{0}C (ice/acetone bath). After 5 min a solution of Bis(4-nitrophenyl)carbonate (260.4 mg, 0.856 mmol) in 5 mL anhydrous acetonitrile was added drop wise to the reaction. The resulting mixture was stirred at rt for 4 h. Reaction progress was monitored with TLC in acetone/DCM (1/10, v/v). The solvent was removed with rotary evaporator; the residue was purified with column chromatography in DCM and acetone as a solvent. The expected compound was isolated at 10% acetone in DCM. Solvent was evaporated and the residue was dried on high vacuum to give a white solid compound **2a** (60 mg, 88.58%); **2b** (26 mg, 38.39%).

^{1}H-NMR of **2a** (400 MHz, DMSO-d_6, 25^{o}C): δ = 10.62 (s, 1 H), 8.37 (d, J = 9.14 Hz, 2 H), 8.06 (d, J = 7.67 Hz, 1 H), 7.62 (d, J = 9.14 Hz, 2 H), 7.12 (d, J = 7.55 Hz, 1 H), 6.35 (t, J = 8.69 Hz, 1 H), 5.58 - 5.41 (m, 1 H), 4.73 - 4.71 (m, 1 H), 4.68 - 4.62 (m, 2 H), 1.58 (s, 9 H), 1.49 (s, 9 H) ppm; ^{13}C-NMR (400 MHz, DMSO-d_6, 25^{o}C): δ = 164.77 (C), 156.10 (C), 154.73 (C), 152.79 (C), 152.66 (C), 152.04 (C), 146.53 (CH), 146.21 (C), 126.38 (CH), 123.55 (CH), 96.28 (CH), 86.32 (C), 84.88 (C), 82.38 (C), 76.62 (CH), 73.79 (CH), 68.06 (CH_2), 28.66 (CH_3), 28.06 (CH_3) ppm. Mass: ESI-MS (*m/z)* Calcd. for $C_{26}H_{30}F_2N_4O_{12}$: 628.18, found: 629.93 $[M+H]^+$.

H-NMR of **2b** (400 MHz, DMSO-d_6, 25^{o}C): δ = 10.64 (s, 1 H), 8.40 (d, J = 9.15 Hz, 2 H), 8.08 (d, J = 7.7 Hz, 1 H), 7.68 (d, J = 9.15 Hz, 2 H), 7.13 (d, J = 7.65 Hz, 1 H), 6.40 (t, J = 8.56 Hz, 1 H), 5.56 (m, 1 H), 4.66 - 4.58 (m, 2 H), 4.49 - 4.44 (m, 1 H), 1.50 (s, 9 H), 1.46 (s, 9 H) ppm; ^{13}C-NMR (400 MHz, DMSO-d_6, 25^{o}C): δ = 164.80 (C), 155.73 (C), 154.73 (C), 153.44 (C), 152.78 (C), 151.66 (C), 146.42 (CH), 126.48 (CH), 123.36 (CH), 96.22 (CH), 86.06 (CH), 83.14 (C), 82.36 (C), 76.68 (CH), 75.51 (CH), 64.0 (CH_2), 28.65 (CH_3), 28.20 (CH_3) ppm; Mass: ESI- MS (*m/z)* Calcd. for $C_{26}H_{30}F_2N_4O_{12}$: 628.18, found: 629.87 $[M+H]^+$.

Synthesis of 2G$_1$/2G$_2$: DIPEA (8.34 µL, 0.047 mmol) was added to the solution of [D-Lys]^6-GnRH (20 mg, 0.015 mmol) in anhydrous DMF (2 mL) under inert atmosphere at ice cooling. After 5 min a solution of **2a/2b** (10 mg, 0.015 mmol) in anhydrous DMF (1 mL) was added drop wise and the resulting mixture was stirred at rt overnight (12 h). The

reaction was monitored with TLC in 10% acetone in DCM to investigate the gemcitabine and in order to track the peptide we used a solution of nBuOH/AcOH/H_2O, 6/2/2, v/v. The solvent was removed under high vacuum and the residue was washed with acetonitrile (2 mL X 2) to give a white solid This crude compound was dissolved in 3 mL (TFA/TIS/ H_2O, 9.5/0.25/0.25, v/v) cleavage cocktail at ice cooling under stirring which was continued for 12 h at rt. The solvent was evaporated, azeotrop with DCM/Hexane (1:1, v/v), the residue was washed with cold diethyl ether (2 mL X 3). The compound was purified with semi preparative HPLC (90/10 to 70/30, ACN/H_2O) for 50 min. The pure fraction was lyophilized to give a white solid compound.**2G$_1$** (12.5 mg, 50.81%); **2G$_2$** (12 mg, 48.78%).

Mass 2G$_1$: ESI-MS (*m/z*): $[M+2H]^{2+}$ calcd. for $C_{69}H_{93}F_2N_4O_{18}$, 771.85; found 771.9, $[M+3H]^{3+}$calcd. 514.9; found 514.9.

Mass 2G$_2$: ESI-MS (*m/z*): $[M+2H]^{2+}$ calcd. for $C_{69}H_{93}F_2N_4O_{18}$, 771.85; found 771.8, $[M+3H]^{3+}$calcd. 514.9; found 514.9.

2.4.2.2 Biological evaluation:

Note: *In forthcoming bilogical evaluation of carbamate conjugates (2G$_1$ and 2G$_2$), we have included GSHG (from section 2.2.3 GSHG conjugate bearing a long linker*) *for comparitive study of Short and Long linkers in bio-conjugation.*

1) Cell uptake:

Determination of intracellular concentrations of 2G$_1$, 2G$_2$, GSHG: Cells (DU145) were plated in 6-well plates at a density of 2 x 10^6 cells/well. Cells were then incubated either 2G$_1$, 2G$_2$, GSHG (10 μM) for selected time points (0.5 h, 1 h, 4 h, 8 h). Incubations were terminated by removing the medium and washing the cells twice with ice cold PBS to remove unbound molecules. The cells were then lysed by adding an ice cold solution of ACN-Water (3:2) and scraping the cell monolayer. Samples were subsequently vortexed, sonicated and centrifuged for three minutes at 16,060 g (Heraeus Biofuge Pico

microcentrifuge, Thermo Scientific, Bonn, Germany). The supernatants were collected, evaporated and stored at -20°C until the day of analysis. Intracellular accumulation of $2G_1$, $2G_2$, GSHG, gemcitabine and dFdU was determined by LC-MS/MS analysis using a stable internal standard as well as $2G_1$, $2G_2$, GSHG, gemcitabine and dFdU standards for the construction of analytical standard curves.

As it can be observed in the *Figure 30* below, both of the conjugates were detected intracellularly suggesting internalization, most likely through the GnRH-R. $2G_1$ and $2G_2$ showed a higher intracellular concentration over time (AUC = 62.8 ng/ million cells x hr) and AUC = 88.7 ng/ million cells x hr) compared to GSHG (AUC = 38.6 ng/ million cells x hr) probably to its enhanced stability compared to GSHG.

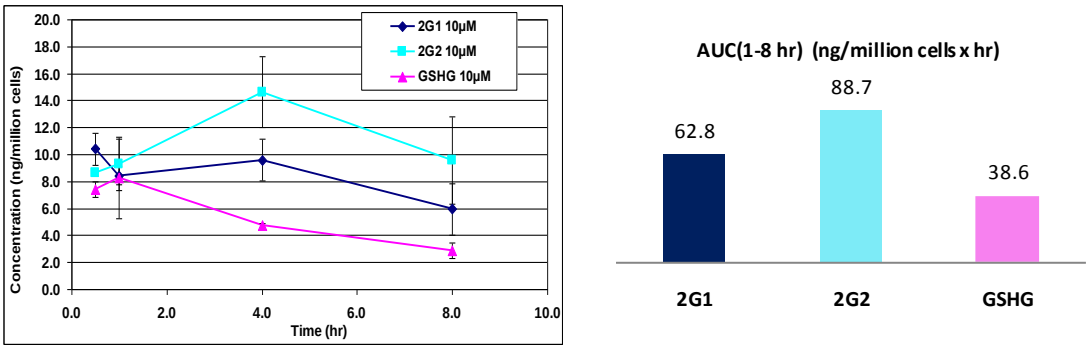

Figure 30: *Intracellular levels of Conjugates ($2G_1$, $2G_2$ and GSHG) over time.*

Regarding intracellular levels of gemcitabine, incubation of $2G_1$ or $2G_2$ did not result in intracellular detection of gemcitabine suggesting that this linkage is most probably very stable and gemcitabine is not released even after 8 h of incubation with this cell culture system. Incubation of GSHG with DU145 cells on the other hand results in increasing levels of gemcitabine over time as seen in the figure below

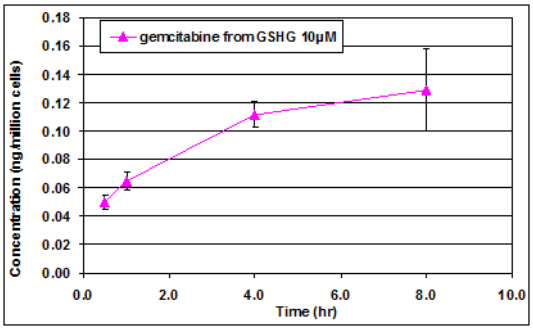

Figure 31: *Intracellular levels of gemcitabine from GSHG.*

Note: Finally, no detectable levels of the inactive metabolite were observed in any of the three incubations (2G$_1$, 2G$_2$, GSHG)

***2) In vitro* cytotoxicity of 2G$_1$, 2G$_2$, GSHG in MCF7 and MDA-MB-231.**

Cells (MDA-MB-231) were plated at a density of 5 x 10^3 cells per well on 96-well plates. After 24 h incubation (37^{o}C, 5% CO_2), the cell medium was removed, and compounds were added at selected concentrations (10-20,000 nM for, GSHG and 500-40,000 nM for 2G$_1$, 2G$_2$), followed by incubation for 72 h. The medium was then removed and the MTT solution (0.3 mg/mL in PBS) was added to cells for 3 h, after which the MTT solution was removed and the formazan crystals were dissolved in 100 µL DMSO. The optical density was measured at 570 nm and a reference wavelength of 690 nm using an absorbance microplate reader. The 50% cytostatic concentration (IC_{50}) was calculated based on a five-parameter logistic equation using SigmaPlot 12 software. Experiments were performed in triplicate. Results are summarized in the table below:

Table 6: *IC_{50} for 2G$_1$, 2G$_2$, GSHG and gemcitabine in MCF7 and MDA-MB-231 cells.*

IC_{50} (nM)	**gemcitabine**	**GSHG**	**2G$_1$**	**2G$_2$**
MCF7	38.0 ± 14.1 (n=3)	55.5 ± 7.2 (n=3)	621.3 ± 113 (n=3)	449.1 ± 87.0 (n=3)
MDA-MB-231	1567 ± 757 (n=5)	2387 ± 1220 (n=3)	>40,000 (n=3)	>40,000 (n=3)

***3) In vitro* stability of 2G$_1$, 2G$_2$, GSHG in human plasma:**

1µM of either 2G$_1$, 2G$_2$, or GSHG were incubated with human plasma. Samples (triplicates of 50 µL) were collected at selected time points (t = 0, 0.08, 0.5, 1, 4 h) and were stored at -80^{o}C after mixing with 150 µL acetonitrile. Samples were then extracted using protein precipitation. The degradation of the tested molecules and the formation of gemcitabine from the conjugates over time are presented below.

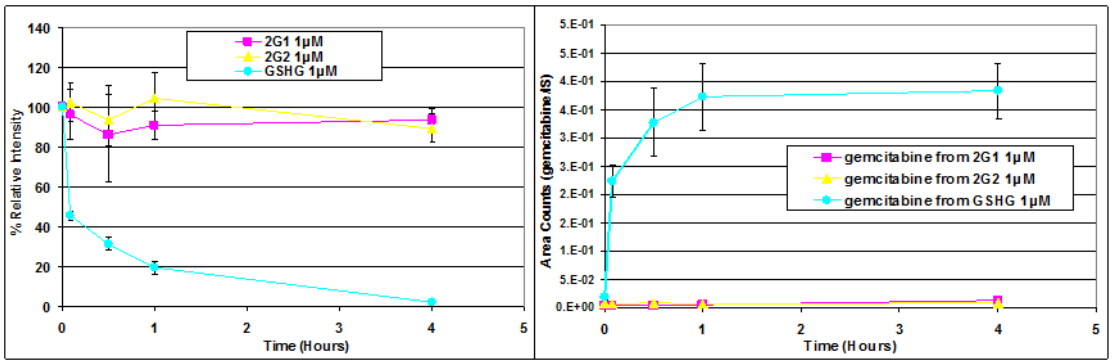

Figure 32: *In vitro stability of $2G_1$, $2G_2$, GSHG in human plasma.*

In order to compare all conjugates tested, they were incorporated in one graph and then classified on the basis of their human plasma stability that is shown in the following *Figure 33*.

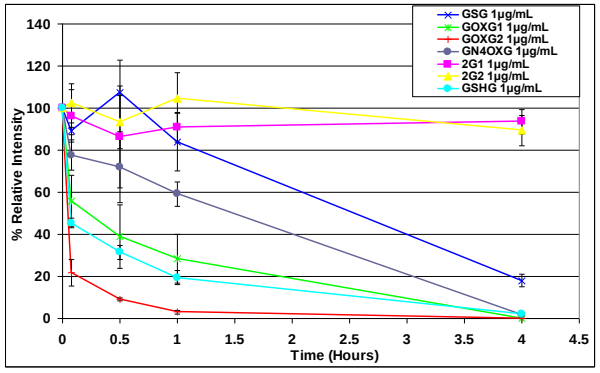

1	$2G_1, 2G_2$
2	GSG
3	GN_4OXG
4	$GOXG_1$, GSHG
5	$GOXG_2$

Figure 33: *Relative stability of all conjugates (Carbonate, Oximes and Carbomates) in human plasma with real time. (**Note:** GSG = GSG_1)*

4) Pharmacokinetics of $2G_1$, $2G_2$ and GSHG.

Animals at the age of 12 weeks were weighed and fasted overnight before dosing (n = 5 per group, male C57BL/6N inbred strain obtained from Charles River, Calco, Italy). Dosing solutions of GnRH conjugates (10 mg/kg or 6.3 µmol/kg) in saline were administered intraperitoneally (IP). A serial tail bleeding protocol was used for the collection of blood samples. Blood samples (10 µL) were collected at selected time points (0.25 h, 0.5 h, 1 h, 2 h, 4 h, 6 h, 8 h) in tubes containing 40 µL citric acid (0.1 M, pH 4.5)

and stored at -80°C until sample extraction. Samples were prepared for quantification by protein precipitation and evaporation. $2G_1$, $2G_2$, gemcitabine and dFdU were quantified by LC-MS/MS analysis. No detectable levels of the inactive metabolite were observed in $2G_1$ or $2G_2$ samples

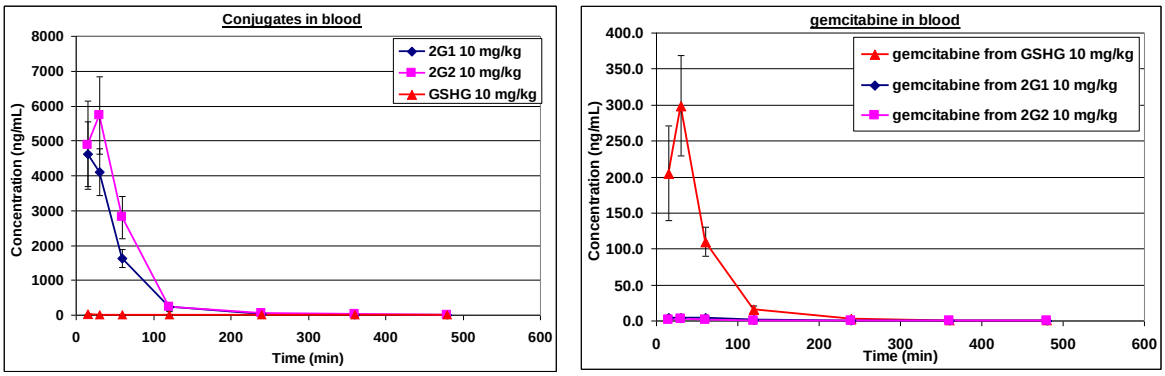

Figure 34: *Blood levels of $2G_1$, $2G_2$ and GSHG and gemcitabine after administration of $2G_1$ $2G_2$ or GSHG.*

In the following *Figure 35* the pharmacokinetic data of $2G_1$ and $2G_2$ are compared with GSG which had been so far the best bioavailability as compared to the other tested conjugates ($3G_2$, $3G_1$).

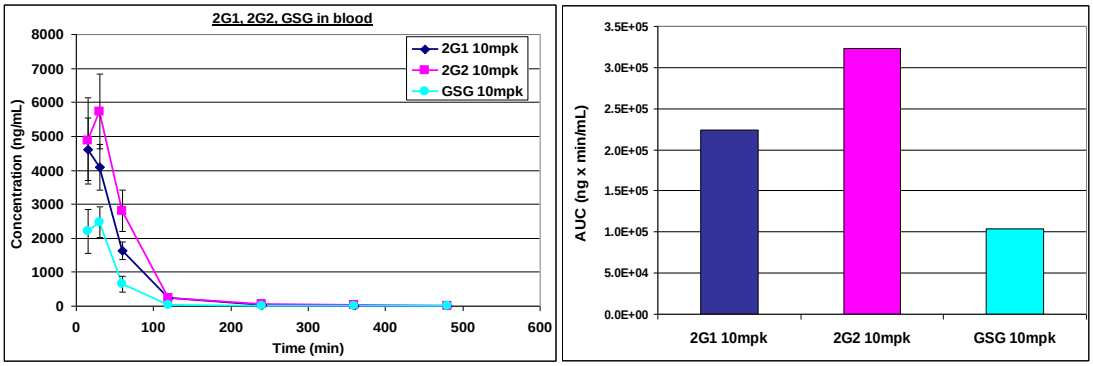

Figure 35: *Blood levels and AUCs of $2G_1$, $2G_2$, GSG. (**Note:** GSG = GSG_1)*

2.4.3 Carbamate bond formation at Gemcitabine's amine (4-NH_2) group using Chloroformates.

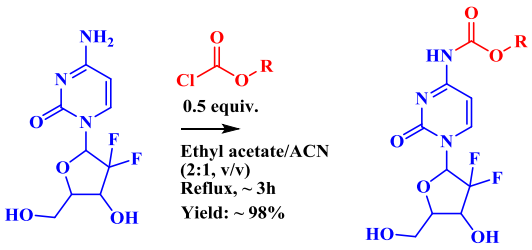

Significant characteristics of our methodology

- Rapid, single step slective carbamate of Gemcitabine at 4-NH.
- Quantitative and qualitative synthesis of gemcitabine prodrug.
- Combination of solvents and stoichiometric ratio of starting materials useful for skipping purification step. Ehtyl acetate and Acetonitrile (2:1, v/v).
- Low reaction cost and simple synthetic procedure.

2.4.3.1 Design, synthesis and characterization:

As we mentioned Gemcitabine is the first line chemotherepatic drug being used in numerous cancers, though its extreme cytotoxicity and intrcellular conversion into the inactive metabolite 2', 2'-difluorodeoxyuridine (dFdU) restricts its exploration as a very effective anticancer drug. This deamination does not allow its enzymatic recognition and conversion to the active phospholyrated analogues that are ready available for incorporation to the DNA and thus are inactivated.[28] To overcome these it is needed to construct Gemcitabine prodrugs that will be prior release of the active parent compound less cytotoxic, less hydrophilic and will eliminate the formation of the inactive metabolite dFdU. A strategy could be to occupy Gemcitabine's 5'-OH (where the phosphorylation takes place) and 4-NH_2 (where deamination happens) through alkylation or acylation to carbonate and carbamate (or amide) respectively.[28] In the former subschapters we discussed about the effect of carbonate bond at the 5'-OH and 3'-OH groups of gemcitabines via different linkers of different size, and illustrated that the resulted compounds adopted metabolic stability and target drug delivery.[18] In the earlier research *Jason T. Weiss et.al*.[28] highlighted the biological activities of different analogues having modification, with a carbamate bond, at the 4-NH_2 and 5'-OH of Gemcitabine. It was concluded that the analogues of gemcitabine bearing carbamate bond at the 4-NH_2 had 23 fold less cytotoxic activity than those that were modified with carbamate bond at the 5'-OH in pancreatic cell lines.[28] We therefore focused on the regioselective modification of the 4-NH_2 of Gemcitabine.

There are many different way to have chemical reaction at 4-NH_2; such as alkylation, acylation[37] (amide and carbamates). But the synthesised prodrugs must get hydrolyse in tumour cell (acidic pH)[31] to release gemcitabine. The 4-N-alkyl derivatives neither were deaminated into dFdU nor got hydrolysed in to Gemcitabine, where 4-N-amide derivative slowly got hydrolysed and simultaneously deaminated.[37]

The carbamate functional group can be easily hydrolyzed with respect to the amide bond,[80] thus carbamate prodrugs could be hydrolysed at the acidic pH of cancer cells[31] and release the parent active compound (gemcitabine). This strategy could surmount from the traditionally requested high dose of gemcitabine and avoid the toxicity to normal cells. Herein, we took efforts to establish a synthetic method for carbamate derivatives of gemcitabine using different chloroformates.

The acylation of gemcitabine at its 4-NH_2 position has been extensively studied by many groups.[37, 81, 35] Acylation (carbamate bond formation) with chloroformates has been reported but using different methods. As per our best knowledge the latest related research is by *Jason T. Weiss et. al.*.[28] This group achieved a selective one step acylation of gemcitabine with chloroformates at the 5'-OH position in the presence of 1,8-Diazabicyclo[5,4,0]undec-7-ene (DBU). For the 4-NH_2 carbamates they had gone through the protection/deprotection (TBS) of 5' and 3' hydroxyl group; finally, after following this long process they obtained a reduced overall reaction yield. Furthermore, a US patent[35] has reported synthesis of similar gemcitabine prodrugs, but that synthetic method had limitations such as lack of selectivity to the 4-NH_2 amine and HPLC was requested for purification, it was time consuming and complicated procedure, requiring also stoichiometric excess of reagents and resulted at low reaction yield.

Herein, we established a new method for selective Gemcitabine 4-N-acylation. This is performed in a single quantitative step. Gemcitabine (dFdC) is refluxed with different chloroformates in ethyl acetate/acetonitrile (2:1, v/v) solution for 3 h. Acylation was achieved selectively at the 4-NH_2 of gemcitabine without any protection of primary (5'-OH) and secondary (3'-OH) hydroxyl groups. The combination of reaction solvents and stoichiometric ratio of starting materials are useful for skipping purification step. These gemcitabine prodrugs may reduce the intracellular deamination and subsequently minimize 2', 2'-difluorodeoxyuridine (dFdU) level. Different functionalities at 4-NH_2 (from chloroformates) are useful for bio orthogonal coupling, conjugation and transportation of gemcitabine into the biological systems.

We are the first one to synthesise this gemcitabine prodrug in high selectivity, one step, rapid, with high purity, almost 100% yield and with simple synthetic procedure. Acylation with chloroformates selectively goes to aromatic amine in presence of aromatic hydroxyl group for the case of 3-aminophenol however, it lacked the presence of primary and secondary alcohols like gemcitabine and this was not explored.[82] This report supports our new method of Gemcitabine 4-NH acylation. We used a two molar ratio of gemcitabine with respect to the chloroformates. This molar ratio played a vital role in purification, since, one mole of gemcitabine reacted with the chloroformate and the second mole was utilized to make an HCl salt of gemcitabine as a side product (*Figure 36*). The side product (gemcitabine.HCl) and the desired product (gemcitabine 4-N-acylation) have

completely different solvent solubility and this allowed us to easily separate the pure desired product from the side product (starting material) after a simple filtration.[81] Specifically, the desired product is soluble in the reaction solvent (ethyl acetate/acetonitrile, 2/1, v/v), whereas the resulted gemcitabine.HCl is precipited out and thus after filtering the reaction mixture we were able to get almost 100% pure compounds.

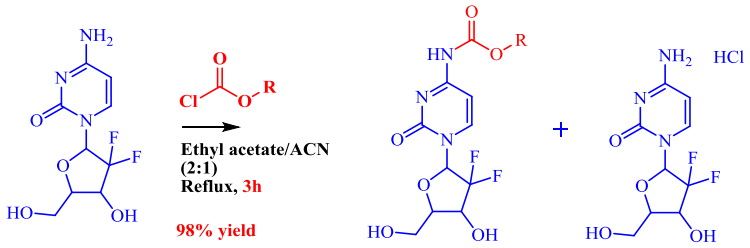

Figure 36: *Chemical synthesis of N-acyl gemcitabine.*

Table 7: *Derivatives of Gemcitabine prodrug and reaction conditions.*

Sr. No.	***R***	***Reaction time***	***% yield***	
1		3 h	98.31%	
2	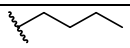	3 h	98.20%	
3		2 h	76.44% *Column purification*	
4	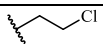 **(*Figure 2*)**	3 h	76.44% *Column purification*	4A = 100%
		12 h	*84.98%*	*4A = 74.55%*
				4B = 25.45%
		40 h	*84.98%*	*4A = 10%*
				4B = 90%
	4A  **4B**	2 h	99.71%	

5		3 h	89.25%
		12 h	98.78%
6	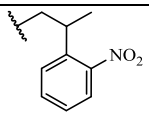	3 h	98.50%
7	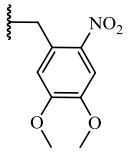	3 h	71.10% (After water workup.)

For all Gemcitabine prodrugs the reaction was almost completed in 3 h. Interesting thing to note was the case of compound **4** for which we found that the reaction was not completed in expected time, and thus we continued the reaction for 12 h and then for 40 h, respectively; we found that during this extended period of time, an additional product was formed **4B** in addition to the expected product **4A**. **4B** came after intramolecular cyclisation of **4A** and was specifically formed after dehydrohalogenation to produce a favourable five membered ring. Intramolecular cyclization was happened in refluxed temperature and also could be boost (2 h) by the addition of the base DIPEA (*Figure 37*). These two derivatives (**4A** and **4B**) of compound **4** were purified by silica gel column chromatography in acetone/DCM as a solvents and confirmed by NMR assignment, (disappearance of 7-NH amide singlet from δ = 11.03 ppm; a change in the chemical shifts of 5-H and 11-H (*Figure 39*) were significant evidences in favour of **4B**).

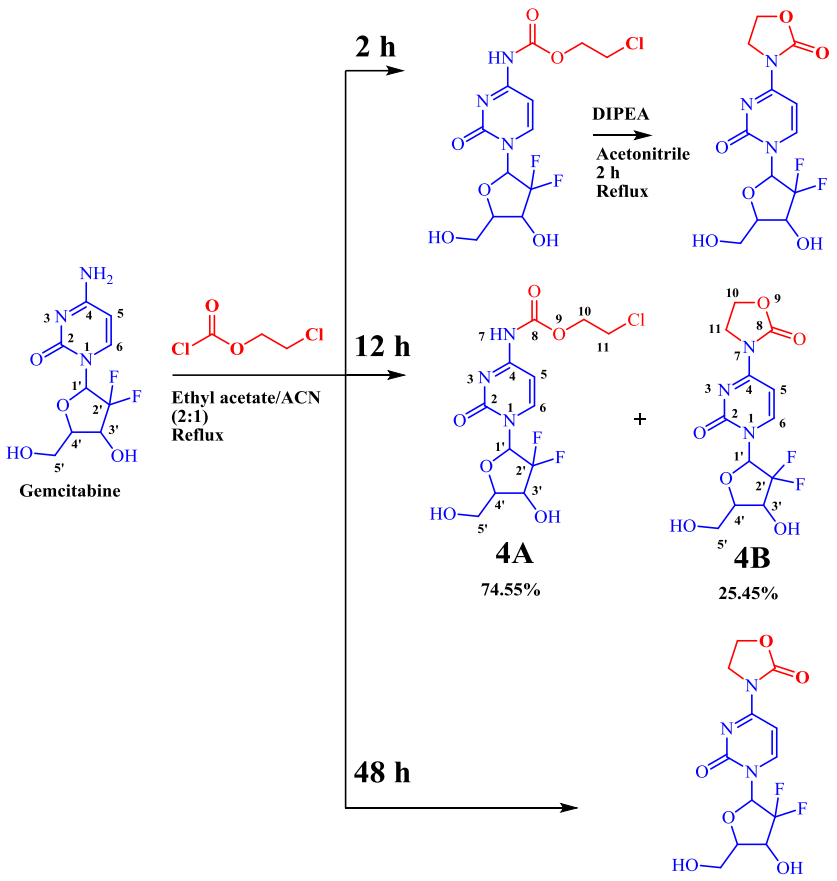

Figure 37: *Intramolecular cyclisation of compound* ***4.***

To further probe the fact that the cyclization takes place in these analogues we performed a reaction with compound **3** which resulted only in the desired and un-cyclized compound. This was expected since a potential cyclized side product was unfavorable, due to ring strain, four carbon ring.

Below we have presented NMR and MS characterization of the Ethyl-(4-N-gemcitabine) carbamate 1 as also of:

a) By NMR:

Characterization of **1** was performed by ^{1}H and ^{13}C correlation in 2D NMR. Following *Figure 38-A* is overlap of ^{1}H NMR of gemcitabine and **1**. In ^{1}H NMR **1** shows new peaks triplet at 1.26 (t, J = 7.0 Hz, 3 H, 11-H) ppm and quarted at 4.20 (q, J = 7.1 Hz, 7.0 Hz, 2 H, 10-H) ppm suggest acylation happen at gemcitabine. Same time 4-NH_2 of

gemcitabine 7.4 (d, J = 14 Hz, 2 H) disappeared to give amide, it showed new peak at 10.86 (s, 1 H, 7 NH). Influence of new acyl group was significant on 5-H as expected.

All these characteristic changes in ^{1}H NMR of **1** were confirmed by HMBC and HSQC (*Figure 38-B*). The new acyl carbonyl carbon (C8) shows cross peak with 7-NH and & 7-NH shows cross peak with C4 and C5. These results are in favour of expected structure of **1**.

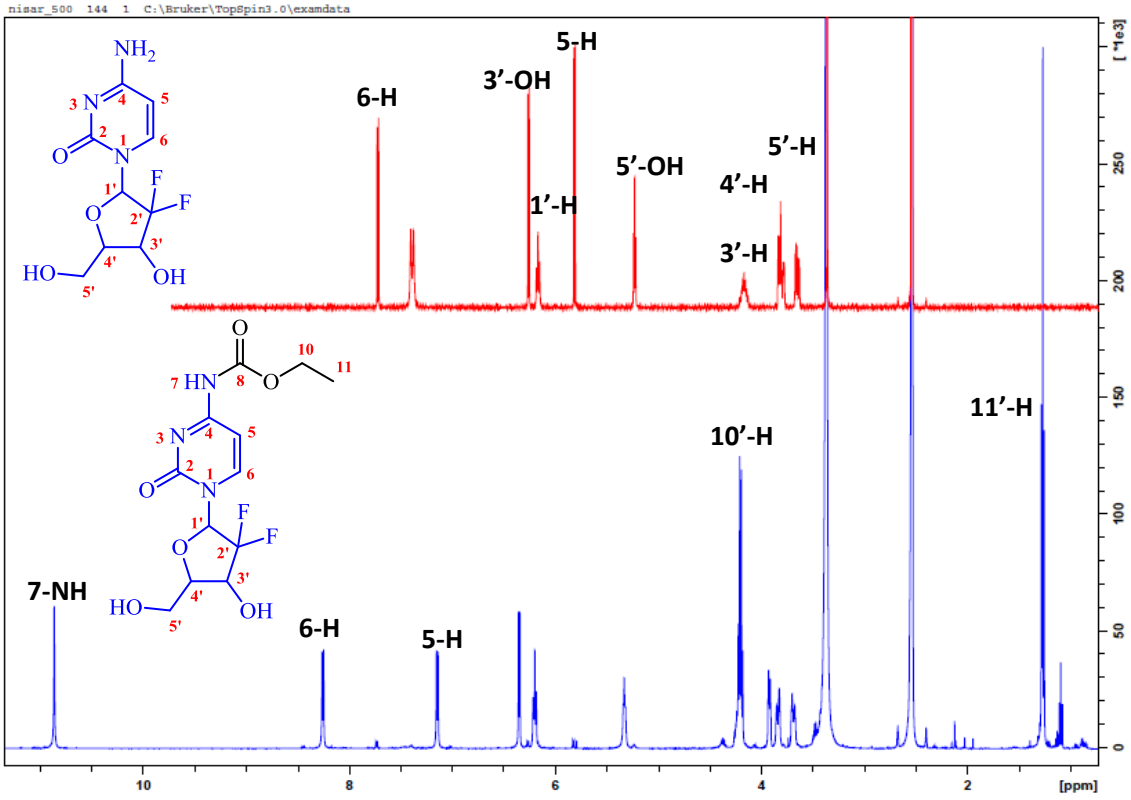

Figure 38-A: *^{1}H NMR (DMSO d_6) Overlap of Gemcitabine and* Ethyl-(4-N-gemcitabine) carbamate *at 500MHz, 298K, B): 2D NMR (HMBC, HSQC) at 500MHz, 298K.*

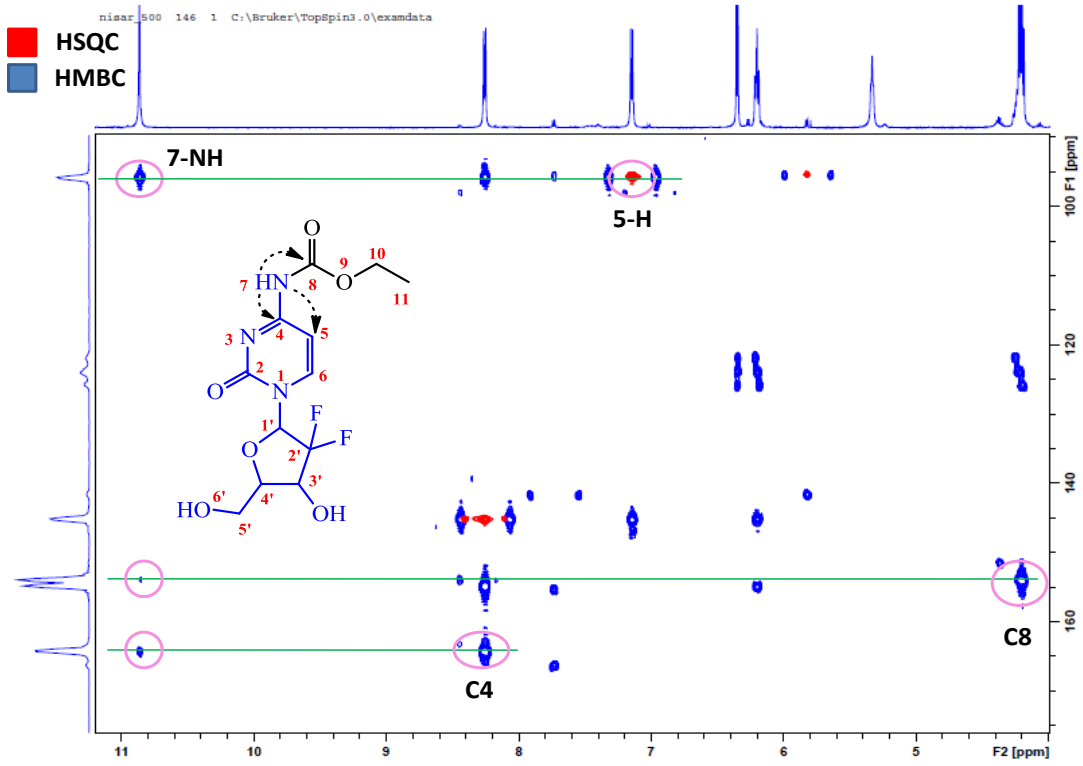

Figure 38-B: *2D NMR (HMBC, HSQC) at 500MHz, 298K.*

.

Following *Figure 39* clearly shows the cyclisation of **4A** into **4B** occurs in long reaction time. The most significant changes that we can see is 7-NH proton disappered and a small shifting of neighbouring proton from the reaction site occured. e.g. as 5-H and 11-H.

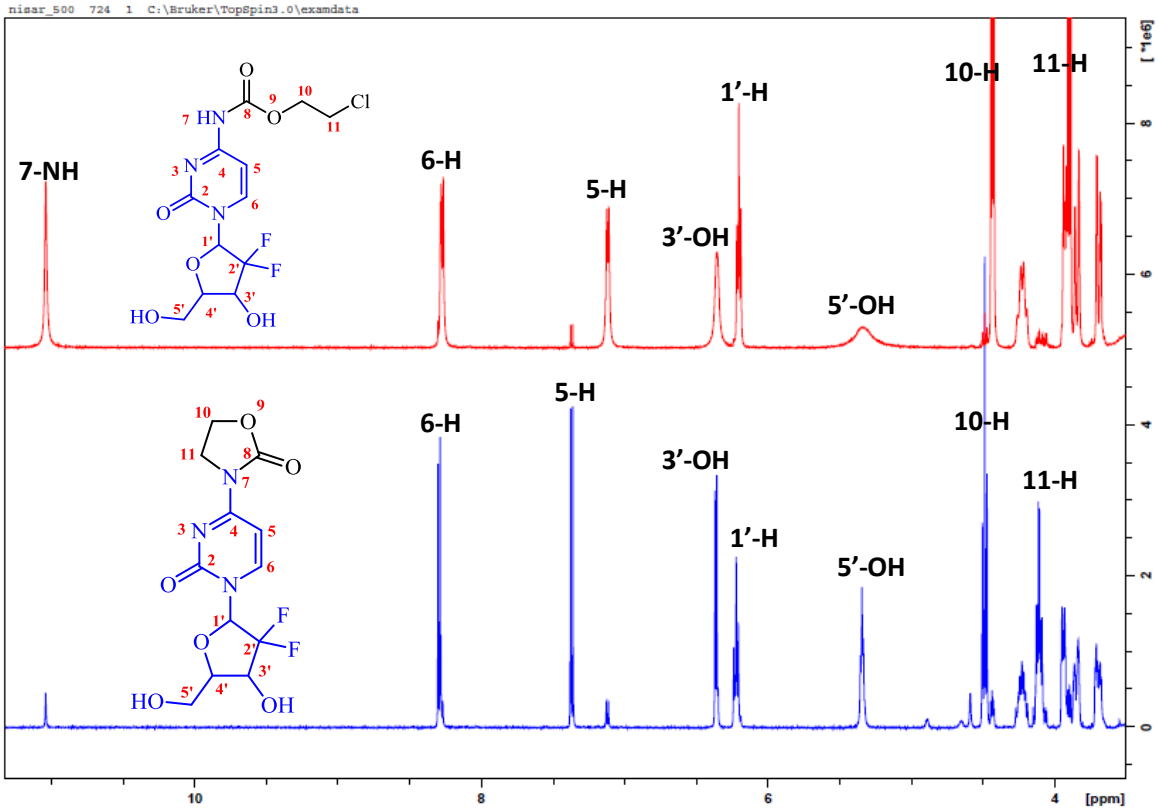

Figure 39: *^{1}H NMR overlaps of **4A** and **4B**.*

b) By Mass:

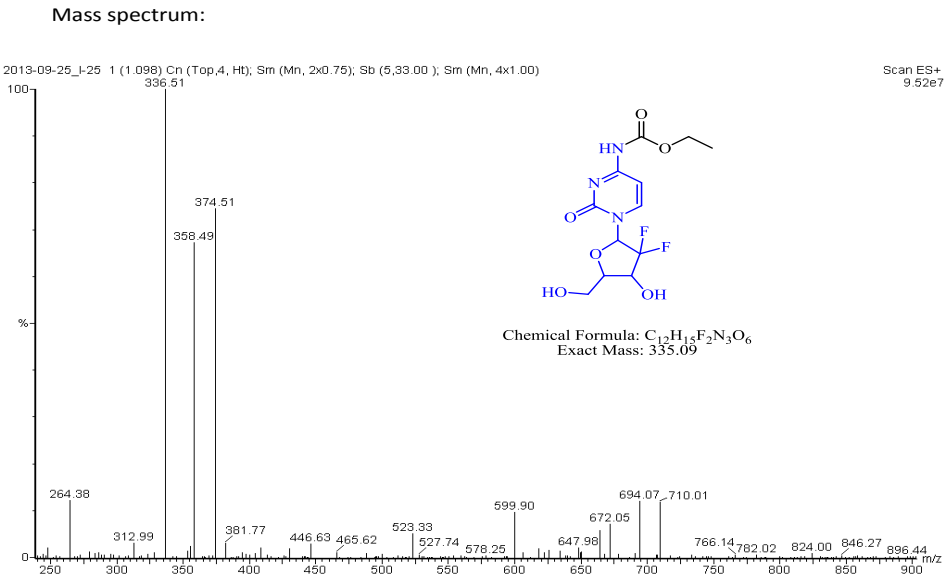

Figure 40: *Mass of Ethyl-(4-N-gemcitabine) carbamate in (0.1 mg in 1 mL 0.1% formic acid in methanol).*

General synthetic procedure for gemcitabine N-acylation:

Under nitrogen atmosphere, the solution of Gemcitabine **(**30 mg, 0.114 mmol) in 15 mL solution of ethyl acetate/acetonitrile (2:1, v/v) was refluxed for 1 h (*Observation:* Gemcitabine gets soluble and reaction mixture becomes almost clear). Ethylchloroformate (5.44 µL, 0.057 mmol) was added and continue reflux. Reaction progress was monitored with TLC (DCM/acetone/ethanol, 5/5/0.5, v/v). After 3 h the reaction mixture was filtered through filter paper, the filtrate was concentrated and dried under high vacuum, to give **1** (14.6 mg, 98.31%) as a white solid. The other chloroformates were synthesized accordingly.

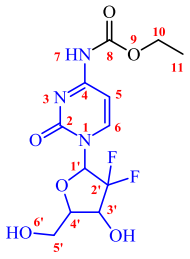

1

Ethyl-(4-N-gemcitabine) carbamate 1:

^{1}H-NMR of **1** (500 MHz, DMSO-d$_6$, 25^{o}C): δ = 10.86 (s, 1 H, 7 NH), 8.25 (d, J = 7.5 Hz, 1 H, 6-H), 7.14 (d, J = 7.5 Hz, 1 H, 5-H), 6.34 (d, J = 6.5 Hz, 1 H, 3'-OH), 6.19 (t, J = 7.5 Hz, 1 H, 1'-H), 5.32 (t, J = 4.5 Hz, 1 H, 5'-OH), 4.22 (m, 1 H, 3'-H), 4.20 (q, J = 7.1 Hz, 7.0 Hz, 2 H, 10-H), 3.92 (m,1 H, 4´-H), 3.83 (d, J = 12.3 Hz, 1 H, 5´a-H), 3.68 (m, 1 H, 5'b-H) 1.26 (t, J = 7.0Hz, 3 H, 11-H) ppm; ^{13}C-NMR (500 MHz, DMSO-d$_6$, 25^{o}C): δ = 164.3 (C4), 154.99 (C2), 154.04 (C8), 145.19 (C6), 123.86 (C2'), 95.63 (C5), 84.86 (C1'), 81.73 (C4'), 69.14 (C3'), 62.22 (C10), 59.6 (C5'), 15.01 (C11) ppm; Mass: MS (ESI^{+}) *m/z*: [M+H]$^{+}$ for $C_{12}H_{15}F_2N_3O_6$: calcd, 335.09; found, 336.51, [M+Na]$^{+}$ for $C_{12}H_{15}F_2N_3O_6Na$: calcd, 357.49; found, 358.49, [M+K]$^{+}$ for $C_{12}H_{15}F_2N_3O_6K$: calcd, 373.09; found, 374.51.

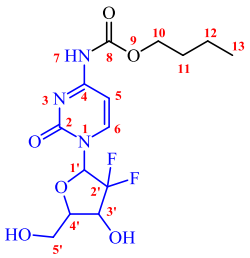

2

n-Butyl-(4-N-gemcitabine) carbamate 2:

^{1}H-NMR of **2** (500 MHz, DMSO-d_6, 25^{o}C): δ = 10.85 (s, 1 H, 7-NH), 8.25 (d, J = 7.65 Hz, 1 H, 6-H), 7.13 (d, J = 7.65 Hz, 1 H, 5-H), 6.34 (d, J = 6.50 Hz, 1 H, 3'-OH), 6.19 (t, J = 7.50 Hz, 1 H, 1'-H), 5.32 (t, J = 5.50 Hz, 1 H, 5'-OH), 4.22 (m, 1 H, 3'-H), 4.15 (t, J = 6.60 Hz, 2 H, 10-H), 3.91 (m, 1 H, 4´-H), 3.83 (m, 1 H, 5´a-H), 3.68 (m, 1 H, 5'b-H) 1.62 (m, 2 H, 11-H), 1.39 (m, 2 H, 12-H), 0.94 (t, J = 7.35 Hz, 3 H, 13-H) ppm; ^{13}C-NMR (500 MHz, DMSO-d_6, 25^{o}C): δ = 164.38 (C4), 154.88 (C2), 154.18 (C8), 145.33 (C6), 123.9 (C2'), 95.55 (C5), 84.76 (C1'), 81.65 (C4'), 69.09 (C3'), 65.75 (C10), 59.48 (C5'), 30.94 (C11), 19.14 (C12), 14.16 (C13) ppm.

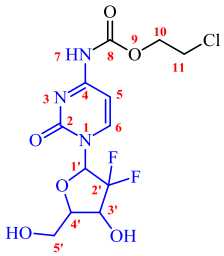

4A

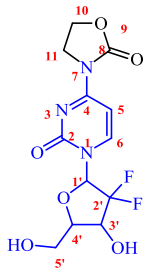

4B

^{1}H-NMR of **4A** (500 MHz, DMSO-d_6, 25^{o}C): δ = 11.03 (s, 1 H, 7-NH), 8.27 (d, J = 7.70 Hz, 1 H, 6-H), 7.11 (d, J = 7.70 Hz, 1 H, 5-H), 6.20 (t, J = 7.60 Hz, 1 H, 1'-H), 4.43 (t, J = 5.30 Hz, 2 H, 10-H), 4.22 (m, 1 H, 3'-H), 3.92 (m, 1 H, 4´-H), 3.89 (t, J = 5.30 Hz, 2 H, 11-H), 3.84 (m, 1 H, 5'a-H), 3.69 (m, 1 H, 5'b-H) ppm; ^{13}C-NMR (500 MHz, DMSO-d_6, 25^{o}C): δ = 164.3 (C4), 154.82 (C2), 153.68 (C8), 145.5 (C6), 129.89 (C2'), 95.64 (C5), 84.79 (C1'), 81.68 (C4'), 69.03 (C3'), 65.93 (C10), 59.45 (C5'), 43.16 (C11) ppm.

^{1}H-NMR of **4B** (500 MHz, DMSO-d$_6$, 25^{o}C): δ = 8.29 (d, J = 7.70 Hz, 1 H, 6-H), 7.36 (d, J = 7.70 Hz, 1 H, 5-H), 6.22 (t, J = 7.60 Hz, 1 H, 1'-H), 4.48 (t, J = 8.0 Hz, 2 H, 10-H), 4.22 (m, 1 H, 3'-H), 4.10 (m, 2 H, 11-H), 3.92 (m, 1 H, 4'-H), 3.84 (m, 1 H, 5'a-H), 3.69 (m, 1 H, 5'b-H) ppm; ^{13}C-NMR (500 MHz, DMSO-d$_6$, 25^{o}C): δ = 162.0 (C4), 155.03 (C8), 154.82 (C2), 144.45 (C6), 123.89 (C2'), 95.64 (C5), 84.79 (C1'), 81.68 (C4'), 69.03 (C3'), 63.37 (C10), 59.45 (C5'), 42.20 (C11) ppm.

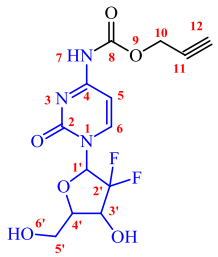

5

^{1}H-NMR of **5** (500 MHz, DMSO-d$_6$, 25^{o}C): δ = 11.10 (s, 1 H, 7-NH), 8.28 (d, J = 7.6 Hz, 1 H, 6-H), 7.11 (d, J = 7.6 Hz, 1 H, 5-H), 6.20 (t, J = 7.4 Hz, 1 H, 1'-H), 4.83 (d, J = 2.35 Hz, 2 H, 10-H), 4.22 (m, 1 H, 3'-H), 3.92 (m, 1 H, 4′-H), 3.84 (m, 1 H, 5′a-H), 3.69 (m, 1 H, 5'b-H) 3.65 (t, J = 2.35 Hz, 1 H, 12-H) ppm; ^{13}C-NMR (500 MHz, DMSO-d$_6$, 25^{o}C): δ = 164.20 (C4), 154.81 (C2), 153.31 (C8), 145.95 (C6), 123.93 (C2'), 95.53 (C5), 84.83 (C1'), 81.68 (C4'), 79.17 (C11), 78.91 (C12), 69.05 (C3'), 59.45 (C5') ppm.

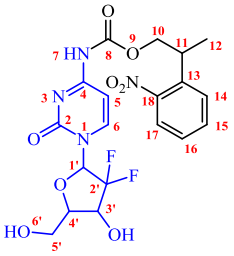

6

^{1}H-NMR of **6** (500 MHz, DMSO-d$_6$, 25^{o}C): δ = 10.89 (s, 1 H, 7-NH), 8.23 (d, J = 7.65 Hz, 1 H, 6-H), 7.87 (d, J = 7.75 Hz, 1 H, 14-H), 7.81 (d, J = 7.75 Hz, 1 H, 17-H), 7.72 (t, J = 7.75 Hz, 1 H, 15-H), 7.52 (t, J = 7.75 Hz, 1 H, 16-H), 7.03 (m, 1 H, 5-H), 6.19 (t, J = 7.50 Hz, 1 H, 1'-H), 4.36 (m, 2 H, 10-H), 4.22 (m, 1 H, 3'-H), 3.91 (m, 1 H, 4′-H), 3.83 (m, 1

H, 5´a-H), 3.68 (m, 1 H, 5'b-H) 3.54 (m, 1 H, 11-H), 1.35 (d, J = 7.0 Hz, 3 H, 12-H) ppm; ^{13}C-NMR (500 MHz, DMSO-d_6, 25°C): δ = 164.17 (C4), 154.78 (C2), 153.86 (C8), 150 (C18), 145.33 (C6), 137.31 (C13), 133.71 (C15), 129.75 (C17), 128.61 (C16), 124.46 (C14), 123.74 (C2'), 95.53 (C5), 84.80 (C1'), 81.68 (C4'), 69.47 (C10), 69.05 (C3'), 59.47 (C5'), 33.61 (C11), 18.49 (C12) ppm.

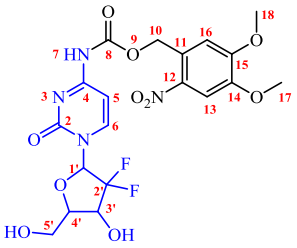

7

^{1}H-NMR of **7** (500 MHz, DMSO-d_6, 25°C): δ = 11.30 (s, 1 H, 7-NH), 8.30 (d, J = 7.55 Hz, 1 H, 6-H), 7.78 (s, 1 H, 13-H), 7.44 (s, 1 H, 16-H), 7.17 (d, J = 7.55 Hz, 1 H, 5-H), 6.35 (d, J = 6.32 Hz, 1 H, 3'-OH), 6.21 (t, J = 7.50 Hz, 1 H, 1'-H), 5.55 (s, 2 H, 10-H), 5.33 (t, J = 5 Hz, 1 H, 5'-OH), 4.23 (m, 1 H, 3'-H), 3.99 (s, 3 H, 18-H), 3.93 (m, 1 H, 4'-H), 3.92 (s, 3 H, 17-H), 3.84 (m, 1 H, 5´a-H), 3.69 (m, 1 H, 5'b-H) ppm; ^{13}C-NMR (500 MHz, DMSO-d_6, 25°C): δ = 164.26 (C4), 154.8 (C2), 154.52 (C15), 153.42 (C8), 148.64 (C14), 145.51 (C6), 139.84 (C12), 127.52 (C11), 123.9 (C2'), 111.04 (C16), 108.78 (C13), 95.42 (C5), 84.77 (C1'), 81.68 (C4'), 69.06 (C3'), 64.55 (C10), 59.45 (C5'), 57.18 (C18), 56.75 (C17) ppm.

2.4.3.2 Application of N-acyl gemcitabine prodrugs:

The different resulted Gemcitabine N-acyl prodrugs have a high potential to be used in a) bio-conjugation, b) cellular imaging and c) photocaging for photon controlled drug release. These different directions are mentioned briefly below:

1) Bioconjugation:

In targeted drug delivery conjugation of carrier and drug are possible via thioether or ether bond. Carrier may be peptides, ligands or enzymes should carry unprotected sulfur or hydroxyl functionality. Nucleophilic substitution reaction can be performed in presence of mild base or even in absence of base if compounds are thermodynamically stable enough.

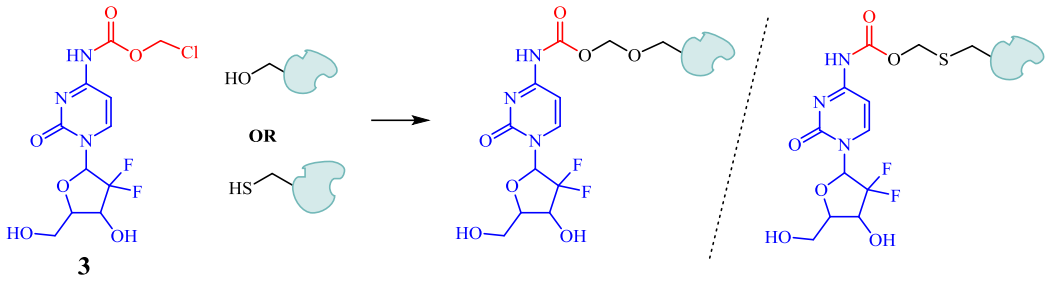

Figure 41: *The possible bio-conjugation of gemcitabine derivatives.*

2) Imaging and subcellular localization:

The established protocol to rapidly construct, via chloroformates, N-acyl derivatives of gemcitabine allowed us to construct a tharanaustic agent (bearing a therapeutic (gemcitabine) and a diagnostic functional group (coumarin)) shown in *Figure 42.*

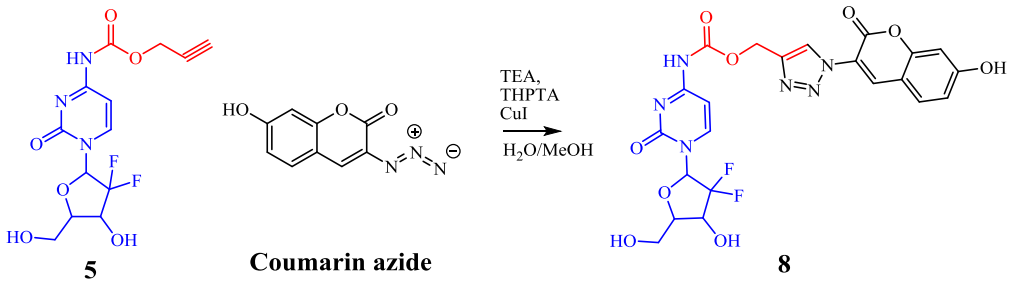

Figure 42: *Molecular hybrid **8** from **5** (alkyne drivative of gemcitabine) and coumarine azide by click reaction.*

In cell uptake or imaging studies the relevant prodrug would be of great importance to indicate the mode of cellular uptake of the prodrug (since it is equipped with a fluorophore). This simple and rapid chemoselective click reaction between the alkyne

group of the gemcitabine intermediate **5** and any azide from any chromophore enables the attachement of any chromophore or biomolecule in gemcitabine.

General procedure for the click reaction:

Gemcitabine-alkyne (5 mg, 14.48 μM), coumarine azide (2.94 mg, 14.48 μM), triethyl amine (2 μL, 5%), CuI (0.1 mg, 1%), Tris(3-hydroxypropyltriazolylmethyl)amine (THPTA) were dissolved in 1 mL solution of methanol/H_2O (2:1), overnight on rt. Solvent was evaporated in rotary evaporator, the residue was washed with diethyl ether several times, to give **8** (6 mg, 75.55%) as a brown solid.

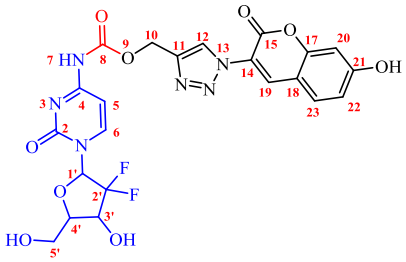

8

^{1}H-NMR of **8** (500 MHz, DMSO-d_6, 25ºC): δ = 11.03 (s, 1 H, 7-NH), 8.68 (s, 1 H, 12-H), 8.65 (s, 1 H, 19-H), 8.28 (d, J = 7.60 Hz, 1 H, 6-H), 7.78 (d, J = 8.50 Hz, 1 H, 23-H), 7.15 (d, J = 7.60 Hz, 1 H, 5-H), 6.94 (dd, J = 8.50, 2.20 Hz, 1 H, 22-H), 6.88 (d, J = 2.20 Hz, 1 H, 20-H), 6.35 (d, J = 6.50 Hz, 1 H, 3'-OH), 6.19 (t, J = 7.50 Hz, 1 H, 1'-H), 5.39 (s, 2 H, 10-H), 5.34 (t, J = 5.50 Hz, 5'-OH), 4.22 (m, 1 H, 3'-H), 3.92 (m, 1 H, 4´-H), 3.84 (m, 1 H, 5´a-H), 3.69 (m, 1 H, 5'b-H) ppm; ^{13}C-NMR (500 MHz, DMSO-d_6, 25ºC): δ = 164.30 (C4), 163.58 (C2'), 156.77 (C15), 155.61 (C17), 154.76 (C2), 153.71 (C8), 145.51 (C6), 142.68 (C11), 137.29 (C19), 131.76 (C23), 126.85 (C12), 120.12 (C14), 115.1 (C22), 111.17 (C18), 102.91 (C20), 95.65 (C5), 84.81 (C1'), 81.69 (C4'), 69.07 (C3'), 59.49 (C5'), 58.91 (C10) ppm.

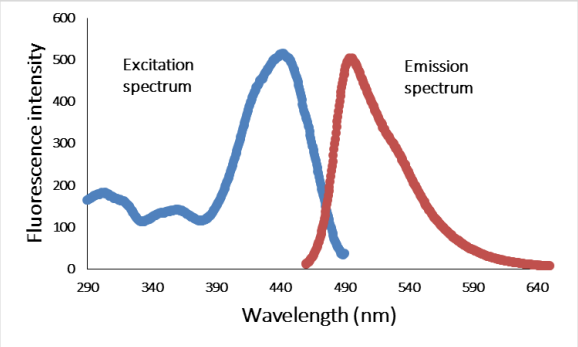

Figure 43: *Gemcitabin-Coumarin absorption and emission spectra*

Above *Figure 43* represents the excitation and emission spectra given by Gemcitabin-Coumarin (**8**) molecular hybrid. Compound **8** was diluted in DMSO and the spectra were performed on a Perkin-Elmer LS-55 spectrofluorometer, using a 1.0 cm Quartz cell (slits = 3 nm). According to the excitation spectrum, the λexc was estimated at 443 nm. Then, the emission was collected upon excitation at 443 nm giving a maximum value at 495 nm.

3) Photon – controlled drug release: A novel photocaged gemcitabine analogue (7):

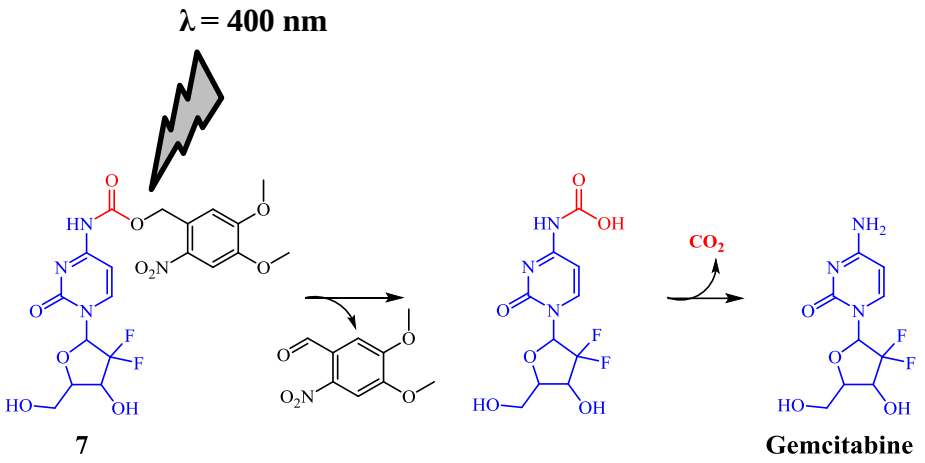

Figure 44: *Photoclevable gemcitabine nalogue (**7**) release gemcitabine after irradiation.*

Photochemistry provides a unique mechanism that enables the active control of drug release in cancer targeting drug delivery. This compound (7) could be investigated for the light-mediated release of gemcitabine, using a photocleavable linker strategy based on o-nitrobenzyl protection.

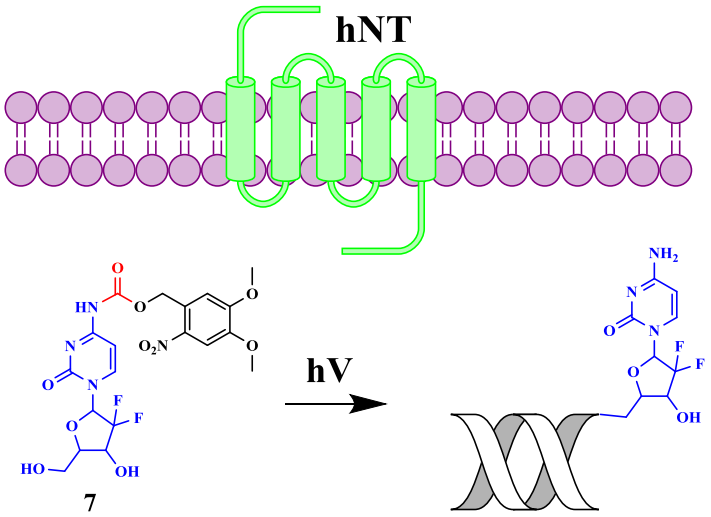

Figure 45: *Compound **7** enters inside the cell through cell membrane by nucleoside transporter and then phoclevage (irradiation cells) of compound **7** gives gemcitabine. Free gemcitabine involved in DNA synthesis, subsequently mask termination resulted apoptosis could happen.*

Photocaging refers to the temporary inactivation of a biologically active molecule using a protective photocleavable group. We used an ortho-nitrobenzyl (ONB)-based photocleavable group at the primary amine of gemcitabine (compound **7**; as described in the above synthesis). Upon UV irradiation of the photocleavable group, the active form of the caged molecule is irreversibly released. Photocaging has been frequently applied in vitro towards the spatiotemporal control of biological processes and the light-triggered payload release from nanoscale materials. This dual mechanism approach to drug delivery (cell targeting and photocontrolled release) could be more effective at enhancing the therapeutic index of an anticancer drug than mechanism alone. We believe that this dual strategy is of particular value for those therapeutic applications that require non-invasive and spatiotemporal drug activation. Future efforts to enhance the scope of potential in vivo applications will focus on investigating the use of longer wavelength light and two-photon excitation. The photocleavage experiments are in process.

2.5 Regioselective Chemical and Rapid Enzymatic Synthesis of a Novel Redox - Antiproliferative Molecular Hybrid between Gemcitabine-Lipoic acid

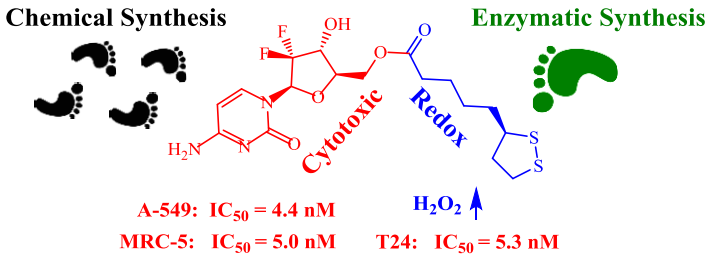

Published:

Sayyad Nisar et al., Regioselective Chemical and Rapid Enzymatic Synthesis of a Novel Redox - Antiproliferative Molecular Hybrid, ***Eur. J. Med. Chem.***, 96:47-57. Apr. 2015.

2.5.1 Introduction

Recent science evidenced the interlinkage of oxidative stress and cancer. Due to the inherent complexity of cancer and its accompanying effect of oxidative stress, novel molecules, containing combinatorial functionalities should be targeted. Herein, we synthesized Gemcitabine-5´-O-lipoate derived from a regioselective coupling of the chemotherapeutic drug Gemcitabine (GEM), a first-line agent for cancer therapy and α-Lipoic acid (LA), a potent antioxidant. Gemcitabine-5´-O-lipoate was obtained in 4 chemical steps. To avoid the tedious and laborious chemical steps we also utilized biocatalysis using immobilized Candida antarctica lipase B (CALB), and the optimum conditions for the regioselective and one-pot synthesis of Gemcitabine-5´-O-lipoate were established by exploiting different solvents (organic solvents and ionic liquids) and enzyme immobilization (acrylic resin and carbon nanotubes). Cytotoxic activity of co-administrating GEM and LA was proven to be synergistic against non-small cell lung cancer cells whereas antagonistic for bladder cancer cells. In contrast, the Gemcitabine-5´-O-lipoate hybrid was found to be superior to the parent compounds against both non-small cell lung cancer and bladder cancer cells were also found to preserve the redox activity of the parent compound LA. The regioselective biotransformation mediated synthesis of the anticancer-antioxidant hybrid illustrates the capacity of biocatalysis to act as an asset in molecular hybridization techniques.

The imbalance between the production of free radicals and reactive oxygen species (ROS) leads to oxidative stress, which affects various signaling pathways in many diseases including cancer. The impact of ROS in cancer includes gene mutations, structural changes in DNA as well as abnormal gene expression, modifications of second-messenger system and blockage of cell- cell communication, depending on the stage of cancer[83]. Since cancer cells are vulnerable to agents that further modulate redox sensitive agents, pro-oxidants emerge as an exciting direction to target tumour cells[84]. Although most studies had focused on the antioxidant activity of bioactive compounds, their pro-oxidant properties, that could mediate specific toxicity against cancer cells due to the low level of antioxidant defenses found in tumours, has been largely omitted[84]. Along these lines there is currently a large array of ongoing clinical trials aiming to exploit novel redox drugs in cancer patients[85]. In the quest to optimize the biological activities of drugs for multifactorial diseases, the

hybrid approach, i.e. to covalently link two distinct potent entities into one molecule, is a promising area and constantly gains ground [86, 87, 18, 88, 89, 90]. As follows, the formulation of a molecular hybrid containing in the same scaffold an anticancer component and an antioxidant/pro-oxidant part, could confer complementary and enhancement biological activity. Thus, we exploited the conjunction of Gemcitabine (GEM) (1) and α-Lipoic acid (LA) (4) in order to produce a hybrid molecule bearing anticancer and antioxidant/pro-oxidant activity. LA (4) is a natural occurring dithiol compound, which is well known as a powerful micronutrient with antioxidant[91, 92] and pro-oxidant properties[93, 94, 95] (*Figure 46*). GEM (1) (2´,2´difluorodeoxycytidine, dFdC, (*Figure 46*) is a synthetic deoxycytidine analogue, with potent anti-tumour activity in various human cancers, such as pancreatic cancer, bladder cancer, breast cancer and non-small cell lung cancer[96, 97], by promoting reduction of neoplastic cell proliferation and apoptosis[98]. It acts as a pro-drug and once it is transported into the cell it is converted to its active form, Gemcitabine triphosphate (dFdCTP), through phosphorylation in its 5´-OH by deoxycytidine kinase. dFdCTP is then incorporated to DNA and causes cell death through inhibition of processes required for DNA synthesis[99]. However, its non-specific toxicity, brief plasma half-life and chemotherapeutic-resistance, acquired i.e. through reduction in the expression of nucleoside transporters responsible for its intracellular uptake, have restricted its utility in clinical oncology. A strategy to reduce its non-specific toxicity as also to surmount deficits in its intracellular uptake in cancer cells could be through its conjugation with LA (4). GEM (1) conjugation to LA (1) should be conducted in a regioselective way and the ideal position will be its 5´-OH, which participates to the phosphorylation leading to its DNA incorporation and cell death[18, 26, 37]. To achieve this synthesis we followed both classical chemical synthesis as also biotransformation-mediated synthesis in an effort to minimize the laborious multistep reactions required to the synthesis of such molecular hybrids. The resulted hybrid molecule, Gemcitabine-5´-O-lipoate (6), was evaluated for its cytotoxic efficacy against two cancer and one normal human cell lines, by measuring cell growth inhibition. In vitro chemosensitivity of the tested cell lines was also evaluated for the isolated chemotherapeutic drug (GEM) (1) and (LA) (4) treating cells either with each compound alone, or in simultaneous and sequential mode of exposure. The combined drug interaction was assessed with the median-effect analysis and the combination index (CI). Gemcitabine-5´-O-lipoate (6) was also exploited for its redox potential in cells.

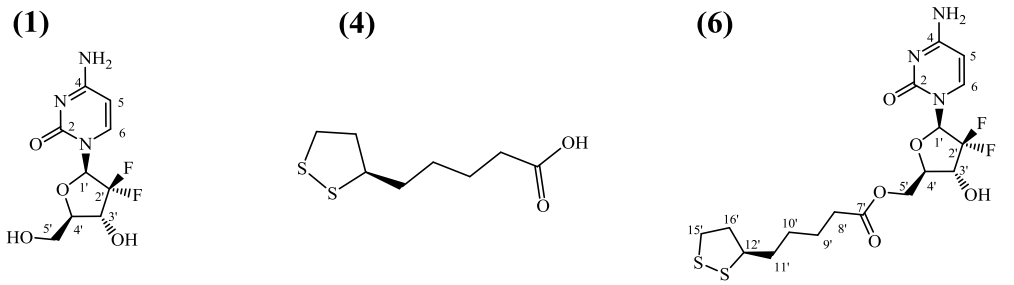

Figure 46: *2D structures of the antitumour compounds GEM (**1**), the antioxidant LA (**4**) and the molecular hybrid Gemcitabine-5'-O-lipoate (**6**).*

2.5.2 Design, synthesis and characterization of the Gemcitabine – Lipoic acid molecular hybrid

The chemical synthetic method for Gemcitabine-5′-*O*-lipoate (**6**) is depicted in *Figure 47A*. LA (**4**) can be coupled to (**1**) at 4-NH_2, 3′-OH, and 5′-OH positions. Development of the Gemcitabine-5′-*O*-lipoate conjugate requires selective protection at 4-NH_2 and 3′-OH of GEM (**1**)[18, 41] prior to LA (**4**)coupling. Transformation of (**1**) into compound (**6**) was achieved via a four-step synthetic process. In order to regioselectively couple LA (**4**) to the 5′-OH position of (**1**), we followed a selective protection/deprotection scheme for the 4-NH_2 and 3′-OH positions. The *tert*-butoxycarbonyl (Boc) group was used as selective protecting group and the synthetic paths previously reported were followed[18, 41]. Briefly, in the first step, the 3′-OH of (**1**) was protected with Boc using di-*tert*-butyl dicarbonate (DBDC) to give product (**2**). Consecutively, (**2**) was protected at the 4-NH_2 with DBDC to give product (**3**). (**3**) was then coupled at its 5′-OH with LA (**4**) with *N,N′*-Dicyclohexylcarbodiimide(DCC) to obtain product (**5**). Finally, TFA mediated Boc deprotection gave the desired Gemcitabine-5′-*O*-lipoate product (**6**). The reaction yields for the four steps were found to be 94%, 60%, 26% and ~ 80%, respectively.

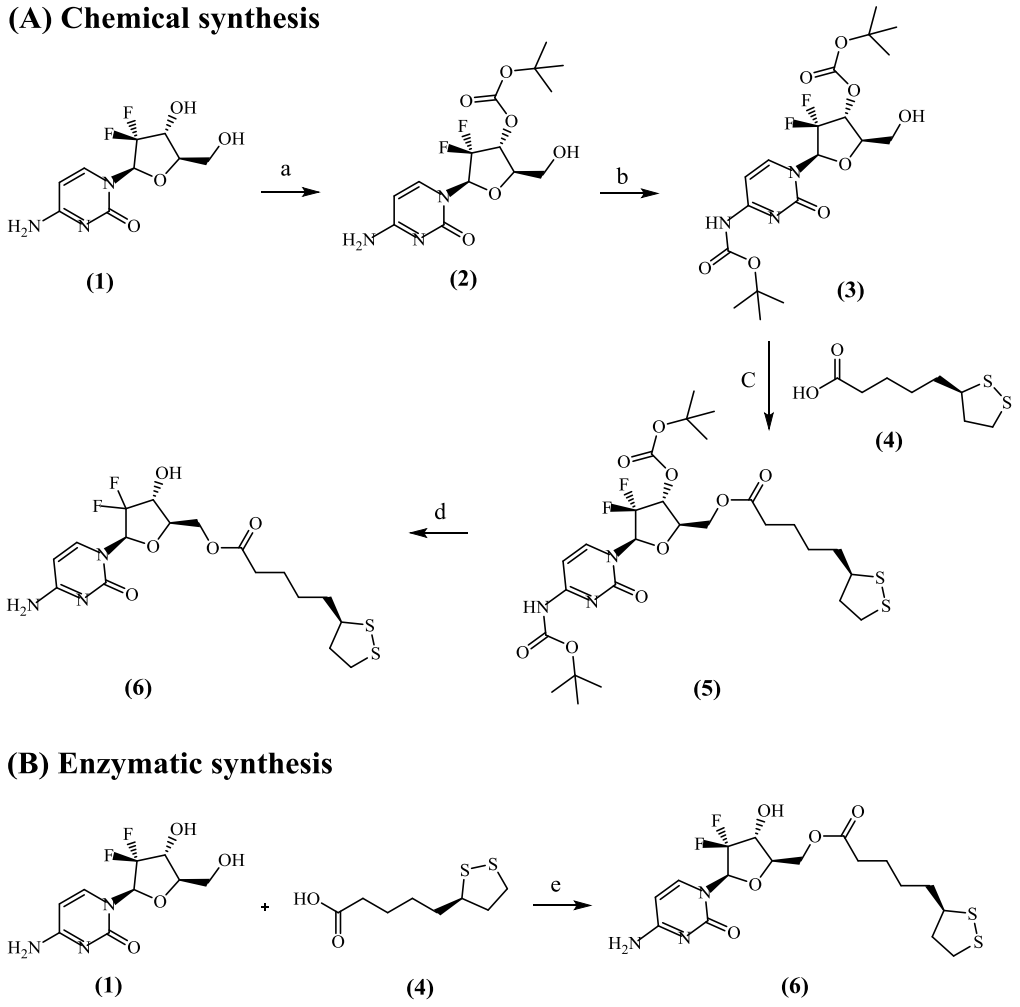

Figure 47: *(A)* ***Chemical synthesis of (6)*** *(Gemcitabine-5´-O-lipoate). Reagents and conditions: (a) Na_2CO_3, DBDC, 1,4-Dioxane, H_2O, rt, 50 h; (b) DBDC, 1,4-Dioxane, 40 ^0C, 70 h; (c) DMAP, DCC, CH_2Cl_2, L-Cysteine, 0 ^0C –rt, 24 h; (d) TFA-CH_2Cl_2 (1/10, v/v), 0 ^0C-rt, 2 h. (B)* ***Enzymatic synthesis of (6)*** *(Gemcitabine-5´-O-lipoate): (e) GEM (1) (1 equiv.), LA (4) (10 equiv.), enzyme CALB, acetonitrile, at 60 ^0C; yield was measured after 72 h by ^1H-NMR and it was found to be ~64%.*

The regioselective coupling of LA (4) to the 5´-OH group of GEM (1) was determined through combinatorial analysis of the 2D ^1H–^{13}C HMBC and ^1H–^{13}C HSQC of the final product. Specifically, the recorded cross peak of the proton H5´ of the GEM (**1**) moiety to carbon C (7´) [^3J (^1H,^{13}C)] of the LA (**4**) moiety unambiguously determined the desired regioselective coupling.

2.5.2.1 Chemical Synthesis and design of the Gemcitabine – Lipoic acid molecular hybrid

Synthesis of 3´-O-(tert-Butoxycarbonyl)Gemcitabine 2: Di-*tert*-butyl dicarbonate (DBDC) (0.414 g, 1.899 mmol) was added to the solution of **1** (0.5 g, 1.899 mmol) and Na_2CO_3 (1.0 g, 9.498 mmol) in dioxane-water (5:1, v/v.) and the reaction was continued at room temperature for 50 h. TLC (CH_2Cl_2-acetone-EtOH, 5:4:1, v/v) showed almost complete consumption of **1**. The reaction mixture was then diluted with water and extracted with ethyl acetate. The combined extract was washed with brine, dried over sodium sulfate and concentrated to dryness under reduced pressure. The residue was washed with diethyl ether to give a white solid **2** (0.65 g, 94 %).

^{1}H-NMR of **2** 400 MHz, DMSO-d_6, 25 ^{o}C**:** δ = 7.63 (d, J = 7.5 Hz, 1 H), 7.41 (d, J = 9.9 Hz, 2 H), 6.21 (t, J = 9.4 Hz, 1 H), 5.80 (d, J = 7.5 Hz, 1 H), 5.25 (t, J = 5.7 Hz, 1 H), 5.16 (m, 1 H), 4.13 (m, 1 H), 3.74 (m, 1 H), 3.63 (m, 1 H), 1.45 (s, 9 H) ppm. ^{13}C-NMR 400 MHz, DMSO-d_6, 25 ^{o}C: δ = 165.74 (C), 154.51 (C), 151.32 (C), 141.37 (CH), 121.60 (CF_2), 94.84 (CH), 83.73 (C), 83.35 (CH), 78.36 (CH), 72.35 (CH), 59.26 (CH_2), 27.16 (CH_3) ppm. Mass**:** (ESI) MS *m/z* Calcd. for $C_{14}H_{19}F_2N_3O_6$: 363.12, found:362.1 $[M-H]^-$.

Synthesis of 4-N-3´-O-Bis(tert-Butoxycarbonyl)Gemcitabine 3: DBDC (3.9 g, 17.9 mmol) was added to the solution of **2** (0.65 g, 1.79 mmol) in dioxane (25 mL) and the resulting mixture was stirred at 40 ^{o}C for 70 h. TLC (CH_2Cl_2-acetone-EtOH, 5:4:1, v/v) showed the complete consumption of **2**. The solvent was removed under reduced pressure and the residue was dissolved in water and extracted with CH_2Cl_2. The combined organic layer was washed with brine, dried over sodium sulfate and concentrated to dryness under reduced pressure. The crude compound was purified by column chromatography (CH_2Cl_2-acetone) to give **3** (0.5 g, 60 %**).**

^{1}H-NMR of **3** 400 MHz, DMSO-d_6, 25 ^{o}C: δ = 10.53 (s, 1 H), 8.09 (d, J = 7.7 Hz, 1 H), 7.08 (d, J = 7.7 Hz, 1 H), 6.26 (t, J = 8.7 Hz, 1 H), 5.30 (t, J = 5.7 Hz, 1 H), 5.19 (m, 1 H), 4.22 (m, 1 H), 3.77 (m, 1 H), 3.67 (m, 1 H), 1.46 (s, 9 H), 1.45 (s, 9 H) ppm. ^{13}C-NMR 400 MHz, DMSO-d_6, 25 ^{o}C: δ = 163.66 (C), 153.89 (C), 151.89 (C), 151.25 (C), 144.77 (CH), 121.47 (CF_2), 95.11 (CH), 84.19 (CH), 83.78 (C), 81.38 (C), 78.94 (CH), 72.24 (CH), 59.15 (CH_2), 27.74 (CH_3), 27.12 (CH_3) ppm. Mass: (ESI) MS *m/z* Calcd. for $C_{19}H_{27}F_2N_3O_8$: 463.18, found: 462.1 $[M-H]^-$

Synthesis of 4-N-3'-O-Bis(tert-Butoxycarbonyl)Gemcitabine-5´-O-lipoate 5: Compounds **3** (0.025 g, 0.054 mmol), **4** (0.013 g, 0.065 mmol) and DMAP (0.019 g, 0.162 mmol) were dissolved in anhydrous CH_2Cl_2 (5 mL) under inert atmosphere. A solution of DCC (0.013 g, 0.064 mmol) in 2 mL of anhydrous CH_2Cl_2 was added drop wise at 0 ^oC. Catalytic amount of L- Cysteine (0.5 %) was added to inhibit polymerization. Reaction was continued for 24 h at room temperature. TLC (CH_2Cl_2-MeOH, 95:05) showed the consumption of **3**. The reaction mixture was filtered and the solvent was evaporated under reduced pressure. The residue was purified with HPLC to give **5** (0.010 g, 26 %).

^{1}H-NMR of **5** 400 MHz, DMSO-d_6, 25 ^oC: δ = 10.55 (s, 1 H), 7.97 (d, J = 7.7 Hz, 1 H), 7.11 (d, J = 7.7 Hz, 1 H), 6.29 (t, J = 8.2 Hz, 1 H), 5.28 (m, 1 H), 4.40 (m, 3 H), 3.59 (m, 1 H), 3.13 (m, 1 H), 2.75 (s, 1 H), 2.38 (m, 3 H), 1.86 (m, 1 H), 1.65 (m, 1 H), 1.54 (m, 3 H), 1.46 (s, 9 H), 1.45 (s, 9 H), 1.37 (m, 2 H) ppm. ^{13}C-NMR 400 MHz, DMSO-d^6, 25 ^oC: δ = 172.61 (C), 163.81 (C), 153.87 (C), 151.99 (C), 151.18 (C), 145.27 (CH), 95.46 (CH), 82.02 (C), 81.54 (C), 76.04 (CH), 73.10 (CH), 62.26 (CH_2), 56.09 (CH), 39.69 (CH_2), 38.16 (CH_2), 34.08 (CH_2), 33.14 (CH_2), 28.10 (CH_2), 27.80 (CH_3), 27.19 (CH_3), 24.14 (CH_2) ppm. Mass: (ESI) MS *m/z* Calcd. for $C_{27}H_{39}F_2N_3O_9S_2$: 651.21, found: 650.1 $[M-H]^-$.

Synthesis of Gemcitabine-5'-O-lipoate 6: Compound **5** (0.010 g) was dissolved in CH_2Cl_2 (5 mL) at 0 ^oC and TFA (0.5 mL) was added drop-wise. The resulting mixture was stirred at room temperature for 2 h. The reaction solvent was evaporated under reduced pressure; the residue was diluted with water and extracted with ethyl acetate. The combined extract was washed with brine, dried over magnesium sulfate and concentrated. The product *Gemcitabine-5'-O-lipoate* (**6**) was purified with HPLC (5.5 mg, 80%).

^{1}H-NMR of **6** 500 MHz, DMSO-d_6, 25 ^oC: δ = 7.54 (d, J = 7.5 Hz, 1 H, 6-H), 7.43 (d, J = 10.35 Hz, 2 H, 4-NH_2), 6.46 (s, 1 H, 3'-OH), 6.20 (t, J = 8.0 Hz, 1 H, 1'-H), 5.83 (d, J = 7.5 Hz, 1 H, 5-H), 4.41 (m, 1 H, 5´a-H), 4.32 (m, 1 H, 5b'-H), 4.22 (m, 1 H, 3´-H), 4.03 (m, 1 H, 4´-H), 3.63 (m, 1 H, 12´-H), 3.20 (m, 1 H, 15'a-H), 3.15 (m, 1 H, 15'b-H), 2.44 (m, 1 H, 16'a-H), 2.41 (m, 2 H, 8'-H), 1.89 (m, 1 H, 16'b-H), 1.69 (m, 1 H, 11'a-H), 1.58 (m, 1 H, 11'-H), 1.57 (m, 2 H, 9'-H), 1.41 (m, 2 H, 10'-H) ppm; ^{13}C-NMR (500 MHz, DMSO-d_6, 25^o C): δ = 173.46 (C7'), 166.42 (C4), 155.37 (C2), 141.96 (C6), 95.59 (C5), 84.38 (C1'), 78.03 (C4'), 70.80 (C3'), 63.21 (C5'), 56.50 (C12´), 40.37 (C16´), 38.80 (C15´), 34.72 (C11´), 33.70 (C8´), 28.54 (C10´), 24.77 (C9') ppm. Mass: (ESI) MS *m/z* Calcd. for $C_{17}H_{23}F_2N_3O_5S_2$: 451.1, found: 452.36 $[M+H]^+$.

The regioselective coupling of LA (**4**) to the 5´-OH group of GEM (**1**) was determined through NMR spectroscopy. *Figure 48* shows the selected regions of 500 MHz ^{1}H-^{13}C HSQC (coloured in red) and ^{1}H-^{13}C HMBC (coloured in black) spectra of Gemcitabine-5´-*O*-lipoate (**6**). The regioselective coupling of LA (**4**) to the 5´-OH group of GEM (**1**) was determined through the recorded cross peak, illustrated with an arrow, of the proton H5´ of the GEM (**1**) moiety to carbon C(7´) [^{3}J(^{1}H,^{13}C)] of the LA (**4**) moiety.

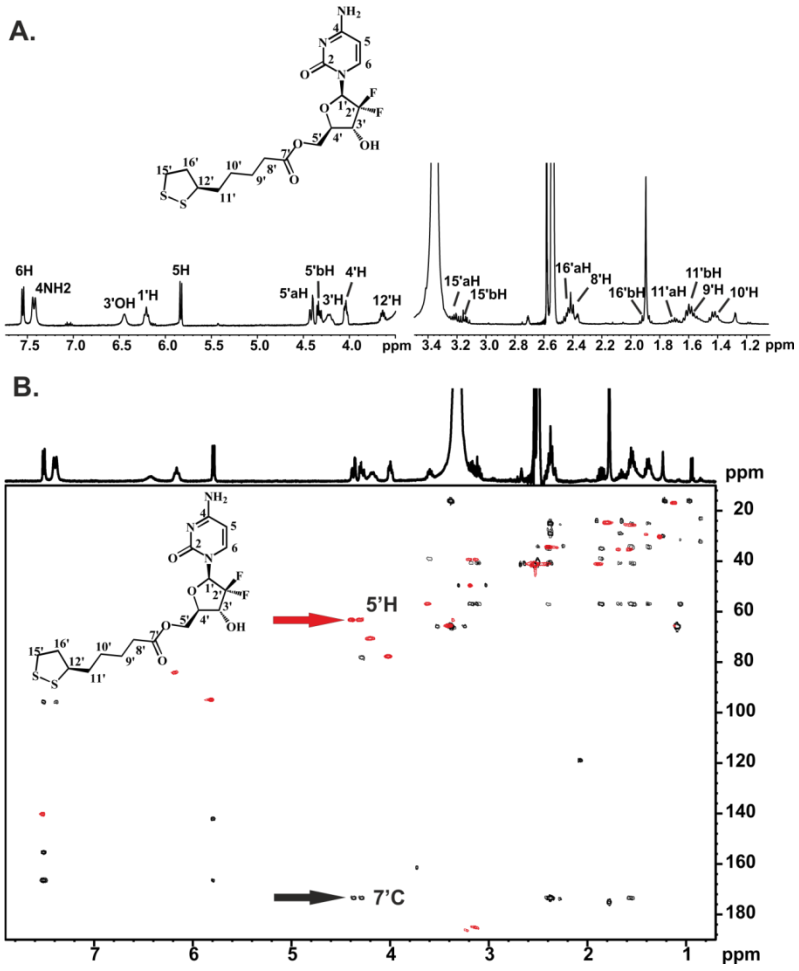

Figure 48: *A.^{1}H-NMR spectra of Gemcitabine-5´-O-lipoate in DMSO-d_6. B. Selected regions of the 500 MHz ^{1}H-^{13}C HSQC (coloured in red) and ^{1}H-^{13}C HMBC (coloured in black) spectra of Gemcitabine-5´-O-lipoate (6).*

2.5.2.2 Enzymatic Designs and synthesis of the Gemcitabine – Lipoic acid molecular hybrid

1 mg of GEM (**1**) (0.0038 mmol) was dissolved in acetonitrile or in 2-methyl-2-butanol or in *tert*-butanol (800 μL), containing 7.84 mg (0.038 mmol) of LA (**4**). The acylation reaction was performed in the presence of 2 mg of enzyme (refers to pure protein) both when Novozym or CNT-CALB preparations were used. The suspension incubated at 60 ^{o}C under shaking (250 rpm). After 72 h the reaction was stopped and the enzyme filtered off. The yield of the product was estimated in the crude reaction mixture by ^{1}H-NMR through integration of the NMR spectrum. The yield was found to be ~ 64 % in acetonitrile, whereas in t-butanol and in 2-methyl-2-butanol no product was detected when Novozym was used.

2.5.3 Biological evaluation of the *Gemcitabine-5´-O-lipoate* (**6**) *hybrid*

1) Cytotoxicity exploitation of the Gemcitabine-5´-O-lipoate (**6**) *hybrid*

Profound cell growth inhibitory effects were observed for Gemcitabine-5´-*O*-lipoate (**6**) and GEM compounds against all cell lines tested after 48 h of exposure. In contrast LA (4) proved to have no effect for all cell lines up to maximum threshold concentration applied (100 μM). Our results revealed that Gemcitabine-5´-*O*-lipoate (**6**) and GEM (**1**) compounds, caused a dose-dependent inhibition of cell proliferation. For all compounds, a 50 % growth-inhibitory effect (IC_{50}) was obtained (*Table 8*).

The *in vitro* cytotoxic activity of Gemcitabine-5´-*O*-lipoate (**6**) seems very promising.Cytotoxic effects of Gemcitabine-5´-*O*-lipoate (**6**) and GEM (**1**) compounds on tested cells were strictly concentration-dependent. For all cell lines tested, Gemcitabine-5´-*O*-lipoate (**6**) found to exhibit the best cytotoxic activity (lower IC_{50} values), followed by GEM. Gemcitabine-5´-*O*-lipoate's IC_{50} values were lower than the corresponding values of GEM (**1**), by 1.54, 1.24 and 1.30 times (in A549, MRC-5 and T24 cells, respectively). A549 lung cancer cells appeared to be more sensitive to Gemcitabine-5´-*O*-lipoate (**6**) (lower IC_{50}), compared to MRC-5 and T24 cells which exerted an equivalent response, which seems to be equipotent against MRC-5 and T24 cells. This finding is of increasing importance since GEM (**1**) is used for the treatment of non-small cell lung cancer [100] and the hybrid compound improves its activity. On the other hand, GEM (**1**) found to exhibit almost the same toxicity to all tested cell lines. These findings suggest that the applied

designing strategy, besides providing a more potent hybrid compound, indicates that LA (**4**) (a nontoxic by itself compound [101, 102, 103]) may be an interesting scaffold to design and develop novel anticancer agents. These results greatly raise the potential for using Gemcitabine-5´-*O*-lipoate (**6**) hybrid molecule in non-small cell lung and bladder cancer treatment.

Table 8: *Cytotoxicity evaluation of the administered compounds expressed in IC_{50} values as determined based on SRB assay.*

IC_{50} values (μM)*			
Compounds	**Cell lines**		
	A-549	**MRC-5**	**T24**
GEM(1)	0.0068	0.0063	0.0069
LA(4)	> 100	> 100	> 100
Gemcitabine-5´-*O*-lipoate (6)	0. 0044	0.0050	0.0053

*IC_{50} values were derived from the corresponding dose-effect curves drawn from sextuplicate determinations with CV lower than 10%. For drug combinations the IC_{50} values correspond to GEM concentrations.

**Statistically significant lower compared to IC_{50} values derived from sequential treatment with LA pretreatment of cells.

2) Monitoring cellular H_2O_2 levels in the presence of the parent compounds and the molecular hybrid

Cells have developed several systems to detoxify ROS, such as ROS-detoxifying enzymes, including superoxide dismutases (SODs) among others. SOD catalyzes the dismutation of superoxide anions to hydrogen peroxide H_2O_2[104] which is further detoxified by catalases. Cancer cells are often catalase deficient and thus more sensitive than normal cells to H_2O_2[105, 106, 107]. Interestingly, antioxidants such as vitamin C can act as pro-oxidants by producing hydrogen peroxide [108] that can damage DNA and cell membranes if not neutralized by catalases [108, 109]. This pro-oxidant (hydrogen peroxide production) effect has been reported for numerous known antioxidants[110]. The antioxidant properties of LA (**4**) have been previously well documented[92]. Since, it is known that LA (**4**) antioxidant properties include the detoxification of singlet oxygen, hydroxyl radical and hypochlorous anion and not a direct effect on H_2O_2, we hypothesized that an indirect effect could be also

observed. Indeed, published data refer that LA (**4**) may increase the activity of superoxide dismutase (SOD), an antioxidant enzyme responsible for the conversion of superoxide anion ($O2^{\cdot-}$) to H_2O_2[111, 112]. Along these lines we evaluated whether the Gemcitabine-5´-*O*-lipoate (**6**) preserved the pro-oxidant behavior of LA (**4**). A549 cells treated with LA (**4**), GEM (**1**) and Gemcitabine-5´-*O*-lipoate (**6**) at the concentration of 1 μM and a time course study at 5, 10 and 30 min, for H_2O_2 detection by flow cytometry, was performed. We found that LA (**4**) alone increased the levels of H_2O_2 5 min after its addition to cells ($p = 0.025$) and this effect was reversed 30 min later as shown in *Figure 49*.

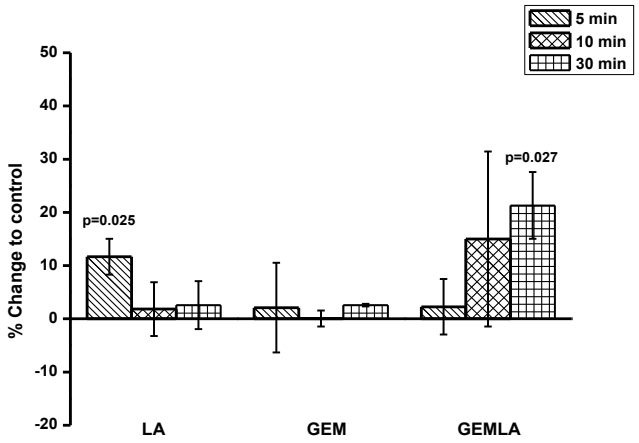

Figure 49: *Evaluation of H_2O_2 status in A549 levels. Cells treated with LA (4), GEM (1) and Gemcitabine-5´-O -lipoate (6) (GEMLA) and H_2O_2 levels were estimated at 5, 10 and 30 min after cells treatment. The results are expressed as % change to control (untreated cells)* ± *SE.*

GEM did not affected the H_2O_2 levels at any time point tested and Gemcitabine-5´-*O*-lipoate (**6**) caused an increase in H_2O_2 levels 30 min after its addition to cells ($p = 0.027$). The increased hydrogen peroxide production through Gemcitabine-5´-*O*-lipoate (**6**) could function in two axes. First this could operate as a ROS detoxification agent that would be beneficial for normal cells. In addition, this could amplify the cytotoxic activity of the anticancer component (GEM (**1**)) through H_2O_2 production that can make catalase deficient cancer cells more vulnerable to cytotoxic agents.

2.5.4 Conclusion

Human lung and bladder cancer cell lines (along with a non-tumour human lung cell line) were selected for the preliminary anti-cancer screening of the tested compound. To assess any modulatory/interactive effect of LA (4) on the cytotoxic activity of the chemotherapeutic drug GEM (1) we explored the mode of cell treatment with the parent compounds in isolation, after a sequential combination and after simultaneous combination. GEM (1) interacts synergistically with LA (1) in most schedules of administration on lung cancer cells, while an antagonistic effect for this combination was apparent for the treatment of bladder cancer and normal lung cells. When GEM (1) is administered in combination with LA (4), higher inhibition in cell growth was observed compared to the action of GEM (1) alone. At the same time, lower doses of the chemotherapeutic drug GEM (1) may be applied (since DRI for GEM (1) found to be higher than 1), alleviating the side effects of the drug. To take advantage of the recorded beneficial effect of co-administration of the two compounds we concomitantly targeted the construction of a molecular hybrid. The unique tasks of hybrid molecule design is challenging since suitable ways to chemically connect the drug components normally suffers from the requested laborious steps of selective protection/deprotection of the parent compounds to obtain the final hybrid. To this end, we explored two different synthetic approaches, including the chemical synthesis and the enzymatic synthesis to obtain the final conjugated product. Through this combinatorial effort we identified the ideal conditions to enzymatically synthesize the requested hybrid in a rapid, regioselective way and in one-pot, avoiding the tedious protection/deprotection steps required in the classical chemical synthesis method. We found that the resulted hybrid Gemcitabine-5´-O-lipoate (6) is more active against non-small cell lung cancer and bladder cancer cells than the widely used chemotherapeutic GEM (1), and also preserves the redox potential of the parent molecule LA (4). In overall, we showed that biocatalysis can act as an asset in molecular hybridization techniques and established a novel redox – anticancer hybrid that could assist in cancer treatment.

Chapter 3: Quercetin

3.1 Introduction:

The herbivorous human diet is enriched of fibers, vitamins, phytosterols, sulfur compounds, carotenoids, organic acids and polyphenols.[113] Polyphenols have a major role in many biological effects including free radical scavenging, modulation of enzymatic activity, inhibition of cell proliferation, antibiotic, anti-allergic and anti-inflammatory[114] as well as prevent degenerative diseases, such as cancer and cardiovascular diseases[113]. Polyphenols are widely distributed group of molecules in plant kingdom, according to their structures they are divided into phenolic acids, flavonoids.

Flavonoid is the Latin word which mean yellow; as they have yellow colour. These are plant secondary metabolites and are present in our everyday diet (apples, onions, grapes, red wine, cereals, vegetable and green tea[115] etc).

Flavonoids are polyphenolic compounds, which are involved in various biological activities such as the inhibition of angiogenesis, oxidative stress and proliferation of cancer cells. Their structure mainly contains two phenyl rings ("A" and "B") and one heterocycle ("C") (*Figure 1*). Flavonoids are divided in three classes 1) Flavones, 2) Isoflavonoids and 3) Neoflavonoids.

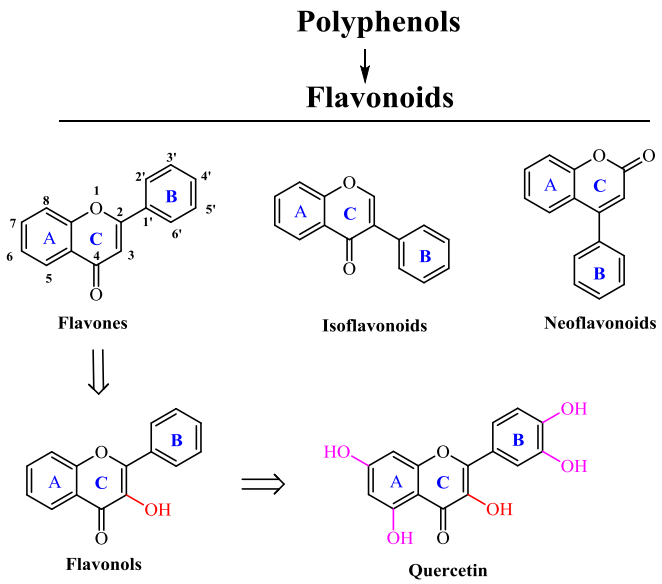

***Figure 1**: Classification of Flavonoids.*

Introduction of one hydroxyl at position 3 in flavones gives flavonols. Quercetin belongs to the group of flavonols, consisting of five hydroxyl group two at each ring

"**A"**and "**B"**. Quercetin was selected among the other flavones because of its abundance in nature, readily availability, present in plasma almost total as conjugates and its absorption and metabolism has been studied in detail.[116] Quercetin shows the wide range of bioactivity profile such as antiviral, antioxidant, antibacterial, and anticancer etc. But has low bioavailability, possibly due to its 5 polar phenol groups.

Importance of hybrid drugs: Despite the fact that several natural polyphenols are being exploited as additives in nutritional, cosmetic and over the counter pharmacological formulations, their activity in vivo is difficult to demonstrate due to their low bioavailability.[117, 113] One interesting approach to overcome the low bioavailability of polyphenols, so as to test and hopefully exploit their activity *in vivo*, relies on chemical modification of the natural compound aimed at increasing solubility.

Drug hybridization, that is the combination of the two parent compounds in a single entity, is an important strategy in drug discovery of novel biocompounds with either improved affinity for one bioreceptor or dual action on more than one bioreceptor related with a multifactorial disease. In addition, the hybrid molecules might improve their therapeutic window through enhancement of their metabolic stability, targeting and enhanced their bioavailability. The molecular hybridization strategy is useful for diseases that are interlinked such as hypertension and oxidative stress. Specifically, antihypertensive drugs exert their protective mechanism through lowering blood pressure. However, a relevant mechanism of cardiovascular disease progression in hypertensive patients may also be the increased oxidative stress at the vascular level. Thus, treatments that present a beneficial effect not only on regulation of blood pressure but also in interference with this oxidative stress have the potential to be a useful tool for the management of these individuals.

We have designed and constructed the following molecular hybrids of quercetin that to analyzed in three subsections:

3.2 Quercetin-aminoacids

3.3 Quercetin-Losartan

3.4 Quercetin-Captopril

3.2 Quercetin-amioacids

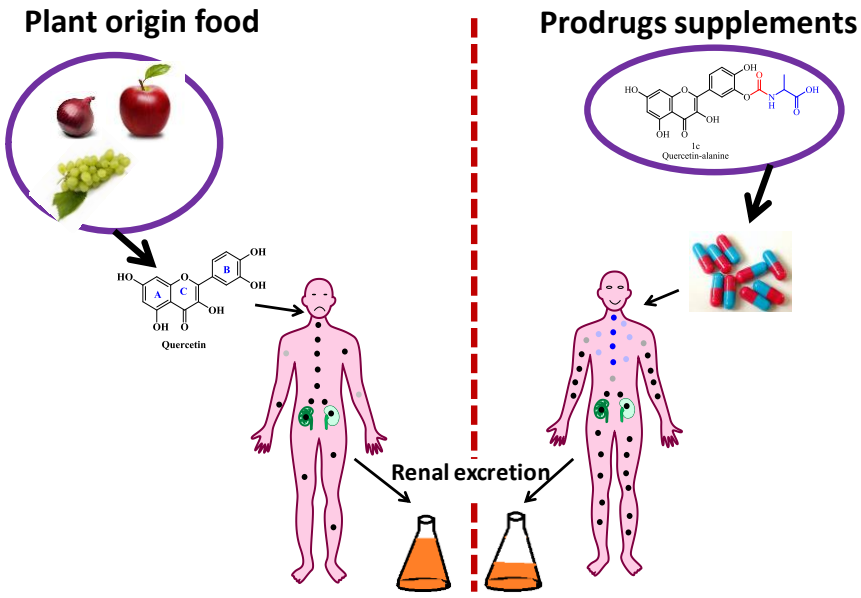

To be submitted.

Nisar Sayyad, et al., Maria V. Chatziathanasiadou[1], Antigoni Katsikoudi[1], Sofia Bellou[2,3,], Serafeim Pappas[1], George D Geromichalos[4], Andreas G. Tzakos[1] **Sculpting A Novel Quercetin Analogue: Compound Optimization for Efficient Delivery and Cytotoxic Activity.**

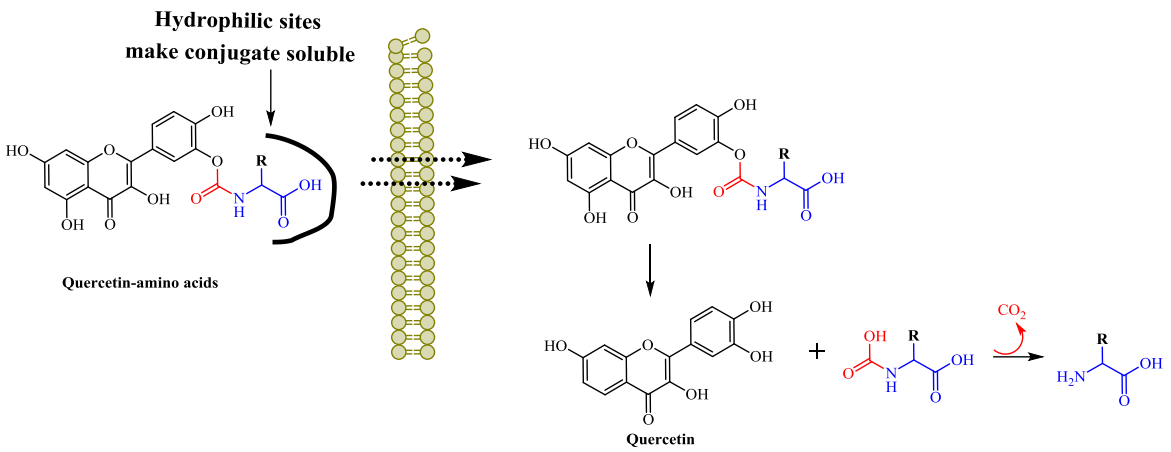

***Figure 2**: Concept of Quercetin-aminoacid prodrugs to enhance its bioavailability.*

3.2.1 Introduction:

Quercetin is one of the prominent antioxidant consumed from the daily diet but its low water solubility and less bioavailability results in its low plasma amount, since most of it is being excreted through metabolism.[22] Quercetin metabolites (methylated, sulfonylated and glucuronidated) are derived through the alkylation or acylation of hydroxyl groups of Quercetin.[115] Therefore chemical derivatization and construction of a prodrug of quercetin targeting these sites (hydroxyl to ester[118, 119] or carbamate bond[120]) could enhance its pharmacokinetic window and bioavailability by making it more water soluble as well as more stable (less metabolized products).

3.2.2 Design, synthesis and characterization:

Water insolubility and low bioavailability was the major obstacle for clinical administration of Quercetin. To overcome this hurdle, O-methylation and O-acetylation were necessary in order to magnify their medical result and avoid the deactivating metabolism.[119] Consequently, to cope up with this limitation we have designed and synthesised Quercetin-amino acid prodrugs via carbamate bond (*Figure 3*), which have extreme water solubility as compared to the parent drug and after hydrolysis it gives active ingredient, Quercetin.[22] The efficacy of these compounds as anticancer agents against

seven cancer and one non-cancer cell lines as also their capacity to binds serum albumin was evaluated.

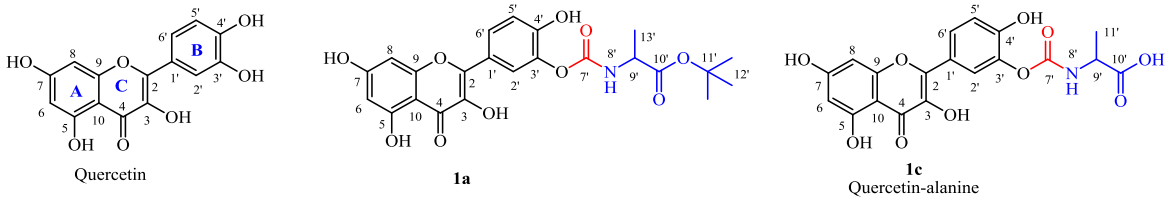

Figure 3: *Quercetin and its Alanine conjugate.*

Initially aminoacids were converted into their *tert*-Butyl ester through reaction of perchloric acid ($HClO_4$) and *tert*-Butyl acetate as a solvent in airtight closed vessel. These *tert*-Butyl esters of aminoacids were transformed into active urethane by Bis(4-nitrophenyl)carbonate (BNPC) and DIPEA, followed by alcoholysis of Quercetin. The alcoholysis is regioselective at ring "B" (*Figure 4*) and two reaction products (regioisomers) are resulted in a 3:1 ratio. Rapid Intramolecular transesterification is the cause for this inseparable regioisomers,[116] ^{1}H NMR confirm this result and shows major isomer was 3'-O-substituted quercetin (1a, 1c) and minor was 4'-O-substituted quercetin (1b, 1d). Final deprotection of the *tert*-Butyl protecting group by non aqueous hydrolysis (TFA/DCM) results in the quercetin-aminoacid conjugate;[22] Aqueous medium results in decomposition to quercetin. We also observed formation of Quercetin in ^{1}H NMR when

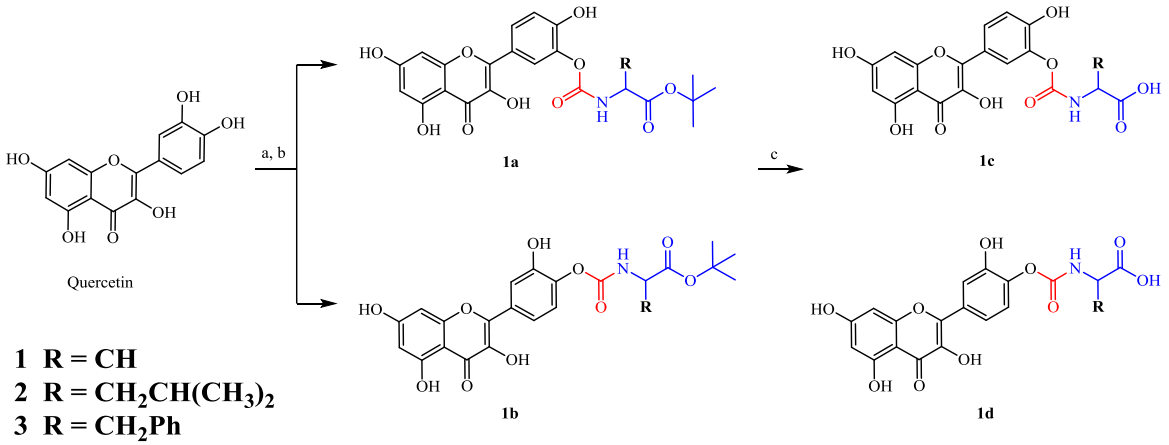

Figure 4: *Synthetic scheme of Quercetin-aminoacids.Regents and Conditions: a*) amino acid O*t*Bu.HCl, *BNPC, DIPEA, THF, rt., 12 h; b) Quercetin, rt. 12 h and c) TFA/DCM (1/10, v/v), 0^{0}C to rt., 4 h.*

the NMR sample was kept in DMSO d_6 around 12 h at room temperature (or 4^0C).

Aminoacids with *tert*-Butyl ester were preferred over methyl or ethyl ester because of their susceptibility for acidic hydrolysis in non aqueous condition. Generally, methyl/ethyl ester needs aqueous acidic or basic condition for hydrolysis, in such condition degradation of carbamate bond occurs prior to methyl ester hydrolysis. Utilization of non aqueous hydrolysis[121] codition gives expected Quercetin-alanine acid but in aqueous hydrolysis degradation of conjugates to parent Quercetin (*Figure 5*).

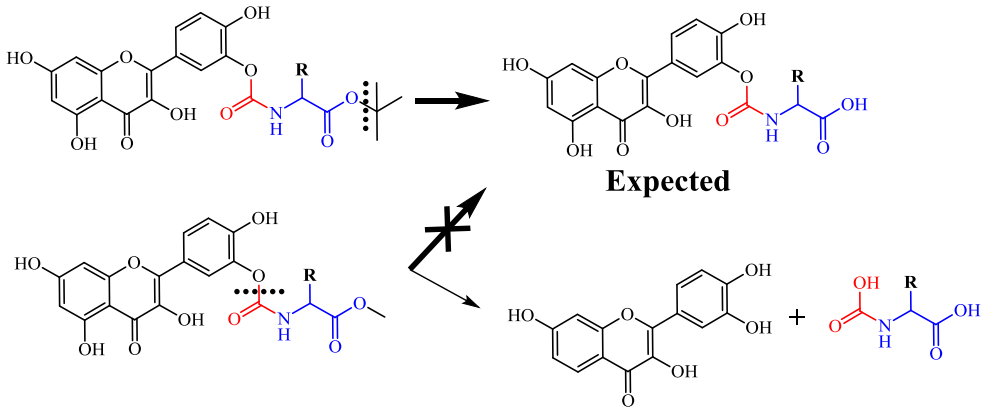

Figure 5: *Hydrolysis of tert*-Butyl *and methyl ester analogues of Quercetin-aminoacids.*

1) Synthesis of Quercetin-aminoacids conjugates

Synthesis of 3'-O-CO-(Ala-OtBu)-Quercetin (1a) and 4'-O-CO-(Ala-OtBu)-Quercetin (1b):

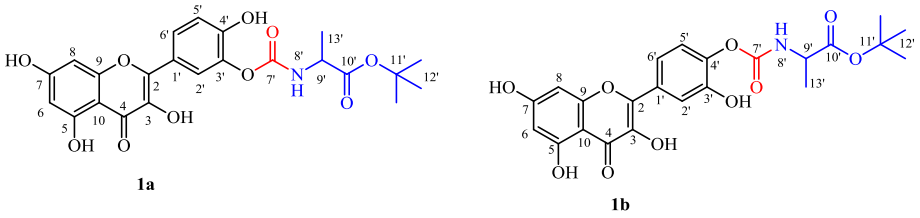

DIPEA (0.191 mL, 1.1 mmol) was added to the solution of H-Ala-O*t*Bu.HCl (100 mg, 0.550 mmol) and Bis(4-nitrophenyl)carbonate (167.46 mg, 0.550 mmol) in anhydrous THF(20 mL) under nitrogen atmosphere and at room temperature. After 12 h Quercetin (166.37 mg, 0.550 mmol) was added and the reaction was continued for 12 h at room temperature. The reaction solvent was evaporated on rotary evaporator; the crude

compound was purified with column chromatography (dichloromethane/methanol, 8:2) to obtain 200 mg (76.7%) of yellow solid.

^{1}H-NMR of **1a** (500 MHz, DMSO-d_6, 25^{o}C): δ = 12.47 (s, 1 H, 5-OH), 10.84 (s, 1 H, 7-OH), 10.40 (s, 1 H, 4'-OH), 9.58 (s,1 H, 3-OH), 8.13 (d, J = 7.3 Hz, 1 H, 8'-NH), 7.94 (dd, J = 8.7 Hz, 2.2 Hz, 1 H, 6'-H), 7.88 (d, J = 2.2 Hz, 1 H, 2'-H), 7.09 (d, J = 8.6 Hz, 1 H, 5'-H), 6.48 (d, J = 2.0 Hz, 1 H, 8-H), 6.23 (d, J = 2.0 Hz, 1 H, 6-H), 4.05- 3.99 (m, 1 H, 9´-H), 1.46 (s, 9 H, 12´-H), 1.35 (d, J = 7.2, 3 H, 13'-H) ppm; ^{13}C-NMR (500 MHz, DMSO-d_6, 25^{o}C): δ = 177.04 (C4), 172.64 (C10'), 164.87 (C7), 161.51 (C5), 157.04 (C9), 154.54 (C7'), 152.5 (C4'), 146.64 (C2), 126.62 (C6´), 123.79 (C2´), 122.50 (C1'), 117.33 (C5´), 103.86 (C10), 98.91 (C6), 94.22 (C8), 81.34(C11'), 50.97 (C9'), 28.40 (C12'), 17.74 (C13') ppm.

^{1}H-NMR of **1b** (500 MHz, DMSO-d_6, 25^{o}C)**:** δ = 12.41 (s, 1 H, 5-OH), 10.89 (s, 1 H, 7-OH), 10.00 (s, 1 H, 3'-OH), 9.69 (s, 1 H, 3-OH), 8.12 (d, J = 7.3 Hz, 1 H, 8'-NH), 7.81 (d, J = 2.0 Hz, 1 H, 2'-H), 7.61 (dd, J = 8.6, 2.0 Hz, 1 H, 6'-H), 7.18 (d, J = 8.6Hz, 1 H, 5'-H), 6.45 (d, J = 2.0 Hz, 1 H, 8-H), 6.24 (d, J = 2.0 Hz, 1 H, 6-H), 4.05- 3.99 (m, 1 H, 9´-H), 1.46 (s, 9 H, 12´-H), 1.35 (d, J = 7.2 Hz, 3 H, 13'-H) ppm; ^{13}C-NMR (500 MHz, DMSO-d_6, 25^{o}C)**:** δ = 177.02 (C4), 172.64 (C10'), 164.86 (C7), 161.65 (C5), 157.00 (C9), 154.50 (C7'), 150.31 (C3'), 146.32 (C2), 140.77 (C4'), 137.75 (C3), 129.4 (C1'), 124.20 (C5´), 119.24 (C6'), 116.55 (C2´), 103.98 (C10), 98.97 (C6), 94.07 (C8), 81.34 (C11'), 50.97 (C9'), 28.40 (C12'),17.74 (C13') ppm.

Mass: MS (ESI) *m/z:* [M-H]$^{-}$ for $C_{23}H_{23}NO_{10}$: calcd, 473.13, found: 472.1.

Synthesis of 3'-O-CO-Ala-Quercetin (1c) and 4'-O-CO-Ala-Quercetin (1d):

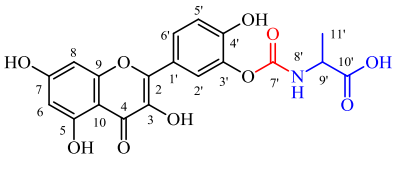

1c

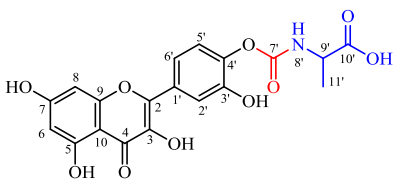

1d

To the solution of **1a** and **1b** (125 mg) in anhydrous dichloromethane (10 mL), TFA (1 mL) was added at 0^0C and the reaction was continued at room temperature for 4 h. A yellow compound was precipitated out was filtered and the solid was washed with anhydrous hexane (5 mL X 2), dried well on high vacuum to afford 63 mg (57%) of a yellow solid compound.

^{1}H-NMR of **1c** (500 MHz, DMSO-d_6, 25^{o}C): δ = 12.66 (bs, 1 H, 11'-OH), 12.47 (s, 1 H, 5-OH), 10.85 (s, 1 H, 7–OH), 10.39 (s, 1 H, 4'-OH), 9.56 (s, 1 H, 3-OH), 8.09 (d, J = 7.4 Hz, 1 H, 8'-NH), 7.93 (dd, J = 8.6 Hz, 2.2 Hz, 1 H, 6'-H), 7.89 (d, J = 2.2 Hz, 1 H, 2'-H), 7.09 (d, J = 8.6Hz, 1 H, 5'-H), 6.50 (d, J = 2.0 Hz, 1 H, 8-H), 6.23 (d, J = 2.0 Hz, 1 H, 6-H), 4.12- 4.06 (m, 1 H, 9′-H), 1.39- 1.37 (m, 3 H, 11′-H) ppm; ^{13}C-NMR (500 MHz, DMSO-d_6, 25^{o}C): δ = 176.5 (C4), 174.7 (C10'), 164.83 (C7), 161.6 (C5), 157.04 (C9), 154.46 (C7'), 152.63 (C4'), 146.57 (C2), 139.4 (C3'), 126.45 (C6′), 123.73 (C2′), 122.77 (C3), 122.66 (C1′), 117.19 (C5′), 103.95 (C10), 103.91 (C8), 99.05 (C6), 50.33 (C9'), 18.13 (C11') ppm.

^{1}H-NMR of **1d** (500 MHz, DMSO-d_6, 25^{o}C): δ = 12.66 (bs, 1 H, 11'-OH), 12.41 (s, 1 H, 5-OH), 10.85 (s, 1 H, 7–OH), 9.99 (s, 1H, 3'-OH), 9.68 (s, 1H, 3-OH), 8.09 (d, J = 7.4 Hz, 1 H, 8'-NH), 7.81 (d, J= 2.1 Hz, 1 H, 2'-H), 7.61 (dd, J = 8.6 Hz, 2.2 Hz, 1 H, 6'-H), 7.19 (d, J = 8.6Hz, 1 H, 5'-H), 6.45 (d, J = 2.0 Hz, 1 H, 8-H), 6.24 (d, J = 2.0 Hz, 1 H, 6-H), 4.12-4.06 (m, 1 H, 9′-H), 1.39- 1.37 (m, 3 H, 11′-H) ppm; ^{13}C-NMR (500 MHz, DMSO-d_6, 25^{o}C): δ = 176.5 (C4), 174.7 (C10'), 164.83 (C7), 161.7 (C5), 156.92 (C9), 154.46 (C7'), 150.22 (C3'), 146.39 (C2), 140.97 (C4'), 129.29 (C1′), 124.10 (C5′), 122.77 (C3), 119.23 (C6′), 116.54 (C2′), 104.06 (C10), 99.12 (C6), 94.02 (C8), 50.1 (C9'), 18.13 (C11') ppm.

Mass: MS (ESI) *m/z:* $[M+H]^+$ for $C_{19}H_{15}NO_{10}$: calcd, 417.07; found: 417.9; 438.0 $[M+Na]^+$.

Similarly we have synthesised all remaining Quercetin-aminoacids analogues.

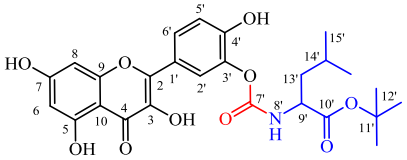

2a

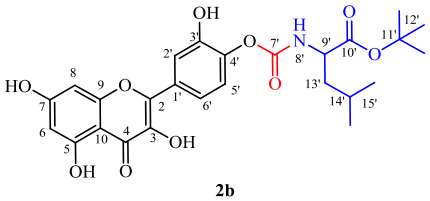

2b

^{1}H-NMR of **2a** (500 MHz, DMSO-d_6, 25^{o}C): δ = 12.47 (s, 1 H, 5-OH), 10.83 (s, 1H, 7-OH), 10.40 (s, 1 H, 4'-OH), 9.57 (s, 1 H, 3-OH), 8.09 (d, J = 7.8 Hz, 1 H, 8'-NH), 7.94 (dd, J = 8.6 Hz, 2.2 Hz, 1 H, 6'-H), 7.88 (d, J = 2.2 Hz, 1 H, 2'-H), 7.08 (d, J = 8.6Hz, 1 H, 5'-H), 6.48 (d, J = 2.0 Hz, 1 H, 8-H), 6.23 (d, J = 2.0 Hz, 1 H, 6-H), 4.01- 3.96 (m, 1 H, 9´-H), 1.82-1.74 (m, 1 H, 14'-H), 1.67-1.60 (m, 1 H, 13'a-H), 1.56-1.52 (m, 1 H, 13´b-H), 1.46 (s, 9 H, 12'-H), 0.93 (d, J = 6.5, 6 H, 15'H) ppm; ^{13}C-NMR (500 MHz, DMSO-d_6, 25^{o}C): δ = 176.7 (C4), 172.5 (C10'), 164.75 (C7), 161.62 (C5), 156.95 (C9), 154.80 (C7'), 152.63 (C4'), 146.58 (C2), 139.90 (C3'), 132.45 (C3), 126.63 (C6'), 123.63 (C2´), 122.62 (C1'), 117.26 (C5´), 103.86 (C10), 99.09 (C6), 94.21 (C8), 81.49 (C11'), 53.89 (C9'), 40.47 (C13'), 28.50 (C12'), 24.96 (C14'), 22.09 (C15') ppm.

^{1}H-NMR of **2b** (500 MHz, DMSO-d_6, 25^{o}C): δ = 12.41 (s, 1 H, 5-OH), 10.89 (s, 1 H, 7-OH), 10.00 (s, 1 H, 3'-OH), 9.68 (s, 1 H, 3-OH), 8.10 (d, J = 7.8 Hz, 1 H, 8'-NH), 7.81 (d, J = 2.2 Hz, 1 H, 2'-H), 7.61 (dd, J = 8.6Hz, 2.2 Hz, 1 H, 6'-H), 7.18 (d, J = 8.6Hz, 1 H, 5'-H), 6.45 (d, J = 2.0 Hz, 1 H, 8-H), 6.24 (d, J = 2.0 Hz, 1 H, 6-H), 4.01- 3.96 (m, 1 H, 9´-H), 1.82-1.74 (m, 1 H, 14'-H), 1.67-1.60 (m, 1 H, 13'a-H), 1.56-1.52 (m, 1 H, 13´b-H), 1.46 (s, 9 H, 12'-H), 0.93 (d, J = 6.5, 6 H, 15'H) ppm; ^{13}C-NMR (500 MHz, DMSO-d_6, 25^{o}C): δ = 172.50 (C10'), 164.93 (C7), 161.73 (C5), 154.80 (C7'), 157.09 (C9), 150.31 (C3'), 146.20 (C2), 141.00 (C4'), 122.62 (C1'), 119.34 (C6´), 117.26 (C5´), 116.56 (C2'), 103.90 (C10), 99.19 (C6), 94.06 (C8), 81.49 (C11'), 53.89 (C9'), 40.47 (C13'), 28.50 (C12'), 24.96 (C14'), 22.09 (C15') ppm.

Mass: MS (ESI) *m/z:* $[M-H]^-$ for $C_{26}H_{29}NO_{10}$: calcd, 515.18, found: 514.2.

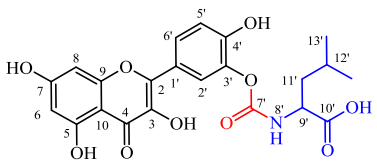

2c

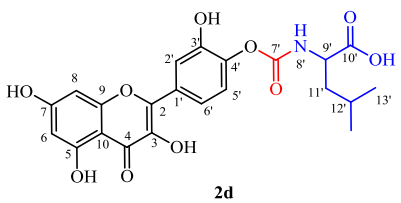

2d

^{1}H-NMR of **2c** (500 MHz, DMSO-d_6, 25^{o}C): δ = 12.67 (bs, 1 H, 10'-OH), 12.47 (s, 1 H, 5-OH), 10.83 (s, 1H, 7-OH), 10.39 (s, 1 H, 4'-OH), 9.57 (s, 1 H, 3-OH), 8.07 (d, J = 8.1 Hz, 1 H, 8'-NH), 7.94 (dd, J = 8.6 Hz, 2.0 Hz, 1 H, 6'-H), 7.89 (d, J = 2.0 Hz, 1 H, 2'-H), 7.08 (d, J = 8.6Hz, 1 H, 5'-H), 6.49 (d, J = 1.8 Hz, 1 H, 8-H), 6.23 (d, J = 1.8 Hz, 1 H, 6-H), 4.08- 4.03 (m, 1 H, 9´-H), 1.82-1.76 (m, 1 H, 12'-H), 1.69-1.62 (m, 1 H, 11'a-H), 1.60-1.54 (m, 1 H, 11´b-H), 0.94 (d, J= 6.5Hz, 6 H, 13'-H) ppm; ^{13}C-NMR (500 MHz, DMSO-d_6, 25^{o}C): δ = 176.76 (C4), 174.77 (C10'), 164.82 (C7), 161.58 (C5), 157.95 (C9), 152.55 (C4'), 146.69 (C2), 139.7 (C3'), 136.77 (C3), 126.54 (C6'), 123.63 (C2´), 117.22 (C5´), 103.91 (C10), 99.09 (C6), 94.27 (C8), 53.08 (C9'), 40.57 (C11'), 24.95 (C12'), 22.00 (C13') ppm.

^{1}H-NMR of **2d** (500 MHz, DMSO-d_6, 25^{o}C): δ = 12.67 (bs, 1 H, 10'-OH), 12.41 (s, 1 H, 5-OH), 10.89 (s, 1 H, 7-OH), 9.96 (s, 1 H, 3'-OH), 9.68 (s, 1 H, 3-OH), 8.07 (d, J = 8.1 Hz, 1 H, 8'-NH), 7.80 (d, J = 2.0 Hz, 1 H, 2'-H), 7.62 (dd, J = 8.6Hz, 2.0 Hz, 1 H, 6'-H), 7.18 (d, J = 8.6 Hz, 1 H, 5'-H), 6.45 (d, J = 1.8 Hz, 1 H, 8-H), 6.24 (d, J = 1.8 Hz, 1 H, 6-H), 4.08-4.03 (m, 1 H, 9´-H), 1.82-1.76 (m, 1 H, 12'-H), 1.69-1.62 (m, 1 H, 11'a-H), 1.60-1.54 (m, 1 H, 11´b-H), 0.94 (d, J = 6.5, 6 H, 13'H) ppm; ^{13}C-NMR (500 MHz, DMSO-d_6, 25^{o}C): δ = 177.01 (C4), 174.77 (C10'), 165.09 (C7), 161.64 (C5), 157.15 (C9), 150.20 (C3'), 146.40 (C2), 141.00 (C4'), 137.76 (C3), 124.08 (C5'), 119.35 (C6´), 116.51 (C2´), 103.95 (C10), 99.24 (C6), 94.02 (C8), 53.08 (C9'), 40.57 (C11'), 24.95 (C12'), 22.00 (C13') ppm.

Mass: MS (ESI) *m/z:* $[M+H]^+$ for $C_{22}H_{21}NO_{10}$: calcd, 459.12; found: 560.1.

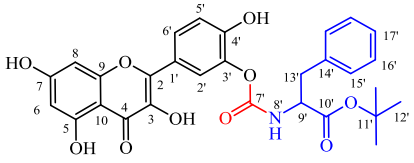

3a

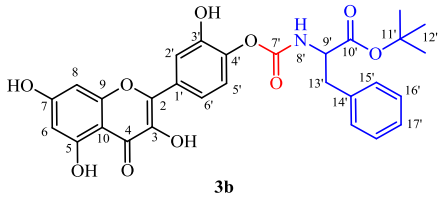

3b

^{1}H-NMR of **3a** (500 MHz, DMSO-d_6, 25^{o}C): δ = 12.47 (s, 1 H, 5-OH), 10.84 (s, 1H, 7-OH), 10.39 (s, 1 H, 4'-OH), 9.57 (s, 1 H, 3-OH), 8.20 (d, J = 7.7 Hz, 1 H, 8'-NH), 7.93 (dd, J = 8.7 Hz, 2.2 Hz, 1 H, 6'-H), 7.82 (d, J = 2.2 Hz, 1 H, 2'-H), 7.36-7.34 (m, 4 H, 15' and 16'-H), 7.30-7.26 (m, 1 H, 17'-H), 7.08 (d, J = 8.7Hz, 1 H, 5'-H), 6.48 (d, J = 2.0 Hz, 1 H, 8-H), 6.23 (d, J = 2.0 Hz, 1 H, 6-H), 4.22- 4.17 (m, 1 H, 9´-H), 3.08-2.98 (m, 2 H, 13'-H), 1.39 (s, 9 H, 12'-H) ppm; ^{13}C-NMR (500 MHz, DMSO-d_6, 25^{o}C): δ = 176.81 (C4),

171.42 (C10'), 164.76 (C7), 161.63 (C5), 156.98 (C9), 154.59 (C7'), 152.45 (C4'), 146.56 (C2), 139.54 (C3'), 138.2 (C14'), 136.89 (C3), 130.03 (C15'), 129.05 (C16'), 127.32 (C17'), 126.69 (C6'), 123.69 (C2′), 122.45 (C1'), 117.25 (C5′), 103.91 (C10), 98.98 (C6), 94.25 (C8), 81.66 (C11'), 57.08 (C9'), 37.56 (C13'), 28.43 (C12') ppm.

^{1}H-NMR of **3b** (500 MHz, DMSO-d_6, 25^{o}C): δ = 12.41 (s, 1 H, 5-OH), 10.88 (s, 1 H, 7-OH), 9.99 (s, 1 H, 3'-OH), 9.68 (s, 1 H, 3-OH), 8.21 (d, J = 7.8 Hz, 1 H, 8'-NH), 7.80 (d, J = 2.1 Hz, 1 H, 2'-H), 7.59 (dd, J = 8.6 Hz, 2.1 Hz, 1 H, 6'-H), 7.36-7.34 (m, 4 H, 15' and 16'-H), 7.30-7.26 (m, 1 H, 17'-H), 7.10 (d, J = 8.6Hz, 1 H, 5'-H), 6.44 (d, J = 2.0 Hz, 1 H, 8-H), 6.24 (d, J = 2.0 Hz, 1 H, 6-H), 4.22- 4.17 (m, 1 H, 9′-H), 3.08-2.98 (m, 2 H, 13'-H), 1.39 (s, 9 H, 12'-H) ppm; ^{13}C-NMR (500 MHz, DMSO-d_6, 25^{o}C): δ = 177.07 (C4), 171.46 (C10'), 164.95 (C7), 161.74 (C5), 157.04 (C9), 154.59 (C7'), 150.27 (C3'), 146.27 (C2), 140.87 (C4'), 138.20 (C14'), 130.03 (C15'), 129.05 (C16'), 127.32 (C17'), 124.05 (C5'), 122.45 (C1'), 119.32 (C6′), 116.59 (C2′), 104.02 (C10), 98.98 (C6), 94.14 (C8), 81.66 (C11'), 57.08 (C9'), 37.56 (C13'), 28.43 (C12') ppm.

Mass: MS (ESI) *m/z* [M-H]$^{-}$ for $C_{29}H_{27}NO_{10}$: calcd, 549.16; found: 548.2.

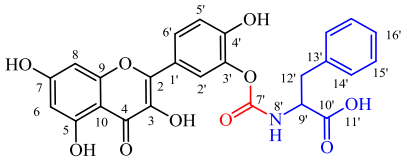

3c

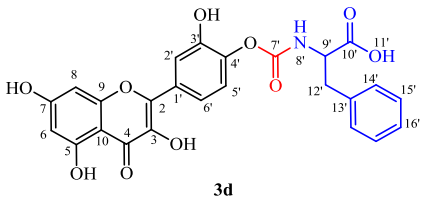

3d

^{1}H-NMR of **3c** (500 MHz, DMSO-d_6, 25^{o}C): δ = 12.88 (bs, 1H, 11'-OH), 12.47 (s, 1 H, 5-OH), 10.85 (s, 1H, 7-OH), 10.37 (s, 1 H, 4'-OH), 9.55 (s, 1 H, 3-OH), 8.14 (d, J = 8 Hz, 1 H, 8'-NH), 7.92 (dd, J = 8.7 Hz, 2.2 Hz, 1 H, 6'-H), 7.79 (d, J = 2.2 Hz, 1 H, 2'-H), 7.36-7.35 (m, 4 H, 14' and 15'-H), 7.31-7.26 (m, 1 H, 16'-H), 7.06 (d, J = 8.6Hz, 1 H, 5'-H), 6.48 (d, J = 2.0 Hz, 1 H, 8-H), 6.23 (d, J = 2.0 Hz, 1 H, 6-H), 4.27- 4.22 (m, 1 H, 9′-H), 3.14 (dd, J = 14.0 Hz, 4.4Hz, 1 H, 12a'-H), 2.99 (dd, J = 9.6Hz, 4.2Hz, 1 H, 12b'-H) ppm; ^{13}C-NMR (500 MHz, DMSO-d_6, 25^{o}C): δ = 174.04 (C10'), 165.03 (C7), 161.77 (C5), 157.07 (C9), 152.45 (C4'), 146.74 (C2), 139.57 (C3'), 138.64 (C13'), 130.02 (C14'), 129.01 (C15'), 127.3 (C16'), 126.70 (C6'), 123.83 (C2′), 122.63 (C1'), 117.40 (C5′), 104.00 (C10), 99.10 (C6), 94.34 (C8), 56.54 (C9'), 37.39 (C12') ppm.

^{1}H-NMR of **3d** (500 MHz, DMSO-d_6, 25^{o}C): δ = 12.88 (bs, 1 H, 11'-OH), 12.40 (s, 1 H, 5-OH), 10.89 (s, 1 H, 7-OH), 9.97 (s, 1 H, 3'-OH), 9.67 (s, 1 H, 3-OH), 8.15 (d, J = 7.8 Hz, 1 H, 8'-NH), 7.78 (d, J = 2. Hz, 1 H, 2'-H), 7.58 (dd, J = 8.6 Hz, 2.1 Hz, 1 H, 6'-H), 7.36-7.35 (m, 4 H, 14' and 15'-H), 7.32-7.26 (m, 1 H, 16'-H), 7.07 (d, J = 8.6Hz, 1 H, 5'-H), 6.44 (d, J = 2.2 Hz, 1 H, 8-H), 6.23 (d, J = 2.2 Hz, 1 H, 6-H), 4.27- 4.22 (m, 1 H, 9´-H), 3.14 (dd, J = 14.0 Hz, 4.4Hz, 1 H, 12a'-H), 2.99 (dd, J = 9.6Hz, 4.2Hz, 1 H, 12b'-H) ppm; ^{13}C-NMR (500 MHz, DMSO-d_6, 25^{o}C): δ = 174.04 (C10'), 165.09 (C7), 161.50 (C5), 157.26 (C9), 150.15 (C3'), 146.74 (C2), 140.84 (C4'), 138.64 (C13'), 130.02 (C14'), 129.64 (C1'), 129.01 (C15'), 127.30 (C16'), 124.16 (C5'), 119.50 (C6´), 116.66 (C2´), 104.00 (C10), 99.10 (C6), 94.23 (C8), 56.54 (C9'), 37.39 (C12') ppm.

Mass: MS (ESI) *m/z* $[M+H]^+$ for $C_{25}H_{19}NO_{10}$: calcd, 493.10; found: 516.0 $[M+Na]^+$.

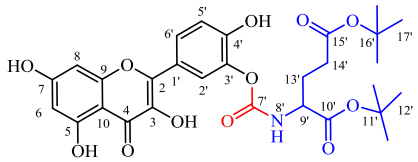

4a

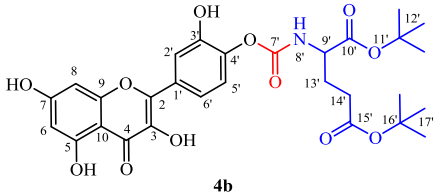

4b

^{1}H-NMR of **4a** (500 MHz, DMSO-d_6, 25^{o}C): δ = 12.47 (s, 1 H, 5-OH), 8.11 (d, J = 7.5 Hz, 1 H, 8'-NH), 7.95 (dd, J = 8.6 Hz, 2.2 Hz, 1 H, 6'-H), 7.8 (d, J = 2.2 Hz, 1 H, 2'-H), 7.09 (d, J = 8.6Hz, 1 H, 5'-H), 6.48 (d, J = 2.0 Hz, 1 H, 8-H), 6.23 (d, J = 2.0 Hz, 1 H, 6-H), 4.04- 3.99 (m, 1 H, 9´-H), 2.00 (m, 2 H, 14'-H), 1.87 (m, 2 H, 13'-H), 1.47 (s, 9 H, 17´-H), 1.45 (s, 9 H, 12'-H) ppm; ^{13}C-NMR (500 MHz, DMSO-d_6, 25^{o}C): δ = 176.81 (C4), 172.31 (C15'), 172.31 (C10'), 164.80 (C7), 161.60 (C5), 157.00 (C9), 154.75 (C7'), 152.44 (C4'), 146.59 (C2), 139.59 (C3'), 126.72 (C6´), 123.73 (C2´), 122.63 (C1'), 117.30 (C5´), 103.92 (C10), 98.96 (C6), 94.25 (C8), 81.7 (C11'), 80.72 (C16'), 54.62 (C9'), 28.48 (C17'), 28.48 (C12'), 27.00 (C14'), 27.00 (C13') ppm.

^{1}H-NMR of **4b** (500 MHz, DMSO-d_6, 25^{o}C): δ = 12.41 (s, 1 H, 5-OH), 8.11 (d, J = 7.5 Hz, 1 H, 8'-NH), 7.81 (d, J = 2.2 Hz, 1 H, 2'-H), 7.62 (dd, J = 8.6, 2.2 Hz, 1 H, 6'-H), 7.18 (d, J = 8.6Hz, 1 H, 5'-H), 6.45 (d, J = 2.0 Hz, 1 H, 8-H), 6.24 (d, J = 2.0 Hz, 1 H, 6-H), 4.04-3.99 (m, 1 H, 9´-H), 2.00 (m, 2 H, 14'-H), 1.87 (m, 2 H, 13'-H), 1.47 (s, 9 H, 17´-H), 1.45

(s, 9 H, 12'-H) ppm; ^{13}C-NMR (500 MHz, DMSO-d_6, 25°C): δ = 177.03 (C4), 172.31 (C10'), 172.30 (C15'), 164.80 (C7), 161.60 (C5), 157.00 (C9), 154.75 (C7'), 150.21 (C3'), 146.36 (C2), 140.86 (C4'), 129.55 (C1´), 124.15 (C5´), 119.33 (C6'), 116.61 (C2´), 103.92 (C10), 98.96 (C6), 94.14 (C8), 81.70 (C11'), 80.72 (C16'), 54.62 (C9'), 28.48 (C17'), 28.48 (C12'), 27.05 (C14'), 27.05 (C13') ppm.

Mass: MS (ESI) *m/z* [M-H]$^-$ for $C_{29}H_{33}NO_{12}$: calcd, 587.20; found: 586.3.

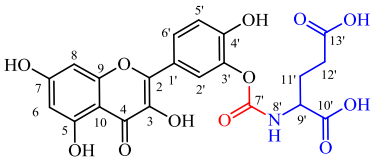

4c

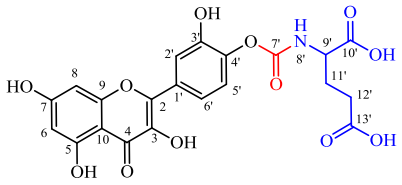

4d

^{1}H-NMR of **4c** (500 MHz, DMSO-d_6, 25°C): δ = 12.85 (bs), 12.47 (s, 1 H, 5-OH), 10.84 (s, 1 H, 7-OH), 10.36 (s, 1 H, 4'-OH), 9.55 (s, 1 H, 3-OH), 8.14 (d, J = 8.2 Hz, 1 H, 8'-NH), 7.92 (dd, J = 8.6 Hz, 2.2 Hz, 1 H, 6'-H), 7.79 (d, J = 2.2 Hz, 1 H, 2'-H), 7.06 (d, J = 8.6Hz, 1 H, 5'-H), 6.48 (d, J = 2.0 Hz, 1 H, 8-H), 6.23 (d, J = 2.0 Hz, 1 H, 6-H), 4.27 - 4.22 (m, 1 H, 9´-H), 3.16 - 3.11 (m, 2 H, 12'-H), 3.01 - 3.29 (m, 2 H, 11'-H) ppm; ^{13}C-NMR (500 MHz, DMSO-d_6, 25°C): δ = 177.01 (C4), 173.77 (C13'), 173.44 (C10'), 164.81 (C7), 161.67 (C5), 156.88 (C9), 154.99 (C7'), 152.26 (C4'), 146.70 (C2), 139.42 (C3'), 126.7 (C6´), 123.83 (C1´), 123.73 (C2'), 117.31 (C5´), 103.99 (C10), 98.98 (C6), 94.25 (C8), 56.46 (C9'), 37.36 (C11'), 37.36 (C12') ppm.

^{1}H-NMR of **4d** (500 MHz, DMSO-d_6, 25°C): δ = 12.85 (bs), 12.41 (s, 1 H, 5-OH), 10.88 (s, 1 H, 7-OH), 9.97 (s, 1 H, 3'-OH), 9.68 (s, 1 H, 3-OH), 8.15 (d, J = 8.2 Hz, 1 H, 8'-NH), 7.78 (dd, J = 2.2 Hz, 1 H, 2'-H), 7.58 (d, J = 8.6, 2.2 Hz, 1 H, 6'-H), 7.07 (d, J = 8.4Hz, 1 H, 5'-H), 6.44 (d, J = 2.0 Hz, 1 H, 8-H), 6.23 (d, J = 2.0 Hz, 1 H, 6-H), 4.27 - 4.22 (m, 1 H, 9´-H), 3.16 - 3.11 (m, 2 H, 12'-H), 3.01 - 3.29 (m, 2 H, 11'-H) ppm; ^{13}C-NMR (500 MHz, DMSO-d_6, 25°C): δ = 177.01 (C4), 173.77 (C13'), 173.44 (C10'), 165.07 (C7), 161.67 (C5), 157.23 (C9), 154.99 (C7'), 150.28 (C3'), 146.50 (C2), 140.89 (C4'), 129.47 (C1´), 124.01 (C5´), 119.30 (C6'), 116.54 (C2´), 104.03 (C10), 98.98 (C6), 94.25 (C8), 56.46 (C9'), 37.36 (C11'), 37.36 (C12') ppm.

Mass: MS (ESI) *m/z* $[M-H]^-$ for $C_{21}H_{17}NO_{12}$: calcd, 475.08; found: 474.0.

2) Characterization of Quercetin-aminoacids analogues:

***a) By NMR: Herein we are introducing an example to indicate the regioselective coupling of the aminoacids in quercetin core*.** To this we used the analogue **1a** and all the remaining analogues were characterised similarly. The ^{1}H NMR of **1a** was recorded at 400 MHz in DMSO-d_6, and 298K. The sample was titrated with 1M solution of picric acid in DMSO-d_6 to make the peaks derived from the phenol groups sharper (the broadening of these hydroxyl protons is due to fast intermolecular exchange which is minimized upon addition of picric acid as our group has recently shown[122]).

Overlapping of the ^{1}H NMR spectra of Quercetin and **1a** (*Figure 6*); clearly indicate the formation of **1a** since we observe: 1) missing of Quercetin's OH-3' peak in **1a** spectra, 2) appearance of new peaks derived from alanine at,

a) 8.13 (d, J = 7.3 Hz, 1 H, 8'-NH),

b) 4.05- 3.99 (m, 1 H, 9´-H),

c) 1.46 (s, 9 H, 12´-H), and

d) 1.35 (d, J = 7.2, 3 H, 13'-H).

These observations lead to the conclusion that acylation of Quercetin by alanine happens to the ring **B** of Quercetin and at the 3'-OH. This result has been unambiguously confirmed by 2D NMR (HMBC and HSQC).

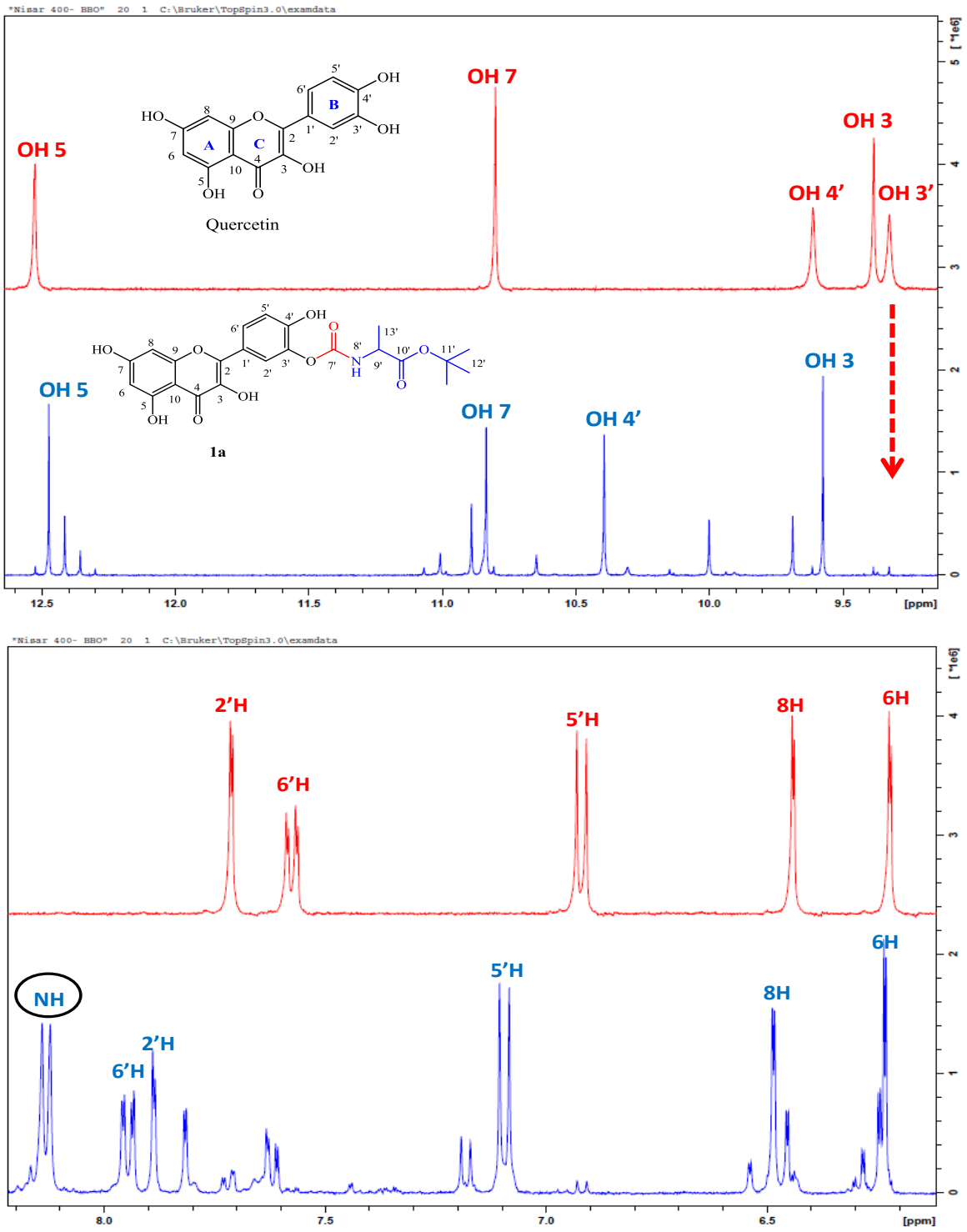

Figure 6: *^{1}H NMR characterisation of Quercetin-alanine coupling.*

b) Mass spectrometry: All Quercetin-aminoacids analogues are susceptible for aqueous hydrolysis, (carbamate is succeptible to hydrolysis). This hydrolysis results were confirmed by mass spectrometry. Samples were prepared just before experiments, were

dissolved in 0.1% formic acid in methanol or 0.1% ammonium acetate in methanol. An example of sample **1c** follows.

MS (ESI) *m/z:* $[M-H]^-$ for $C_{19}H_{15}NO_{10}$: calcd, 417.07; found: 438.0 [M+Na].

Here 438.0 is the molecular ion peak of compound **1c**, and in the same time there is the presence of the 300.9 peak which corresponds to Quercetin (m/z: 302.23) (*Figure 7*).

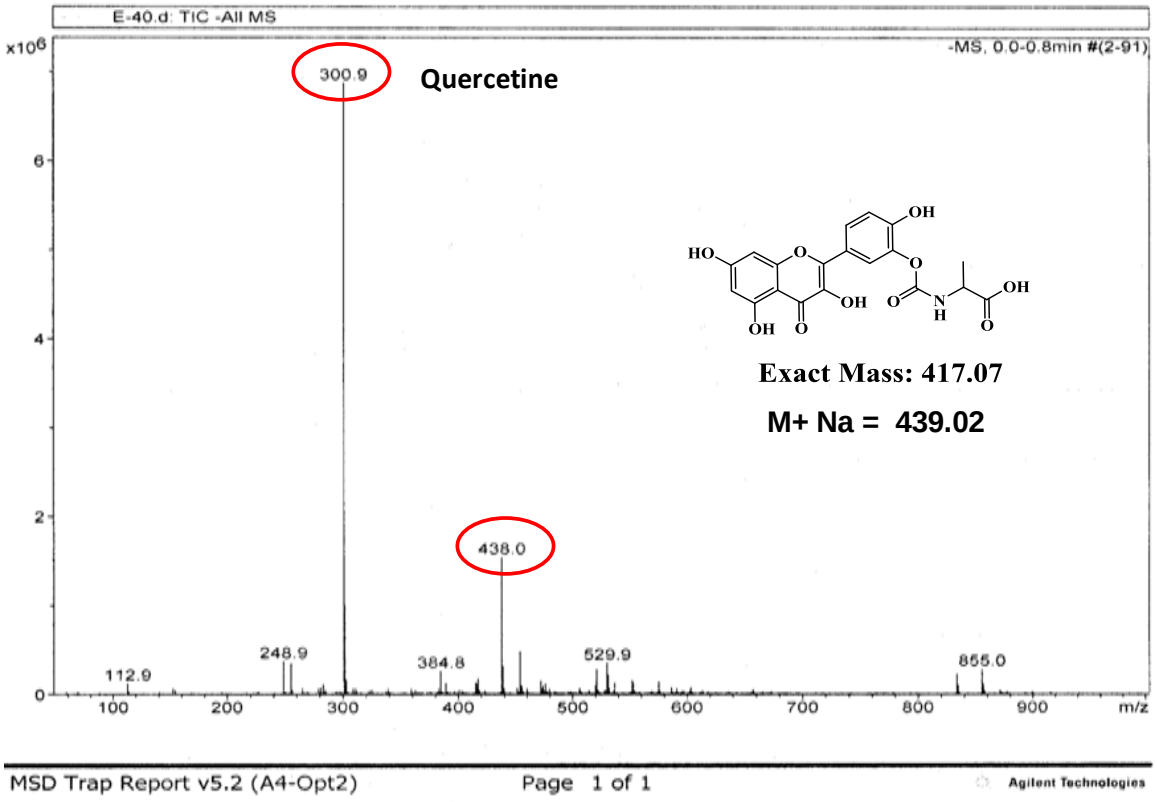

Figure 7: *Mass spectrum of* ***1c.***

3.2.3 Biological evaluation:

Cytotoxic activity:

Our results revealed that both administered agents, caused a dose-dependent inhibition of cell proliferation. For all compounds, a 50% growth-inhibitory effect (IC_{50}) was obtained. The calculated IC_{50} (μM) values are shown in *Table 1*. In *Figure 7* are illustrated the dose-effect curves for all treated cell lines, demonstrating the different chemosensitivity of the

cell lines to both compounds. As depicted in *Table 1*, the Quercetin analogue (QUE/ALA) found to be more active than QUE, exhibiting 2 to 4 fold lower IC_{50} values.

Table 1: *Cytotoxicity evaluation of QUE and QUE/ALA expressed in IC_{50} values as determined based on SRB assay.*

Compound	**IC_{50} values (μM)***									
	Cell lines									
	HeLa	A549	MRC-5	MCF-7	T24	HepG2	Colo-205	LNCaP	4T1	N2a
QUE	150	256	50	79	250	54	301	130	69.5	68.7
QUE/ALA	40	71	26	25	126	40	141	34	28	26.5

**IC_{50} values were derived from the corresponding dose-effect curves drawn from sextuplicate determinations with CV lower than 5%.*

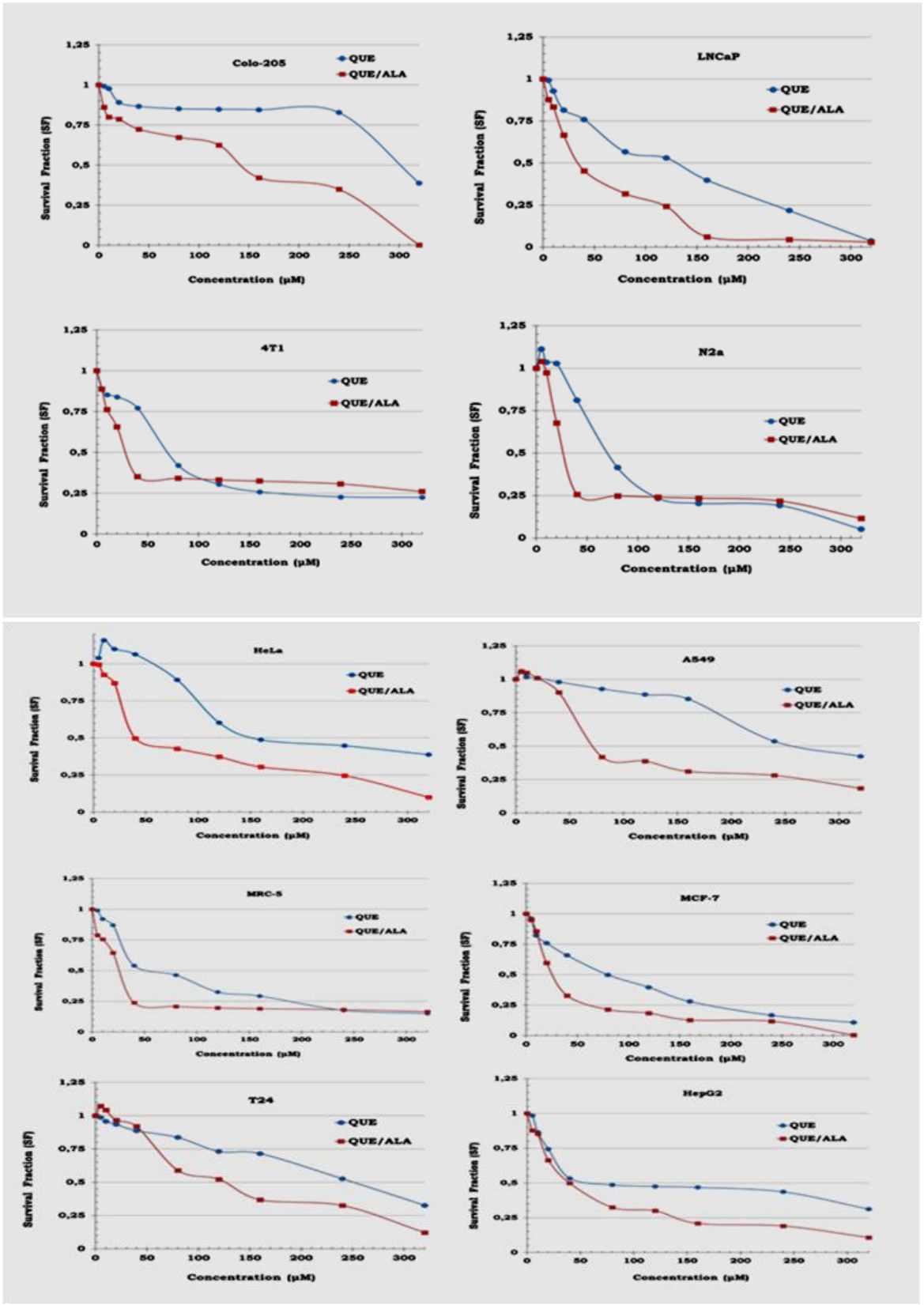

Figure 7: *Dose-effect survival plots for QUE and QUE/ALA against a panel of human and murine cell lines 72 h after the administration of agents. Cytotoxicity was estimated via SRB assay (each point represents mean of six replicate wells.*

3.3 Quercetin-Losartan

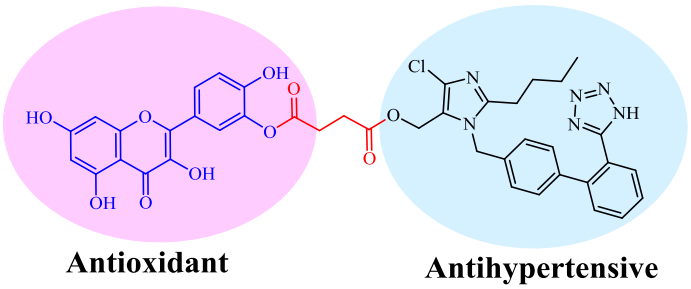

Manuscript under preparation

Sayyad Nisar et al. Molecular Hybridization targeting hypertension and cancer.

3.3.1 Introduction:

In this article we are introducing a new hybrid drug with dual functionality: anti-hypertension and antioxidant. It is well known that hypertension and oxidative stress are interlinked; Losartan and Quercetin are being used as parent compounds to compete hypertension and oxidative stress, respectively.

It has been established that oxidative stress can cause cardiovascular disease progression in hypertensive patients.[123] The currently used antihypertensive drugs are mostly angiotensin converting enzyme (ACE) inhibitors and they prevent the conversion of Angiotensin I into Angiotensin II. Due to their side effect (e.g. cough) they have somehow been displaced by antagonists of the angiotensin II GPCR receptor AT1[124]. What is interesting to note is that angiotensin II besides taking an active role in cardiovascular disease it also lead to tissue damages[125] by increasing oxidative stress[124]. Thus, oxidative stress treatment can play a vital role in the antihypertensive therapy.

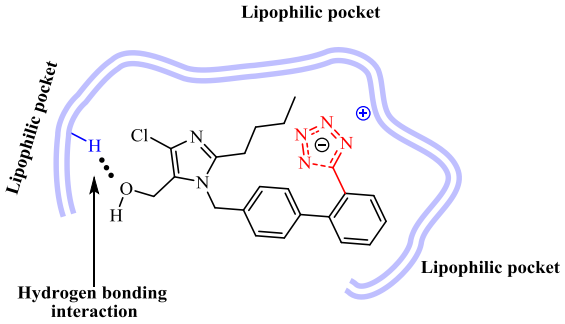

Figure 8: *Losartan and its interaction of hypothetical model of Angiotensin II receptor.*

Losartan is one of the marketed drugs that act as an antagonist for angiotensin II to the AT1 receptor. We selected Losartan **2** on the basis of the work by *David J. Carini et. al.*[126]; where it was pinpointed that substitution of the tetrazole ring at the ortho position of biphenyl of losartant enhanced its affinity for the AT1 receptor as well as its antihypertensive potency.[126] In addition, recent studies highlighted the role of losartan to bear enhanced anticancer properties.[127]

The aforementioned interlinkage of hypertension and oxidative stress as also implication of losartant and quercetin in cancer prompted us to design a new molecular hybrid drug bearing both functional cores. We hypothesised that this hybrid molecule would act as better anti-hypertensive, antioxidant and anticancer compound.

3.3.2 Design, synthesis and characterization:

The designed hybrid **3** is illustrated in *Figure 9* that was achieved through coupling of the hydroxymethyl group of Losartan and hydroxyl group from Quercetin (via carbonate bond) using hemisuccinate as a spacer.

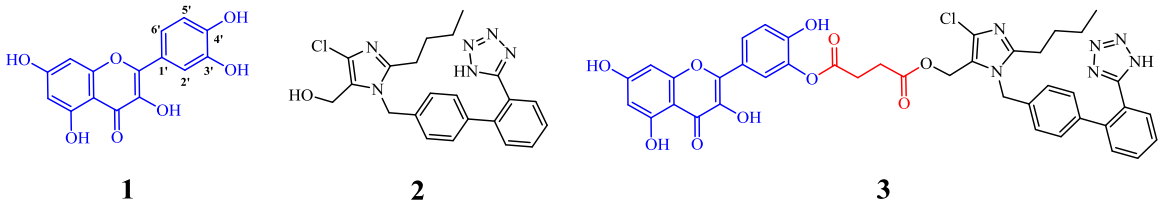

1 **2** **3**

Figure 9: *Quercetin, Losartan and their hybrid.*

Interesting thing to note is that this hybrid is equipped with two ester bonds that could have a difference in the rate of their hydrolysis and this could play a dominant role in drug release and subsequent activity. A scenario is that losartan will be released first leaving as intermediate the aqueous soluble quercetin-4'-succinic acid (due to the carboxylic acid terminal)[22] which could be trapped inside the cell and consequently quercetine could be released, thus enhancing its bioavailability (*Figure 10*).

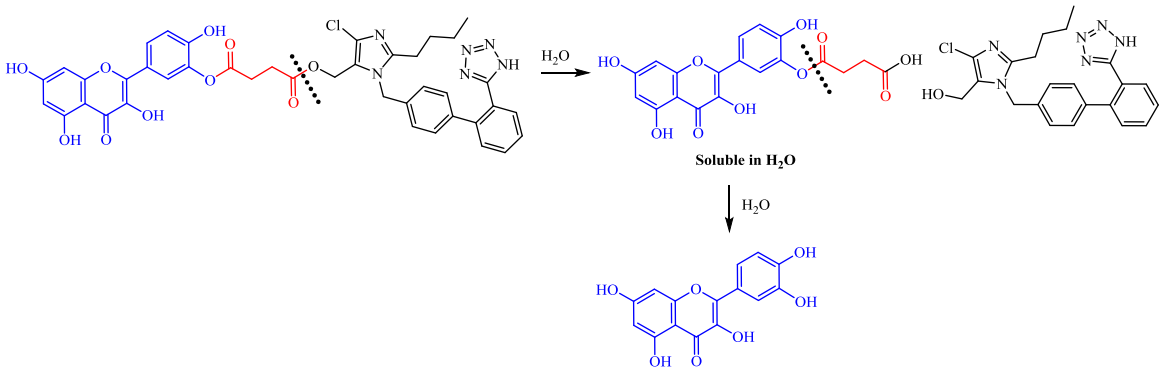

Figure 10: *The sites of hydrolysis and release of parent drugs from the Quercetin-Losartan hybrid.*

To achieve the synthesis of the relevant prodrug, the tetrazole ring of Losartan was protected with the trityl group for the ease of purification in the upcoming steps.[126] Trityl protected losartan **4** was converted to its succinic acid derivative **5** at the hydroxymethyl position using Diisopropyl ethyl amine (DIPEA) and succinic anhydride[18]. The esterification reaction of **5** with Quercetin hydroxyl (3'-OH, major) was conducted using

N-(3-Dimethylaminopropyl)-N′-ethylcarbodiimide hydrochloride (EDCI.HCl), 1-Hydroxybenzotriazole hydrate (HOBt) in Dimethylformamide (DMF).[128] The reaction resulted to **6** as a mixture of regioisomers of Quercetin at 3' and 4' (3:1).[22] Prior to the final acidic (DCM/TFA/TIS, 8.5/1/0.5, v/v) deprotection of the trityl group, the compound was purified with silica gel column chromatography.

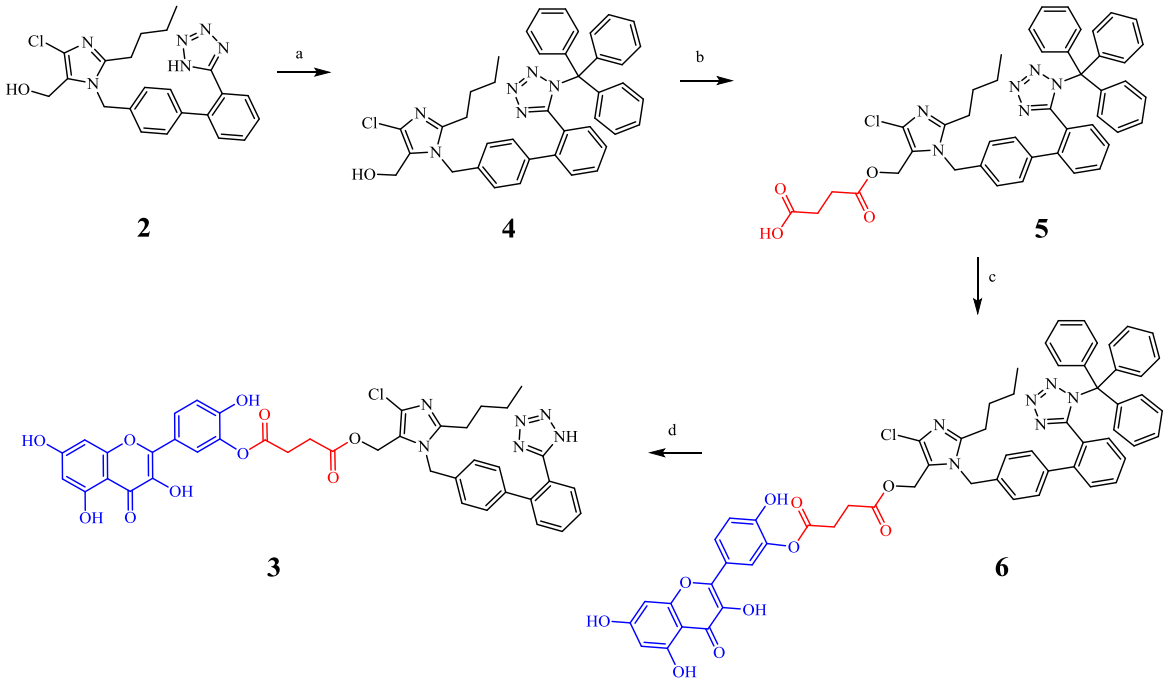

Figure11: *Chemical synthesis of the Queecetin-Losartan hybrid. Reagent and Conditions: a) Trityl chloride, Triethyl amine, DCM, rt, 2 h; b) Succinic anhydride, Diisopropyl ethyl amine, acetonitrile, rt, 12 h; c) Quercetin, EDC.HCl, HOBt, DMF, 60^{0}C, 1 h; d) DCM/TFA/TIS (8.5/1/0.5, v/v), 0^{0}C to rt, 4 h.*

Synthesis of N-trityl Losartan 4: Triethyl amine (165.0 µL, 2.5 mmol) was added to the solution of losartan (200 mg, 0.472 mmol) in 10 mL anhydrous dichloromethane (DCM) under inert atmosphere. After 5 min a solution tritylchloride (184.56 mg, 0.662 mmol) in 5 mL anhydrous DCM was added drop wise and the reaction was continued at rt for 2 h. TLC (DCM/MeOH, 9.5/0.5, v/v) illustrates the formation of a new spot and consumption of almost all losartan. The solvent was evaporated and the residue was dried well to give compound **4** (310 mg, 98.5%) as a white solid. The compound was used for next reaction without further purification.

Synthesis of N-trityl-Losartan succinic acid 5:

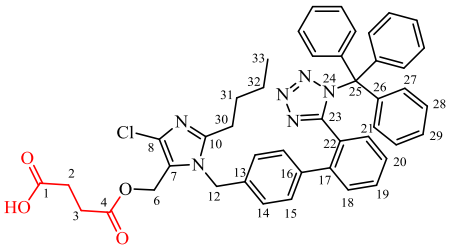

4

Diisopropyl ethyl amine (DIPEA) (818.15 µL, 4.696 mmol) was added to a solution of **4** (78 mg, 0.117 mmol) and succinic anhydride (29.37 mg, 0.293 mmol) in anhydrous acetonitrile (5 mL) under inert atmosphere. The reaction was continued on rt for 12 h. TLC (DCM/MeOH, 10/1, v/v) shows the consumption of **4**. The solvent was evaporated on rotary evaporator, the residue was dissolved in 5 mL of water and extracted with ethyl acetate (5 mL X 3).The combined organic layers were washed with brine, dried over sodium sulfate and concentrated to give **5** (86 mg, 95.86%) as a crude brown solid compound.

^{1}H-NMR of **5** (500 MHz, DMSO-d_6, 25^{o}C): δ = 12.23 (bs, 1 H, COOH), 7.84 - 7.81 (m, 1 H, 21-H), 7.66 - 7.63 (m, 1 H, 19-H), 7.59 - 7.56 (m,1 H, 20-H), 7.47 - 746 (m, 1 H, 18-H), 7.43- 7.27 (m, 9 H, 28 and 29-H), 7.11 (d, J = 8.2 Hz, 2 H, 15-H), 6.91 - 6.88 (m, 6 H, 27-H), 6.88 (d, J = 8.1 Hz, 2 H, 14-H), 5.20 (s, 2 H, 12-H), 4.92 (s, 2 H, 6-H), 2.46 (t, J = 7.7 Hz, 2 H, 30-H), 2.36 (t, J = 6.3 Hz, 2 H, 3-H), 2.27 (t, J = 6.3 Hz, 2 H, 2-H), 1.53 - 1.46 (m, 2 H, 31-H), 1.23 - 1.16 (m, 2 H, 32-H), 0.78 (t, J = 7.4 Hz, 3 H, 33-H) ppm. ^{13}C-NMR (500 MHz, DMSO-d_6, 25^{o}C): δ = 174.06 (C1), 172.44 (C4), 164.28 (C23), 149.48 (C10), 141.83 (C17), 141.79 (C22), 141.66 (C26), 140.34 (C16), 136.07 (C13), 131.29 (C18), 131.11 (C19), 130.92 (C21), 130.23 (C27), 139.94 (C15), 129.05 (C7), 128.96 (C29), 128.61 (C28), 128.49 (C20), 126.27 (C14), 121.42 (C8), 83.09 (C25), 54.48 (C6), 47.12 (C12), 29.42 (C31), 29.08 (C3), 28.98 (C2), 26.41 (C30), 22.18 (C32), 14.13 (C33) ppm. Mass: MS (ESI^{-}) *m/z* $[M-H]^{-}$ for $C_{45}H_{41}ClN_6O_4$: calcd,764.29; found, 763.27.

Synthesis of compound 6:

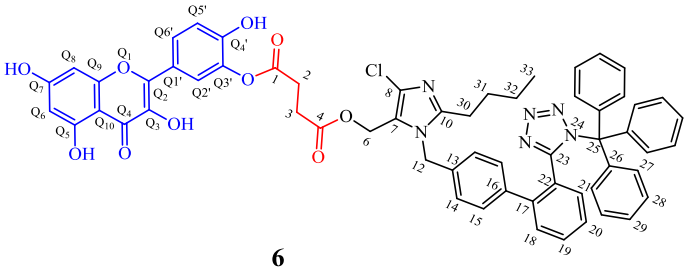

6

The solution of **5** (50 mg, 0.065 mmol) were added Quercetin (29.63 mg, 0.098 mmol), N-(3-Dimethylaminopropyl)-N′-ethylcarbodiimide hydrochloride (EDCI.HCl) (31.35 mg, 0.163 mmol) and 1-Hydroxybenzotriazole hydrate (HOBt) (17.67 mg, 0.130 mmol) in anhydrous DMF under inert atmosphere and were heated at 60^0C for 2 h. TLC (DCM/MeOH, 9.5/0.5, v/v) illustrated shows the formation of a new spot, and almost consumption of **5**. The reaction solvent was removed under high vacuum and the residue was purified with column chromatography (DCM/ methanol). The pure expected fraction was collected at 1% methanol in DCM, it was concentrated and dried to give product **6** (25 mg, 36.45%) as a yellow sticky compound.

^{1}H-NMR of **6** (500 MHz, DMSO-d_6, 25^{o}C): δ = 12.44 (s, 1 H, Q5-OH), 10.85 (s, 1 H, Q7-OH), 10.41 (s, 1 H, Q4'-OH), 9.60 (s, 1 H, Q3-OH), 7.97 (dd, J = 8.76, 2.26 Hz, 1 H, Q6'-H), 7.86 (d, J = 2.26 Hz, 1 H, Q2'-H), 7.81 (m, 1 H, 21-H), 7.60 (m, 1 H, 19-H), 7.56 (m,1 H, 20-H), 7.44 (m, 1 H, 18-H), 7.39 (m, 3 H, 29-H), 7.35 (m, 6 H, 28-H), 7.11 (d, J = 8.76 Hz, 1 H, Q5'-H), 7.08 (d, J = 8.20 Hz, 2 H, 15-H), 6.90 (m, 6 H, 27-H), 6.86 (d, J = 8.2 Hz, 2 H, 14-H), 6.45 (d, J = 2.0 Hz, 1 H, Q8-H), 6.23 (d, J = 2.0 Hz, Q6-H), 5.19 (s, 2 H, 12-H), 4.97 (s, 2 H, 6-H), 2.77 (m, 2 H, 2-H), 2.46 (m, 2 H, 3-H), 2.43 (m, 2 H, 30-H), 1.48 (m, 2 H, 31-H), 1.17 (m, 2 H, 32-H), 0.77 (t, J = 7.35 Hz, 3 H, 33-H) ppm; ^{13}C-NMR (500 MHz, DMSO-d_6, 25^{o}C): δ = 176.69 (C Q4), 172.15 (C4), 171.16 (C1), 164.91 (C Q7), 164.22 (C23), 161.73 (C Q5), 157.08 (C Q9), 151.67 (C Q4'), 149.46 (C10), 146.37 (C Q2), 141.85 (C17), 141.70 (C26), 140.30 (C16), 138.87 (C Q3') 136.94 (C Q3), 136.20 (C13), 131.38 (C18), 131.22 (C19), 130.99 (C21), 130.24 (C27), 130.09 (C15), 128.96 (C29), 128.61 (C28), 128.58 (C20), 127.19 (C Q6'), 126.34 (C14), 123.19 (C Q2'), 121.34 (C8), 117.66 (C Q5'), 103.92 (C Q10), 99.00 (C Q6), 94.22 (C Q8), 83.09 (C25), 54.74 (C6), 47.23 (C12), 29.52 (C31), 29.05 (C3 and C2), 26.48 (C30), 22.18 (C32), 14.20 (C33) ppm. Mass: MS (ESI$^-$) *m/z* [M-H]$^-$ for $C_{60}H_{49}ClN_6O_{10}$: calcd, 1048.32; found, 1047.30.

Synthesis of compound molecular hybrid 3:

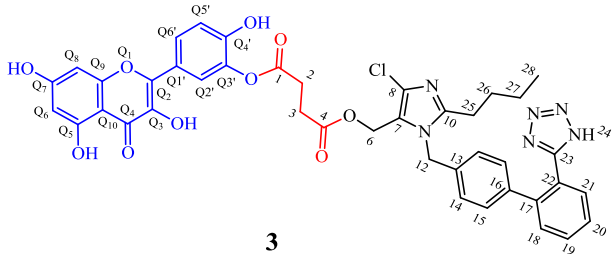

3

Compound **6** (48 mg) was dissolved in 5 mL of the cleavage cocktail DCM/TFA/TIS, 8.5/1/0.5, v/v at 0^0C to rt for 4 h. TLC (DCM/MeOH, 9.5/0.5, v/v) illustrated the formation of a new spot, and almost consumption of **6**. The reaction solvent was removed on rotary evaporator and the residue was washed with hexane (1 mL X 2) and diethyl ether (1 mL X 2) simultaneously, dried well to give compound **3** (35 mg, 94.82%) as a yellow solid.

^{1}H-NMR of **3** (500 MHz, DMSO-d_6, 25^{o}C): δ = 16.25 (bs, 1 H, 24-NH), 12.45 (s, 1 H, Q5-OH), 10.85 (s, 1 H, Q7-OH), 10.42 (s, 1 H, Q4'-OH), 9.60 (s, 1 H, Q3-OH), 7.97 (dd, J = 8.5, 2.1 Hz, 1 H, Q6'-H), 7.86 (d, J = 2.2 Hz, 1 H, Q2'-H), 7.67 (m, 1 H, 21-H), 7.59 (m, 1 H, 19-H), 7.58 (m, 1 H, 20-H), 7.67 (m, 1 H, 18-H), 7.11 (m, 1 H, Q5'-H), 7.11 (d, J = 8.1 Hz, 2 H, 15-H), 6.96(d, J = 8.1 Hz, 2 H, 14-H), 6.47 (d, J = 2.1 Hz, 1 H, Q8-H), 6.23 (d, J = 2.1 Hz, Q6-H), 5.26 (s, 2 H, 12-H), 5.06 (s, 2 H, 6-H), 2.81 (m, 2 H, 3-H), 2.54 (m, 2 H, 25-H), 2.46 (t, J = 6.5 Hz, 2 H, 2-H), 1.51 (m, 2 H, 26-H), 1.28 (m, 2 H, 27-H), 0.83 (t, J = 7.30 Hz, 3 H, 28-H) ppm; ^{13}C-NMR (500 MHz, DMSO-d_6, 25^{o}C): δ = 172.22 (C4), 171.18 (C1), 164.98 (C Q7), 161.71 (C Q5), 157.01 (C Q9), 151.81 (C Q4'), 149.66 (C10), 146.44 (C Q2), 141.87 (C17), 139.30 (C16), 138.91 (C Q3') 136.82(C13), 131.30 (C21), 131.28 (C19), 131.26 (C18), 129.94 (C15), 129.13 (C7), 128.53 (C20), 127.21(C Q6'), 126.56 (C14), 123.11 (C Q2'), 121.46 (C8), 117.60 (C Q5'), 103.94 (C Q10), 98.91 (C Q6), 94.17 (C Q8), 54.73 (C6), 47.18 (C12), 29.52 (C26), 29.02 (C3), 28.91 (C2), 26.47 (C25), 22.27 (C27), 14.22 (C28) ppm. Mass: MS (ESI$^-$) *m/z* $[M-H]^-$ for $C_{41}H_{35}ClN_6O_{10}$: calcd, 806.21; found, 805.2.

Mass spectrum of 3: Mass spectrum of final compound **3** in 0.1% formic acid in methanol show expected mass: Calcd, 806.21; found, 805.2. $[M-H]^-$ and 807.2 $[M+H]^+$. MS2 of peak 807.2 gives 405.1. The fragments 405.1 might be from intermediate Quercetin-succinic acid (calcd, 402.06.), mass spectrum is as following *Figure 12*.

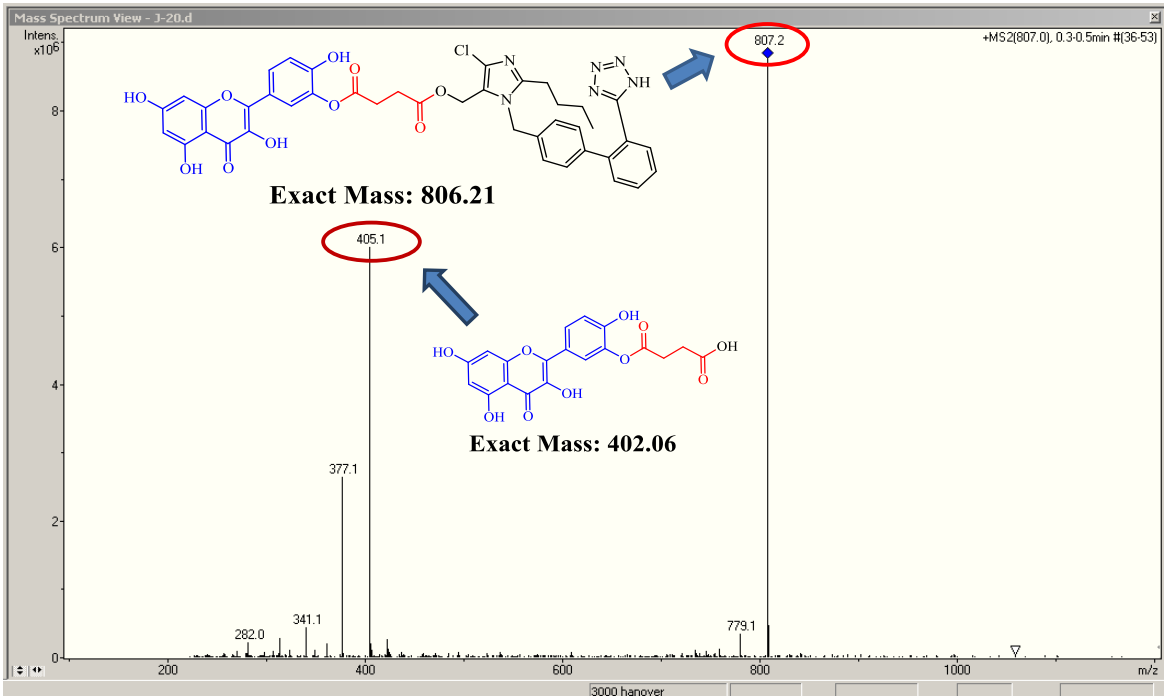

Figure 12: *Mass spectrum of final hybrid* ***3****.*

3.3.3 Biological evaluation:

The biological evaluation of this analogue is in process (binding affinity to the AT1 and AT2 receptors by the group of R. Widdob, Monash University, Australia and Cancer related experiments by Sayed Nelofer, Imperial College, UK).

3.4. Quercetin-Captopril

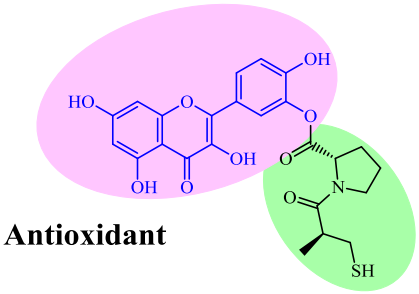

Antioxidant

Antihypertensive

3.4.1 Introduction:

In current time research on hypertension gain worldwide importance, because of it high frequency and risk factor associated with cardiovascular disease. So it has been identified as one of the risk factor for mortality. Angiotensin converting enzyme (ACE) maintains the arterial blood pressure by maintaining conversion of Angiotensin-I (decapeptide) to angiotensin-II (octapeptide). Inhibition of ACE reduce the concentration of Angiotensin II and subsequently blood pressure.[129] Therefore ACE inhibition plays an important role in the regulation of hypertension,[130, 129] as also regulation of the progression of renal disease through reducing the glomerular pressure and proteinuria.[129]

Captopril is one of the ACE inhibitors being currently used for the treatment of hypertension.[129] Captopril interacts with the active site of ACE [130, 129] (*Figure 13*). Captopril has two stereo centers (*Figure 13*) and its **S** enantiomer is 100 times more active than the **R** configuration[131].

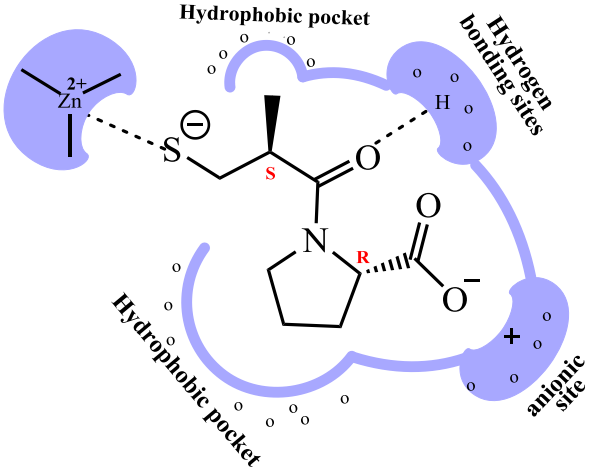

Figure 13: *Interaction of Captopril with the catalytic site of ACE.*

Herein, on the basis of the interlinkage of oxidative stress and hypertension, we exploited the potential of formation of a molecular hybrid with enhanced therapeutic index consisted of a potent antioxidant (quercetin) and the antihypertensive agent captopril.

3.4.2 Design, synthesis and characterization

Captopril bears two sites, sulfur and a carboxylic acid for the formation of the hybrid with Quercetin. Since, the sulfure group of captopril is implicated in the interaction with Zn^{2+} in the active site of ACE; we targeted conjugate formation with Quercetin through its carboxylic acid moiety. To achieve this it was necessary to follow a protection/ deprotection scheme both for sulfur as well as for the carboxylic group of Captopril (*Figure 14*).

We used different protection schemes for the sulfur of captopril (*tert*-Butyl and Trityl protection). Due to the free carboxylic acid of captopril, the sulfur protection was not quantitative and conversion to ethyl ester **2** was requested. Generally methyl/ethyl ester formation is simple, however, in the specific compounds care has to be taken since extra equivalents of thionyl chloride[132] results in a undesired product. Both trityl **3** and *tert*-Butyl **7** protections of sulfur reactions was qualitative and quantitative. The *tert*-Butyl protection was performed with perchloric acid ($HClO_4$) and *tert*-Butyl acetate; whereas trityl protection was achieved using trityl chloride and triethyl amine (TEA) as a base. Classical aq. KOH mediated hydrolysis results to compounds **4**/**8** for further coupling with Quercetin. The coupling of **4**/**8** and Quercetin was achieved in presence of EDCI.HCl, HOBt in DMF[128]. The last reaction resulted to inseparable mixture of regioisomers at positions 3' and 4' hydroxyl (in a ratio 3:1[22]). Final deprotection of sulfur (compound **5**) to obtain product **6** was carried out with a mixture of TFA/DCM/TIS (9/0.75/0.25; v/v). TIS (Triisopropyl silane) was used as carbocation scavenger. Interestingly, we were not able to have conversion of **9** to **6** in acidic non aqueous medium, even after the addition of 2.5% water (TFA/TIS/H_2O; 9.5/0.25/0.25, v/v). Using harsh aqueous conditions to hydrolyze compound **9** resulted in the parent compounds Quercetin and Captopril. It is there more pinpointed the importance of having a different and more acid labile protecting group (Trt) for the sulfur group of captopril.

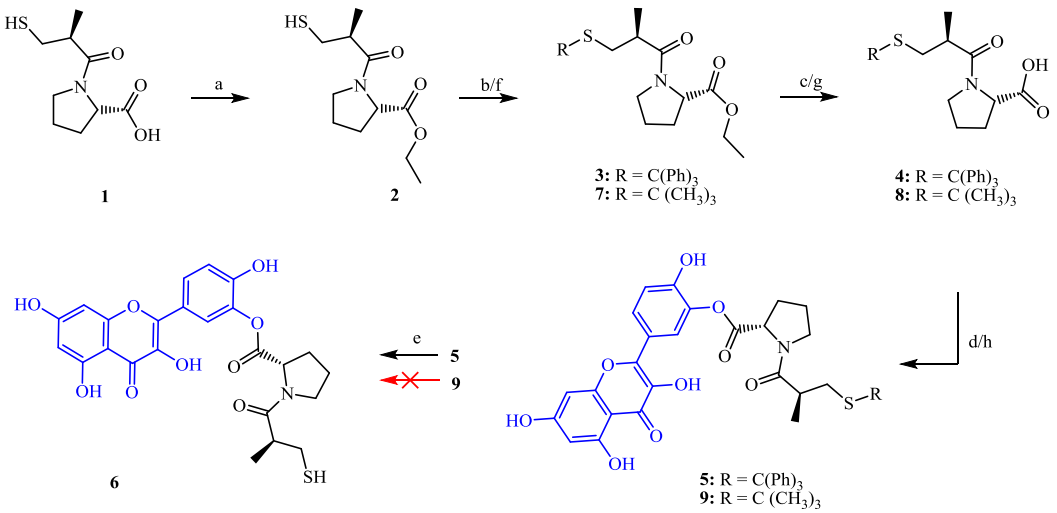

Figure14: *Synthetic scheme of Quercetin-Captopril. Reagents and conditions: a)Ethanol, $SOCl_2$, 60^0C, 4-5 h; b) $C(Ph_3)Cl$ (Trityl chloride), Triethyl amine (TEA), DCM, rt, 2 h; c) KOH (1N), $MeOH/H_2O$, 65^0C, 12 h; d) Quercetin, EDCI.HCl, HOBt, DMF, 60^0C, 1 h; e) TFA/DCM/TIS (9/0.75/0.25; v/v), rt, 4 h; f) $HClO_4$, $CH_3COO(CH_3)_3$, 0^0C - rt, 4 h; g) KOH (1M), $MeOH/H_2O$, rt, 24 h; h) Quercetin, EDCI.HCl, HOBt, DMF, 60^0C, 1 h.*

The synthetic methodology we used to construct the relevant hybrid is analyzed below.

Synthesis of 2:

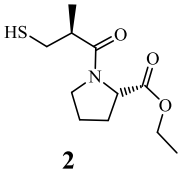

Captopril (500 mg, 2.303 mmol) was dissolved in 12.5 mL ethanol and Thionyl chloride (50 µL, 0.689 mmol) was added dropwise (ice cooling), and then heating at 60^0C was continued for 4-5 h. TLC (10% methanol in DCM (stain in Ioadine to see captipril) illustrated consumption of captopril and formation of two new spots related to the two regioisomers). The reaction solvent was evaporated on rotary evaporator, dried under high vacuum to give product **2** (560 mg, 99.19%) as a colourless viscous liquid.

^{1}H-NMR of **2** (250 MHz, DMSO-d_6, 25^0C): δ = 4.34 (dd, J = 4.5, 4.1 Hz, 1H), 4.15 - 4.02 (m, 2H), 3.72 - 3.52 (m, 2H), 2.84 – 2.73 (m, 1H), 2.70 – 2.62 (m, 1H), 2.51 – 2.40 (m, 1H), 2.30 (t, J = 8.2 Hz, 1H), 2.25 – 2.14 (m, 1H), 2.01 – 1.90 (m, 2H), 1.90 – 1.81 (m, 1H), 1.19 (t, J = 7.1 Hz, 3H), 1.09 (d, J = 6.7 Hz, 3H) ppm; ^{13}C-NMR (250 MHz, DMSO-

d_6, 25^0C): δ = 173.61 (C=O)), 172.78 (C=O), 61.12 (CH_2), 59.25 (CH), 47.45 (CH_2), 42.07 (CH), 29.57 (CH_2), 27.93 (CH_2), 25.34 (CH_2), 17.47 (CH_3), 14.92 (CH_3) ppm. Mass: MS (ESI^-) *m/z* $[M-H]^-$ for $C_{11}H_{19}NO_3S$: calcd, 245.11; found: 444.10.

Synthesis of compound 3:

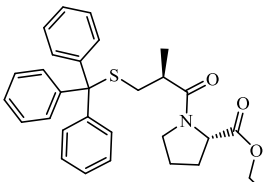

3

TEA (99.64 µL, 0.713 mmol) was added to a solution of **2** (70 mg, 0.285 mmol) and Trityl chloride (111.45 mg, 30.399 mmol) in 10 mL anhydrous DCM. The reaction was continued on rt for 2 h. TLC (5% Ethanol in DCM) illustrated the formation of a new spot consumption of **2**. The reaction mixture was diluted with 10 mL of water, then the residue was extracted with DCM (10 mL X 3), the combined organic layers were washed with brine, dried over sodium sulfate, concentrated, dried to give product **3** (139 mg). The crude compound was used fot the next reaction.

Synthesis of 4:

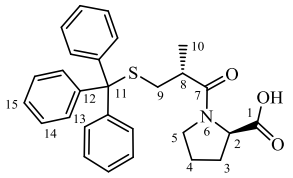

4

Compound **3** (139 mg, 0.285 mmol) was dissolved in 10 mL methanol, 1M aq. KOH (10 mL) was added at ice and the reaction was continued reflux (65^0C) for 12 h. TLC (5% methanol in DCM, stained in Iodine) showed consumption of **3** and formation of a new polar spot. The solvent (methanol) was evaporated on rotary evaporator; the aqueous layer (solid precipitate) was filtered through filter paper. Filtrate was extracted with ethyl acetate (5 mL X 1), the aqueous layer was acidify with dil. HCl till pH ~ 4 (Note: *Careful about pH, more acidic will deprotect sulfur)* ,the residue was extracted with ethyl acetate (10 mL X 3), washed with brine, dried over sodium sulfate, concentrated, dried to give compound **4** (77 mg, 58.72%) as a white solid.

^{1}H-NMR of **4** (500 MHz, DMSO-d_6, 25^{o}C): δ = 12.41 (bs, 1 H, 1-H), 7.36 (s, 12 H, 13, 14-H), 7.32- 7.28 (m, 3H, 15-H), 4.20 (dd, J = 8.2, 3.3 Hz, 1 H, 2-H), 3.30 (m, 2 H, 5-H), 2.58 (m, 1 H, 9a-H), 2.17 (m, 1 H, 8-H), 2.15- 2.11 (m, 1 H, 3a-H), 2.02 (dd. J = 6.23, 5.91 Hz, 1 H, 9b-H), 1.88 (m, 2 H, 4-H), 1.84- 1.80 (m, 1 H, 3b-H), 0.86 (d, J = 6.54, 3 H, 10-H) ppm; ^{13}C-NMR (500 MHz, DMSO-d_6, 25^{o}C): δ = 174.19 (C1), 173.0 (C7), 145.32 (C12), 129.92 (C14), 128.77 (C13), 127.47 (C15), 67 (C11), 58.94 (C2), 46.98 (C5), 37.76 (C8), 35.19 (C9), 29.28 (C3), 25.04 (C4), 17.53 (C10) ppm. Mass: MS (ESI^{-}) *m/z*: $[M-H]^{+}$ for $C_{28}H_{29}NO_3S$:calcd, 459.19; found, 458.17.

Synthesis of 5:

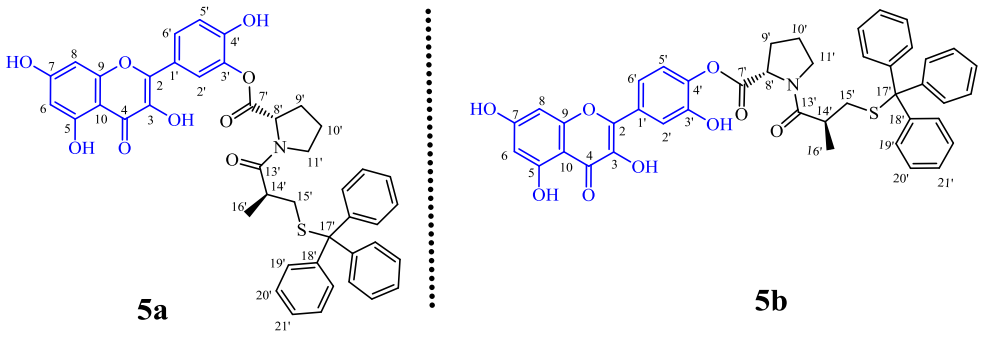

5a **5b**

A solution of **4** **(**65 mg, 0.146 mmol), Quercetin (50.27 mg, 0.166 mmol), EDCI.HCl **(**69.97 mg, 0.365 mmol) and HOBt **(**39.45 mg, 0.292 mmol) in 5 mL anhydrous DMF under nitrogen atmosphere was heated at 60^{0}C for 1 h.TLC (5% methanol in DCM) showed the formation of a new spot, and almost consumption of **4**. The solvent was evaporated with high vacuum, the crude compound was used for silica gel column chromatography purification in DCM and methanol as solvent.The pure expected spot was collected at 0.75% methanol in DCM.The pure fractions were concentrated and dried well to give product **5** (61 mg, 57.98%) as a yellow solid.

^{1}H-NMR of **5a** (500 MHz, DMSO-d^{6}, 25^{o}C): δ = 12.45 (s, 1 H, 5-OH), 10.85 (s, 1 H, 7-OH), 10.43 (s, 1 H, 4'-OH), 9.61 (s,1 H, 3-OH), 7.96 (dd, J = 8.65, 2.2 Hz, 1 H, 6'-H), 7.82 (d, J = 2.02 Hz, 1 H, 2'-H), 7.39 - 7.38 (m, 12 H, 19', 20'-H), 7.31 - 7.28 (m, 3 H, 21'-H), 7.09 (d, J = 8.87 Hz, 1 H, 5'-H), 6.47 (d, J = 2.0 Hz, 1 H, 8-H), 6.23 (d, J = 2.0 Hz, 1 H, 6-H), 4.58 (dd, J = 8.56, 4.36 Hz, 1 H, 8'-H), 3.47- 3.43 (m, 2 H, 11'-H), 2.69 - 2.63 (m, 1 H, 15'a-H), 2.36 - 2.30 (m, 1 H, 9'a-H), 2.26 - 2.20 (m, 1 H, 14'-H), 2.19 - 2.14 (m, 1 H, 9'b-H), 2.09 - 2.04 (m, 1 H, 15'b-H), 2.03 - 1.98 (m, 2H, 10'-H), 0.89 (d, J = 7.10 Hz, 3 H,

16'-H) ppm; ^{13}C-NMR (500 MHz, DMSO-d^6, 25^{o}C): δ = 176.9(C4), 173.61 (C13'), 170.81 (C7'), 165.2 (C7), 161.63 (C5), 157.08 (C9), 151.71 (C4'), 146.37 (C2), 145.41 (C18'), 138.97 (C3'), 136.91 (C3), 129.9 (C20'), 128.78 (C19'), 127.52 (C21'), 127.22 (C6´), 122.98 (C2´), 117.36 (C5´), 103.99 (C10), 98.97 (C6), 94.15 (C8), 64.24 (C17'), 59.02 (C8'), 47.18 (C11'), 37.88 (C14'), 35.09 (C15'), 29.26 (C9'), 25.13 (C10'), 17.54 (C16') ppm.

^{1}H-NMR of **5b** (500 MHz, DMSO-d^6, 25^{o}C): δ = 12.39 (s, 1 H, 5-OH), 10.90 (s, 1 H, 7-OH), 10.04 (s, 1 H, 3'-OH), 9.74 (s,1 H, 3-OH), 7.82 (d, J = 2.02 Hz, 1 H, 2'-H), 7.63(dd, J = 8.53, 2.10 Hz, 1 H, 6'-H), 7.39 - 7.38 (m, 12 H, 19', 20'-H), 7.31 - 7.28 (m, 3 H, 21'-H), 7.11 (d, J = 8.87 Hz, 1 H, 5'-H), 6.45 (d, J = 2.0 Hz, 1 H, 8-H), 6.24 (d, J = 2.0 Hz, 1 H, 6-H), 4.57 (dd, J = 8.56, 4.36 Hz, 1 H, 8'-H), 3.47- 3.43 (m, 2 H, 11'-H), 2.69 - 2.63 (m, 1 H, 15'a-H), 2.36 - 2.30 (m, 1 H, 9'a-H), 2.26 - 2.20 (m, 1 H, 14'-H), 2.19 - 2.14 (m, 1 H, 9'b-H), 2.09 - 2.04 (m, 1 H, 15'b-H), 2.03 - 1.98 (m, 2H, 10'-H), 0.89 (d, J = 7.10 Hz, 3 H, 16'-H) ppm; ^{13}C-NMR (500 MHz, DMSO-d^6, 25^{o}C): δ = 177.2 (C4), 173.61 (C13'), 170.81 (C7'), 165.2 (C7), 161.63 (C5), 157.08 (C9), 149.6 (C3'), 145.99 (C2), 145.41 (C18'), 140.50 (C4'), 137.9 (C3), 129.9 (C20'), 128.78 (C19'), 127.52 (C21'), 123.55 (C5´), 119.5 (C6'), 116.67 (C2´), 103.99 (C10), 98.97 (C6), 94.15 (C8), 67.24 (C17'), 59.02 (C8'), 47.18 (C11'), 37.88 (14'), 35.09 (C15'), 29.26 (C9'), 25.13 (C10'), 17.54 (C16') ppm.

Mass: MS (ESI$^-$) *m/z* [M-H]$^-$ for $C_{43}H_{37}NO_9S$: calcd, 743.22; found: 742.20.

Synthesis of 6:

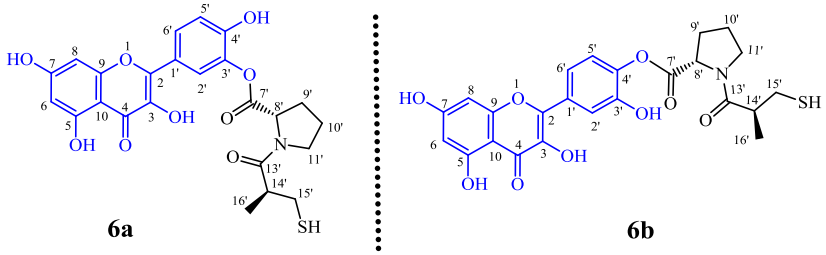

Compound **5** (35 mg) in 2.5 mL cleavage cocktail (TFA/DCM/TIS, 9/0.75/0.25; v/v) was stirred at 0^{0}C rt for 4 h. The solvent was evaporated using azeotrop with DCM/Hexane (1:1, 5mL X 3); the resulted solid was dissolved in a minimum amount of DCM (~ 1 mL) and was then precipitated out with hexane (~ 5 mL). The residue was then centrifugated

and the solid was dried well on high vacuum to give compound **6** (20 mg, 84.78%) as a yellow solid.

^{1}H-NMR of **6a** (500 MHz, DMSO-d_6, 25^{o}C): δ = 12.45 (s, 1 H, 5-OH), 10.85 (s, 1 H, 7-OH), 10.44 (s, 1 H, 4'-OH), 9.63 (s,1 H, 3-OH), 7.98 (dd, J = 8.68, 2.2 Hz, 1 H, 6'-H), 7.85 (d, J = 2.21 Hz, 1 H, 2'-H), 7.11 (d, J = 8.76 Hz, 1 H, 5'-H), 6.47 (d, J = 1.98 Hz, 1 H, 8-H), 6.23 (d, J = 1.98 Hz, 1 H, 6-H), 4.65 (dd, J = 8.70, 4.64 Hz, 1 H, 8'-H), 3.78 (m, 2 H, 11'-H), 2.88 - 2.84 (m, 1 H, 14'-H), 2.77 - 2.71 (m, 1 H, 15'a-H), 2.52 (m, 1 H, 15'b-H), 2.40 - 2.39 (m, 1 H, 9'a-H), 2.25 - 2.21 (m, 1 H, 9'b-H), 2.11 - 2.04 (m, 2 H, 10'-H), 1.12 (d, J = 6.81 Hz, 3 H, 16'-H) ppm; ^{13}C-NMR (500 MHz, DMSO-d_6, 25^{o}C): δ = 176.84 (C4), 174.13 (C13'), 170.93 (C7'), 165.07 (C7), 161.74 (C5), 157.13 (C9), 151.84 (C4'), 146.41 (C2), 138.96 (C3'), 137.05 (C3), 127.32 (C6′), 123.07 (C2′), 117.44 (C5′), 104.12 (C10), 98.99 (C6), 94.26 (C8), 59.13 (C8'), 47.43 (C11'), 41.98 (C14'), 29.43 (C9'), 27.73 (C15'), 25.31 (C10'), 17.29 (C16') ppm.

^{1}H-NMR of **6b** (500 MHz, DMSO-d_6, 25^{o}C): δ = 12.39 (s, 1 H, 5-OH), 10.90 (s, 1 H, 7-OH), 10.05 (s, 1 H, 3'-OH), 9.74 (s,1 H, 3-OH), 7.83 (d, J = 2.05 Hz,1 H, 2'-H), 7.65 (dd, J = 8.47, 2.04 Hz, 1 H, 6'-H), 7.15 (d, J = 8.43 Hz, 1 H, 5'-H), 6.45 (d, J = 1.98 Hz, 1 H, 8-H), 6.24 (d, J = 1.98 Hz, 1 H, 6-H), 4.63 (dd, J = 8.70, 4.64 Hz, 1 H, 8'-H), 3.78 (m, 2 H, 11'-H), 2.88 - 2.84 (m, 1 H, 14'-H), 2.77 - 2.71 (m, 1 H, 15'a-H), 2.52 (m, 1 H, 15'b-H), 2.40 - 2.39 (m, 1 H, 9'a-H), 2.25 - 2.21 (m, 1 H, 9'b-H), 2.11 - 2.04 (m, 2 H, 10'-H), 1.11 (d, J = 6.56 Hz, 3 H, 16'-H) ppm; ^{13}C-NMR (500 MHz, DMSO-d_6, 25^{o}C): δ = 174.13 (C13'), 170.93 (C7'), 165.24 (C7), 161.82 (C5), 157.13 (C9), 146.22 (C2), 140.47 (C4'), 138.1 (C3), 123.68 (C5'), 119.54 (C6′), 116.77 (C2'), 104.12 (C10), 98.99 (C6), 94.26 (C8), 59.13 (C8'), 47.43 (C11'), 41.95 (C14'), 29.43 (C9'), 27.73 (C15'), 25.31 (C10') 17.29 (C16') ppm.

Synthesis of compound 7:

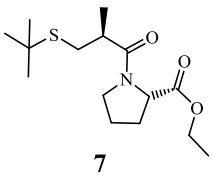

7

Compound **2** (560 mg, 2.284 mmol) was dissolved in 10 mL *tert*-Butyl acetate and then perchloric acid (116.82 µL, 1.941 mmol) was added drop wise under ice stirring was continued rt for 4 h. The solvent was evaporated; the residue was diluted with 20 mL water and neutralized with sodium bicarbonate ($NaHCO_3$). The residue was extracted with ethyl acetate (15 mL X 3), the combined organic layers were washed with brine, dried over sodium sulfate and concentrated to give compound **7** (650 mg, 94.46%) as a pale yellow liquid.

^{1}H-NMR of **7** (250 MHz, DMSO-d_6, 25^o C): δ = 4.30 (dd, J = 8.74, 4.1 Hz, 1 H), 4.17 - 4.01 (m, 2 H), 3.60 (t, J = 6.7 Hz, 2 H), 2.80 – 2.68 (m, 2 H), 2.49 – 2.40 (m, 1 H), 2.27 – 2.13 (m, 1 H), 2.00 - 2.90 (m, 2 H), 1.90 – 1.81 (m, 1 H), 1.28 (s, 9 H), 1.19 (t, J = 7.1 Hz, 3 H), 1.11 (d, J = 6.4 Hz, 3 H) ppm; ^{13}C-NMR (250 MHz, DMSO-d_6, 25^o C): δ = 173.84 (C=O), 172.83 (C=O), 61.16 (CH_2), 59.31 (CH), 47.51 (CH_2), 42.84 (C), 39.05 (CH), 32.08 (CH_2), 31.65 (CH_3), 29.59 (CH_2), 25.34 (CH_2), 18.11 (CH_3), 14.95 (CH_3) ppm. Mass: MS (ESI) *m/z* $[M+H]^+$ for $C_{15}H_{27}NO_3S$: calcd, 301.17; found: 302.17.

Synthesis of compound 8:

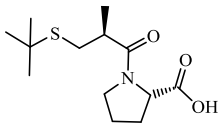

8

Compound **7** (85 mg, 0.282 mmol) was dissolved in methanol (2 mL).1M aq. KOH (2 mL) was then added at ice cooling and the reaction was continued on rt for 24 h. (***Observation*****:** light pink colour of **7** in methanol was disappeared after addition of aq. KOH.) TLC (10% methanol in DCM; stained in Iodine) illustrated the consumption of starting material and formation of a polar spot. The solvent was evaporated, the residue was dissolved in 5 mL water and extracted with ethyl acetate (3 mL X 2).The aqueous layer was acidified with dil. HCl until pH ~ 4, extracted with ethyl acetate 3 mL X 3. The combined organic layers were washed with brine, dried over sodium sulfate and concentrated to give compound **8** (75 mg, 97.30%) as a yellow liquid.

^{1}H-NMR of **8** (250 MHz, DMSO-d_6, 25^o C): δ = 12.40 (bs, 1 H), 4.25 (dd, J = 8.67, 3.5 Hz, 1 H), 3.59 (t, J = 6.60 Hz, 2 H), 2.80 – 2.70 (m, 2 H), 2.48 – 2.41 (m, 1 H), 2.21 – 2.10 (m,

1 H), 1.99 - 1.90 (m, 2 H), 1.87 – 1.81 (m, 1 H), 1.28 (s, 9 H), 1.10 (t, J = 6.38 Hz, 3 H), ppm; ^{13}C-NMR (250 MHz, DMSO-d_6, 25^o C): δ = 174.36 (C=O), 173.71 (C=O), 59.23 (CH), 47.48 (CH_2), 42.84 (C), 38.99 (CH), 32.17 (CH_2), 31.66 (CH_3), 29.65 (CH_2), 25.30 (CH_2), 18.12 (CH_3), ppm. Mass: MS (ESI) *m/z* [M-H]$^-$ for $C_{13}H_{23}NO_3S$: calcd, 273.14, found: 272.13.

Synthesis of 9:

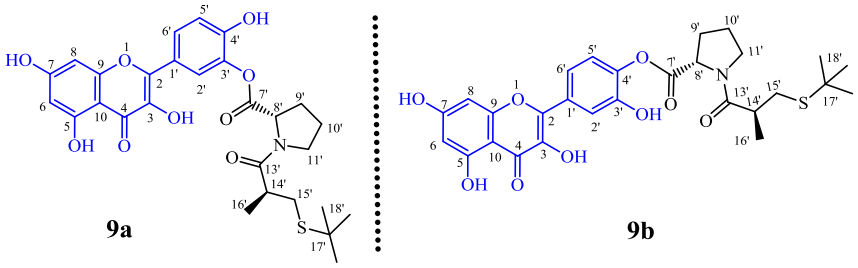

9a **9b**

Toa solution of **8 (**100 mg, 0.366 mmol) in anhydrous DMF (10 mL) under nitrogen atmosphere, Quercetin (126.0 mg, 0.417 mmol), EDCI.HCl (175.4 mg, 0.915 mmol) and HOBt (98.93 mg, 0.732 mmol) were added and the reaction was heated at 60^{0}C for 1 h.TLC (5% methanol in DCM) showed almost consumption of **8** and formation of a new spot.The solvent was evaporated under high vacuum, the crude compound was used for silica gel column chromatography purification in DCM and methanol as solvent. The desired product was collected at 1% methanol in DCM and the pure fraction was concentrated and dried to give compound **9** (52 mg, 25.49%) as a yellow solid.

^{1}H-NMR of **9a** (500 MHz, DMSO-d_6, 25^{o}C): δ = 12.45 (s, 1 H, 5-OH), 10.85 (s, 1 H, 7-OH), 10.44 (s, 1 H, 4’-OH), 9.63 (s,1 H, 3-OH), 7.98 (dd, J = 8.64, 2.24 Hz, 1 H, 6’-H), 7.85 (d, J = 2.24 Hz, 1 H, 2’-H), 7.11 (d, J = 8.78 Hz, 1 H, 5'-H), 6.47 (d, J = 2.05 Hz, 1 H, 8-H), 6.23 (d, J = 2.0 Hz, 1 H, 6-H), 4.62 (dd, J = 8.70, 4.34 Hz, 1 H, 8'-H), 3.71 (m, 2 H, 11'-H), 2.83 - 2.81 (m, 1 H, 14'-H), 2.83 - 2.80 (m, 1 H, 15'a-H), 2.54 (m, 1 H, 15'b-H), 2.40 - 2.39 (m, 1 H, 9'a-H), 2.24 - 2.19 (m, 1 H, 9'b-H), 2.10 - 2.04 (m, 2 H, 10'-H), 1.31 (s, 9 H, 18'-H), 1.15 (d, J = 6.25 Hz, 3 H, 19'-H) ppm; ^{13}C-NMR (500 MHz, DMSO-d_6, 25^{o}C): δ = 176.88 (C4), 174.24 (C13’), 170.78 (C7'), 164.84 (C7), 161.63 (C5), 156.89 (C9), 151.67 (C4’), 146.21 (C2), 138.87 (C3'), 136.89 (C3), 127.24 (C6'), 122.98 (C2´), 117.31 (C5´), 103.99 (C10), 98.93 (C6), 94.14 (C8), 59.09 (C8'), 47.37 (C11’), 42.8 (C17'), 38.85 (C14'), 31.79 (C15'), 31.41 (C18'), 29.33 (C9'), 25.19 (C10'), 17.87 (C19') ppm.

^{1}H-NMR of **9b** (500 MHz, DMSO-d_6, 25^{o}C): δ = 12.39 (s, 1 H, 5-OH), 10.90 (s, 1 H, 7-OH), 10.04 (s, 1 H, 3'-OH), 9.74 (s,1 H, 3-OH), 7.83 (d, J = 2.09 Hz, 1 H, 2'-H), 7.65 (dd, J = 8.53, 2.09 Hz, 1 H, 6'-H), 7.15 (d, J = 8.53 Hz, 1 H, 5'-H), 6.45 (d, J = 2.07 Hz, 1 H, 8-H), 6.24 (d, J = 2.0 Hz, 1 H, 6-H), 4.60 (dd, J = 8.53, 4.30 Hz, 1 H, 8'-H), 3.71 (m, 2 H, 11'-H), 2.83 - 2.81 (m, 1 H, 14'-H), 2.83 - 2.80 (m, 1 H, 15'a-H), 2.54 (m, 1 H, 15'b-H), 2.40 - 2.39 (m, 1 H, 9'a-H), 2.24 - 2.19 (m, 1 H, 9'b-H), 2.10 - 2.04 (m, 2 H, 10'-H), 1.31 (s, 9 H, 18'-H), 1.14 (d, J = 6.04 Hz, 3 H, 19'-H) ppm; ^{13}C-NMR (500 MHz, DMSO-d_6, 25^{o}C): δ = 176.88 (C4), 174.24 (C13'), 170.78 (C7'), 165.1 (C7), 161.63 (C5), 156.89 (C9), 149.6 (C3'), 146.21 (C2), 140.4 (C4'), 123.54 (C5′), 119.53 (C6'), 116.64 (C2′), 103.99 (C10), 98.93 (C6), 94.14 (C8), 59.09 (C8'), 47.37 (C11'), 42.8 (C17'), 38.85 (14'), 31.79 (C15'), 31.41 (C18'), 29.33 (C9'), 25.19 (C10'), 17.87 (C19') ppm.

3.4.3 Biological evaluation:

Biological experiments for this analogue are in progress by our collaborators Tim Crook, Sayed Nelofer in Imperial College, UK

Chapter 4: GnRH-Sunitinib conjugates

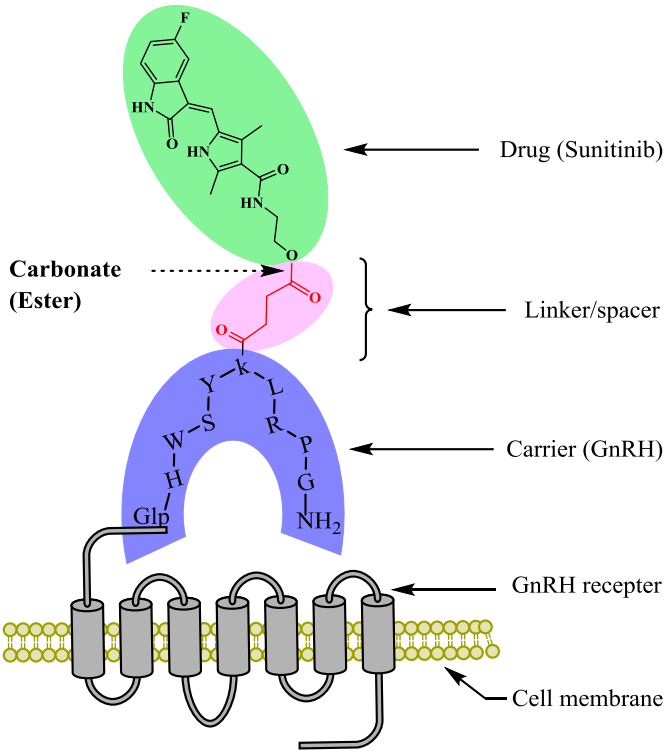

Submitted:

Orestis Argyros[1], Theodoros Karampelas[1], Xenofontas Asbos[3], Nisar Sayyad[3] et. al.

SUNITINIB-GNRH CONJUGATES FOR THE TARGETED TREATMENT OF TUMOURS, Clinical Cancer Research.

4.1 Introduction

The concept of generating novel cancer therapies that target specific cell-surface receptors has been a driving force of drug development over the past few years.[133, 134] This idea is based on the knowledge that certain cell-surface receptors in tumour cells are either mutated (*e.g.*, EGFR) or over-expressed (*e.g.*, HER-2, GnRH-R), compared to normal cells[135, 2] and these alterations provide "druggable" opportunities. Driven by this fact we previously showed the successful targeting of gonadotropin releasing hormone receptor (GnRH-R) in GnRH-R positive prostate cancer (CaP) using a conjugate of a GnRH peptide linked to the cytotoxic drug Gemcitabine.[18] A similar doxorubicin based conjugate (called AN152) proved efficacious in pre-clinical studies, and has now advanced to phase III clinical trials for various solid malignancies; a significant achievement that highlights the power of this targeted concept.[136, 137]

The GnRH-R is a member of G-protein-coupled receptors with the characteristic seven transmembrane domains connected by extracellular and intracellular loops.[2, 1] It is normally present in the pituitary gland and in smaller amounts in other tissues, but upregulation of its expression has been reported in prostate, breast and other cancers.[1, 3] The main ligand for this receptor is the decapeptide hormone GnRH-I, which upon binding transmits signals from the GnRH-R to the nucleus through the MAPK/Erk1/2 signaling pathway,[3, 138] regulating reproduction.[5] Interestingly an anti-proliferative role of GnRH-I on hormone independent CaP has also been reported, providing additional opportunities for the treatment of this tumour by directly affecting cancer cells apart from the pituitary.[139, 140]

Supplementary to dysregulation of cell surface receptor another key factor promoting tumour progression is angiogenesis; a process orchestrated by cytokines released from the tumour itself to sprout new vessels and support tumour growth. The prospect of angiogenesis as a target for cancer therapy lead to the development of numerous anti-angiogenic agents which inhibit phosphorylation (hence, activation) of certain receptors like the vascular endothelial growth factor receptors (VEGFRs) types 1/2 and platelet-derived growth factor receptors (PDGFR-α/β).[141] Current clinical efforts in the treatment of patients with solid tumours (including CaP) evaluate combinational strategies with molecules that simultaneously inhibit tumour and stromal cell growth.[142,143] We decided to pursue this concept and apply a bimodal treatment on GnRH-R positive cancers, by

generating novel GnRH-based molecules conjugated to a leading anti-angiogenic drug, Sunitinib.

Sunitinib (SU11248; Sutent) is a rationally designed small molecule that emerged as a pharmacologically improved version of the indolin-2-one Semaxanib.[144] It is orally available and able to inhibit phosphorylation of several receptor tyrosine kinases (RTKs) including VEGFRs-1/2, PDGFR-α/β, c-Kit and FLT-3, with an IC_{50} below 100nM.[145, 146] In CaP and other solid tumours, the VEGF, PDGF and c-Kit signaling pathways are critical in driving transduction of extracellular signals controlling angiogenesis, tumour growth and metastasis.[147, 148]

The success of Sunitinib in clinical trials led to its FDA approval for renal cell carcinoma, imatinib-resistant gastrointestinal stromal tumour and of pancreatic neuroendocrine malignancies. However, clinical trials of Sunitinib in other solid tumours, such as prostate[149] and breast cancer[150] were halted in phase III based on the lack of statistically significant overall survival rates in patients despite successful pre-clinical efficacy[145] and prolongation of progression free survival. The latter clinical results suggest that better patient selection or increased specificity of Sunitinib delivery at the site of action, through a targeting peptide may lead to improved efficacy while minimizing off-target effects.

In addition, generation of Sunitinib based conjugates may address another important issue, the rapid but reversible resistance of tumour cells to Sunitinib treatment.[151] Blockage of VEGFR-2 by small molecules such as Sunitinib causes vascular and tumoural regression. Nevertheless, tumour collapse also causes central tumour regions of hypoxia and a corresponding up-regulation of hypoxia inducible factors that may help in circumvent of VEGFR-inhibited signalling pathways and promote evasion from VEGFR inhibitors in peripheral areas. In this latter phase of circumvention, tumour cells upregulate the expression of other pro-angiogenic factors (*e.g.,* PDGF/ PDGFR) that reactivate angiogenesis in a VEGFR-independent manner.[152] To overcome this phenomenon, combination therapies of Sunitinib with other targeted agents (e.g., compounds against the Phosphatidyl inositol 3 kinase) may be used.[153] Alternatively and at least for GnRH-R positive tumours, the resistance of the peripheral rim of viable tumour cells can be overcomed by utilizing a GnRH conjugated version of Sunitinib, exploiting the additional anti-proliferative effect of the GnRH peptide itself.

Following Sunitinib approval, few groups have reported the generation of a small number of analogues, with most of them modifying the pyrrole ring of Sunitinib.[154,155,156,157] This

was based on crystallization studies[158] revealing that the drug part involved in kinase phosphorylation inhibition is the indolin-2-one core, whereas the C4 position on the pyrrole ring had minimal interaction with the active kinase centre. Thus, substitution at this position might serve as a key for improving pharmaceutical properties as shown by Toceranib, a drug approved by the FDA for the treatment of c-Kit driven canine mast cell tumour.[156] Other analogues have also been described[159,160] but as far as we know, there have been no reports of a conjugated version of Sunitinib or any of its analogues to a targeting moiety, possibly due to the lack of chemically linkable groups in Sunitinib. Such a conjugation may overcome limited clinical success on some solid tumours by increasing the drug payload specifically to the site of action for selected patient populations.

The results of preclinical studies for six novel Sunitinib analogues (named SANs 1-6), which were rationally designed to be linkable to a targeting peptide while still maintaining their anti-angiogenic properties are reported in this manuscript.

The application of peptide-drug conjugates in the clinic promises to achieve higher efficacy with increased safety. In the current manuscript we investigated the possibility of conjugating a targeting peptide to an analogue of Sunitinib, a multi-kinase inhibitor with a strong clinical record against several solid tumours. Prostate and breast cancer trials with Sunitinib revealed an improved Progression Free Survival but not Overall Survival, suggesting that better patient selection or a more specific drug delivery to the tumour site may lead to an improved clinical outcome. Thus, we generated a conjugated molecule consisting of a potent Sunitinib Analogue (SAN1) linked to [D-Lys^6]-GnRH moiety and evaluated it *in vivo* in a GnRH-R cancer model. *In vivo* efficacy of SAN1 and SAN1GSC was assessed in prostate cancer mouse xenografts by tumour volume measurements, immunohistochemistry and by determining the phosphorylation status of 39 kinases. We demonstrated an improved delivery and efficacy on animals which were treated with the conjugate compared to control. This targeted approach is applicable to other GnRH-R expressing tumours as well as other receptors by alteration of the targeting peptide.

4.2 Design, synthesis and characterization:

Synthesis and characterization:

The sunitinib analogue SAN1 (1) has a free hydroxyl group which was used to make carboxylic ester based bio conjugates with [D-Lys^6]-GnRH. Reaction of **1** and succinic

anhydride resulted in sunitinib-hemisuccinate (2). HATU mediated coupling of acid **2** with the ε-amino group of [D-Lys^6]-GnRH afforded bioconjugate **3**.

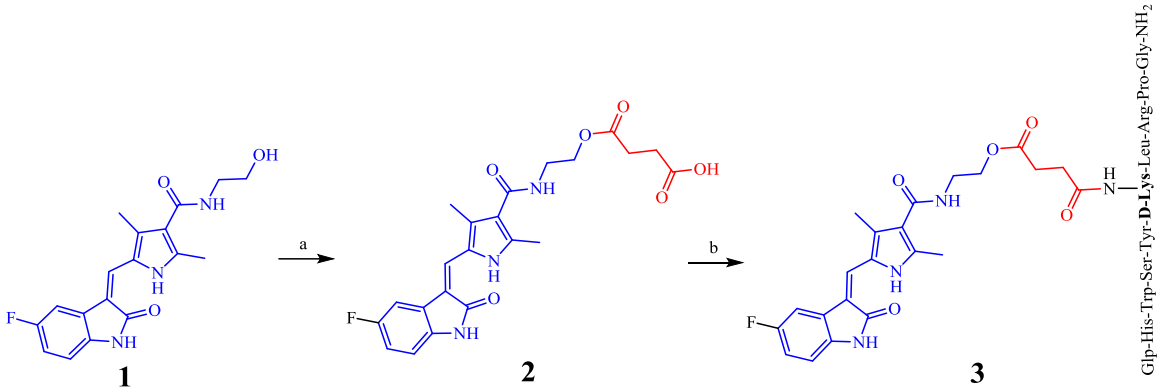

Figure 1: *Chemical Synthesis of **3**, Reagents and Conditions: a) succinic anhydride, DMAP, TEA, DMF, rt, 12 h; b) [D-Lys^6]-GnRH, HATU, DIPEA, DMF.*

Synthesis of 2: To a solution of **1** (50 mg, 0.145 mmol), succinic anhydride (116.57 mg, 1.165 mmol) and 4-Dimethylaminopyridine (17.80 mg, 0.145 mmol) in anhydrous DMF (10 mL) was added Triethyl amine (406.76 µL, 2.914 mmol). The reaction mixture was stirred at room temperature overnight. The resulting mixture was concentrated under reduced pressure to give the crude product which was purified by HPLC to give hemisuccinate **2** (40 mg, 62%) as a yellow solid.

^{1}H-NMR of **2** (500 MHz, DMSO-d$_6$, 25^{o}C): δ = 13.72 (s, 1 H, 15-NH), 10.93 (s, 1 H, 1-NH), 7.80 (dd, J = 9.5, 2.4 Hz, 1 H, 5-H),7.76 (s, 1 H, 17-NH), 7.75 (s, 1 H, 10-H), 6.96 (dt, J = 9.0, 2.4 Hz, 1 H, 7-H), 6.88 (m, 1 H, 8-H), 4.17 (t, J = 5.6 Hz, 2 H, 19-H), 3.50 (t, J = 5.6 Hz, 2 H, 18-H), 2.55 (m, 2 H, 22-H), 2.52 (m, 2 H, 23-H), 2.46 (s, 3 H, 14a-H), 2.44 (s, 3 H, 12a-H) ppm; ^{13}C-NMR (500 MHz, DMSO-d$_6$, 25^{o}C): δ = 174.23 (C24), 173.18 (C21), 170.40 (C2), 165.76 (C16), 158.94 (C6), 137.39 (C14), 135.5 (C9), 131.25 (C12), 128.13 (C3) 126.71 (C11), 125.63 (C10), 121.54 (C13), 115.54 (C4), 113.11 (C7), 110.73 (C8), 106.69 (C5), 63.5 (C19), 38.44 (C18), 29.54 (C22 and C23), 13.87 (C14a), 11.12 (C12a) ppm. Mass: MS (ESI$^-$) *m/z*: [M-H]$^-$ for $C_{22}H_{22}FN_3O_6$:calcd.443.15, found 442.14.

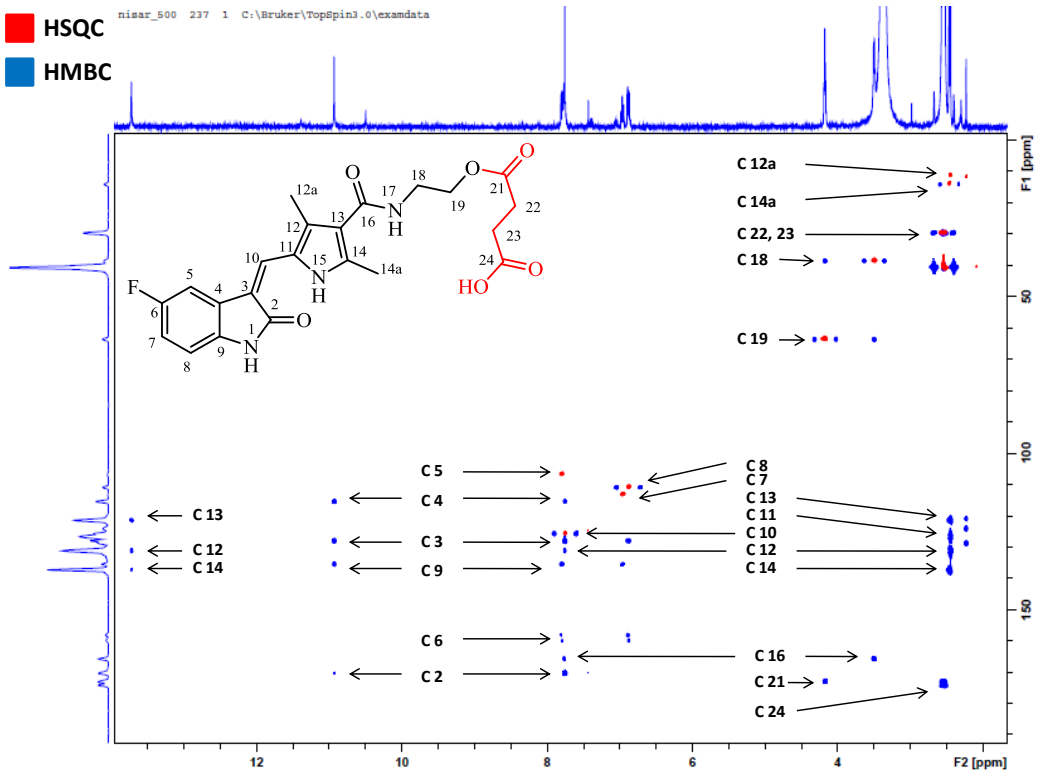

Figure 2: *2D NMR (HMBC, HSQC) of* ***2****.*

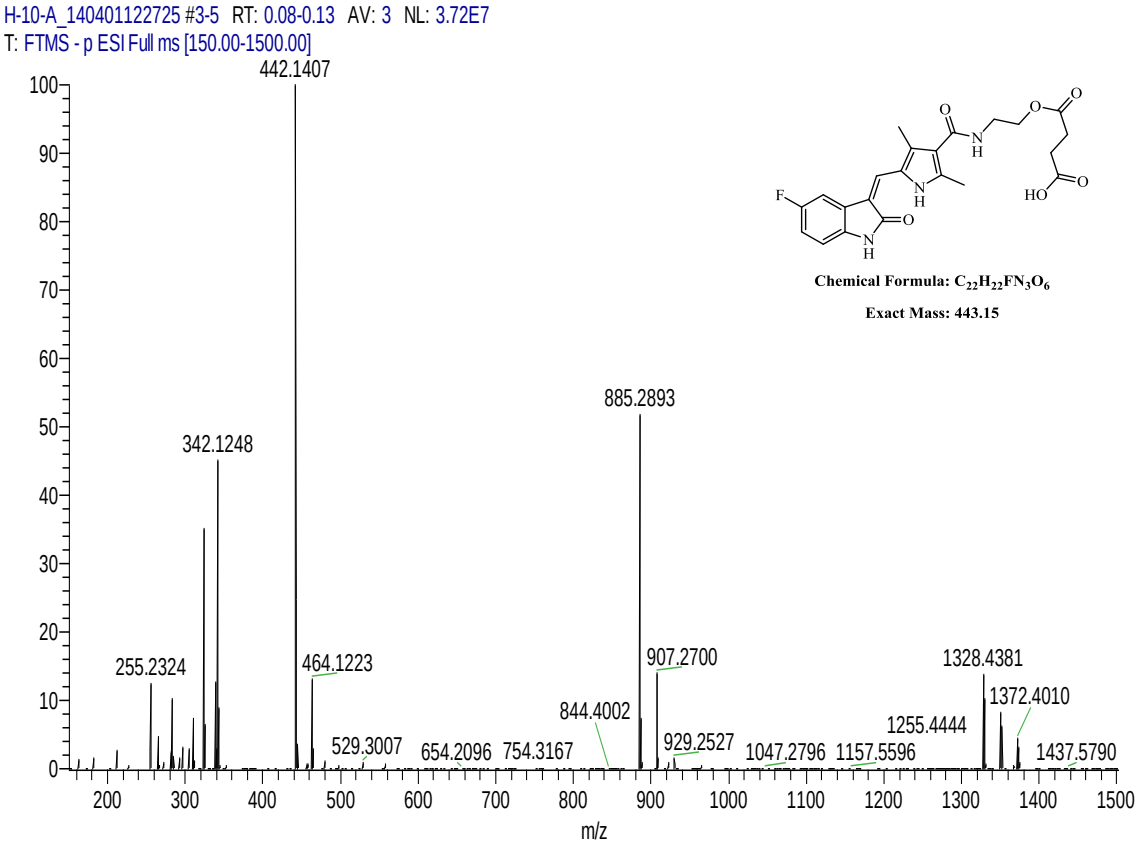

Figure 3: *Mass spectrum of* ***2****.*

Synthesis of 3: To a solution of acid **2** (50 mg, 0.112 mmol), HATU (42.58 mg, 0.112 mmol) and DIPEA (98.2 µL, 0.564 mmol) in 10 mL of DMF, a solution of [D-Lys^6]-GnRH (140 mg, 0.112 mmol) in 5 mL of DMF was added drop wise. The reaction mixture was stirred at room temperature for 12 h and the solvent was removed under reduced pressure. The crude product was purified by HPLC to give conjugate **3** (52 mg, 27.46%). as a yellow solid.

Mass: MS (ESI$^+$) *m/z* for $C_{81}H_{104}FN_{21}O_{18}$: calcd, 1677.99; found, 840.4 $[M+2H]^{2+}$.

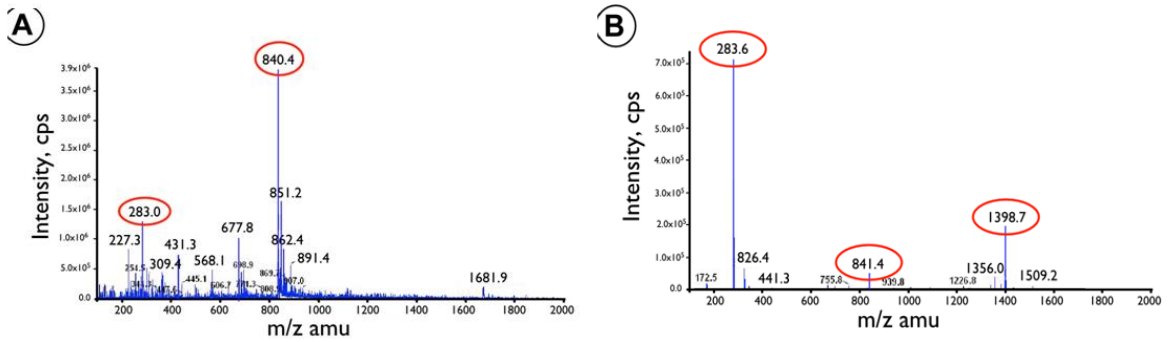

Figure 4: *Mass spectrum of compound* ***3****. Representative MS/MS analysis of parent ion (SAN1GSC) with m/z 840.4 showing the main fragments (product ions) with m/z 283.6 and 1398.7 corresponding to the main SAN1 product ion and a fragment ion consisting of the [D-Lys^6]-GnRH-Succinate linker****.***

MS analysis

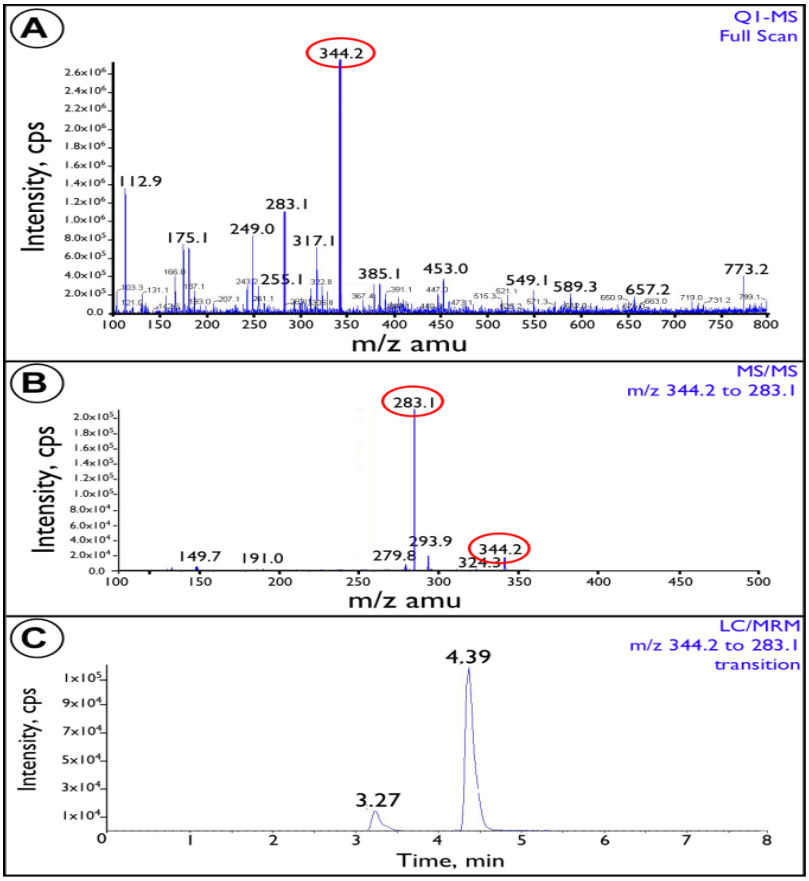

Figure 5: *(A) Representative positive electrospray ionization (ESI$^+$) mass spectra of SAN1 showing the main ionized form (m/z 344.1) corresponding to M+1 of SAN1. (B) Representative MS/MS analysis of parent ion with m/z 344.1 showing the main fragment (product ion) with m/z = 283.1. (C) LC/MRM chromatogram depicts the separation of SAN1 (10 ng on column) and demonstrating the two geometric isomers (E and Z).*

4.3 Biological evaluation

Molecular Docking Analysis

Molecular docking analysis was performed to all synthesized SANs using the catalytic domains from three key kinases (VEGFR-2, PDGFR-β, c-Kit) in order to simulate binding affinity. The estimated inhibition constant K_i was not affected in comparison to Sunitinib for all of the molecules examined, remaining in the low nanomolar range (*Figure 6A*). The calculated values for all the different sunitinib analogues and a representative complex of

SAN1 together with VEGFR-2 are shown in *Figure 6A*.

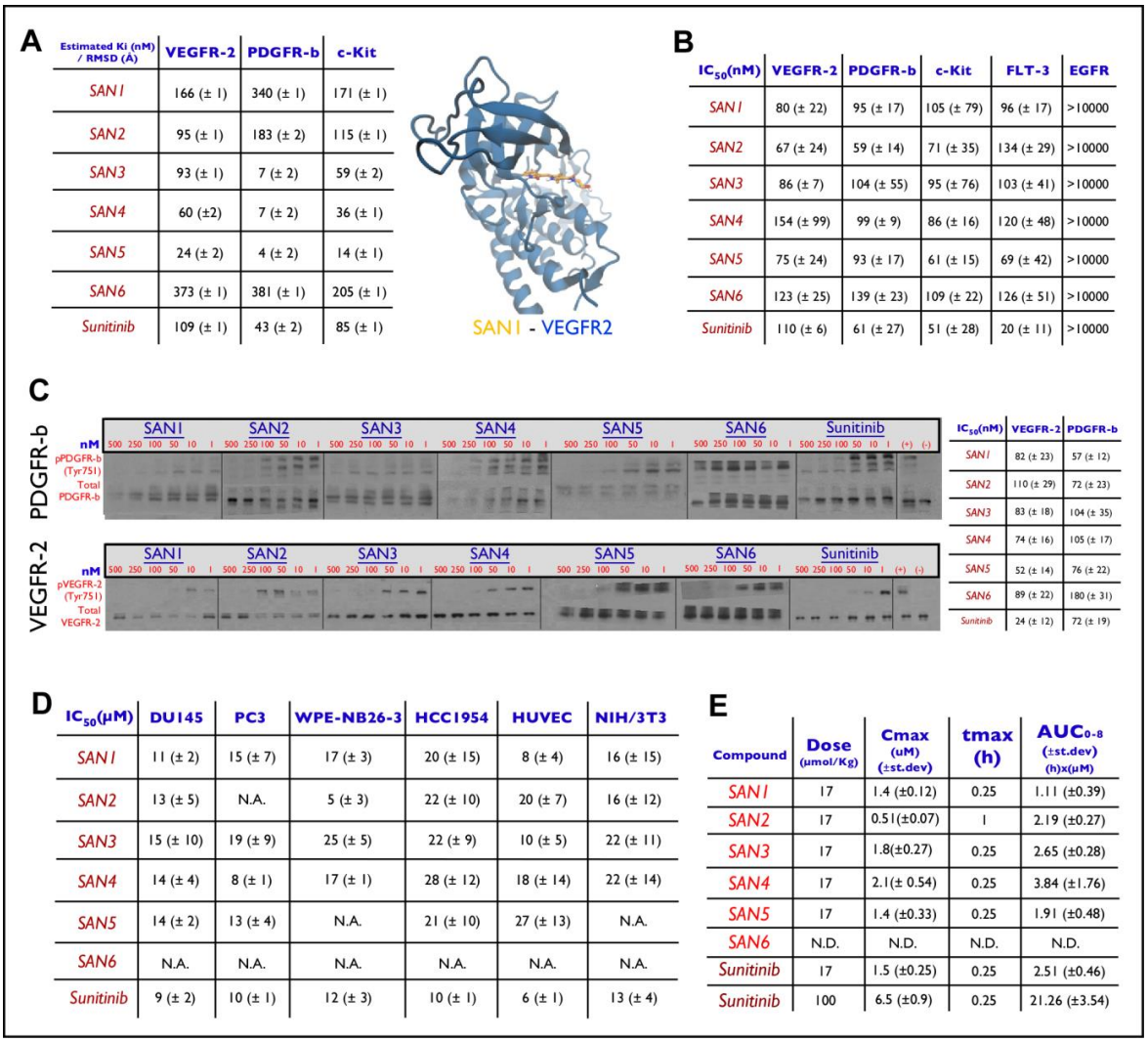

Figure 6: ***(A)*** *Docking results for Sunitinib and the synthesized analogues SAN 1-6. The estimated inhibition constant K_i is given in nM and the root-mean-square deviation (RMSD) from the initial crystallographic pose of Sunitinib in Å.* ***(B)*** *Summary of in vitro kinase activity of VEGFR-2, PDGFR-β, c-Kit, FLT-3 and EGFR in the presence of Sunitinib or SANs 1-6. Each IC_{50} value is the average of three independent experiments, performed in duplicate, (± SD).* ***(C)*** *Cell based auto-phosphorylation assay for PDGFR-β and VEGFR-2 in the presence of Sunitinib or SANs 1-6. Each IC_{50} value is the average of three independent experiments (± SD).* ***(D)*** *MTT cytotoxicity assay in a panel of cell lines. DU145, PC3 and WPE1-NB26-3 are CaP, HCC1954 is a Breast Cancer cell line, HUVE cells are human endothelial expressing high levels of VEGFR-2 and NIH/3T3 are murine fibrobasts expressing high levels of PDGFR-β. Each IC_{50} value is the average of three independent experiments performed in triplicate (± SD).* ***(E)*** *Pharmacokinetic evaluation*

of the most potent SANs (1-5) versus Sunitinib. Male NOD/SCID mice (n = 4) were dosed (IP) with each drug at a dose of 17 μmol/Kg, and blood samples were collected at selected time points. Drug Levels were monitored by LC-MS/MS. The areas under the curve (AUCs) for each treatment were calculated as a measure of drug exposure over time.

Biochemical Kinase Assays

The potency of all SANs was experimentally evaluated in biochemical assays against purified GST-tagged proteins (VEGFR-2, PDGFR-β, c-Kit, FLT-3) as shown in *Figure 6B*. All SANs inhibited the specific RTK targets with IC_{50} values ranging from 0.02 to 0.1 μM. Those potencies were comparable to Sunitinib but also to Sorafenib and Pazopanib, two other anti-angiogenic drugs that were used as positive controls. Another RTK (EGFR) that is not affected by Sunitinib was used as a control for specificity and results confirmed that drug concentrations up to 10 μM of either Sunitinib or any of the six SANs did not inhibit EGFR phosphorylation.

Cellular ligand-dependent phosphorylation assay

The inhibition of phosphorylation of VEGFR-2 and PDGFR-β, was further confirmed in HUVEC and NIH/3T3 cells, using a Western blot based cellular ligand-dependent phosphorylation assay as shown in *Figure 6C*. Sunitinib showed a calculated cellular IC_{50} value of 24 (± 12) nM (for VEGFR-2) and 72 (± 19) nM for PDGFR-β respectively. Similar potencies were observed for all six SANs with calculated cellular IC_{50} values ranging from 52-180 nM *Figure 6C.*

SANs Exhibit Anti-proliferative Potential in vitro.

The anti-proliferative effect of the six SANs was assessed in three GnRH-R positive CaP cell lines (DU145, PC3, WPE1-NB26-3) one GnRH-R positive breast cancer (HCC1954) one endothelial (HUVEC) and one fibroblast cell line (NIH/3T3). Results and calculated IC_{50} values compared to Sunitinib are shown in *Figure 6D*. SAN1 proved potent in all cell lines with HUVEC and DU145 being the most sensitive cell lines (IC_{50s}: 8 ± 4 μM and 11 ± 2 μM respectively) whereas SAN2 was especially efficacious against the WPE1-NB26-3 (IC_{50}: 5 ± 3 μM). SAN1 and SAN2 were also the most potent SANs in NIH/3T3 cells (IC_{50}: 16 ± 11 μM for SAN1 and 16 ± 12 μM for SAN2). SANs 3-5 showed intermediate

efficacies while SAN6 showed no potency in any of the cell lines (IC_{50}>100 μM) and was thus discarded from further evaluation.

Pharmacokinetic Evaluation of selected SANs

The most promising SANs (SAN1-5) were evaluated for their pharmacokinetic parameters in mice, following IP administration (17 μmol/Kg). Sunitinib maximum blood concentrations were achieved at 0.25 h (1.5 μM) with an $AUC_{0–8h}$ of 2.51 h x μM. SANs 1-5 were rapidly absorbed reaching highest blood concentrations averaging from 0.51 to 2.1 μM at 0.25 to 1 h after dosing (*Figure 6E*). The levels of SAN1 peaked at 0.25 h with an $AUC_{0–8h}$: 1.11 h x μM, whereas the maximum AUC was noted for SAN4 ($AUC_{0–8h}$: 1.91 h x μM). Signs of discomfort and toxicity (without mortality) were observed in mice that received SAN2, prohibiting further evaluation. According to the biochemical assays, drug levels of approximately 100 nM are needed for the inhibition of the target kinases (see *Figure 6 A-C*). The pharmacokinetic experiments suggested that following IP dosing, concentrations of at least 100 nM could be sustained for 4 h post-dose for all the molecules that were tested. In order to maintain the circulating drug levels for 24 h a single IP administration of a higher dose (100 μmol/Kg) was selected for Sunitinib. Based on the described pharmacokinetic and biological readouts combined with a facile synthetic route, SAN1 was singled-out as a lead candidate compound for follow up efficacy studies in mice.

<u>In vivo Studies</u>

Antitumour Efficacy Studies with SAN1

In order to determine whether SAN1 treatment could eradicate tumours as effectively as Sunitinib, mice bearing established DU145 tumours were treated with each molecule at 100 μmol/Kg/day (equal to 40 mg/Kg for Sunitinib) for 19 days. On the basis of caliper measurements, tumour growth delay was observed in all mice treated with Sunitinib (*Figure 7A*) with an average tumour size at day 19 of 312 (± 123) mm^3 and an average tumour weight at the day of sacrifice of 0.2 g compared to 1181 (± 105) mm^3 ($p<0.0001$) and 0.87g ($p=0.005$) for vehicle treated mice respectively (*Figure 7B*). Importantly, tumour growth delay was also observed in DU145 xenografted mice treated with a similar dose of SAN1 (100 μmol/Kg/day). The results are depicted in *Figure 7A*, showing an average

tumour size at day 19 of 455 (± 137) mm^3 for SAN1 ($p<0.001$ compared to vehicle treated mice). Additionally, the average tumour weight at sacrifice was 0.37 g for SAN1, (*Figure 7B*), statistically significant ($p=0.005$) compared to vehicle treated mice. Concentrations of Sunitinib and SAN1 in blood and tumour tissue were calculated at 2 h after a final dose on d 19 (shown in *Figure 7C*). Sunitinib's blood concentrations were 4.7 (± 0.1) μM, whereas levels at tumour tissue were 17 (± 9.3) μM. The values for SAN1 in the tumour tissue were significantly lower, at 0.4 (± 0.1) μM, but definitely higher than the IC_{50} levels determined for inhibition of phosphorylation of the target kinases. It should be noted that Sunitinib is more lipophilic compared to SAN1 (as evident in their logP values), a property that supports drug accumulation in the tumour tissue over the treatment period.

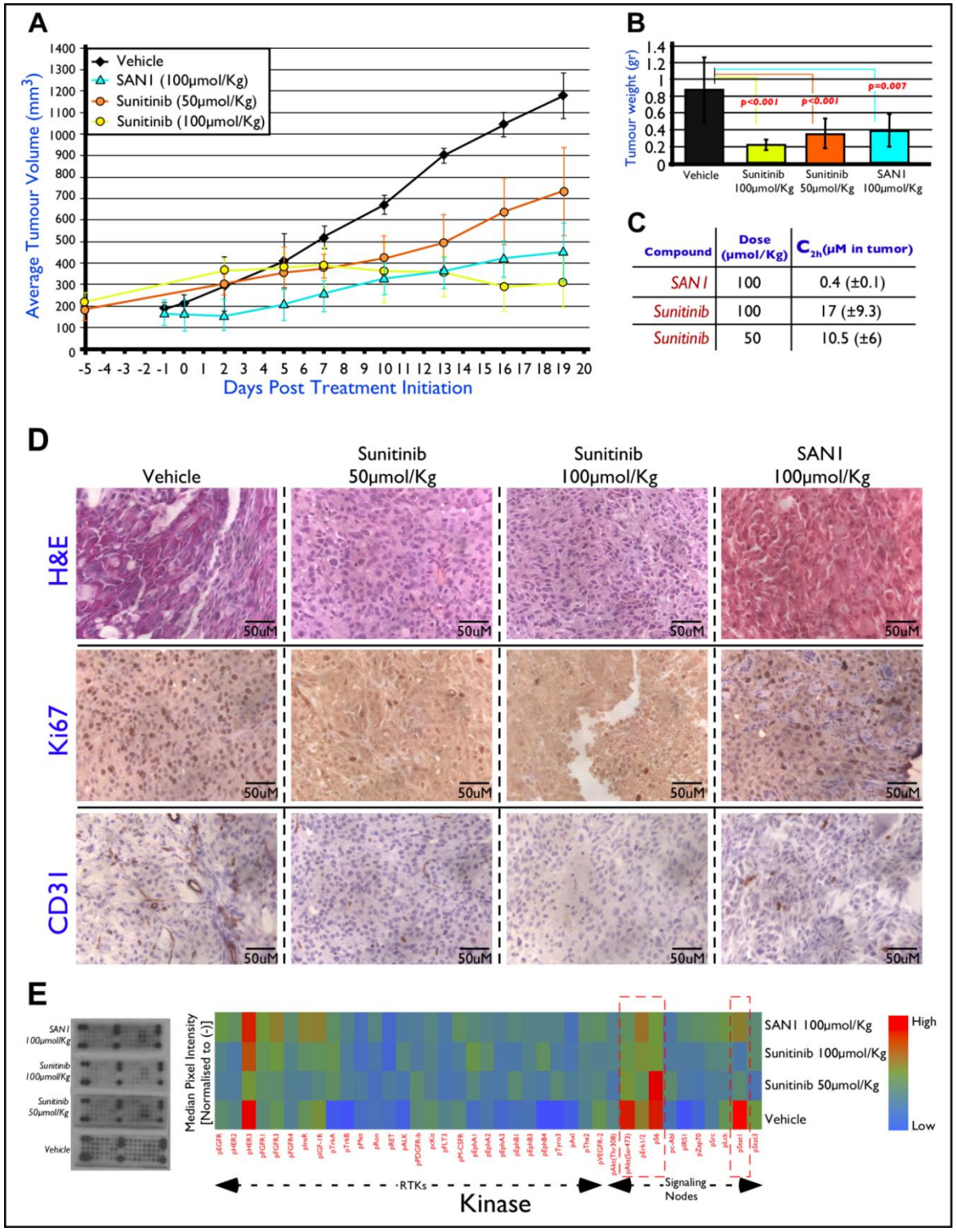

Figure 7: *Therapeutic efficacy of SAN1 and Sunitinib in NOD/SCID mice xenografted with DU145 cells.* ***(A)*** *Tumour growth inhibition. Mice were dosed (IP) daily with SAN1 (100 µmol/Kg), Sunitinib (50 and 100 µmol/Kg) or vehicle. Each point represents the mean of at least 10 tumour volumes resulting from at least five mice ± SD.* ***(B)*** *Average tumour weight at day of sacrifice (d19) between treatment groups. Each bar is the average of 10 tumours*

for each treatment and error bars represent ± SD. On each case P values are calculated using the two-tailed, two-sample unequal variance distribution t test. ***(C)*** *Average intratumoural drug levels as measured by LC-MS/MS at two hours post a final dose on d19, ± SD.* ***(D)*** *Histological sections of xenograft tissue harvested on day of sacrifice (d19) (hematoxylin/eosin staining). Immunohistochemical analysis showed marked decrease in cell proliferation (Ki67) and reduced angiogenesis (CD31+) in drug versus vehicle treated mice. Tumours were fixed, paraffin-embedded, sectioned, immunostained and counterstained with hematoxylin. Representative x40 fields are shown. Scale bar: 50 μM* ***(E)*** *Heat map analysis showing the In vivo phosphorylation status of 39 kinases on drug versus vehicle treated mice at two hours post a final dose on d19. Data represent the average of 10 tumours from five mice for each treatment. A marked upregulation of pAkt (Ser473), pS6 and pStat1 on the vehicle treated mice is noted and highlighted.*

In vivo Target Modulation Studies.

The molecular mechanism behind the *in vivo* efficacy of SAN1 was investigated by histological, immunohistochemical and target modulation analysis of tumours resected from treated and untreated animals. Hematoxylin and eosin stained tissue sections were performed to identify tumour histology (*Figure 3D*). IHC analysis using antibodies against Ki-67 and CD31 showed a marked reduction in cell proliferation and reduced angiogenesis in Sunitinib treated mice as well as with the SAN1 treated mice (*Figure 3D*). The Ki-67 assessed proliferation indices of mice treated with Sunitinib at 100 μmol/Kg, 50 μmol/Kg and mice treated with SAN1 at 100 μmol/Kg or vehicle were 24.1 (± 10.5), 41.6 (± 8.8), 43.9 (± 8.2) and 119.9 (± 27) respectively.

In order to further elucidate the mechanism of action of SAN1 in treated mice, we investigated the phosphorylation status of 39 kinases in extracts of tumour tissue and compared it to tumour extracts of vehicle and Sunitinib treated mice (*Figure 7E*). A marked upregulation of pAkt (Ser473), pS6 and pStat1 was noted in vehicle treated but not in drug treated mice. Thus, a combination mechanism of reduced pro-angiogenic factors in the tumour microenvironment (evident in IHC) together with the downregulation of pAkt (Ser473), pS6 and pStat1 offers a likely explanation for the efficacy observed in drug-treated animals.

Generation of a [D-Lys^6]-GnRH-SAN1 conjugate - In vitro Studies

Based on the *in vivo* efficacy profile, SAN1 was selected for conjugation to the [D-Lys^6]-GnRH targeting peptide exploiting the free hydroxyl group of SAN1. Given our prior experience with the Gemcitabine-GnRH molecules[18] we followed a similar linking strategy for SAN1 to [D-Lys^6]-GnRH, resulting in SAN1GSC molecule as shown in *Figure 8A*.

Molecular docking analysis predicted that SAN1GSC would remain potent, with a calculated Ki=28 (± 2) nM for VEGFR-2, Ki=51 (± 2) nM for c-Kit and Ki=65 (± 2) nM for PDGFR-β (*Figure 8B*).

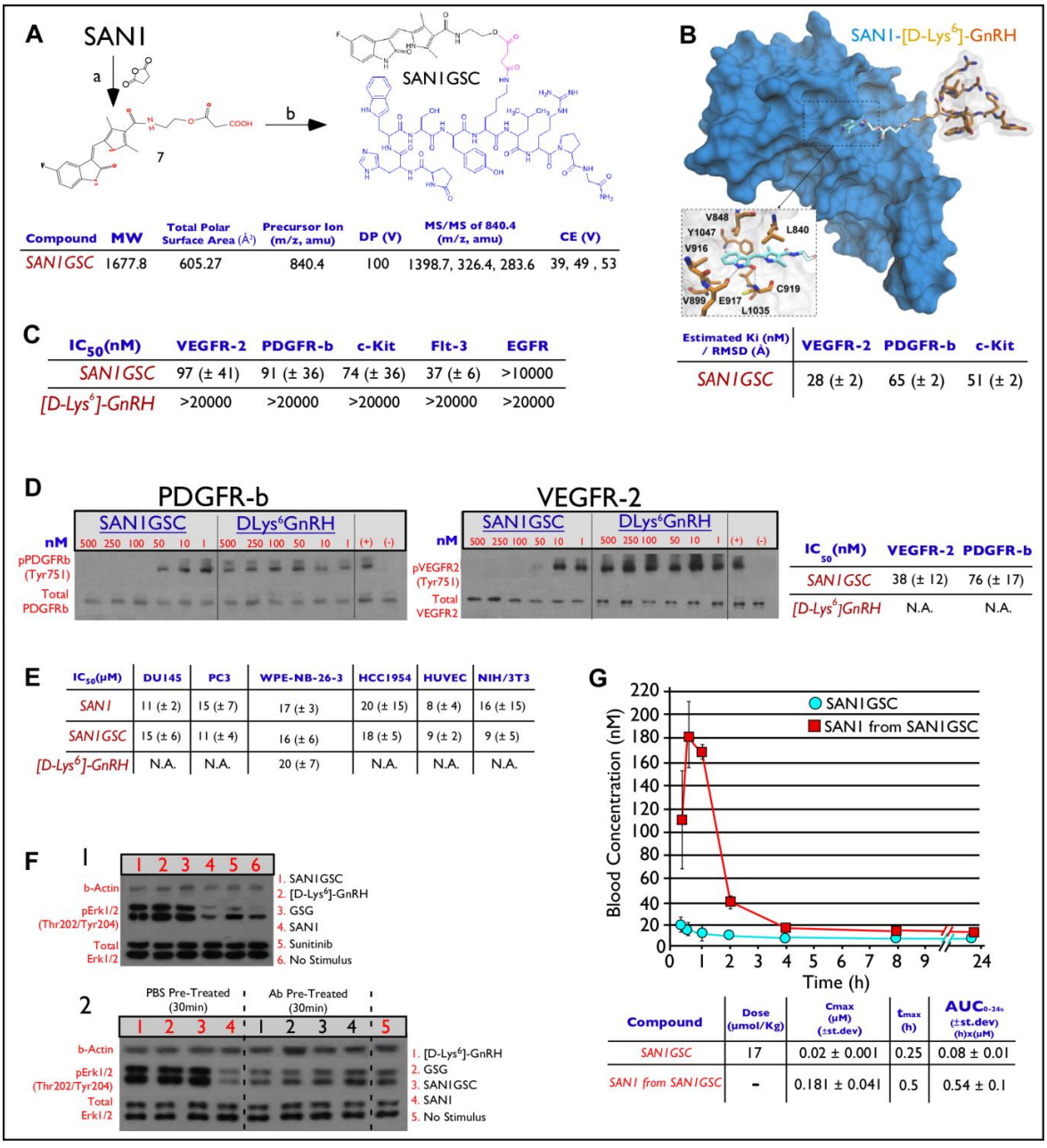

Compound	MW	Total Polar Surface Area (Å^2)	Precursor Ion (m/z, amu)	DP (V)	MS/MS of 840.4 (m/z, amu)	CE (V)
SAN1GSC	1677.8	605.27	840.4	100	1398.7, 326.4, 283.6	39, 49 , 53

IC$_{50}$(nM)	VEGFR-2	PDGFR-b	c-Kit	Flt-3	EGFR
SAN1GSC	97 (± 41)	91 (± 36)	74 (± 36)	37 (± 6)	>10000
[D-Lys^6]-GnRH	>20000	>20000	>20000	>20000	>20000

Estimated Ki (nM) / RMSD (Å)	VEGFR-2	PDGFR-b	c-Kit
SAN1GSC	28 (± 2)	65 (± 2)	51 (± 2)

IC$_{50}$ (nM)	VEGFR-2	PDGFR-b
SAN1GSC	38 (± 12)	76 (± 17)
[D-Lys^6]GnRH	N.A.	N.A.

IC$_{50}$(μM)	DU145	PC3	WPE-NB-26-3	HCC1954	HUVEC	NIH/3T3
SAN1	11 (± 2)	15 (± 7)	17 (± 3)	20 (± 15)	8 (± 4)	16 (± 15)
SAN1GSC	15 (± 6)	11 (± 4)	16 (± 6)	18 (± 5)	9 (± 2)	9 (± 5)
[D-Lys^6]-GnRH	N.A.	N.A.	20 (± 7)	N.A.	N.A.	N.A.

Compound	Dose (μmol/Kg)	Cmax (μM) (±st.dev)	t_{max} (h)	AUC$_{0\text{-}24h}$ (±st.dev) (h)x(μM)
SAN1GSC	17	0.02 ± 0.001	0.25	0.08 ± 0.01
SAN1 from SAN1GSC	-	0.181 ± 0.041	0.5	0.54 ± 0.1

Figure 8: (A) *Key properties and synthesis of SAN1GSC from SAN1 and [D-Lys^6]-GnRH.* ***Reagents and Conditions:*** *(a) DMF, DMAP, NEt_3, rt; (b) [D-Lys^6]-GnRH, DMF, HATU, $NiPr_2Et$.* ***(B)*** *Molecular representation of the energy minimized model of VEGFR-2 catalytic domain (blue surface) in complex with the SAN1GSC conjugate (sticks) that is colour-coded with cyan carbons for the Sunitinib analogue SAN1 and orange for the [D-Lys^6]-GnRH peptide. The SAN1 linker and D-Lys^6 domains are highlighted. Inset illustrates a close-up view of the ATP-binding site with the SAN1 moiety of the conjugate (cyan) and the key interacting residues (orange). Intermolecular hydrogen bonds are shown with dotted lines and the other atom colours are blue for N, red for O, yellow for S and pink for F.* ***(C)*** *Summary of in vitro kinase activity of VEGFR-2, PDGFR-β, c-Kit, FLT-3 and EGFR in the presence of SAN1GSC and [D-Lys^6]-GnRH. Each IC_{50} value is the average of three independent experiments, performed in duplicate, (± SD).* ***(D)*** *Cell based auto-phosphorylation assay for PDGFR-β and VEGFR-2 in the presence of SAN1GSC and [D-Lys^6]-GnRH. Each IC_{50} value is the average of three independent experiments (± SD).* ***(E)*** *MTT cytotoxicity assay in a panel of cell lines. DU145, PC3 and WPE1-NB26-3 (stably over-expressing the human GnRH-R) are CaP, HCC1954 is Breast Cancer cell lines, HUVE cells are human endothelial expressing high levels of VEGFR-2 and NIH/3T3 are murine fibrobasts expressing high levels of PDGFR-β. Each IC_{50} value is the average of three independent experiments performed in triplicate (± SD).* ***(F)*** *SAN1GSC activates the Erk1/2 pathway through binding to the GnRH-R.* ***1.*** *The WPE1-NB26-3 cell line shows increased phosphorylation of Erk1/2 only after stimulation by the ligand [D-Lys^6]-GnRH or SAN1GSC that contains this ligand. GSG a Gemcitabine-[D-Lys^6]-GnRH conjugate described previously, was used as a positive control due to its known GnRH-R binding studies.* ***2.*** *Phosphorylation of Erk1/2 following treatment with SAN1GSC, [D-Lys^6]-GnRH or GSG is absent when cells are pretreated for 30 min with an antibody against the human GnRH-R.* ***(G)*** *Pharmacokinetic evaluation of SAN1GSC. Male NOD/SCID mice (n = 4) were dosed (IP) with each drug at a dose of 17 μmol/Kg, and blood samples were collected at selected time points. Drug Levels of SAN1GSC and SAN1 formed from its breakdown were monitored by LC-MS/MS. The areas under the curve (AUCs) for each treatment were calculated as a measure of drug exposure over time.*

In vitro evaluation of SAN1GSC

SAN1GSC was evaluated in a series of relevant assays to ensure that the conjugation process did not affect the mechanism of action of SAN1. Incubation of SAN1GSC with GST-tagged VEGFR-2, PDGFR-β and c-KIT resulted in the inhibition of phosphorylation of each of these kinases with an IC_{50} of 97 (± 41), 91 (± 36) and 74 (± 36) nM respectively but not of the EGFR (*Figure 8C*). Incubation of [D-Lys^6]-GnRH with all the kinases did not result in any inhibition of phosphorylation. SAN1GSC was equipotent to SAN1 in terms of cellular toxicity in various cell lines with the calculated IC_{50} ranging from 9-18 μM (*Figure 8D*). Finally, Western blot analysis showed that SAN1GSC inhibited phosphorylation of VEGFR-2 and PDGFR-β, with a low nanomolar potency (38 ±12 nM for VEGFR-2 and 76 ±17 nM for PDGFR-β, shown in *Figure 8E*).

Binding of SAN1GSC to GnRH-R with subsequent activation of the pErk1/2 signaling pathway was investigated by setting-up an indirect method based on the WPE1-NB26-3 cell line (*Figure 8F*). Initially we demonstrated that among the three CaP cell lines used in this study only in the WPE1-NB26-3 cell line, stably modified to over-express the GnRH, activation of pErk1/2 was observed following stimulation with [D-Lys^6]-GnRH or our previously described GSG_1 conjugate. Incubation of WPE1-NB26-3 cells with SAN1GSC resulted in a robust phoshporylation of Erk1/2 similar to when the same cells were stimulated by [D-Lys^6]-GnRH or GSG (lanes 1-3 in *Figure 8F-1*). Such an effect was abrogated, when cells were pretreated with a GnRH-R antibody (*Figure 8F-2*), suggesting that pErk1/2 activation was a result of direct binding of SAN1GSC to GnRH-R.

Pharmacokinetic evaluation of SAN1GSC

A single IP administration of 17 μmol/Kg of SAN1GSC in mice led to conjugate blood concentrations averaging 20 nM at 0.25 h following dosing with an $AUC_{0–24h}$ of 0.08 h x μM (*Figure 8E*). Levels of SAN1 formed from the break-up of SAN1GSC peaked at 0.5 h with a Cmax of 181 nM at 0.5 h and an $AUC_{0–24h}$: 0.54 h x μM. Interestingly, SAN1 released from SAN1GSC was higher than 100 nM, an estimated level required for effective inhibition of phosphorylation of the target kinases. Moreover conjugation of SAN1 to [D-Lys^6]-GnRH improved the solubility of SAN1 in saline.

***In vivo* studies using SAN1GSC**

Antitumour Efficacy Studies

Mice bearing established DU145 tumours were dossed with equimolar amounts of SAN1GSC, SAN1 and [D-Lys^6]-GnRH for a total period of 21 days. Tumour growth delay occurred in all mice treated with SAN1GSC (*Figure 9A*), with an average tumour size at day 21 of 689 (±102) mm^3, a significantly smaller tumour in comparison to SAN1 treated mice [1010 (±114) mm^3, $p < 0.001$] and of [1248 (±108) mm^3, $p < 0.001$] for mice treated with [D-Lys^6]-GnRH. On the day of sacrifice (d21) average tumour weight for SAN1GSC treated mice was 0.50 g compared to 0.75 g for SAN1 treated mice, ($p=0.038$, *Figure 9B*) and 0.82 g for [D-Lys^6]-GnRH treated mice ($p=0.003$, *Figure 9B*).

To investigate if SAN1GSC dosing increased the drug payload to the tumour site, levels of SAN1, SAN1GSC and of SAN1 formed from SAN1GSC in the blood and tumour tissue were measured at 1 h post-dose (final dose) after 21 days of treatment (*Figure 9C*). Blood concentrations of SAN1GSC were 5nM, whereas levels at tumour tissue were also evident. Additionally, blood levels of SAN1 were 210 (± 110) nM whereas levels of SAN1 formed from SAN1GSC were 250 (± 50) nM. It should be noted that measurements of SAN1 in the tumour tissue revealed four times higher SAN1 in SAN1GSC treated mice compared to SAN1 treated mice (114 ± 33 versus 31 ± 1 nM). This is also evident when we looked at the tumour/blood (t/b) ratio for each treatment, where SAN1 formed from SAN1GSC demonstrated a t/b ratio of almost 0.5 compared to less than 0.2 t/b ratio for SAN1 treated mice.

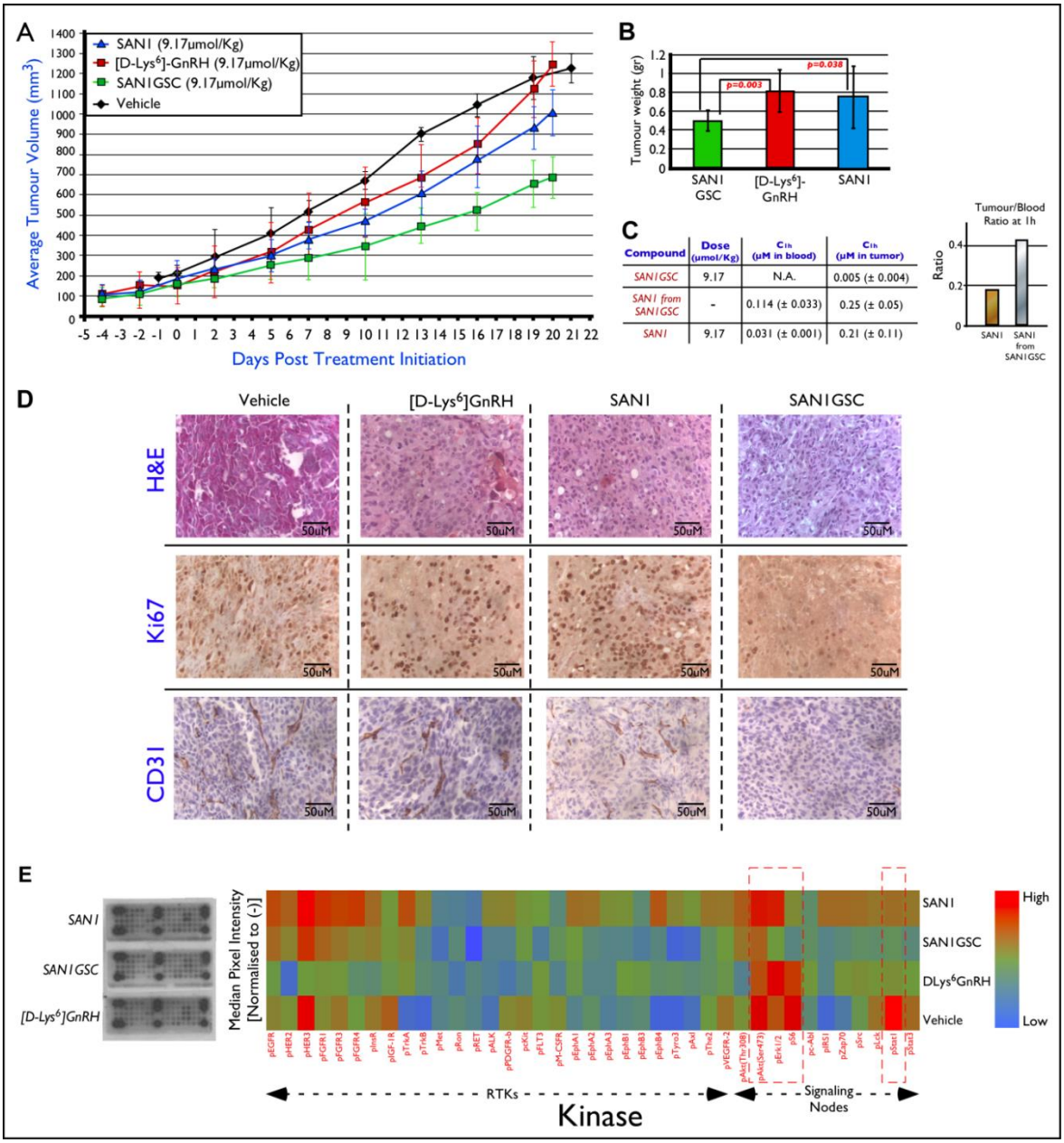

Figure 9: *Therapeutic efficacy of SAN1GSC (9.17 µmol/Kg), versus equimolar amounts of SAN1 and [D-Lys^6]-GnRH in NOD/SCID mice xenografted with DU145 cells.* ***(A)*** *Tumour growth inhibition. Mice were dosed (IP) daily with SAN1GSC, SAN1 or [D-Lys^6]-GnRH. Each point represents the mean of at least 10 tumour volumes resulting from at least five mice ± SD.* ***(B)*** *Average tumour weight at day of sacrifice (d21) between treatment groups. Each bar is the average of 10 tumours for each treatment and error bars represent ± SD. On each case P values are calculated using the two-tailed, two-sample unequal variance distribution t test.* ***(C)*** *Average intratumoural drug levels as measured by LC-MS/MS at one hour post a final dose on d21, ± SD. SAN1 formed from the SAN1GSC is four times higher than SAN1 treated mice, despite the fact that blood levels are similar, resulting in a*

higher blood/tumour ratio on SAN1GSC treated mice ***(D)*** *Histological sections of xenograft tissue harvested on day of sacrifice (d21) (hematoxylin/eosin staining). Immunohistochemical analysis showed marked decrease in cell proliferation (Ki67) and reduced angiogenesis (CD31+) in SAN1GSC versus SAN1 and [D-Lys^6]-GnRH treated mice. Tumours were fixed, paraffin-embedded, sectioned, immunostained and counterstained with hematoxylin. Representative x40 fields are shown. Scale bar: 50 μM.* ***(E)*** *Heat map analysis showing the In vivo phosphorylation status of 39 kinases on drug versus vehicle treated mice at one hour post a final dose on d21, Data represent the average of 10 tumours from five mice for each treatment. A marked upregulation of pAkt (Ser473), pS6 and pStat1 is again noted in most treatment groups except SAN1GSC treated mice. In every case, vehicle treated mice are used for comparative studies.*

In vivo **Target Modulation Studies.**

The molecular mechanism responsible for the efficacy observed with SAN1GSG compared to other treatments was investigated using the methodology described above. IHC analysis in tumour sections using antibodies against Ki-67 and CD31 showed a marked reduction in cell proliferation and reduced angiogenesis in SAN1GSC treated compared to SAN1 or [D-Lys^6]-GnRH treated mice (*Figure 9D*). The Ki-67-assessed proliferation indices of mice treated with SAN1GSC were 53.5 (± 10.8), for SAN1 122.5 (± 45.5), and for [D-Lys^6]-GnRH 91.6 (± 31.3) respectively. Additionally, the average number of CD31+ cells in tumour sections of mice treated with SAN1GSC were 9.75 (± 2.5), for SAN1 26 (± 7.3) and for [D-Lys^6]-GnRH 29 (± 5.4) respectively (*Figure 9D*).

Finally, results from the panel of 39 kinases in extracts of tumour tissue are shown in *Figure 7E*. A marked upregulation of pAkt (Ser473), pErk1/2, pS6 was again noted in vehicle, [D-Lys^6]-GnRH and SAN1 treated mice but was absent from SAN1GSC treated mice. This correlated nicely with results from IHC and measurement of drug levels in the tumour tissue, demonstrating a general downregulation of angiogenic and signaling proteins in the SAN1GSC treated group.

4.4 Discussion

The targeting of GnRH-R expressing tumours with GnRH based therapeutics is a promising evolving field in the area of personalized treatment. The clinical application of this concept became evident following the conjugation of a GnRH peptide to doxorubicin, currently in Phase III clinical trials.[136] Based on our own experience[18] and a better understanding of CaP biology and angiogenesis[143] we surmised that a more efficient strategy would be to combine a small anti-angiogenic molecule active against various kinases with the targeting peptide [D-Lys^6]-GnRH. Such a conjugate should specifically deliver the multi-kinase inhibitor to the site of action, reducing off-target effects and possibly lowering the dose required for efficacy. The drug chosen for our studies, Sunitinib, has been extensively used in the clinic for the treatment of solid tumours with a known mechanism of action[161] and off-target toxicity[162]. In CaP clinical trials, Sunitinib failed to receive regulatory approval despite a statistically significant progression free survival,[149] suggesting that a better patient selection could lead to an improved outcome.

Due to the lack of "linkable" free groups of Sunitinib, we rationally designed and synthesized six analogues (SANs 1-6) that maintained their efficacy but could also be coupled to targeting peptides. Indeed, molecular docking analysis to three key angiogenic RTKs revealed that all SANs assumed a bound conformation similar to Sunitinib while remaining efficacious at the low nanomolar scale. This was verified experimentally in an extensive series of *in vitro* biochemical and cellular experiments as well as pharmacokinetic studies of SANs 1-5 in mice, which demonstrated *in vitro* efficacy and bioavailability in mouse models. Evaluation of all experimental data combined with a facile chemical synthesis scheme singled out SAN1 as the lead compound for further development using an *in vivo* androgen independentCaP xenograft animal model.

SAN1 treatment was well tolerated and proved efficacious in inhibiting tumour growth when compared to vehicle and slightly less potent than Sunitinib treated animals. Efficacy of Sunitinib at the administered dose verified previously published reports[163,164] for the specific animal model and dosing scheme. Immunohistochemical analysis on tumour sections from treated and untreated animals revealed reduced CD31 and Ki67 positive cells, demonstrating that inhibition of angiogenesis is at least one mechanism by which SAN1 achieved its efficacy on the particular tumour model of CaP. This was further

supported by mass spectrometry based measurements in tumour samples, revealing that levels of SAN1 at two hours after dosing were above the IC_{50} required for efficacy as determined in the *in vitro* experiments. Bearing in mind that Sunitinib and its novel analogue SAN1 are designed to be multi-kinase inhibitors we investigated their effect in a panel of 39 kinases and showed that several key kinases (pErk1/2, pS6, pStat1) were phosphorylated in vehicle treated animals, but not in any of the drug treated animals. Since the abovementioned kinases are second messengers in signaling pathways and apart from pS6 are not known to be directly inhibited by Sunitinib (37) (or SAN1), further research is required to delineate the exact mechanism of action. Certainly inhibition of pS6 by Sunitinib and the involvement of pS6 in promoting angiogenesis[165] provide a direct link for the observed efficacy. Additionally, there was a clear overall trend of reduced kinase phosphorylation in the treated versus untreated animals. It is worth mentioning, that the direct targets of Sunitinib (and SAN1), namely VEGFR-2, PDGFR-β, c-Kit and FLT3 were present in the panel of kinases we examined, but detectable levels were low and no statistically significant differences could be observed.

Building on the efficacy of SAN1, we investigated whether linking of [D-Lys^6]-GnRH to SAN1 would lead to an enhanced delivery of the active molecule to the tumour site. Thus SAN1GSC was generated followed by extensive *in vitro* and *in silico* evaluation. Results demonstrated that SAN1GSC maintained its anti-angiogenic and cytotoxic properties with IC_{50} values similar to those of unconjugated SAN1. A potentially wider role of SAN1GSC for the treatment of other GnRH-R positive tumours was provided by the inclusion in our studies of a breast cancer cell line positive for the GnRH-R (HCC1954). Importantly, we demonstrated that SAN1GSC activated the GnRH-R through the pErk1/2 pathway, revealing at least one mechanism by which SAN1GSC enters the target cell.

The succinate linker used in SAN1GSC aimed to provide stability in blood while releasing active SAN1 to the tumour site as shown in the PK and *in vivo* efficacy studies. PK analysis revealed low levels of free circulating SAN1 in the blood, possibly a desirable feature expected to minimize off-target effects, while daily administrations of 9.17 μmol/Kg SAN1GSC were well tolerated and proved efficacious in the androgen independent CaP xenograft model. Importantly, measurements of SAN1 in tumour sample specimens showed four times higher levels of intracellular SAN1 released from SAN1GSC than levels of SAN1 delivered on its own. These levels are well within the efficacious IC_{50} values as estimated in the *in vitro* assays and explain the efficacy seen in SAN1GSC versus

SAN1 treated animals. It is worth mentioning that our xenograft CaP model was androgen independent, and a statistically significant anti-proliferative effect of the [D-Lys^{6}]-GnRH peptide was not observed. However, SAN1GSC contains a potent agonist peptide of the GnRH-R and could certainly exert a central effect through the pituitary in androgen dependent forms of CaP by lowering testosterone levels.[166] Immunohistochemical analysis in conjunction to the phosphorylation status of 39 kinases support these observations, with reduced CD31 positive cells and lower phosphorylation of pErk1/2, pS6, pStat1 among others, similar to when animals were treated with either Sunitinib or high dose of SAN1.

In conclusion, we have generated a series of novel readily conjugatable anti-angiogenic compounds to treat various forms of cancer based on the clinically successful drug Sunitinib. The lead compound in the current study (SAN1) proved potent *in vivo,* a phenomenon associated with reduced angiogenesis and inhibition of several kinases. Importantly, we demonstrated for the first time the direct conjugation of SAN1 to a targeting moiety and showed an enhanced delivery to the tumour. To our knowledge this is the first time that an anti-angiogenic small molecule inhibitor is conjugated to a targeting peptide and our concept is certainly applicable to other solid tumour types expressing the GnRH-R or even to other types of receptors by swiftly altering the targeting peptide.

Chapter 5: Side projects I worked in the frame of PhD thesis

In addition to my interest of working in the bioconjugate formation of different drugs, my intense interest to explore novel bioactive cores that are used in the lab resulted me to interfere with an array of different side projects that are presented below.

5.1 Y6-DOTA

5.2 Compound 21

5.3 NMR study of Gemcitabine

5.1 Y6 – DOTA conjugate

5.1.1 Introduction:

G-protein-coupled receptors (GPCRs) orchestrate most cellular responses to neurotransmitters and hormones.[167] They form a major therapeutic platform for an array of diseases, with 50% of clinically marketed drugs targeting this receptor family.[168] GPCR subtypes within a subfamily usually posses distinct functional and pharmacological profiles,[169] thus development of subtype selective ligands has immense untapped therapeutic potential. This is clearly evident for two of the Angiotensin II (AII) receptor subtypes, AT1R and AT2R. Although, they are recognized with similar affinity by the hormone AII (NH_2-DRVYIHPF-OH),[170, 171] the effects of the AT2R activation (vasodilation, apoptosis and antiproliferation) antagonise those mediated by AT1R (cellular growth and proliferation for AT1)[172, 173] Since AT2R stimulation has been implicated in tumour suppression,[174, 175] tissue repair and regeneration, this receptor has been assigned as an important pharmaceutical drug target.[174, 176, 177] Our lab has recently discovered and patented a novel compound which we termed Y6-AII that bears the sequence DRVYIYPF (UK and US patent) which presented enhanced affinity and selectivity over the AT2 receptor. Our lab was also awarded a Developmental Gap Fund award from the Medical Research Council for the further development of this compound. One direction we tackled is to construct a theranaustic agent which could be used in radiotherapy and tumour diagnosis in positron emission tomography in collaboration with the Paul Scherrer Institute (PSI) and Prof. Martin Behe for the application of our analogue in performance of Positron emission tomography (PET). PET is a nuclear medicine, functional imaging technique that produces a three-dimensional image of functional processes in the body. This methodology allows exploring the possibility ofcancer metastasis (i.e., spreading to other sites) and is the most common type of PET scan in standard medical care (90% of current scans). A relevant potential benefit can be adapted by our analogue since it selectively recognizes the AT2 receptor which is over-expressed in cancer cells.

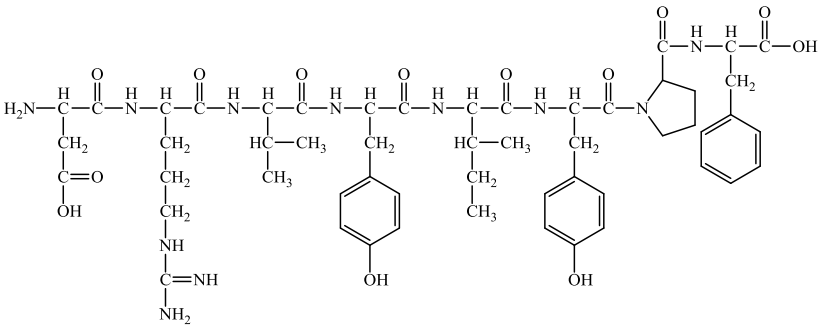

NH_2-DRVYIYPF-OH (1)

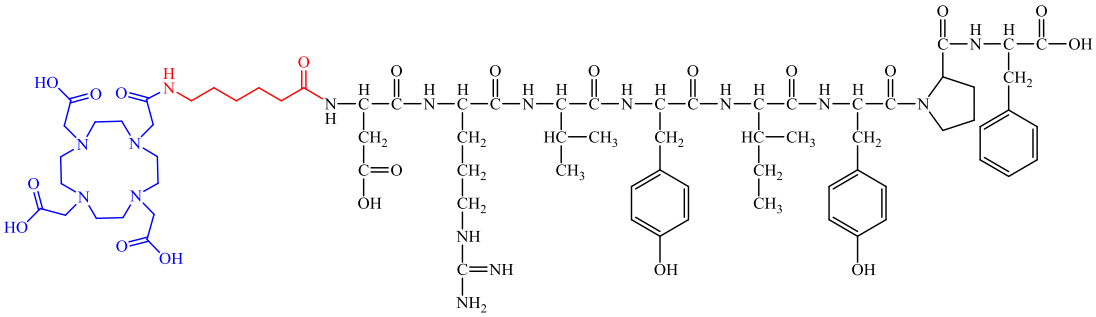

DOTA-aminohexanoic-DRVYIYPF (2)

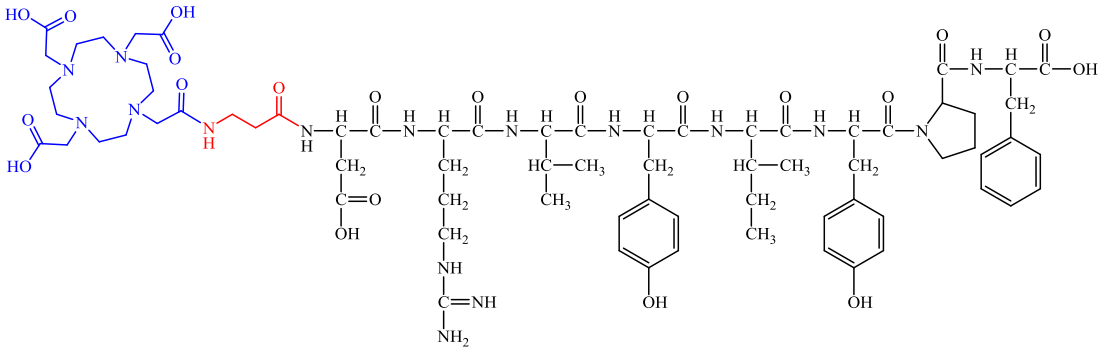

DOTA-beta-alanine-DRVYIYPF (3)

***Figure 1**: Design analogue of DOTA*

5.1.2 Design, synthesis and characterization:

AT2 (1) peptide was synthesised by classical method of peptide synthesis by using fmoc strategy on trityl chloride resin. After completing required aminoacid sequence, linker / spacer (6-Aminohexanoic acid or beta alanine) was added at N-terminal of petide, by amide bond. Subsequent fmoc deprotection (with 20% piperidine in DMF) gives compound **5**. The solid phase peptide bond formation between **5** and DOTA-tri-*t*Bu ester

(6) was carried out with HATU and DIPEA under inert atmosphere. Final clevage of peptide from resin (and deprotection of *t*Bu ester) was performed with clevage cocktail (TFA / TIS / H_2O (9.5/0.5/0.5, v/v) for 4 h. Crude compoud 2 and 3 were purified by washing with solvents (ACN/hexane, 1:2).

Note: *DOTA-tri-tBu ester after deprotection of tBu ester is reactive with metal ions to form very stable complex. We therefore have avoided the HPLC purification as well as application of any metal wares in synthesis; the water used in clevage was also deionised.*

Table 1: *Reagents and conditions for peptide (AT2) synthesis.*

Sr. no.	**Description**	**Deatails**
1	Resin	Trityl chloride
2	Deprotection of Fmoc	Pipyridine 20% in DMF
3	Coupling reagents	HOBt (3 equiv.), DIC (3 equiv.) and HATU/DIPEA
4	Acetylation0	Acetic anhydride (3 equiv.) and Pyridine (20 mL)
5	Cleavage cocktail	TFA / TIS / H_2O (9.5/0.5/0.5, v/v)
6	Solvents	DMF and DCM
7	**Kaiser test:** A few resin balls were placed in test tube and 3-4 drops from each 3 solution were added. The tube was place in boilling water for ~30 seconds. Observed the coloured resin balls.	**Solution 1:** 5 g Ninhydrine in 100 mL Ethanol **Solution 2:** 2 mL (0.001m) KCN in 100 mL Pyridine **Solution 3:** 400 mg Phenol in 100 mL Ethanol

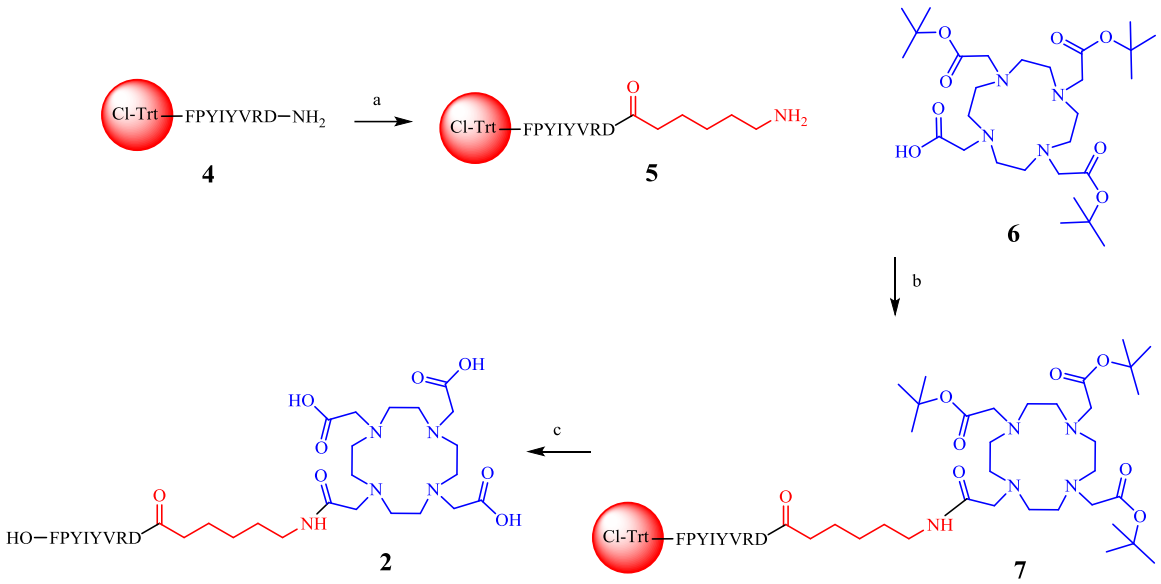

Figure 2: *Synthesis of* ***2*** *reacgent and conditions: a) Fmoc-aminohexanoic acid, HATU (1.5 equiv.), DIPEA (5 equiv.), DMF rt, 12 h; 20% piperidine in DMF; b) HATU (2 equiv.), DIPEA (3 equiv.), DMF, rt 12 h; c) TFA-TIS-H_2O (9.5/0.25/0.25, v/v), rt, 4 h.*

Synthesis of 5: Solid phase synthesis of peptide **4** on trityl chloride resin was continued with coupling of Fmoc-aminohexanoic acid to the α-amine of aspartic acid from C-terminal of peptide by HATU (1.5 equiv.) and DIPEA (5 equiv.). Reaction vessel was rotated for 12 h at rt. Resin washed with DMF (3 mL X 3), DCM (3 mL X 3) and DMF (3 mL X 3). Solution of

20% piperdine in DMF (5 mL X 2) for 10 min each at rt then resin was washed with DMF, DCM and DMF, Test Kaiser shows blue colour resin.

Synthesis of 7: The solution of **5** (0.045 mmol), **6** (51.5 mg, 0.090 mmol), HATU (34.22 mg, 0.090 mmol) and DIPEA (23.51 µL, 0.135 mmol) in DMF (2 mL) were added in reaction vessel under inert atmosphere then continued rotation for 12 h at rt. Resin was washed with DMF (3 mL X 3), DCM (3 mL X 3), DMF (3 mL X 3). Test Kaiser showed a colourless resin.

Synthesis of 2: ***Cleavage of peptide from resin:*** Resin balls were transfered in round bottom flask; 1 mL (TFA-TIS-H_2O (9.5/0.25/0.25, v/v)) cleavage cocktail was added and stirred at 0^0C to rt for 4 h. Reaction mixture filtered, filtrate evaporated and azeotrop with

DCM/hexane (1:1), sticky compound became white solid after addition of cold diethyl ether, removed ether layer by centrifuge, dry well on high vacuum gives **7** (10 mg, ~ 14.5%) as white solid compound.

Similaraly, we have synthesised the analogue **3** (DOTA-beta alanine-AT2). Both the compounds (**2** and **3**) were characterised by mass and analytical HPLC, and presented high purity without any HPLC purification. The relevent peptide were then coupled to the radio active nuclide Lu-177 by our colleagues in PSI and used directly in PET scanning in mice.

Characterization by Mass:

Mass of **2**: MS (ESI^+) *m/z* for $C_{75}H_{110}N_{16}O_{21}$: calcd, 1570.80; found, 1572.79 $[M+H]^+$, 786.36 $[M+2H]^{2+}$

Mass of **3**: Mass (ESI^+) *m/z* for $C_{72}H_{104}N_{16}O_{21}$: calcd, 1528.76; found, 1529.74 $[M+H]^+$., 765.33 $[M+2H]^{2+}$.

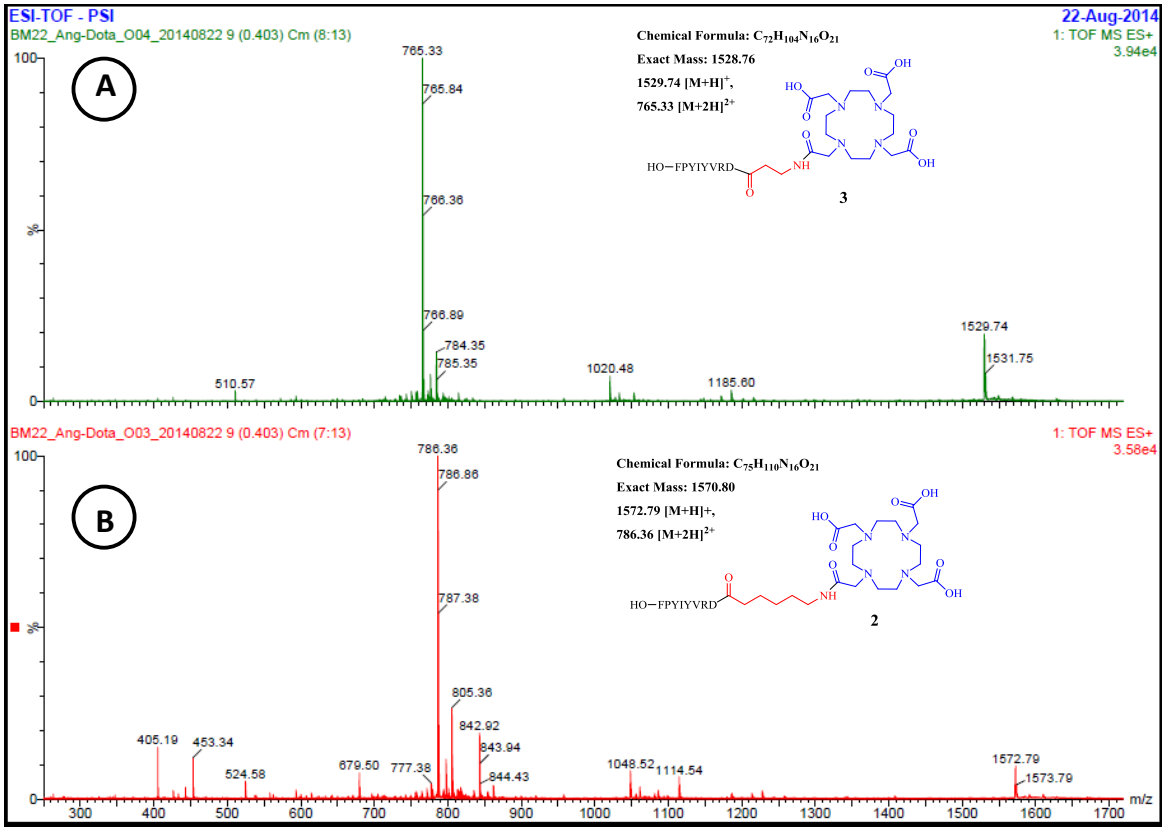

***Figure 3**: Mass spectum of compound **2** and **3**: A) compound **3**; B) compound **2**.*

Characterization by Analytical HPLC: ***C***ompound **2** dissolved in H_2O (0.6 mM) and use for analytical HPLC in ACN/H_2O (5:95-100:00) at λ = 254 nm for 45 min run. The chromatogram shows two peaks in all of three compounds (almost 1:1 in **2** and **3)**, this is bacause of amino acid proline has cis and trans isomers[178] (*Figure 4*).

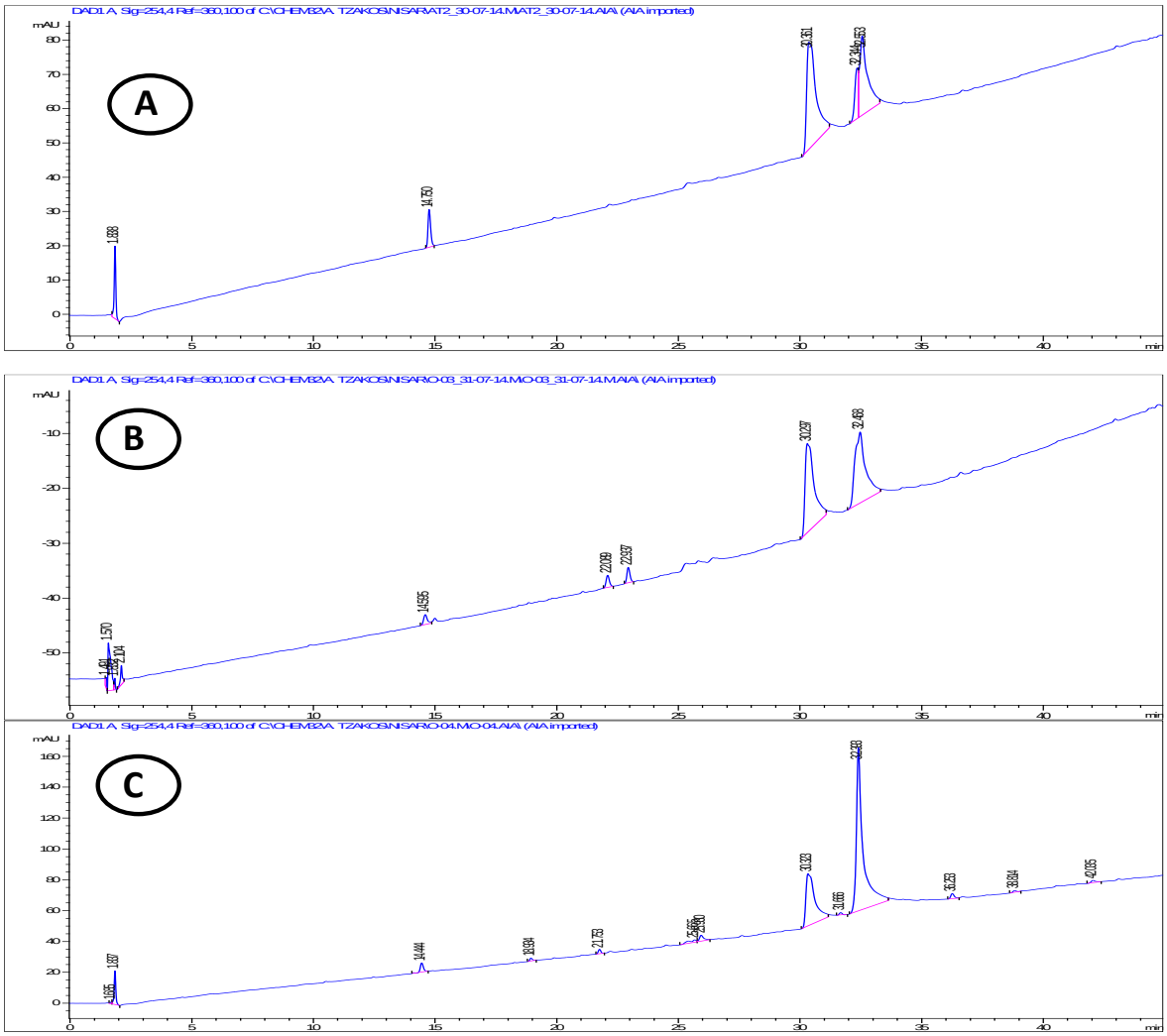

Figure 4: *Analytical HPLC of compound* ***AT2***, ***2***, *and* ***3:*** ***A)*** *AT2;* ***B)*** *DOTA-aminohexanoic-AT2; (2);* ***C)*** *DOTA-beta-alanine-AT2 (3).*

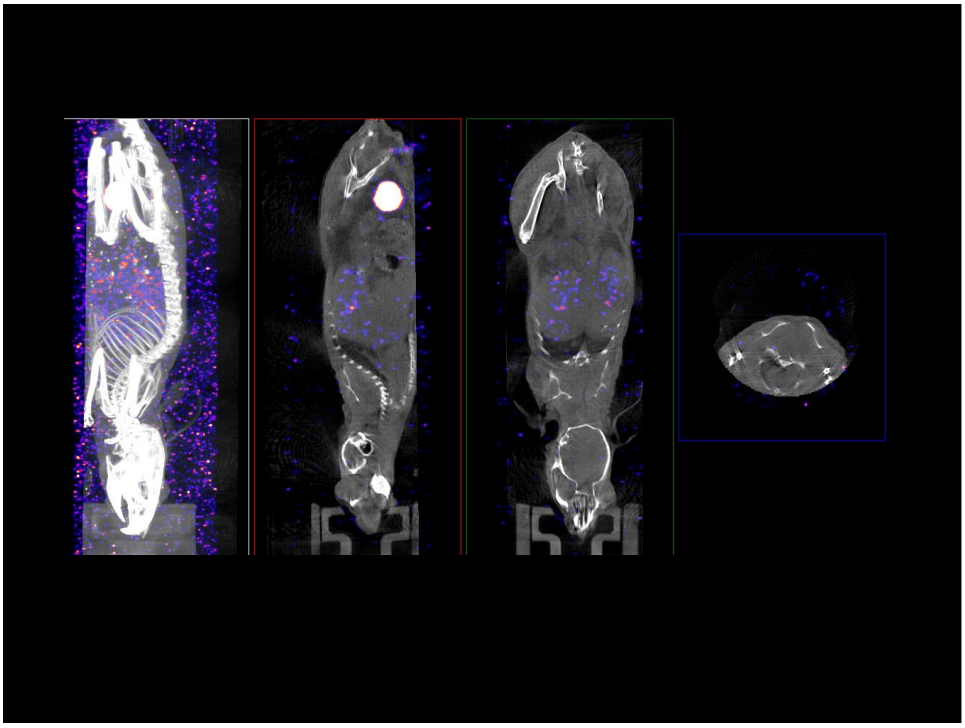

***Figure 5**: PET scanning of the Lu^{177} -Y6-AII analogue in mice indicating the regioselective localization.*

5.2 Compound 21

5.2.1 Introduction:

Very recently a compound termed compound 21 was developed as a selective AT2 receptor agonist that illustrated to have a good potency in trauma brain injury and spinal cord injury. The structure of this compound can be seen below.

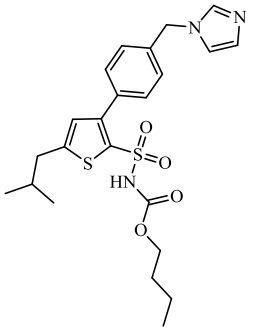

21

In order to compare the activity of this established compound in trauma brain injury and spinal cord injury with our compound **21**, on the frame of the DGF award, we went on to synthesize this compound. The biological experiments of our analogue compound 21 are conducted in collaboration with Prof. Adina Michael-Titus, Centre for Neuroscience and Trauma, Blizard Institute of Cell and Molecular Science, London, UK.

5.2.2 Design, synthesis and characterization:

Synthesis of Compound 21

Compound 21 was synthesized as reported by Yiqian Wan et. al.[179] and Kevin et. al.[180] Thiophene-2-sulphonylchloride was quantitatively converted into its N-*trt*-butyl sulfonamide derivative and then selectively alkylated at position 5 of thiophene. The *n*-BuLi was used as a base to form anion nucleophilic substitution of Iodine from 1-Iodo-2-methylpropane to give compound **2**. Although two equivalents of base *n*-BuLi [180] were added the reaction wasn't quantitative; unreacted **1a** was recovered by silica gel column chromatography. (More *n*-BuLi was avoided, to get rid of alkylation at position 3 also). Similaraly, boronation was achieved selectively at position 3 of thiophene by two equivalents of *n*-BuLi. The formed anion was quenched with Triisopropyl borate after acidic work up to give intermediate compound **3**.

The second intermediate **5** was synthesised by N-alkylation of Imidazole by 4-bromobenzyl bromide in the presence of KOH as a base. Substitution of benzylic bromide was achieved selectively, but the reaction yield was low since additional KOH may help to convert 4-Bromobenzylbromide into 4-Bromobenzylalcohol.[179]

Suzuki coupling is one of the most efficiently used reactions for C-C bond formation in Organic Chemistry. The palladium catalysed cross coupling of boronic acid **3** with aryl halide **5** gives the alkylated compound **6**. In this reaction, to some extent we are getting compound **2**, propably due to the use of NaOH (from Suzuki reaction) removed boronation from **3**. Deprotection of *tert*-butyl from sufonamide with acidic condition gave amine which subsequently acylated by *n*-butyl chloroformate in the presence of pyrrolidinopyridine as a base to give the final compound **21**. Almost after each reaction compounds were purified by silica gell chromatography.

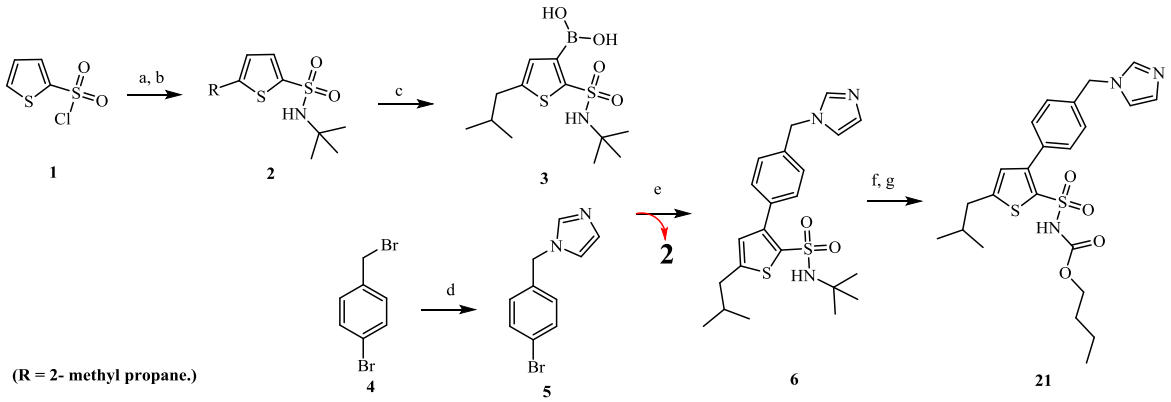

Figure 1: *a) t-BuNH$_2$, CH$_2$Cl$_2$, reflux 10 min.; b) RI (1-Iodo-2-methylpropane), n-BuLi, THF, rt 1 h; c) n-BuLi, B(-OPr^i)$_3$, HCl, rt, 1 h; d) Imidazole, KOH, DMSO,rt, 3 h; e) Pd(PPh$_3$)$_4$, aq. NaOH, Toluene, Ethanol, reflux, 3 h; f) TFA, Toluene, CH$_2$Cl$_2$, rt, 12 h; g) n-butyl chloroformate, pyrrolidinipyridine, pyridine, rt, 12 h.*

Characterization by 2D NMR (HMBC, HSQC): All the above synthesised compounds were characterised by NMR to ensure the reactions and sites of substitution. All that structures were confirmed by 2D NMR (HMBC, HSQC), assignments are shown in following *Figure 2.*

1) Alkylation: As we have mentioned earlier on the basis of previous report isobutyl group was selectively added at 5-thiophene, this statement has been confirmed after assignments, by overlaping HSQC and HMBC spectra. The absence of one aromatic proton (5-H) and cross peak of 6-H with C5, C4, C3 and C2 are in favour of addition of isobutyl group; but specific site where addition reaction happened was confirmed by the most important coupling cross peak of 7-H with only C5 (*Figure 2-A*).

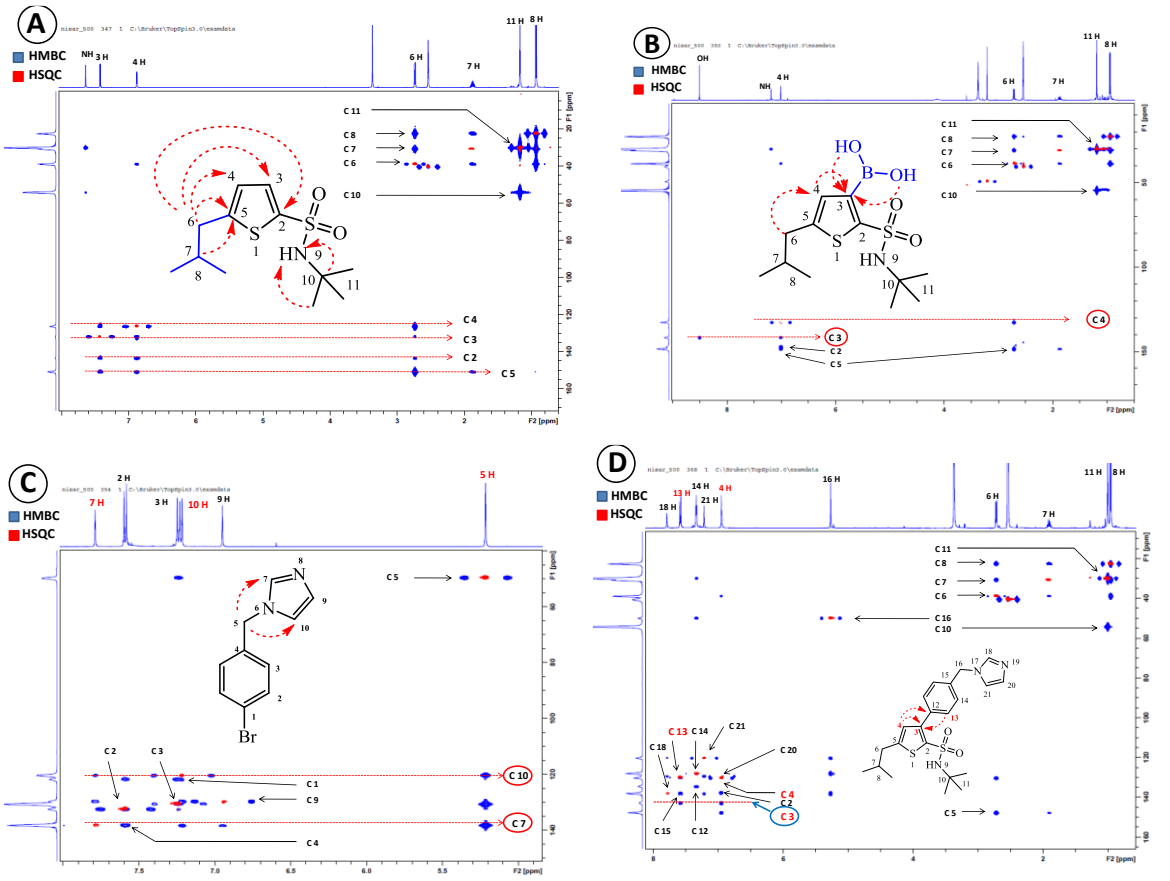

Figure 2*: 2D NMR (HMBC, HSQC) assignment of above synthesised compiunds.*

2) Boronation: Appearance of singlet at δ = 8.5 for two identical hydroxyl protons same time absence of one aromatic proton agree with addition of boronation at thiophene and coupling of 6-H proton with C4 were as 4-H with C3 confirm the boronation happened at 3-thiophene. In addition to these results, two hydroxyls from boronic acid also shows coupling with C3 (*Figure 2-B*).

3) N-alkylation of Imidazole: Intermediate **5** was synthesised by dehydrobromination. Even after the compound 4-Bromobenzyl bromide has two bromine, but reaction happened selectively at benzylic bromide. This result was confirmed by NMR assignments (*Figure 2-C*), the cross peaks of benzylic 5-H with imidazole protons 7-H and 10-H.

4) Suzuki Coupling: Boronic acid from compund **3** was substituted by compound **5**. Elimination of hydroxyl singlet and appearance of additional peak from compound 5, but the important cross peak between aromatic proton 13-H with C3 and 4-H with C12 are in favour of arylation of thiophene by Suzuki reaction (*Figure 2-D*).

Synthesis of 1a:

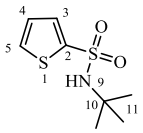

1a

Compound **1 (**5 g, 0.027 mol) was dissolved in 25 mL of anhydrous DCM and *tert*-butyl amine (5.8 mL, 0.054 mol) was added drop wise at rt, under inert atmosphere. The reaction was continued at rt for 1 h and then refluxed for 10 min. TLC (EtOAc/Hexane, 2/8, v/v) showed consumption of **1.** The reaction mixture was diluted with 50 mL H_2O and extracted with DCM (30 mL X 3).The combined organic layers were washed with brine and dried over sodium sulfate, concentrated on rotary evaporator, dried well on high vacuum to obtain compound **1a** (6.0 g, 99.68%) as a white solid compound.

^{1}H-NMR (250 MHz, DMSO-d_6, 25^{o}C): δ = 7.90 (dd, J = 2.5, 1.36 Hz, 1 H), 7.73 (bs, 1 H), 7.60 (dd, J = 1.86, 1.36 Hz, 1 H), 7.16 (dd, J = 3.69, 2.5 Hz, 1 H), 1.17 (s, 9 H) ppm; ^{13}C-NMR (250 MHz, DMSO-d_6, 25^{o}C): δ = 146.69 (C), 132.77 (CH), 132.01 (CH), 128.32 (CH), 54.63 (C), 30.44 (CH_3) ppm. Mass: ESI-MS (*m/z)* for $C_8H_{13}NO_2S_2$: calcd, 219.04; found, 241.9 $[M+Na]^+$.

Synthesis of compound 2:

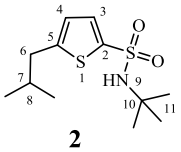

2

Compound **1a** (6.45 g, 0.029 mol) was dissolved in 150 mL anhydrous THF, under inert atmosphere and ice cooling. 2.5 M *n*-BuLi in hexane (23.55 mL, 0.058 mol) was added drop wise (10-15 min). After 20 min 1-Iodo-2-methylpropane (4.06 mL, 0.035 mol) was added drop wise at ice cooling. The resulting mixture was stirred at rt for 1 h.TLC (EtOAc/Hexane, 2/8, v/v) showed the formation of a new spot and unreacted **1a**. The reaction mixture was poured in 100 mL aq. ammonium chloride solution, extracted with ethyl acetate (50 mL X 3), the combined organic layers were washed with brine, dried over sodium sulfate and concentrated. The crude compound was purified with silica gel column chromatography in hexane and ethyl acetate as a solvent. The pure compound was collected (at 6% Ethyl acetate in hexane), concentrated and dried well on high vacuum to obtain compound **2** (3.9 g, 48.14%) as a yellow viscous compound.

^{1}H-NMR (500 MHz, DMSO-d_6, 25^{o}C): δ = 7.64 (s, 1 H, 9-NH), 7.42 (d, J = 3.67 Hz, 1 H, 3-H), 6.88 (d, J = 3.67 Hz, 1 H, 4-H), 2.73 (d, J = 7.05 Hz, 2 H, 6-H), 1.87 (m, 1 H, 7-H), 1.17 (s, 9 H, 11-H), 0.93 (d, J = 6.61 Hz, 6 H, 8-H) ppm; ^{13}C-NMR (500 MHz, DMSO-d_6, 25^{o}C): δ = 150.94 (C5), 143.51 (C2), 132.0 (C3), 126.38 (C4), 54.37 (C10), 39.16 (C6), 30.98 (C7), 30.3 (C11), 22.65 (C8) ppm.

Synthesis of compound 3:

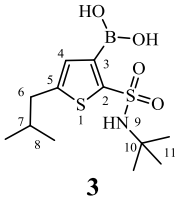

3

Compound **2** (517 mg, 1.879 mmol) was dissolved in 50 mL anhydrous THF, under inert atmosphere and at ice cooling 2.5 M *n*-BuLi in hexane (1.5 mL, 3.758 mmol) was added drop wise (the reaction mixture becomes colourless to pale yellow). After 15 min triisopropyl borate (650.5 µL, 2.818 mmol) was added drop wise at ice cooling. The

resulting mixture was stirred at rt for 1 h. TLC (EtOAc/Hexane, 2/8, v/v) showed almost consumption of **2**. The reaction mixture was poured in 20 mL of 2 N aq. HCl, extracted with ethyl acetate (20 mL X 3). The combined organic layers were washed with brine, dried over sodium sulfate and concentrated. The crude compound was purified with column chromatography in hexane and ethyl acetate as a solvent. The pure compound collected (at 15% ethyl acetate in hexane), concentrated and dried well on high vacuum to obtain compound **3** (535 mg, 89.21%) as a pale yellow sticky compound.

^{1}H-NMR (500 MHz, DMSO-d_6, 25^{o}C): δ = 8.50 (s, 2 H, OH), 7.18 (s, 1 H, 9-NH), 7.00 (s, 1 H, 4-H), 2.71 (d, J = 7.0 Hz, 2 H, 6-H), 1.86 (m, 1 H, 7-H), 1.18 (s, 9 H, 11-H), 0.94 (d, J = 6.6 Hz, 6 H, 8-H) ppm; ^{13}C-NMR (500 MHz, DMSO-d_6, 25^{o}C): δ = 148.70 (C5), 147.51 (C2), 141.8 (C3), 132.9 (C4), 54.68 (C10), 38.6 (C6), 31.0 (C7), 30.24 (C11), 22.70 (C8) ppm.

Synthesis of 5:

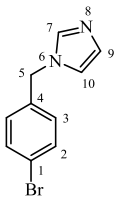

5

Imidazole (164.7 mg, 2.420 mol) was added to the solution of KOH (0.679 g, 12.102 mol) in 7 mL DMSO (DMSO was dried over molecular sives). After 2 h compound **4** (1 g, 4.034 mol) was added under ice cooling and stirring was continued for 1 h. TLC (EtOAc/Hexane, 1/9, v/v) showed the consumption of **4**. The reaction mixture was diluted with 10 mL water, extracted with diethyl ether (10 mL X 3). The combined organic layers were washed with brine, dried over sodium sulfate and concentrated. The crude compound was purified with silica gel column chromatography in DCM and methanol as a solvent. The pure compound was collected (1-2% methanol in DCM and 0.05% formic acid as eluent), concentrated and dried under high vacuum to give compound **5** (350 mg, 36.76%) as a yellow viscus compound.

^{1}H-NMR (500 MHz, DMSO-d_6, 25^{o}C): δ = 7.78 (s, 1 H, 7-H), 7.59 (d, J = 8.40 Hz, 2 H, 2-H), 7.24 (d, J = 8.40 Hz, 2 H, 3-H), 7.21 (t, J = 1.2 Hz, 1 H, 10-H), 6.94 (t, J = 1.0 Hz, 1 H,

9-H), 5.21 (s, 2 H, 5-H) ppm; ^{13}C-NMR (500 MHz, DMSO-d_6, 25^{o}C): δ = 138.34 (C7), 138.17 (C4), 132.37 (C2), 130.48 (C3), 129.77 (C9), 121.81 (C1), 120.33 (C10), 49.47 (C5) ppm. Mass: ESI-MS (*m/z)* for $C_{10}H_9BrN_2$: calcd, 237.10; found, 238.9 $[M+H]^+$.

Synthesis of compound 6:

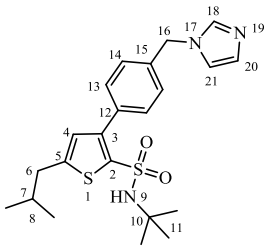

6

The solution of compound **3 (**415 mg, 1.300 mmol**) 5** (202.5 mg, 0.858 mmol) in Toluene (30 mL) and Ethanol (3 mL) was degased for 5 min**;** then addition of 3 mL of 1 M NaOH and Pd $(PPh_3)_4$ (28.85 mg, 0.024 mmol) followed and the reaction mixture was heated to reflux for 3 h under inert atmosphere, TLC (DCM/MeOH, 9.5/0.5, v/v) showed consumption of **3** and **5**. The reaction mixture was diluted with 40 mL ethyl acetate and washed with 10 mL of water and brine, the organic layer was dried over sodium sulfate and concentrated. The crude compound was purified with silica gel column chromatography in DCM and methanol as a solvent. The pure compound was collected (2-4% methanol in DCM), concentrated and dried well under high vacuum to obtain compound **6** (230 mg, 41.02%) as a yellow solid.

^{1}H-NMR (500 MHz, DMSO-d_6, 25^{o}C): δ = 7.79 (s, 1 H, 18-H), 7.58 (d, J = 8.10 Hz, 2 H, 13-H), 7.33 (d, J = 8.10 Hz, 2 H, 14-H), 7.33 (s, 1 H, 9-NH), 7.22 (s, 1 H, 21-H), 6.95 (s, 1 H, 4-H), 6.94 (s, 1 H, 20-H), 5.27 (s, 2 H, 16-H), 2.27 (d, J = 7.02 Hz, 2 H, 6-H), 1.90 (m, 1 H, 7-H), 1.00 (s, 9 H, 11-H), 0.95 (d, J = 6.57 Hz, 6 H, 8-H) ppm; ^{13}C-NMR (500 MHz, DMSO-d_6, 25^{o}C): δ = 147.93 (C5), 143.04 (C3), 138.22 (C15), 138.04 (C18), 137.8 (C2), 134.65 (C12), 130.4 (C4), 130.04 (C13), 129.49 (C20), 128.05 (C14), 120.31 (C21), 54.4 (C10), 49.93 (C16), 38.77 (C6), 30.63 (C7), 29.98 (C11), 22.6 (C8) ppm. Mass: ESI-MS (*m/z)* for $C_{22}H_{29}N_3O_2S_2$: calcd, 431.17; found, 432.1 $[M+H]^+$.

Synthesis of compound 21:

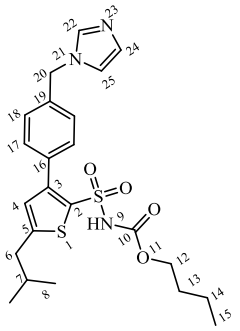

21

A solution of **6** (225 mg, 0.544 mmol) and anisole (300 µL) in 10 mL TFA was stirred at rt overnight. The solvent was evaporated with an azeotrop with acetonitrile (5 mL X 2). The residue was dissolved in anhydrous pyridine (3 mL), addition of pyrrolidinopyridine (80.70 mg, 0.544 mmol) followed by *n*-butyl chloroformate (666.6 µL, 5.173 mmol) at ice cooling under inert atmosphere. The reaction was continued overnight at rt. The solvent was evaporated using an azeotrop with acetonitrile (10 mL X 2). The residue was dissolved in ethyl acetate (100 mL) and washed with 10% aq. citric acid (20 mL), water (20 mL) and brine simultaneously. The organic layer was dried over sodium sulfate. The crude compound was purified with silica gel column chromatography, the pure compound (10-15% methanol in DCM) was concentrated and dried well under high vacuum to obtain compound **21** (175 mg, 70.57%) as a pale yellow solid.

^{1}H-NMR (500 MHz, DMSO-d_6, 25^{o}C): δ = 8.27 (s, 1 H, 22-H), 7.64 (d, J = 8.2 Hz, 2 H, 17-H), 7.44 (s, 1 H, 24-H), 7.33 (d, J = 8.2 Hz, 2 H, 18-H), 7.20 (s, 1 H, 25-H), 6.91 (s, 1 H, 4-H), 5.33 (s, 2 H, 20-H), 3.85 (t, J = 6.47 Hz, 2 H, 12-H), 2.70 (d, J = 6.80 Hz, 2 H, 6-H), 1.90 (m, 1 H, 7-H), 1.42 (m, 2 H, 13-H), 1.23 (m, 2 H, 14-H), 0.97 (d, J = 6.65 Hz, 6 H, 18-H), 0.86 (t, J = 7.34 Hz, 3 H, 15-H) ppm; ^{13}C-NMR (500 MHz, DMSO-d_6, 25^{o}C): δ = 154.72 (C10), 147.93 (C5), 142.48 (C3), 137.53 (C22), 137.1 (C19), 135.08 (C16), 130.27 (C17), 129.88 (C4), 127.98 (C18), 126.84 (C25), 121.11 (C24), 65.0 (C12), 50.56 (C20), 38.86 (C6), 31.15 (C13), 30.66 (C7), 22.67 (C8), 19.17 (C14), 14.21 (C15) ppm. Mass: ESI-MS (*m/z)* for $C_{23}H_{29}N_3O_4S_2$: calcd, 475.16; found, 476.74 $[M+H]^+$.

5.3 NMR study of Gemcitabine

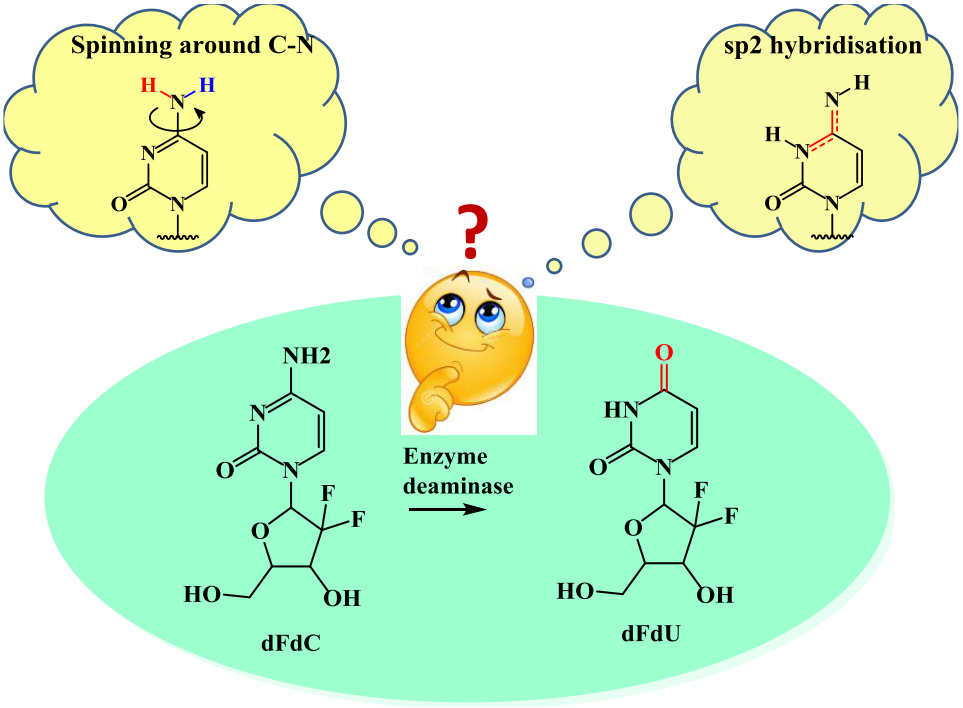

To be submitted:

Title: Solvent dependent chemical exchange in Gemcitabine: the role of hybridization

5.3.1 Introduction:

As we have mentioned in the previous chapters Gemcitabine is an anticancer drug that is used for the treatment of various cancer tumours, however it suffers from poor stability in plasma[26] and in liver,[181] since it converted to its inactive metabolite 2',2'-deoxydifluorouridine (dFdU) via hydrolytic deamination at 4-amine by the enzyme cytidine deaminase. The actual mechanism of gemcitabine deamination is still not well known. *Andriy L. Potyahaylo et. al.*[182] reported the unusual behaviour of cytosine concerning the interconversion of amino group within nucleotide bases to occur through three topologically and energetically different ways: The first way is the **inversion of amine group** and the other two are oppositely directed anisotropically **hindered rotation of amino group** around exocyclic bond (4C-NH_2). This interconversion of the amino group within nucleotide bases is controlled by the following factors:

1) pπ-conjugation of 4-amine lone pair with aromatic π-electron system.
2) Intramolecular hydrogen bonding.
3) Steric factors.

On the frame of this work we identified that the following two chacteristics of cytidine can be assigend to gemcitabine: 1) Chemical exchange resulted from the rotation of 4-NH_2 hydrogen around the C-N bond and 2) Hybridization state of the 4-amine: The lone electron pair of the 4-amine can conjugate with the π electron system of the heterocycle ring resulting in a sp3 to sp2 hybridization of the 4-amine.

These two characteristics of gemcitabine may help to understand well the deamination mechanism.

Chemical exchange: In gemcitabine, rotation of the 4-amine protons around the C-N bond is an example of chemical exchange phenomenon between two equally populated sites; this is the procedure where the nuclei exchange with two or more environments (magnetic) in which they have different NMR parameters (e.g. chemical shift (δ), coupling constant (J) etc.). For simplicity and better understanding we have compared the chemical exchange phenomenon with the rotation of fan blades around their axis (*Figure 1*).When the fan runs slowly then someone can see (count) its blades but when it starts running faster then it seems as a circle. Similarly, slow spinning (slow chemical exchange) of the two different

hydrogen (nucleus) of 4-amine around its C-N axis can result in to distinguished NMR signals that can appear as two different peaks in the spectra; however, when the spinning is fast then these signals are inseperable in the NMR timescale. This happens when nucleus changes its magnetic environment quickly in the NMR timescale then they can not be "recognized" as different nucleus and gives an average (single) peak for the two protons and vice versa.

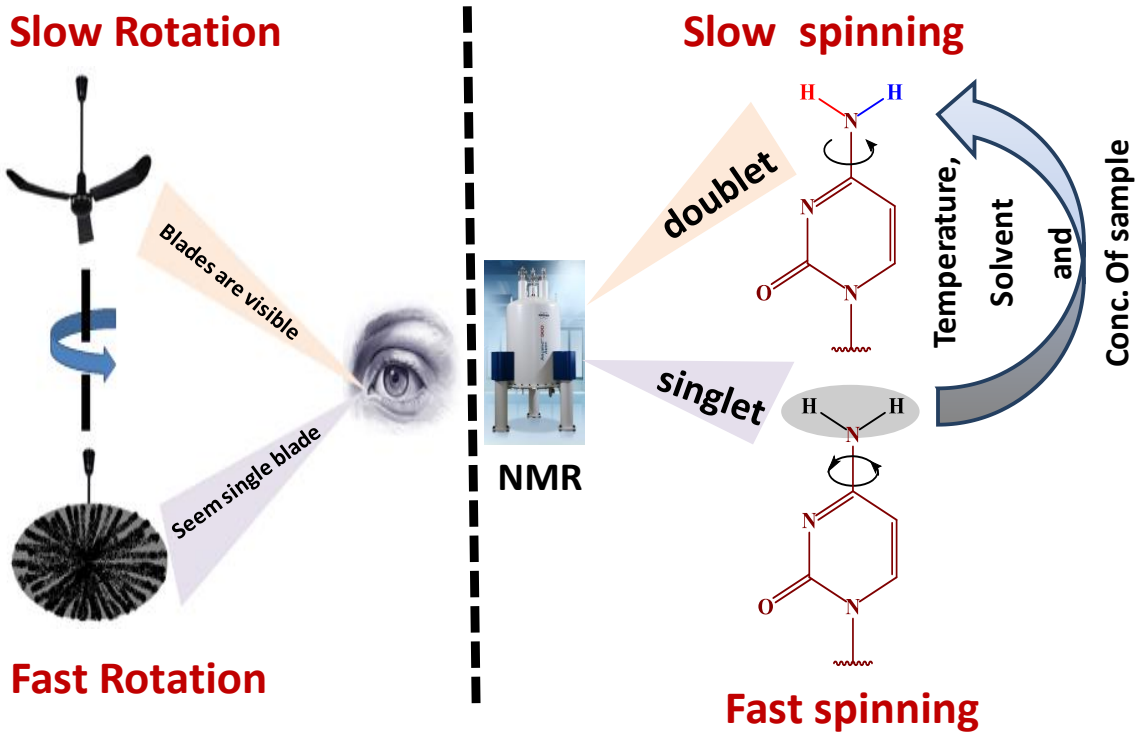

Figure 1: *An analogy of rotation of protons around C-N bond to understand "NMR timescale" phenomenon.*

5.3.2 Results and discussion:

If we are able to slow down this C-N spinning, it is possible to see each individuals magnetic environments i.e. two separate NMR peaks. Following are the factors which we used to reduce the exchanging of the magnetic environment.

1) Temperature: Lowering temperature.[183]

2) Concentration/ dilution.[182]

3) Solvents.

4) Gemcitabine.HCl salt.

The ^{1}H NMR of gemcitabine was taken in DMSO d_6 as a solvent and the assignment is shown in *Figure 2A*, to confirm the amine and alcohol (exchangeable proton) we have taken another ^{1}H NMR in D_2O, where the exchangeable resonance dissapeared. One significant characteristic of gemcitabine that was observed in ^{1}H NMR (400 MHz) is the presence of the peak with the characteristics. δ = 7.38 ppm, d, J = 14.65 Hz, 2 H, 4-NH_2; that responds to the two protons (4-NH_2) from gemcitabine indicating that they are not identical. It was a driving force for us to perform the following temperature and solvents experiments.

Temperature dependent chemical exchange:

We have performed variable temperature experiments to ensure that the observed characteristic is a conformational transformation and not a configuration changes that happen in gemcitabine. As shown in *Figure 2B* in the same NMR tube containing 15 mM gemcitabine in DMSO d_6 we gradually reduced the temperature to 288K and then heated up to 298K.

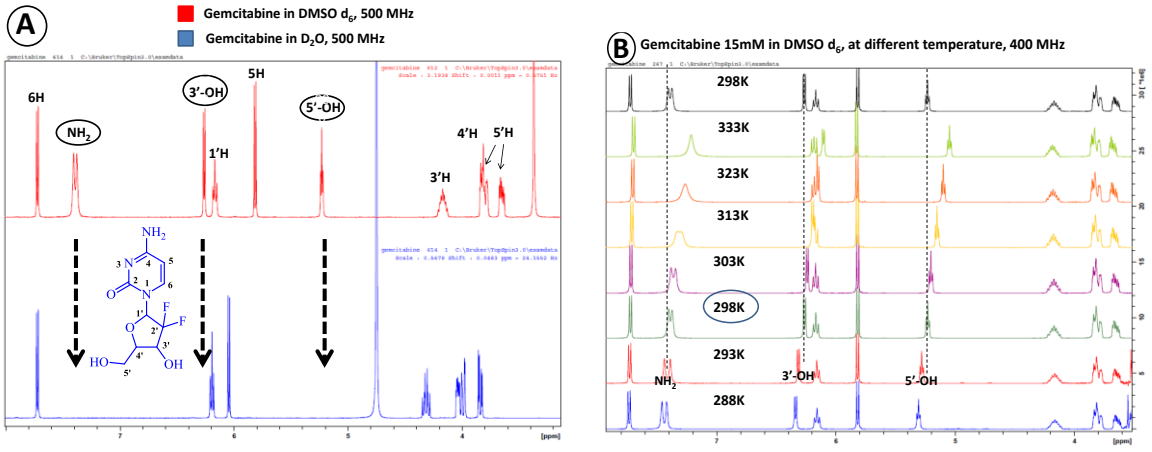

Figure 2: *^{1}H NMR of gemcitabine: A) Exchangeable proton (-NH_2, -OH) are replaced by Deuterium from D_2O; B) Gemcitabine at variable temperature.*

The ^{1}H NMR of gemcitabine at various temperatures (*Figure 2B*) shows linear changes (First order kinetics) in the chemical shift of amine and hydroxyl protons, but the peak of interest, 4-NH_2 at δ = 7.39 is present as a doublet. By going to low temperature we obtained two distinct doublets and as temperature increases the two peaks merge to a singlet. Thus, we indicated that by lowering temperature we succeded to reduce the chemical exchange and trap the two different environments.

Concentration and solvents dependent chemical exchange:

Concentration/dilution of compound plays an important role to create a barrier in C-N similarly to temperature. In high concentration there is a high possibility of intermolecular hydrogen bonding interaction (self association of molecules). In the report of *Andriy L. Potyahaylo et. al.*[182] it was indicated that the rotation of 4-amine is hindered at high concentration; however, we proved that this rotation is not dependent on self association (aggregation) in gemcitabine. As shown in *Figure 3* the amine protons are very much distinct in all different concentration used: 1, 15 and 50 mM concentration in DMSO d_6, 400 MHz. To the best of our knowledge we are the first to report the effect of the solvent as a barrier for the rotation around the C-N bond in gemcitabine. The ^{1}H NMR experiments of gemcitabine at different solvents illustrates some exciting results about the correlation between solvent and chemical exchange (*Figure 3).* In acetone d_6 there is better separation of the peaks at 0.2 mM concentration as compared to DMSO d_6 at higher concentration (7.5 mM). In acetonitrile d_3 the rotations was not stilled and a single peak was observed both at 0.2 and 8 mM concentration. The explanation for this restricted rotation in case of acetone d_6 may be the solute-solvent interaction through hydrogen bonding.

Temperature dependence ^{1}H NMR chemical shift of gemcitabine amine and hydroxyl protons: As explained above (*Figure 3)* the solvent plays an important role in the chemical exchange process. The ^{1}H NMR of gemcitabine in different solvents were taken in different temperature and the chemical shift of the exchangeable protons i.e. amine, and hydroxyl were recorded and are listed in *Table 1.* As we move from DMSO to acetone and to acetonitrile the chemical shift value of the amine is shifted almost by 1 ppm. This is due to the different ability of the different solvents to form hydrogen bond and their solvation

ability.[184] Following *Figure 4* shows the temperature dependence chemical shifts of the amine protons.

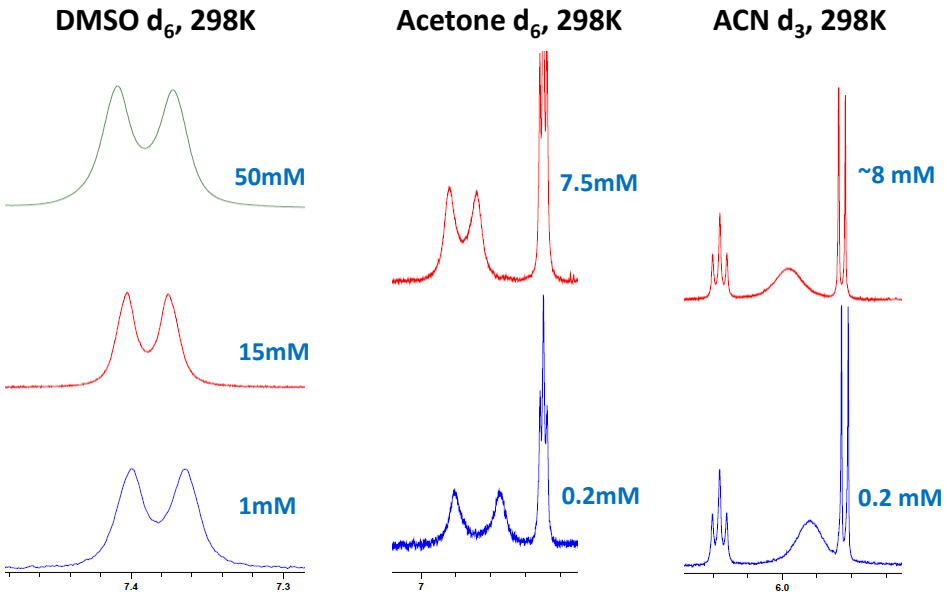

Figure 3: *Effect of concentration and solvent on the chemical exchange.*

.

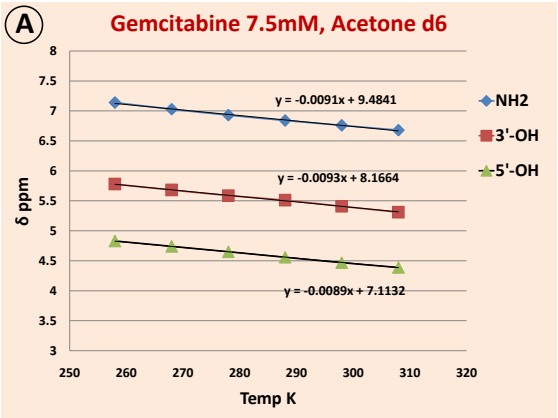

Figure 4: *Temperature dependencies of -NH_2 and -OH of gemcitabine in acetone d_6 at 7.5mM concentration.*

Table.1*: Chemical shift of exchangeable proton of gemcitabine in different solvents*

NMR solvents	**Chemical shift in ppm**		
	4-NH_2	**3'-OH**	**5'-OH**
DMSO d_6	7.38	6.26	5.23
Acetone d_6	6.67	5.38	4.45
acetonitrile d_3	5.98	4.10	3.33

.

Tautomerism/Hybridization state of amine (sp3 to sp2):

In gemcitabine, it was crucial to understand the involvement of pπ lone pairs of electron into the heterocycle π electron system. Lone pairs of 4-amine are in conjugation with the heterocyclic system therefore gemcitabine shows two tautomeric forms the amino and imino. In the imino the 4C-N bond becomes double bond. There is one more possible resonance structure, if conjugation of lone pairs continues till 2-cabonyl to provide the gemcitabine enol form (*Figure 5*). The reported crystal structure study of gemcitabine is in favour of these resonance (enol and imino form) structures because the bond length of 4C-N is almost the same like the double bond 5C=6C.[185]

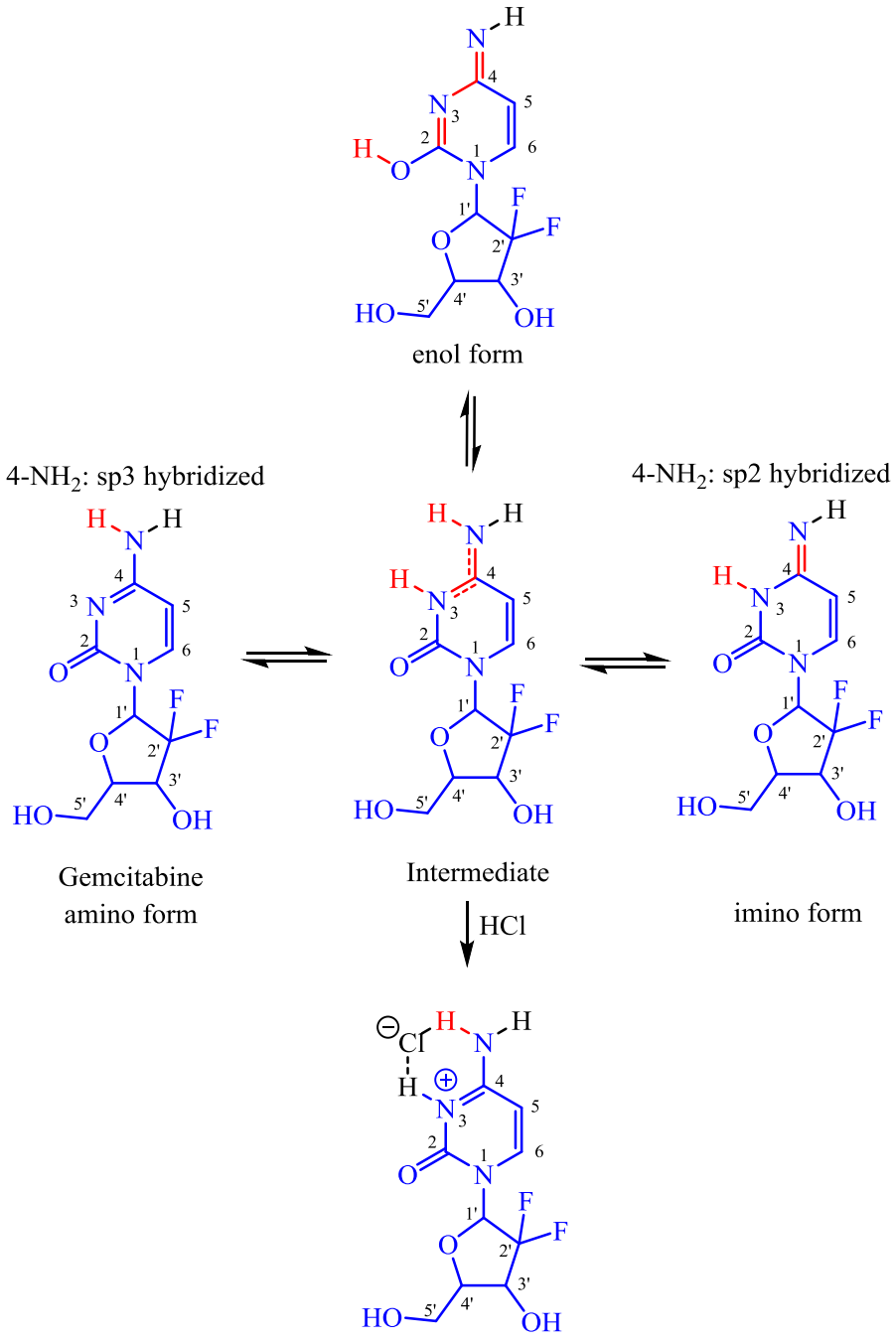

Figure 5: *Hybridization of amine and Gemcitabine.HCl salt.*

In addition to this we had the following observations:

1) Ninhydrin inactive: It is well known reaction for detection of amines or ammonia, primary amine condensed with ninhydrine and gives Schiff base which shows

very intense blue or purple colour. Gemcitabine did not show any colour after ninhydrine test that is in accordance to the absence of primary amine

2) Amide coupling was not succeeded with 1:1 molar ratio of any carboxylic acid and gemcitabine: Generally 1:1 molar ratio of amine (Primary) and carboxylic acid were reacting in presence of several coupling reagents. The reactivity (reaction time) and yield of such reactions changes according to the chemical environments around the amine or acid. In the case of gemcitabine we observed that by using 1 equiv. of gemcitabine and 1 equiv. of acid there is no product formation unless we use excess (3 equiv.) gemcitabine.

The above two results are in favour of the fact that the gemcitabine 4-amine lone pair is involved in π electron delocalization with the heterocycle and the amine behaves as sp2 hybridized. This double bond could create a rotation barrier for the interconversion of the amines in nucleotides.

Gemcitabine.HCl salt:

Once gemcitabine is protonated at position 3-N using hydrochloric acid, the cation and anions formed are linked together by hydrogen bonding.[186] This might be one possible way to trap or to minimise the exocyclic rotation of amine. The ^{1}H NMR of the Gemcitabine.HCl is shown in *Figure 6* and indicates the presence of two different peaks (δ = 9.78 and 8.71) for the 4-amine hydrogen, indicating the absence of any exocyclic amine rotation. Similarly, this protonation at position 3-N of gemcitabine may assist the conservation of the amine sp3 hybridization by blocking the conjugation of amine lone pair of electron with the heterocycle (*Figure 5*). This may be one reason for using Gemcitabine.HCl salt over plane gemcitabine in synthesis of many gemcitabine prodrugs or conjugates of gemcitabine at 4-amine.[38, 26, 187, 33]

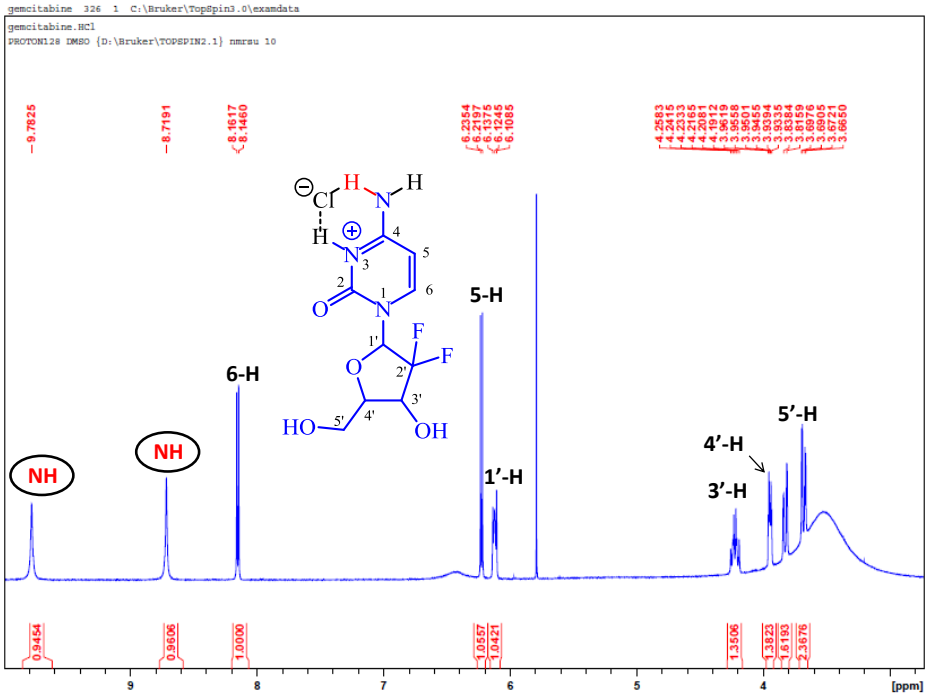

Figure 6: *^{1}H NMR of Gemcitabine.HCl in DMSO d_6, 298 K, 500MHz.*

5.3.3 Proposed mechanism for deamination

Following these observations we herein would like to provide a potential mechanism for the enzyme mediated deamination of gemcitabine by water. Enzyme cytidine deaminase form hydrogen bonding interaction with amine and minimise the chemical exchange/rotation of amine around C-N bond. Then the 3-N gets protonated by water. After resonance stabilisation of quaternary amine cation, nucleophilic attack of water molecule at carbon 4 removes the amine just like sn2 reaction mechanism (*Figure 7*).

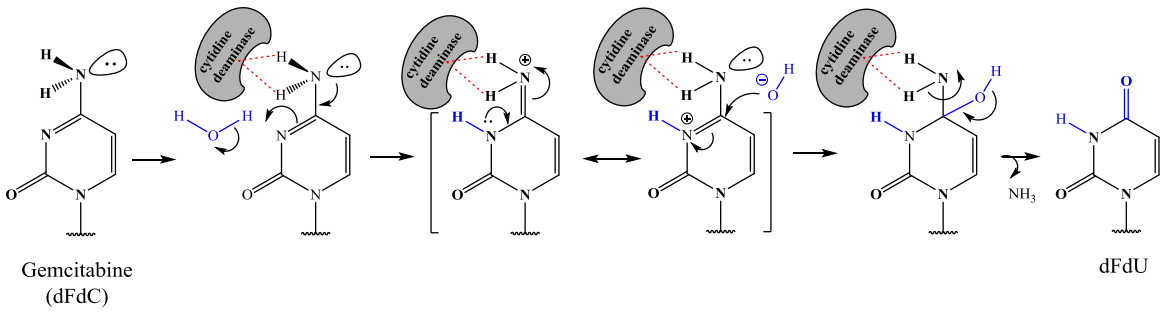

Figure 7: *Proposed mechanism for enzymatic deamination of gemcitabine.*

In this way gemcitabine (dFdC) was converted into its inactive metabolites dFdU. If we have proposed the right mechanism then we can minimise dFdU just by designing a gemcitabine prodrugs with hydrophobic substitution at position 5, not methyl but we can try ethyl, isobutyl or tert-butyl. This substitution will help to minimise the hindered amine rotation (chemical exchange) as well as create a hydrophobic pocket and steric hindrance to attack water molecule. Because, deaminase enzyme, hydrogen bonding in nucleotide base pair or in an intermolecular interaction only one side of cytosine (gemcitabine) is protected/covered and other side is free for water to attack like sn2 mechanism.

Conclusion

GnRH-Gemcitabine conjugates:

Androgen-independent CaP is a condition in which patients have limited treatment options and therefore expansion of the available therapeutic strategies is critical. The concept of using GnRH agonistic peptides for conjugation to small molecule anticancer drugs such as doxorubicin or docetaxel has been described in the past and the preclinical success of that strategy resulted in the birth of a promising targeted delivery field.[188, 10–13, 189] More importantly, the specific approach has advanced to clinical development stages; AN-152, a GnRH-doxorubicin conjugate has been evaluated in phase I and II trials with promising outcomes in GnRH-R positive patients with breast, endometrial and ovarian cancer.[14]

The anticancer drug chosen for our studies, gemcitabine, has been extensively used for the treatment of solid tumours. Its antiproliferative effect in androgen-independent CaP cell lines[61] gave rise to clinical expectations but its benefit in androgen-independent CaP patients was modest mainly due to its peripheral toxicity.[62–64] As targeted delivery cannot be based only on a simplified hypothesis that a cancer cell specific ligand will lead to preferable interaction and internalization of the drug in the cancer cell, other important factors should be taken into consideration, such as systemic targeting, tumour penetration, tumour heterogeneity.[190] For this reason, in this thesis the focus was not only to enrich the repository of GnRH conjugates with new chemical entities which target GnRH-R positive cancer cells, but also to improve the therapeutic potential of gemcitabine, a very potent drug with poor pharmacokinetic properties.[58, 59] These conjugate molecules would ideally operate as prodrugs of gemcitabine with favorable pharmacokinetic properties by protecting it from its rapid inactivation and provide alternative entrance point into the cell for gemcitabine (through the GnRH-R), a pivotal attribute to overcome resistance to gemcitabine treatment often caused by nucleoside transporter deficiency.[59, 60]

[D-Lys^6]-GnRH, a potent GnRH-R agonist was chosen for conjugation to gemcitabine. The D-Lys^6 position offers an amino side chain appropriate for conjugation reactions since the specific amino acid side chain does not participate in the binding to the GnRH-R.[7, 48, 49] GnRH-gemcitabine conjugates containing different linkers and with different gemcitabine conjugation sites were synthesized and evaluated. NMR studies in

representative GnRH-gemcitabine conjugates demonstrated that conjugation of gemcitabine to the GnRH peptide does not alter significantly the structural conformation required for successful binding to the GnRH-R. Furthermore, the described GnRH-gemcitabine conjugates exhibited high binding affinity to the GnRH-R.

Medium linkers via Carbonate bond:

For the *in vitro* evaluation of the GnRH-gemcitabine conjugates, two androgen-independent CaP cell lines were used (DU145, PC3) with confirmed expression of GnRH-R. Among the synthesized GnRH-gemcitabine conjugates that were assessed with respect to their antiproliferative potential *in vitro*, $3G_2$, GSG_1 and GSG_2 exhibited the most prominent effects, similar to those of gemcitabine. Selected molecules ($3G_2$ and GSG_1) were then evaluated in pharmacokinetic animal experiments due to superior stability in cell culture media. Although the criterion of stability in cell culture might seem arbitrary, the rapid cleavage of these analogues was not a desirable property since ultimately some level of stability would be necessary in order for the conjugates to "present" themselves to the site of action (cancer cell). Administration of GSG_1 in mice for pharmacokinetic evaluation, when compared to administration of gemcitabine or $3G_2$, resulted in more sustained levels of gemcitabine in blood, indicating potential for enhanced efficacy. Moreover, less dFdU was produced after administration of GSG_1 compared to administration of gemcitabine or $3G_2$ suggesting that GSG_1 renders gemcitabine less vulnerable to rapid inactivation. This finding led to the selection of GSG_1 as the lead compound of the current study. The sustained levels of gemcitabine and reduced levels of dFdU in blood after GSG_1 administration was further confirmed in tissue distribution experiments in mice bearing xenografts. Moreover, GSG_1, which was shown to be active in antiproliferative assays, could be delivered to the tumour site at appreciable levels. It should be noted that our tumour measurements were based on homogenization of the whole tumour and presumably lack some important information regarding drug intratumoural levels (e.g. measurements at different parts of a tumour might be affected by differences in interstitial fluid pressure).

The protective effect of GSG_1 was further supported by cell uptake experiments where incubation of GSG_1 in DU145 cells suggested that GSG_1 enters the cell and releases gemcitabine in a relatively slow rate, leading to sustained intracellular gemcitabine levels combined with lower levels of dFdU when compared to incubation with gemcitabine.

Although passive diffusion of GSG_1 cannot be ruled out, pre-incubation of DU145 cells with [D-Lys^6]-GnRH limited GSG_1 cell uptake, suggesting a key role of the GnRH-R in the selective cellular entry of GSG_1.

The efficacy of GSG_1 was evaluated in an *in vivo* xenograft animal model. GSG_1 was efficacious in inhibiting tumour growth when compared to gemcitabine or [D-Lys^6]-GnRH at the same molar dose, which were not significantly different from the vehicle. As in previously published reports,[191–193] gemcitabine efficacy was achieved at a dose exceeding 100 mg/kg (120 mg/kg) for the specific animal model and dosing scheme. Since GSG_1 efficacy was achieved with a significantly lower dose when compared to gemcitabine (approximately 25 times), it can be suggested that GSG_1 administration might have advantages in comparison to gemcitabine with respect to off target toxicity.

Although the exact mechanism of action for the efficacy achieved with the GSG_1 has not been fully delineated, it should be emphasized that a strong component that adds to the efficacy of GSG_1 is the enhanced exposure of gemcitabine following dosing combined with a decrease in circulating levels of the inactive metabolite (dFdU). As was recently demonstrated by Frese *et al*[194], approaches which favorably alter gemcitabine's biodistribution properties (e.g., enhanced intratumoural concentration) have important implications for the treatment of a variety of tumours.

In conclusion, the lead compound presented in this thesis, GSG_1, shows a potent anticancer effect that appears to be associated with a dual mode of action: 1) improved efficacy due to reduced metabolic inactivation of gemcitabine and 2) targeted delivery to cancer cells over-expressing the GnRH-R. We believe that the work presented herein could lead to valuable insights associated with gemcitabine treatment and possibly improve the therapeutic options of androgen independent CaP patients.

Above explanation introduced the GSG_1 as convenient conjugates, show improved efficacy as well as targeted drug delivery. By considering GSG_1 as reference conjugate we have synthesised and performed the biological evaluation of various bioconjugates according to variable length of linkers (e.g. long linkers: GSHG, short linker: $2G_1$ and $2G_2$) as well as bifunctional (two hydrolysable sites) linker conjugates such as $GOXG_1$, $GOXG_2$ and GN_4OXG.

GnRH-Gemcitabine: Long linker (GSHG) via carbonate and short linkers ($2G_1$ and $2G_2$) via carbamate bond:

For the short linker ($2G_1$ and $2G_2$) and long linkers (GSHG) celluptake in androgen-independent CaP cell line (DU145) shows high concentration of celluptake for short linkers as compared to long linker GSHG. Also the incubation of $2G_1$ or $2G_2$ did not result in intracellular detection of gemcitabine suggesting that this linkage is most probably very stable and gemcitabine is not released even after 8 h of incubation with this cell culture system. Incubation of GSHG with DU145 cells on the other hand results in increasing levels of gemcitabine over time.

The most promissing result observed from these conjugates was that, no detectable levels of the inactive metabolite were observed in any of the three incubations ($2G_1$, $2G_2$, GSHG). From GSHG we can conclude that in binconjugation not only functional group but also the length of linker is important for cell uptake and its metabolism.

Bifunctional bio-conjugates (*$GOXG_1$, $GOXG_2$ and GN_4OXG):*

We have established a new chemistry for rapid formation of oxime bonds in bioconjugation. Conjugates $GOXG_1$ and $GOXG_2$ are consisted of oxime and carbonates where as GN_4OXG bear oxime and amide. All these three conjugates suprisingly shows low stability than GSG_1 both in cell culture as well as in human plasma. $GOXG_2$ was the least stable and gives highest quantity of gemcitabine after metabolisum. GN_4OXG is the combination of oxime and amide and therefore get metabolised slowly. The best analogue from these three was $GOXG_1$ which shows the moderate stability and high concentration of gemcitabine release both in cell culture as well as in human plasma. Conclude that the combination of oxime and carbonate/amide lower the stability of conjugates than oxime or carbonate alone.

In order to compare all GnRH-gemcitabine conjugates synthesised and tested, they were all incorporated in one graph on the basis of: **Human plasma Stability** *(Figure 1).* According to this stability order someone can easily select the linkers and functional group in the synthesis of bioconjugation. e.g. the most stable conjugates ($2G_1$ and $2G_2$) carmbamate bond can be used for the slow release of parent drug to get long term effect. This may be useful for the protection of particular drug from the metabolic inactivation to

improve the efficacy. Conjugate $GOXG_2$ was the least stable conjugate. As we know oxime is the stable functional group but after combination with the carbonate or amide it became less stable this will help to achive higher concentration of parent drug in short time.

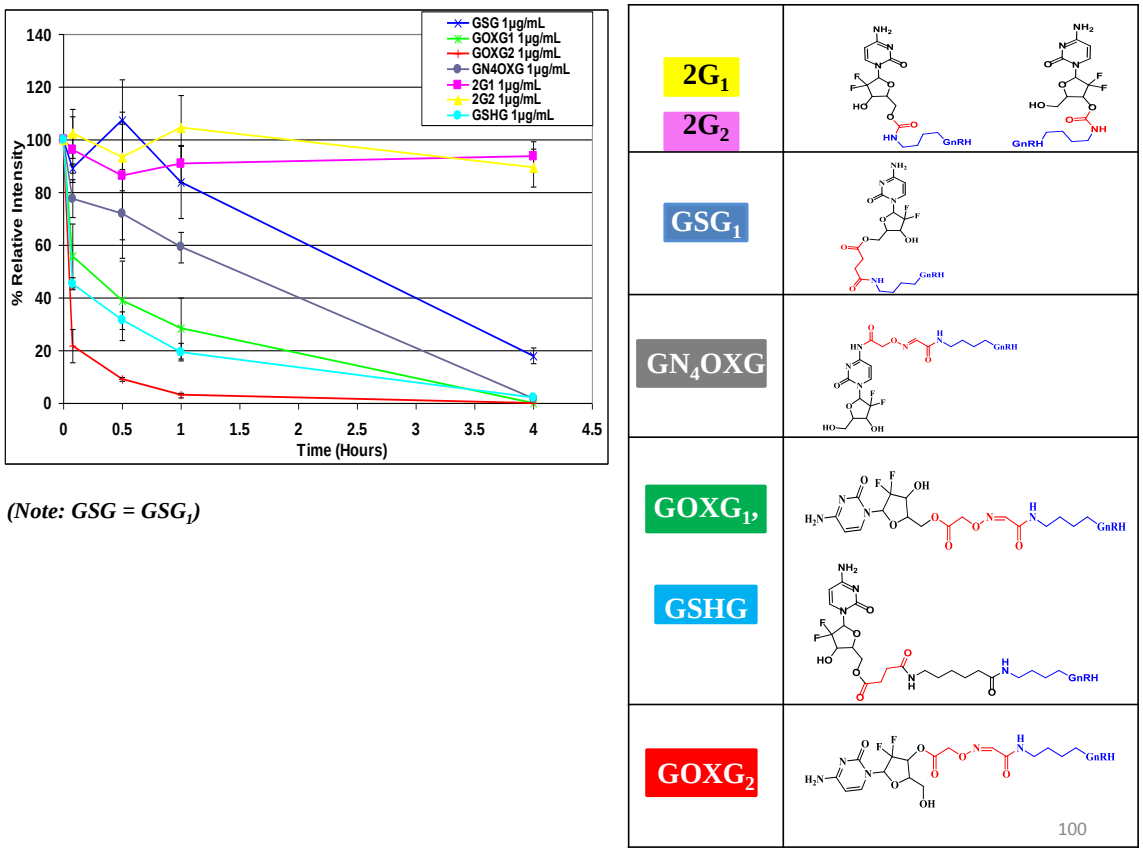

(Note: GSG = GSG_1)

***Figure 1**: Order of stability of all GnRH-gemcitabine conjugates in human plasma*

GnRH-Sunitinib Conjugate:

We have rationally synthesized novel antiangiogenic sunitinib analogues that can be readily coupled to a targeting peptide and demonstrate for the first time that a SAN1-GnRH conjugate is efficacious *in vitro* and *in vivo* in GnRH-R expressing tumours.

A series of novel readily linkable antiangiogenic compounds to treat various forms of cancer based on the clinically successful drug sunitinib. The lead compound in the current study (SAN1) proved potent *in vivo*, an attribute associated with reduced angiogenesis and inhibition of several kinases. Importantly, for the first time we demonstrated a direct conjugation of sunitinib analogue to a targeting moiety and showed

an enhanced delivery to the tumour. The concept is certainly applicable to other solid tumour types expressing the GnRH-R or even to other types of receptors by altering the targeting peptide.

Molecular hybrides:

- ***Gemcitabine-Lipoic acid:*** We found that the hybrid Gemcitabine-5´-O-lipoate is more active against non-small cell lung cancer and bladder cancer cells than the widely used chemotherapeutic Gemcitabine, and also preserves the redox potential of the parent molecule Lipoic acid. In overall, we showed that a novel redox – anticancer hybrid that could assist in cancer treatment.

- ***Gemcitabine:*** We have established a new regioselective method for one pot coupling of different functional groups to the amine group of the cytotoxic agent gemcitabine. By using this method we have synthesised seven different gemcitabine derivatives, characterised by 1D (^{1}H NMR) and 2D NMR (HMBC, HSQC) and also presented different applications.

- ***Quercetin:*** We have presented synthesis of the different hybrids of quercetin for different purpose. Quercetin-aminoacids hybrids are useful for improving biological availability by improving aqueous solubility (quercetin-glutamic acid) of quercetin, which was the major cause of quercetin low bioavailability.

  Also the quercetin (antioxidant and anticancer) used for conjugation with the Losartan and Captopril drugs, which are used for antihypertension. Because hypertension and oxidative stress are inetrlinked, as we know lowering blood pressure is the only treatment available for hypertensive patients, and therefore lowering blood pressure causes oxidative stress in vascular level in hypertension treatment. Therefore our molecular hybride Quercetin-Losartan and Quercetin-Cprotpil will help to minimise hypertension as well as generated oxidative stress.

- **For the first time we have explained the Solvent dependant chemical exchange phenomenon between two equally populated sites (4-NH_2 of Gecitabine).**
- **We are the first to identify the formation of side product driven from a widely used coupling reagent (HATU) at unprotected tyrosine hydroxyl group in liquid phase amide coupling and also determined the optimal conditions to be used.**

Summary (In English)

Despite the progress in techniques for cancer prevention, detection and treatment, as well as for increasing the public awareness in recent years, this disease is projected to become the leading cause of death worldwide. This is due to the fact that cancer is not a static entity that can be easily monitored and manipulated. It is characterized by a dynamic and time dependent network of constantly altered molecular and cellular interactions between players in different pathways.

Chemotherapy is still one of the primary modalities for the treatment of cancer. However, the application of free anticancer drugs has several drawbacks due to the high toxicity, the lack of selectivity and the low bioavailability.

The main objective of the current PhD thesis was to improve the activity mainly of antiproliferative drugs but also of other drugs and bioactive compounds. To achieve this, two axes were followed; a: Design, synthesis and biological evaluation of bioconjugates for selective drug delivery and tumour targeting and b: Design and synthesis of molecular hybrids.

Regarding to the design, synthesis and biological evaluation of bioconjugates for selective drug delivery and tumour targeting, two antiproliferative drugs were studied gemcitabine and sunitinib. Selective drug delivery was achieved by the conjugation of these drugs to gonadotropin-releasing hormone (GnRH) peptide in order to target the GnRH receptor, which is found to over express in different tumour cells. First the chemistry of drug-peptide conjugation was studied and more specific the oxime bonds, the carboxylic acid ester bonds and the carbamate bonds in chemical linkers. Then the biological evaluation of bioconjugates was tested in androgen-independent CaP cell lines followed by the pharmacokinetic study in mice. The results showed that the bioconjugates showed better anticancer activity or stability than the parent drugs. In this way, effective concentration of drugs at target can be achieved by selecting the linker with specific bonds according to required condition of particular drug.

In relation to the design and synthesis of molecular hybrids the synthesis of hybrids of the anticancer drug gemcitabine and of the natural antioxidant/anticancer compound quercetin were studied. The hybrid product of gemcitabine with a prooxidant natural compound lipoic acid showed better anticancer and prooxidant activity than the parent compounds. About quercetin: synthesis of the different hybrids of quercetin for different purposes presented. First quercetin-aminoacids hybrids are useful for improving biological availability by improving aqueous solubility (quercetin-glutamic acid) of quercetin, which was the major cause of quercetin low bioavailability. And second the quercetin (antioxidant and anticancer) used for conjugation with the Losartan and Captopril drugs, which are used for antihypertension. Because hypertension and oxidative stress are interlinked, as we know lowering blood pressure is the only treatment available for hypertensive patients, and therefore lowering blood pressure causes oxidative stress in vascular level in hypertension treatment. Therefore our molecular hybrid Quercetin-Losartan and Quercetin-Cprotpil will help to minimize hypertension as well as generated oxidative stress.

Περήληψη

(Summary in Greek)

Τα τελευταία χρόνια, παρά την πρόοδο στις τεχνικές για την πρόληψη, την ανίχνευση, την θεραπεία του καρκίνου αλλά και την ενημέρωση της κοινής γνώμης, η ασθένεια αυτή προβλέπεται να καταστεί κύρια αιτία θανάτου παγκοσμίως. Αυτό οφείλεται στο γεγονός ότι ο καρκίνος δεν είναι μία στατική οντότητα που μπορεί εύκολα να παρακολουθείται και να χειραγωγείται. Αλλά ο καρκίνος χαρακτηρίζεται από ένα δυναμικό και χρονοεξαρτόμενο δίκτυο μοριακών και κυτταρικών αλληλεπιδράσεων που διαρκώς μεταβάλλεται.

Η χημειοθεραπεία αποτελεί ακόμα μία από τις κύριες μεθόδους αντιμετώπισης του καρκίνου. Ωστόσο η εφαρμογή των αντικαρκινικών φαρμάκων σε ελεύθερη μορφή έχει πολλά μειονεκτήματα λόγω, της υψηλής τοξικότητας, της έλλειψης επιλεκτικότητας και της χαμηλής βιοδιαθεσιμότητας των φαρμάκων αυτών.

Ο κυρίως στόχος της παρούσας διδακτορικής διατριβής ήταν η βελτίωση της δραστικότητας φαρμάκων (κυρίως αντικαρκινικών) καθώς και άλλων βιοδραστικών ενώσεων. Για το σκοπό αυτό ακολουθήθηκαν δύο άξονες: α) Σχεδιασμός, σύνθεση και βιολογική αξιολόγηση βιοσυζυγών για την εκλεκτική απελευθέρωση φαρμάκου και στόχευση όγκων και β) Σχεδιασμός και σύνθεση υβριδικών ενώσεων.

Αναφορικά με το πρώτο σκέλος της διατριβής, τον σχεδιασμός, τη σύνθεση και τη βιολογική αξιολόγηση βιοσυζυγών για την εκλεκτική απελευθέρωση φαρμάκου και στόχευση όγκων, μελετήθηκαν δύο ευρέως γνωστά αντικαρκινικά φάρμακα, η γεμσιταμπίνη και η σουνιτινίμπη. Η εκλεκτική απελευθέρωση αυτών των φαρμάκων επιτεύχθηκε με την σύζευξή τους σε γοναδοεκλυτίνη με στόχο τον μεμβρανικό υποδοχέα GnRH , ο οποίος έχει βρεθεί να υπερεκφράζεται σε πολλά είδη καρκινικών κυττάρων. Αρχικά, μελετήθηκε η χημεία σύζευξης φαρμάκου με πεπτίδιο. Πιο συγκεκριμένα μελετήθηκαν δεσμοί όπως αυτός της οξίμης καθώς και εστερικοί δεσμοί τόσο καρβοξυλικού οξέος όσο και του καρβαμικού, ως χημικοί συνδέτες. Στη συνέχεια μελετήθηκε η βιολογική αξιολόγηση των βιοσυζυγών που συντέθηκαν σε

ανδρογονοανεξάρτητες κυτταρικές σειρές CaP και ακολούθησε η φαρμακοκινητική μελέτη σε ποντίκια. Τα αποτελέσματα έδειξαν ότι τα βιοσυζυγή που συντέθηκαν στην παρούσα διατριβή εμφάνισαν βελτιωμένη αντικαρκινική δράση ή σταθερότητα από τα μητρικά φάρμακα. Συμπερασματικά, η επιθυμητή συγκέντρωση του φαρμάκου μπορεί να επιτευχθεί με την κατάλληλη επιλογή μορίου συνδέτη ανάλογα με την χημεία του φαρμάκου.

Όσο αφορά το δεύτερο σκέλος της παρούσας διατριβής, τον σχεδιασμό και την σύνθεση υβριδικών μορίων μελετήθηκε η σύνθεση υβριδικών μορίων του αντικαρκινικού φαρμάκου γεμσιταμπίνη και του φυσικού αντιοξειδωτικού / αντικαρκινικού φλαβονοειδούς, κερσετίνη. Τα αποτελέσματα έδειξαν ότι το υβριδικό μόριο της γεμσιταμπίνης με το φυσικό προοξειδωτικό λιποϊκό οξύ εμφάνισε καλύτερη αντικαρκινική και προοξειδωτική δράση από της πρόδρομες ενώσεις. Αναφορικά με την κερσετίνη, παρουσιάζεται η σύνθεση διαφορετικών υβριδίων για διαφορετικούς σκοπούς. Έτσι, τα υβριδικά μόρια της κερσετίνης με αμινοξέα είναι χρήσιμα για την βελτίωση της βιολογικής διαθεσιμότητας του φλαβονοειδούς βελτιώνοντας την υδατοδιαλυτότητά της (κερσετίνη-γλουταμινικό οξύ), που αποτελεί τον κύριο παράγοντα μειωμένης βιοδιαθεσιμότητας του συγκεκριμένου και όχι μόνο φλαβονοειδούς. Επιπλέον, καθώς το οξειδωτικό στρες συμβάλει στην υπέρταση και όπως γνωρίζουμε η μείωση της αρτηριακής πίεσης είναι η μόνη διαθέσιμη θεραπεία για τους υπερτασικούς ασθενείς, ενώ παράλληλα η μείωση της αρτηριακής πίεσης προκαλεί το οξειδωτικό στρες σε επίπεδο αγγείων στη θεραπεία της υπέρτασης, μελετήθηκε, η σύνθεση υβριδικών μορίων του φυσικού αντιοξειδωτικού κερσετίνη με τα αντιυπερτασικά φάρμακα λοσαρτάνη και captopril. Ως εκ τούτου, τα μοριακά υβριδικά μόρια Κερσετίνη-λοσαρτάνη και Κερσετίνη-Caprotpil πιστεύεται ότι θα βοηθήσουν στην μείωση της υπέρτασης, καθώς καταπολεμάται το οξειδωτικό στρες.

References

1. Limonta, P. *et al.* GnRH receptors in cancer: from cell biology to novel targeted therapeutic strategies. *Endocr. Rev.* **33,** 784–811 (2012).

2. Millar, R. P. & Newton, C. L. Current and future applications of GnRH, kisspeptin and neurokinin B analogues. *Nat. Rev. Endocrinol.* **9,** 451–66 (2013).

3. Morgan, K. *et al.* Gonadotropin-releasing hormone receptor levels and cell context affect tumour cell responses to agonist in vitro and in vivo. *Cancer Res.* **68,** 6331–40 (2008).

4. Pazaitou-Panayiotou, K. *et al.* Gonadotropin-releasing hormone neuropeptides and receptor in human breast cancer: correlation to poor prognosis parameters. *Peptides* **42,** 15–24 (2013).

5. Millar, R. P. *et al.* Gonadotropin-releasing hormone receptors. *Endocr. Rev.* **25,** 235–75 (2004).

6. Mező, G. & Manea, M. Receptor-mediated tumour targeting based on peptide hormones. *Expert Opin. Drug Deliv.* **7,** 79–96 (2010).

7. Schally, A. V & Nagy, A. Cancer chemotherapy based on targeting of cytotoxic peptide conjugates to their receptors on tumours. *Eur. J. Endocrinol.* **141,** 1–14 (1999).

8. Teicher, B. A. & Chari, R. V. J. Antibody conjugate therapeutics: challenges and potential. *Clin. cancer Res. an Off. J. Am. Assoc. Cancer Res.* **17,** 6389–6397 (2011).

9. Mullard, A. Maturing antibody-drug conjugate pipeline hits 30. *Nat. Rev. Drug Discov.* **12,** 329–332 (2013).

10. Nagy, A. *et al.* Cytotoxic analogs of luteinizing hormone-releasing hormone containing doxorubicin or 2-pyrrolinodoxorubicin, a derivative 500-1000 times more potent. *Proc. Natl. Acad. Sci. U. S. A.* **93,** 7269–7273 (1996).

11. Manea, M. *et al.* Enhanced enzymatic stability and antitumour activity of daunorubicin-GnRH-III bioconjugates modified in position 4. *Bioconjug. Chem.* **22,** 1320–1329 (2011).

12. Aggarwal, S. *et al.* [DLys(6)]-luteinizing hormone releasing hormone-curcumin conjugate inhibits pancreatic cancer cell growth in vitro and in vivo. *Int. J. Cancer* **129,** 1611–1623 (2011).

13. Sundaram, S., Durairaj, C., Kadam, R. & Kompella, U. B. Luteinizing hormone-releasing hormone receptor-targeted deslorelin-docetaxel conjugate enhances efficacy of docetaxel in prostate cancer therapy. *Mol. Cancer Ther.* **8,** 1655–65 (2009).

14. Engel, J., Emons, G., Pinski, J. & Schally, A. V. AEZS-108 : a targeted cytotoxic analog of LHRH for the treatment of cancers positive for LHRH receptors. *Expert Opin. Investig. Drugs* **21,** 891–899 (2012).

15. Wendeler, M., Grinberg, L., Wang, X., Dawson, P. E. & Baca, M. Enhanced catalysis of oxime-based bioconjugations by substituted anilines. *Bioconjug. Chem.* **25,** 93–101 (2014).

16. Kool, E. T., Crisalli, P. & Chan, K. M. Fast alpha nucleophiles: structures that undergo rapid hydrazone/oxime formation at neutral pH. *Org. Lett.* **16,** 1454–7 (2014).

17. Agten, S. M. *et al.* Chemoselective oxime reactions in proteins and peptides by using an optimized oxime strategy: the demise of levulinic acid. *Chembiochem* **14,** 2431–4 (2013).

18. Karampelas, T. *et al.* GnRH-gemcitabine conjugates for the treatment of androgen-independent prostate cancer: Pharmacokinetic enhancements combined with targeted drug delivery. *Bioconjug. Chem.* **25,** 813–823 (2014).

19. Ai, S. *et al.* Biological Evaluation of a Novel Doxorubicin - Peptide Conjugate for Targeted Delivery to EGF Receptor-Overexpressing Tumour Cells. 375–386 (2011).

20. Schally, A. V & Nagy, A. Cancer chemotherapy based on targeting of cytotoxic peptide conjugates to their receptors on tumours. *Eur. J. Endocrinol.* **141,** 1–14 (1999).

21. Hansen, K. T., Faarup, P. & Bundgaard, H. Carbamate ester prodrugs of dopaminergic compounds: synthesis, stability, and bioconversion. *J. Pharm. Sci.* **80,** 793–8 (1991).

22. Kim, M. K., Park, K., Yeo, W., Choo, H. & Chong, Y. In vitro solubility, stability and permeability of novel quercetin-amino acid conjugates. *Bioorg. Med. Chem.* **17,** 1164–71 (2009).

23. Guo, Z. & Gallo, J. M. Selective Protection of 2 ′ , 2 ′ -Difluorodeoxycytidine (Gemcitabine). 8319–8322 (1999).

24. Chitkara, D., Mittal, A., Behrman, S. W., Kumar, N. & Mahato, R. I. Self-Assembling, Amphiphilic Polymer − Gemcitabine Conjugate Shows Enhanced Antitumour E ffi cacy Against Human Pancreatic Adenocarcinoma. (2013).

25. Mini, E., Nobili, S., Caciagli, B., Landini, I. & Mazzei, T. Cellular pharmacology of gemcitabine. *Ann. Oncol.* **17 Suppl 5,** v7–12 (2006).

26. Bender, D. M. *et al.* Synthesis, crystallization, and biological evaluation of an orally active prodrug of gemcitabine. *J. Med. Chem.* **52,** 6958–61 (2009).

27. Pratt, S. E. *et al.* Efficacy of low-dose oral metronomic dosing of the prodrug of gemcitabine, LY2334737, in human tumour xenografts. *Mol. Cancer Ther.* **12,** 481–90 (2013).

28. Weiss, J. T. *et al.* Development and Bioorthogonal Activation of Palladium-Labile Prodrugs of Gemcitabine. (2014).

29. Zhao, C. *et al.* Synthesis and biological evaluation of oral prodrugs based on the structure of gemcitabine. *Chem. Biol. Drug Des.* **80,** 479–88 (2012).

30. Orbán, E. *et al.* In vitro degradation and antitumour activity of oxime bond-linked daunorubicin-GnRH-III bioconjugates and DNA-binding properties of daunorubicin-amino acid metabolites. *Amino Acids* **41,** 469–83 (2011).

31. Tannock, I. F., Rotin, D. & Hot, D. Acid pH in Tumours and Its Potential for Therapeutic Exploitation Perspectivesin CancerResearch Acid pH in Tumours and Its Potential for Therapeutic Exploitation1. 4373–4384 (1989).

32. Choi, S. K. *et al.* A photochemical approach for controlled drug release in targeted drug delivery. *Bioorg. Med. Chem.* **20,** 1281–90 (2012).

33. Labroli, M. a. *et al.* Syntheses of 5′-amino-2′,5′-dideoxy-2′,2′-difluorocytidine derivatives as novel anticancer nucleoside analogs. *Tetrahedron Lett.* **55,** 598–602 (2014).

34. Griffey, R. H. & Sanghvi, Y. S. Synthesis of 5'-0-Amino-2'-deoxypyrimidine and Purine Nucleosides: BuildingBlocks for Antisense Oligonucleosidesl,t. 5150–5156 (1995).

35. Publications, O. (12) Umted States Patent. **2,** (2010).

36. Chu, W. *et al.* New N-substituted 9-azabicyclo[3.3.1]nonan-3alpha-yl phenylcarbamate analogs as sigma2 receptor ligands: synthesis, in vitro characterization, and evaluation as PET imaging and chemosensitization agents. *Bioorg. Med. Chem.* **17,** 1222–31 (2009).

37. Pulido, J., Sobczak, A. J., Balzarini, J. & Wnuk, S. F. Synthesis and cytostatic evaluation of 4-N-alkanoyl and 4-N-alkyl gemcitabine analogues. *J. Med. Chem.* **57,** 191–203 (2014).

38. Das, M., Jain, R., Agrawal, A. K., Thanki, K. & Jain, S. Macromolecular Bipill of Gemcitabine and Methotrexate Facilitates Tumour-Speci fi c Dual Drug Therapy with Higher Bene fi t-to-Risk Ratio. (2014).

39. Maly, D. J. *et al.* Expedient Solid-Phase Synthesis of Fluorogenic Protease Substrates Using the 7-Amino-4-carbamoylmethylcoumarin (ACC) Fluorophore. 910–915 (2002).

40. Zhang, D. *et al.* Facile rearrangement of N4-(α-aminoacyl)cytidines to N-(4-cytidinyl)amino acid amides. *Tetrahedron Lett.* **49,** 2052–2055 (2008).

41. Guo, Z. & Gallo, J. M. Selective Protection of 2 ′ , 2 ′ -Difluorodeoxycytidine (Gemcitabine). 8319–8322 (1999).

42. Jemal, A. *et al.* Global cancer statistics. *CA. Cancer J. Clin.* **61,** 69–90 (2011).

43. Nelson, W. G., De Marzo, A. M. & Isaacs, W. B. Prostate Cancer. *N. Engl. J. Med.* **349,** 366–381 (2003).

44. Miyamoto, H., Messing, E. M. & Chang, C. Androgen deprivation therapy for prostate cancer: Current status and future prospects. *Prostate* **61,** 332–353 (2004).

45. Labrie, F. Endocrine therapy of prostate cancer: optimal form and timing. *J. Clin. Endocrinol. Metab.* **80,** 1066–1071 (1995).

46. Limonta, P. & Manea, M. Gonadotropin-releasing hormone receptors as molecular therapeutic targets in prostate cancer: Current options and emerging strategies. *Cancer Treat. Rev.* (2013). doi:10.1016/j.ctrv.2012.12.003

47. Oudard, S. Progress in emerging therapies for advanced prostate cancer. *Cancer Treat. Rev.* **39,** 275–289 (2013).

48. Millar, R. P. GnRHs and GnRH receptors. *Anim. Reprod. Sci.* **88,** 5–28 (2005).

49. Millar, R. P. Gonadotropin-Releasing Hormone Receptors. *Endocr. Rev.* **25,** 235–275 (2004).

50. Sealfon, S. C. Molecular Mechanisms of Ligand Interaction with the Gonadotropin-Releasing Hormone Receptor. *Endocr. Rev.* **18,** 180–205 (1997).

51. Payne, H. & Mason, M. Androgen deprivation therapy as adjuvant/neoadjuvant to radiotherapy for high-risk localised and locally advanced prostate cancer: recent developments. *Br. J. Cancer* **105,** 1628–1634 (2011).

52. Harrison, G. S., Wierman, M. E., Nett, T. M. & Glode, L. M. Gonadotropin-releasing hormone and its receptor in normal and malignant cells. *Endocr. Relat. Cancer* **11,** 725–748 (2004).

53. Cheung, L. W. T. & Wong, A. S. T. Gonadotropin-releasing hormone: GnRH receptor signaling in extrapituitary tissues. *FEBS J.* **275,** 5479–5495 (2008).

54. Tieva A, Stattin, P., Wikström, P., Bergh, A. & Damber, J. E. Gonadotropin-releasing hormone receptor expression in the human prostate. *Prostate* **47,** 276–284 (2001).

55. Straub, B. *et al.* Increased incidence of luteinizing hormone-releasing hormone receptor gene messenger RNA expression in hormone-refractory human prostate cancers. *Clin. cancer Res. an Off. J. Am. Assoc. Cancer Res.* **7,** 2340–2343 (2001).

56. Carmichael, J. The role of gemcitabine in the treatment of other tumours. *Br. J. Cancer* **78 Suppl 3,** 21–25 (1998).

57. Mackey, J. R. *et al.* Functional nucleoside transporters are required for gemcitabine influx and manifestation of toxicity in cancer cell lines. *Cancer Res.* **58,** 4349–4357 (1998).

58. Ueno, H., Kiyosawa, K. & Kaniwa, N. Pharmacogenomics of gemcitabine: can genetic studies lead to tailor-made therapy? *Br. J. Cancer* **97,** 145–151 (2007).

59. Mini, E. Cellular pharmacology of gemcitabine. *Ann. Oncol.* **17,** v7–v12 (2006).

60. Moysan, E., Bastiat, G. & Benoit, J.-P. Gemcitabine versus Modified Gemcitabine: a review of several promising chemical modifications. *Mol. Pharm.* **10,** 430–44 (2013).

61. Muenchen, H. J. *et al.* The study of gemcitabine in combination with other chemotherapeutic agents as an effective treatment for prostate cancer. *Anticancer Res.* **20,** 735–740 (2000).

62. Buch-Hansen, T. Z. *et al.* Phase I/II study on docetaxel, gemcitabine and prednisone in castrate refractory metastatic prostate cancer. *Cancer Chemother. Pharmacol.* **66,** 295–301 (2010).

63. Garcia, J. A., Hutson, T. E., Shepard, D., Elson, P. & Dreicer, R. Gemcitabine and docetaxel in metastatic, castrate-resistant prostate cancer: results from a phase 2 trial. *Cancer* **117,** 752–757 (2011).

64. Morant, R. *et al.* Response and palliation in a phase II trial of gemcitabine in hormone-refractory metastatic prostatic carcinoma. Swiss Group for Clinical Cancer Research (SAKK). *Ann. Oncol. Off. J. Eur. Soc. Med. Oncol. / ESMO* **11,** 183–188 (2000).

65. Biraboneye, A. C. *et al.* Potential neuroprotective drugs in cerebral ischemia: new saturated and polyunsaturated lipids coupled to hydrophilic moieties: synthesis and biological activity. *J. Med. Chem.* **52,** 4358–69 (2009).

66. Karampelas, T., Argyros, O., Sayyad, N. & Spyridaki, K. Preclinical Evaluation of GnRH-Gemcitabine Conjugates for the Treatment of Prostate Cancer : Targeted Drug Delivery Combined with Pharmacokinetic Enhancements. 1–36

67. Carpino, L. A., Ionescu, D. & El-Faham, A. Peptide Coupling in the Presence of Highly Hindered Tertiary Amines. *J. Org. Chem.* **61,** 2460–2465 (1996).

68. Carpino, L. A. 1-Hydroxy-7-azabenzotriazole. An efficient peptide coupling additive. *J. Am. Chem. Soc.* **115,** 4397–4398 (1993).

69. Han, S.-Y. & Kim, Y.-A. Recent development of peptide coupling reagents in organic synthesis. *Tetrahedron* **60,** 2447–2467 (2004).

70. Albericio, F., Bofill, J. M., El-Faham, A. & Kates, S. A. Use of Onium Salt-Based Coupling Reagents in Peptide Synthesis 1. *J. Org. Chem.* **63,** 9678–9683 (1998).

71. Albericio, F., Bofill, J. M., El-faham, A. & Kates, S. A. Use of Onium Salt-Based Coupling Reagents in Peptide Synthesis 1. 9678–9683 (1998).

72. Crisalli, P. & Kool, E. T. Water-soluble organocatalysts for hydrazone and oxime formation. *J. Org. Chem.* **78,** 1184–9 (2013).

73. Manea, M. *et al.* Enhanced Enzymatic Stability and Antitumour Activity of Daunorubicin-GnRH-III Bioconjugates Modified in Position 4. (2011).

74. Skarlas, T. *et al.* Influenza virus H5N1 hemagglutinin (HA) T-cell epitope conjugates: design, synthesis and immunogenicity. *J. Pept. Sci.* **17,** 226–32 (2011).

75. Lelle, M., Frick, S. U., Steinbrink, K. & Peneva, K. Novel cleavable cell-penetrating peptide-drug conjugates: synthesis and characterization. *J. Pept. Sci.* **20,** 323–33 (2014).

76. Chelius, D. & Shaler, T. A. Capture of peptides with N-terminal serine and threonine: a sequence-specific chemical method for Peptide mixture simplification. *Bioconjug. Chem.* **14,** 205–11

77. Geoghegan, K. F., Emery, M. J., Martin, W. H., McColl, A. S. & Daumy, G. O. Site-directed double fluorescent tagging of human renin and collagenase (MMP-1) substrate peptides using the periodate oxidation of N-terminal serine. An apparently general strategy for provision of energy-transfer substrates for proteases. *Bioconjug. Chem.* **4,** 537–44

78. Schottelius, M., Berger, S., Poethko, T., Schwaiger, M. & Wester, H. Development of Novel 68 Ga- and GnRHR-Targeting Efficiency F-Labeled GnRH-I Analogues with High. 1256–1268 (2008).

79. Bahta, M. *et al.* Oxime-based linker libraries as a general approach for the rapid generation and screening of multidentate inhibitors. *Nat. Protoc.* **7,** 686–702 (2012).

80. V. C. Armstrong, D. W. F. and R. B. M. The hydrolysis of amides, esters, and related compounds in acid solution. Part I. Amides, carbamates, and ureas. J. Chem. Soc. B, 1968, 1099-1103.

81. Lee, J. *et al.* N-Alkoxysulfamide, N-hydroxysulfamide, and sulfamate analogues of methionyl and isoleucyl adenylates as inhibitors of methionyl-tRNA and isoleucyl-tRNA synthetases. *Bioorg. Med. Chem. Lett.* **13,** 1087–1092 (2003).

82. Maly, D. J. *et al.* Expedient Solid-Phase Synthesis of Fluorogenic Protease Substrates Using the 7-Amino-4-carbamoylmethylcoumarin (ACC) Fluorophore. 910–915 (2002).

83. Reuter, S., Gupta, S. C., Chaturvedi, M. M. & Aggarwal, B. B. Oxidative stress, inflammation, and cancer: how are they linked? *Free Radic. Biol. Med.* **49,** 1603–16 (2010).

84. Martin-Cordero, C., Leon-Gonzalez, A. J., Calderon-Montano, J. M., Burgos-Moron, E. & Lopez-Lazaro, M. Pro-oxidant natural products as anticancer agents. *Curr. Drug Targets* **13,** 1006–28 (2012).

85. Wondrak, G. T. Redox-directed cancer therapeutics: molecular mechanisms and opportunities. *Antioxid. Redox Signal.* **11,** 3013–69 (2009).

86. Nepali, K., Sharma, S., Sharma, M., Bedi, P. M. S. & Dhar, K. L. Rational approaches, design strategies, structure activity relationship and mechanistic insights for anticancer hybrids. *Eur. J. Med. Chem.* **77,** 422–87 (2014).

87. Papadopoulou, A. A. *et al.* Enzymatic hybridization of α-lipoic acid with bioactive compounds in ionic solvents. *Bioresour. Technol.* **136,** 41–8 (2013).

88. Pingaew, R. *et al.* Synthesis, biological evaluation and molecular docking of novel chalcone-coumarin hybrids as anticancer and antimalarial agents. *Eur. J. Med. Chem.* **85,** 65–76 (2014).

89. Janga, S. C. & Tzakos, A. Structure and organization of drug-target networks: insights from genomic approaches for drug discovery. *Mol. Biosyst.* **5,** 1536–48 (2009).

90. Bernini, R. *et al.* Synthesis of a novel ester of hydroxytyrosol and α-lipoic acid exhibiting an antiproliferative effect on human colon cancer HT-29 cells. *Eur. J. Med. Chem.* **46,** 439–46 (2011).

91. Gorąca, A. *et al.* Lipoic acid - biological activity and therapeutic potential. *Pharmacol. Rep.* **63,** 849–58 (2011).

92. Packer, L., Witt, E. H. & Tritschler, H. J. alpha-Lipoic acid as a biological antioxidant. *Free Radic. Biol. Med.* **19,** 227–50 (1995).

93. Bhatti, F. *et al.* Mechanisms of antioxidant and pro-oxidant effects of alpha-lipoic acid in the diabetic and nondiabetic kidney. *Kidney Int.* **67,** 1371–80 (2005).

94. Cakatay, U. Pro-oxidant actions of alpha-lipoic acid and dihydrolipoic acid. *Med. Hypotheses* **66,** 110–7 (2006).

95. Moini, H., Packer, L. & Saris, N.-E. L. Antioxidant and prooxidant activities of alpha-lipoic acid and dihydrolipoic acid. *Toxicol. Appl. Pharmacol.* **182,** 84–90 (2002).

96. Rocha Lima, C. M. *et al.* Single-agent gemcitabine and gemcitabine/irinotecan combination (irimogem) in non-small cell lung cancer. *Semin. Oncol.* **26,** 43–50; discussion 71–2 (1999).

97. Zoli, W. *et al.* Docetaxel and gemcitabine activity in NSCLC cell lines and in primary cultures from human lung cancer. *Br. J. Cancer* **81,** 609–15 (1999).

98. Hertel, L. W. *et al.* Evaluation of the antitumour activity of gemcitabine (2',2'-difluoro-2'-deoxycytidine). *Cancer Res.* **50,** 4417–22 (1990).

99. Plunkett, W. *et al.* Gemcitabine: metabolism, mechanisms of action, and self-potentiation. *Semin. Oncol.* **22,** 3–10 (1995).

100. Gwyther, S. J., Aapro, M. S., Hatty, S. R., Postmus, P. E. & Smith, I. E. Results of an independent oncology review board of pivotal clinical trials of gemcitabine in non-small cell lung cancer. *Anticancer. Drugs* **10,** 693–8 (1999).

101. Balachandar, A. V, Malarkodi, K. P. & Varalakshmi, P. Protective role of DLalpha-lipoic acid against adriamycin-induced cardiac lipid peroxidation. *Hum. Exp. Toxicol.* **22,** 249–54 (2003).

102. Al-Majed, A. A., Gdo, A. M., Al-Shabanah, O. A. & Mansour, M. A. Alpha-lipoic acid ameliorates myocardial toxicity induced by doxorubicin. *Pharmacol. Res.* **46,** 499–503 (2002).

103. Selvakumar, E., Prahalathan, C., Sudharsan, P. T. & Varalakshmi, P. Protective effect of lipoic acid on cyclophosphamide-induced testicular toxicity. *Clin. Chim. Acta.* **367,** 114–9 (2006).

104. Molina-Heredia, F. P. *et al.* Detoxification of superoxide without production of H2O2: antioxidant activity of superoxide reductase complexed with ferrocyanide. *Proc. Natl. Acad. Sci. U. S. A.* **103,** 14750–5 (2006).

105. Benade, L., Howard, T. & Burk, D. Synergistic killing of Ehrlich ascites carcinoma cells by ascorbate and 3-amino-1,2,4,-triazole. *Oncology* **23,** 33–43 (1969).

106. Verrax, J. *et al.* In situ modulation of oxidative stress: a novel and efficient strategy to kill cancer cells. *Curr. Med. Chem.* **16,** 1821–30 (2009).

107. Yoo, D. G. *et al.* Alteration of APE1/ref-1 expression in non-small cell lung cancer: the implications of impaired extracellular superoxide dismutase and catalase antioxidant systems. *Lung Cancer* **60,** 277–84 (2008).

108. Casciari, J. J. *et al.* Cytotoxicity of ascorbate, lipoic acid, and other antioxidants in hollow fibre in vitro tumours. *Br. J. Cancer* **84,** 1544–50 (2001).

109. Koch, C. J. & Biaglow, J. E. Toxicity, radiation sensitivity modification, and metabolic effects of dehydroascorbate and ascorbate in mammalian cells. *J. Cell. Physiol.* **94,** 299–306 (1978).

110. Sakagami, H. *et al.* Production of hydrogen peroxide and methionine sulfoxide by epigallocatechin gallate and antioxidants. *Anticancer Res.* **21,** 2633–41

111. Perera, J., Tan, J. H., Jeevathayaparan, S., Chakravarthi, S. & Haleagrahara, N. Neuroprotective effects of alpha lipoic Acid on haloperidol-induced oxidative stress in the rat brain. *Cell Biosci.* **1,** 12 (2011).

112. Maritim, A. C., Sanders, R. A. & Watkins, J. B. Effects of alpha-lipoic acid on biomarkers of oxidative stress in streptozotocin-induced diabetic rats. *J. Nutr. Biochem.* **14,** 288–94 (2003).

113. Silberberg, M. *et al.* The bioavailability of polyphenols is highly governed by the capacity of the intestine and of the liver to secrete conjugated metabolites. *Eur. J. Nutr.* **45,** 88–96 (2006).

114. Bravo, L. Polyphenols: Chemistry, Dietary Sources, Metabolism, and Nutritional Significance. *Nutr. Rev.* **56,** 317–333 (2009).

115. Leary, K. A. O. *et al.* Metabolism of quercetin-7- and quercetin-3-glucuronides by an in vitro hepatic model : the role of human b -glucuronidase , sulfotransferase , catechol- O - methyltransferase and multi-resistant protein 2 (MRP2) in ¯ avonoid metabolism. **65,** 479–491 (2003).

116. Biasutto, L., Marotta, E., De Marchi, U., Zoratti, M. & Paradisi, C. Ester-based precursors to increase the bioavailability of quercetin. *J. Med. Chem.* **50,** 241–53 (2007).

117. Manach, C., Williamson, G., Morand, C. & Scalbert, A. Bioavailability and bioefficacy of polyphenols in humans . I . Review of 97 bioavailability studies 1 – 3. **81,** 230–242 (2005).

118. Picq, M., Prigent, A. F., Némoz, G., André, A. C. & Pacheco, H. Pentasubstituted quercetin analogues as selective inhibitors of particulate 3':5'-cyclic-AMP phosphodiesterase from rat brain. *J. Med. Chem.* **25,** 1192–8 (1982).

119. Kyriakou, E. *et al.* Unexpected enzyme-catalyzed regioselective acylation of flavonoid aglycones and rapid product screening. *Org. Biomol. Chem.* **10,** 1739–42 (2012).

120. Kim, M. K., Park, K., Yeo, W., Choo, H. & Chong, Y. In vitro solubility, stability and permeability of novel quercetin-amino acid conjugates. *Bioorg. Med. Chem.* **17,** 1164–71 (2009).

121. Theodorou, V., Skobridis, K., Tzakos, A. G. & Ragoussis, V. A simple method for the alkaline hydrolysis of esters. *Tetrahedron Lett.* **48,** 8230–8233 (2007).

122. Charisiadis, P., Primikyri, A., Exarchou, V., Tzakos, A. & Gerothanassis, I. P. Unprecedented ultra-high-resolution hydroxy group (1)H NMR spectroscopic analysis of plant extracts. *J. Nat. Prod.* **74,** 2462–6 (2011).

123. Stocker, R. & Keaney, J. F. Role of Oxidative Modifications in Atherosclerosis. 1381–1478 (2004).

124. García, G. *et al.* New losartan-hydrocaffeic acid hybrids as antihypertensive-antioxidant dual drugs: Ester, amide and amine linkers. *Eur. J. Med. Chem.* **50,** 90–101 (2012).

125. Daugherty, A. & Cassis, L. Angiotensin II-Mediated Development of Vascular Diseases. **14,** 117–120 (2004).

126. Carini, D. J. *et al.* Nonpeptide Angiotensin I1 Receptor Antagonists: The Discovery of a Series of N-(Biphenylylmethy1)imidazoles as Potent, Orally Active Antihypertensives. 2525–2547 (1991).

127. Chauhan, V. P. *et al.* Angiotensin inhibition enhances drug delivery and potentiates chemotherapy by decompressing tumour blood vessels. *Nat. Commun.* **4,** 2516 (2013).

128. Tanaka, R. *et al.* Novel 3alpha-methoxyserrat-14-en-21beta-ol (PJ-1) and 3beta-methoxyserrat-14-en-21beta-ol (PJ-2)-curcumin, kojic acid, quercetin, and baicalein conjugates as HIV agents. *Bioorg. Med. Chem.* **17,** 5238–46 (2009).

129. Geng, Q., Sun, X., Gong, T. & Zhang, Z. Peptide − Drug Conjugate Linked via a Disul fi de Bond for Kidney Targeted Drug Delivery. (2012).

130. Hassan, M., Tehrani, H., Zarghi, A. & Jabarian, L. E. Design and Synthesis of New Imidazole Derivatives of Captopril. 37–41 (2005).

131. Chirumamilla, R. R., Marchant, R. & Nigam, P. Review Captopril and its synthesis from chiral intermediates. **127,** 123–127 (2001).

132. Moss, G. P. *et al.* Design, synthesis and characterization of captopril prodrugs for enhanced percutaneous absorption. *J. Pharm. Pharmacol.* **58,** 167–77 (2006).

133. Harmsen, S. & Kok, R. J. Kinase inhibitor conjugates. *Curr. Pharm. Des.* **18,** 2891–900 (2012).

134. Tai, W., Shukla, R. S., Qin, B., Li, B. & Cheng, K. Development of a Peptide À Drug Conjugate for Prostate Cancer Therapy. 901–912 (2011).

135. Martini, M., Vecchione, L., Siena, S., Tejpar, S. & Bardelli, A. Targeted therapies: how personal should we go? *Nat. Rev. Clin. Oncol.* **9,** 87–97 (2012).

136. Liu, S. V *et al.* Phase I, Dose-Escalation Study of the Targeted Cytotoxic LHRH Analog AEZS-108 in Patients with Castration- and Taxane-Resistant Prostate Cancer. *Clin. Cancer Res.* **20,** 6277–83 (2014).

137. Popovics, P., Schally, A. V, Szalontay, L., Block, N. L. & Rick, F. G. Targeted cytotoxic analog of luteinizing hormone-releasing hormone (LHRH), AEZS-108 (AN-152), inhibits the growth of DU-145 human castration-resistant prostate cancer in vivo and in vitro through elevating p21 and ROS levels. *Oncotarget* **5,** 4567–78 (2014).

138. Morgan, K. *et al.* Elevated GnRH receptor expression plus GnRH agonist treatment inhibits the growth of a subset of papillomavirus 18-immortalized human prostate cells. *Prostate* **71,** 915–28 (2011).

139. White, C. D., Stewart, A. J., Lu, Z.-L., Millar, R. P. & Morgan, K. Antiproliferative effects of GnRH agonists: prospects and problems for cancer therapy. *Neuroendocrinology* **88,** 67–79 (2008).

140. Dondi, D. *et al.* Growth-inhibitory effects of luteinizing hormone-releasing hormone (LHRH) agonists on xenografts of the DU 145 human androgen-independent prostate cancer cell line in nude mice. *Int. J. Cancer* **76,** 506–11 (1998).

141. Al-Husein, B., Abdalla, M., Trepte, M., Deremer, D. L. & Somanath, P. R. Antiangiogenic therapy for cancer: an update. *Pharmacotherapy* **32,** 1095–111 (2012).

142. Ostman, A. The tumour microenvironment controls drug sensitivity. *Nat. Med.* **18,** 1332–4 (2012).

143. Karlou, M., Tzelepi, V. & Efstathiou, E. Therapeutic targeting of the prostate cancer microenvironment. *Nat. Rev. Urol.* **7,** 494–509 (2010).

144. Fong, T. A. *et al.* SU5416 is a potent and selective inhibitor of the vascular endothelial growth factor receptor (Flk-1/KDR) that inhibits tyrosine kinase catalysis, tumour vascularization, and growth of multiple tumour types. *Cancer Res.* **59,** 99–106 (1999).

145. Mendel, D. B. *et al.* In vivo antitumour activity of SU11248, a novel tyrosine kinase inhibitor targeting vascular endothelial growth factor and platelet-derived growth factor receptors: determination of a pharmacokinetic/pharmacodynamic relationship. *Clin. Cancer Res.* **9,** 327–37 (2003).

146. Sun, L. *et al.* Discovery of 5-[5-fluoro-2-oxo-1,2- dihydroindol-(3Z)-ylidenemethyl]-2,4-dimethyl-1H-pyrrole-3-carboxylic acid (2-diethylaminoethyl)amide, a novel tyrosine kinase inhibitor targeting vascular endothelial and platelet-derived growth factor receptor tyrosi. *J. Med. Chem.* **46,** 1116–9 (2003).

147. Di Lorenzo, G. *et al.* Expression of proto-oncogene c-kit in high risk prostate cancer. *Eur. J. Surg. Oncol.* **30,** 987–92 (2004).

148. Harper, M. E., Glynne-Jones, E., Goddard, L., Thurston, V. J. & Griffiths, K. Vascular endothelial growth factor (VEGF) expression in prostatic tumours and its relationship to neuroendocrine cells. *Br. J. Cancer* **74,** 910–6 (1996).

149. Michaelson, M. D. *et al.* Randomized, placebo-controlled, phase III trial of sunitinib plus prednisone versus prednisone alone in progressive, metastatic, castration-resistant prostate cancer. *J. Clin. Oncol.* **32,** 76–82 (2014).

150. Bergh, J. *et al.* First-line treatment of advanced breast cancer with sunitinib in combination with docetaxel versus docetaxel alone: results of a prospective, randomized phase III study. *J. Clin. Oncol.* **30,** 921–9 (2012).

151. Hammers, H. J. *et al.* Reversible epithelial to mesenchymal transition and acquired resistance to sunitinib in patients with renal cell carcinoma: evidence from a xenograft study. *Mol. Cancer Ther.* **9,** 1525–35 (2010).

152. Niu, G. & Chen, X. Vascular endothelial growth factor as an anti-angiogenic target for cancer therapy. *Curr. Drug Targets* **11,** 1000–17 (2010).

153. Makhov, P. B. *et al.* Modulation of Akt/mTOR signaling overcomes sunitinib resistance in renal and prostate cancer cells. *Mol. Cancer Ther.* **11,** 1510–7 (2012).

154. Patyna, S. *et al.* SU14813: a novel multiple receptor tyrosine kinase inhibitor with potent antiangiogenic and antitumour activity. *Mol. Cancer Ther.* **5,** 1774–82 (2006).

155. Prakash, C. R., Theivendren, P. & Raja, S. Indolin-2-Ones in Clinical Trials as Potential Kinase Inhibitors : A Review. **2012,** 62–71 (2012).

156. London, C. A. *et al.* Multi-center, placebo-controlled, double-blind, randomized study of oral toceranib phosphate (SU11654), a receptor tyrosine kinase inhibitor, for the treatment of dogs with recurrent (either local or distant) mast cell tumour following surgical excision. *Clin. Cancer Res.* **15,** 3856–65 (2009).

157. Dolman, M. E. M. *et al.* Targeting of a platinum-bound sunitinib analog to renal proximal tubular cells. *Int. J. Nanomedicine* **7,** 417–33 (2012).

158. Laird, A. D. *et al.* SU6668 is a potent antiangiogenic and antitumour agent that induces regression of established tumours. *Cancer Res.* **60,** 4152–60 (2000).

159. Noh, G. T. *et al.* Sunitinib--CLIO conjugate: a VEGFR/PDGFR-targeting active MR probe. *Mol. Imaging Biol.* **16,** 340–9 (2014).

160. Caballero, J. *et al.* Synthesis, in silico, in vitro, and in vivo investigation of 5-[^{11}C]methoxy-substituted sunitinib, a tyrosine kinase inhibitor of VEGFR-2. *Eur. J. Med. Chem.* **58,** 272–80 (2012).

161. Kumar, R. *et al.* Myelosuppression and kinase selectivity of multikinase angiogenesis inhibitors. *Br. J. Cancer* **101,** 1717–23 (2009).

162. Aparicio-Gallego, G. *et al.* New insights into molecular mechanisms of sunitinib-associated side effects. *Mol. Cancer Ther.* **10,** 2215–23 (2011).

163. Brooks, C. *et al.* Preclinical evaluation of sunitinib, a multi-tyrosine kinase inhibitor, as a radiosensitizer for human prostate cancer. *Radiat. Oncol.* **7,** 154 (2012).

164. Cumashi, A. *et al.* Sunitinib malate (SU-11248) alone or in combination with low-dose docetaxel inhibits the growth of DU-145 prostate cancer xenografts. *Cancer Lett.* **270,** 229–33 (2008).

165. Liu, L.-Z., Zheng, J. Z., Wang, X.-R. & Jiang, B.-H. Endothelial p70 S6 kinase 1 in regulating tumour angiogenesis. *Cancer Res.* **68,** 8183–8 (2008).

166. Katsila, T. *et al.* Evaluation of a stable gonadotropin-releasing hormone analog in mice for the treatment of endocrine disorders and prostate cancer. *J. Pharmacol. Exp. Ther.* **336,** 613–23 (2011).

167. Venkatakrishnan, A. J. *et al.* Molecular signatures of G-protein-coupled receptors. *Nature* **494,** 185–94 (2013).

168. Lagerström, M. C. & Schiöth, H. B. Structural diversity of G protein-coupled receptors and significance for drug discovery. *Nat. Rev. Drug Discov.* **7,** 339–57 (2008).

169. Katritch, V., Kufareva, I. & Abagyan, R. Structure based prediction of subtype-selectivity for adenosine receptor antagonists. *Neuropharmacology* **60,** 108–15 (2011).

170. Tzakos, A. G. *et al.* On the molecular basis of the recognition of angiotensin II (AII). NMR structure of AII in solution compared with the X-ray structure of AII bound to the mAb Fab131. *Eur. J. Biochem.* **270,** 849–60 (2003).

171. Tzakos, A. G., Gerothanassis, I. P. & Troganis, A. N. On the structural basis of the hypertensive properties of angiotensin II: a solved mystery or a controversial issue? *Curr. Top. Med. Chem.* **4,** 431–44 (2004).

172. De Gasparo, M., Catt, K. J., Inagami, T., Wright, J. W. & Unger, T. International union of pharmacology. XXIII. The angiotensin II receptors. *Pharmacol. Rev.* **52,** 415–72 (2000).

173. Ichiki, T. *et al.* Effects on blood pressure and exploratory behaviour of mice lacking angiotensin II type-2 receptor. *Nature* **377,** 748–50 (1995).

174. Doi, C. *et al.* Angiotensin II type 2 receptor signaling significantly attenuates growth of murine pancreatic carcinoma grafts in syngeneic mice. *BMC Cancer* **10,** 67 (2010).

175. Pickel, L. *et al.* Over-expression of angiotensin II type 2 receptor gene induces cell death in lung adenocarcinoma cells. *Cancer Biol. Ther.* **9,** 277–85 (2010).

176. Steckelings, U. M. *et al.* Non-peptide AT2-receptor agonists. *Curr. Opin. Pharmacol.* **11,** 187–92 (2011).

177. Ludwig, M., Steinhoff, G. & Li, J. The regenerative potential of angiotensin AT2 receptor in cardiac repair. *Can. J. Physiol. Pharmacol.* **90,** 287–93 (2012).

178. Friebe, S., Hartrodt, B., Neubert, K. & Krauss, G. J. High-performance liquid chromatographic separation of cis-trans isomers of proline-containing peptides. II. Fractionation in different cyclodextrin systems. *J. Chromatogr. A* **661,** 7–12 (1994).

179. Wan, Y., Wallinder, C., Plouffe, B., Pettersson, A. & Nyberg, F. Design , Synthesis , and Biological Evaluation of the First Selective Nonpeptide AT 2 Receptor Agonist. **313,** 5995–6008 (2004).

180. Kevin, N. J. Substituted phenylthiophene benzoylsulfonamides with potent binding affinity to angiotensin ii at1 and at2 receptors. **4,** 189–194 (2000).

181. Pratt, S. E. *et al.* Efficacy of low-dose oral metronomic dosing of the prodrug of gemcitabine, LY2334737, in human tumour xenografts. *Mol. Cancer Ther.* **12,** 481–90 (2013).

182. Potyahaylo, A. L., Samijlenko, S. P., Stepanyugin, A. V. & Hovorun, D. M. <title>Unusual behavior of cytosine amino group signal in <formula><roman>1</roman></formula>H NMR spectra in DMSO depending on its concentration</title>. **5507,** 190–194 (2004).

183. Phenomenon, T. H. E. INTRODUCTION TO CHEMICAL EXCHANGE. 1–16 (2001).

184. Kontogianni, V. G. *et al.* Hydrogen bonding probes of phenol -OH groups. *Org. Biomol. Chem.* **11,** 1013–25 (2013).

185. Singh, U. C., Deeter, J. B., Hertel, L. W., Kroin, J. S. & Initio, A. QUANTUM MECHANICAL AND X-RAY CRYSTALLOGRAPHIC STUDIES OF GEMCITABINE AND. **20,** 459–467 (1996).

186. Sivalakshmidevi, a. *et al.* 2′-Deoxy-2′,2′-difluorocytidine monohydrochloride (Gemcitabine hydrochloride). *Acta Crystallogr. Sect. E Struct. Reports Online* **59,** o1435–o1437 (2003).

187. Zhao, C. *et al.* Synthesis and biological evaluation of oral prodrugs based on the structure of gemcitabine. *Chem. Biol. Drug Des.* **80,** 479–88 (2012).

188. Nagy, A. *et al.* Cytotoxic analogs of luteinizing hormone-releasing hormone containing doxorubicin or 2-pyrrolinodoxorubicin, a derivative 500-1000 times more potent. *Proc. Natl. Acad. Sci. U. S. A.* **93,** 7269–73 (1996).

189. Nagy, A. Targeting of Cytotoxic Luteinizing Hormone-Releasing Hormone Analogs to Breast, Ovarian, Endometrial, and Prostate Cancers. *Biol. Reprod.* **73,** 851–859 (2005).

190. Kwon, I. K., Lee, S. C., Han, B. & Park, K. Analysis on the current status of targeted drug delivery to tumours. *J. Control. release Off. J. Control. Release Soc.* **164,** 108–114 (2012).

191. Jantscheff, P. *et al.* Liposomal gemcitabine (GemLip)-efficient drug against hormone-refractory Du145 and PC-3 prostate cancer xenografts. *Prostate* **69,** 1151–1163 (2009).

192. Kanzaki, M. *et al.* Low concentrations of the histone deacetylase inhibitor, depsipeptide, enhance the effects of gemcitabine and docetaxel in hormone refractory prostate cancer cells. *Oncol. Rep.* **17,** 761–767 (2007).

193. Boven, E., Schipper, H., Erkelens, C. A., Hatty, S. A. & Pinedo, H. M. The influence of the schedule and the dose of gemcitabine on the anti-tumour efficacy in experimental human cancer. *Br. J. Cancer* **68,** 52–56 (1993).

194. Frese, K. K. *et al.* nab-Paclitaxel potentiates gemcitabine activity by reducing cytidine deaminase levels in a mouse model of pancreatic cancer. *Cancer Discov.* **2,** 260–269 (2012).

195. Emons, G. *et al.* Efficacy and safety of AEZS-108 (LHRH agonist linked to doxorubicin) in women with advanced or recurrent endometrial cancer expressing LHRH receptors: a multicenter phase 2 trial (AGO-GYN5). *Int. J. Gynecol. Cancer* **24,** 260–5 (2014).